

GEOMETRIC CHARACTERISTICS OF CLOUDS FROM CEILOMETER MEASUREMENTS AND RADIO SOUNDING METHODS

Montserrat Costa Surós

Dipòsit legal: Gi. 1888-2014
<http://hdl.handle.net/10803/284084>



<http://creativecommons.org/licenses/by/4.0/deed.ca>

Aquesta obra està subjecta a una llicència Creative Commons Reconeixement

Esta obra está bajo una licencia Creative Commons Reconocimiento

This work is licensed under a Creative Commons Attribution licence



Universitat de Girona

**GEOMETRIC CHARACTERISTICS OF CLOUDS
FROM CEILOMETER MEASUREMENTS AND
RADIO SOUNDING METHODS**

DOCTORAL THESIS

Montserrat Costa Surós

2014



DOCTORAL THESIS

**GEOMETRIC CHARACTERISTICS OF CLOUDS FROM CEILOMETER
MEASUREMENTS AND RADIOSOUNDING METHODS**

Montserrat Costa Surós

2014

Doctoral Programme in Experimental Sciences and Sustainability

Supervisors:

Josep Calbó Angrill

José Abel González Gutiérrez

Thesis submitted for the degree of Doctor of Philosophy by the University of Girona

El Dr. Josep Calbó Angrill i el Dr. José Abel González Gutiérrez, professors titulars del Departament de Física de la Universitat de Girona,

CERTIFIQUEN:

Que aquest treball, titulat “Geometric characteristics of clouds from ceilometer measurements and radiosounding methods”, que presenta la Montserrat Costa Surós per a l’obtenció del títol de doctora, ha estat realitzat sota la seva direcció.

I, perquè així consti i tingui els efectes oportuns, signen aquest document.

Dr. Josep Calbó Angrill

Dr. José Abel González Gutiérrez

Girona, 29 de juliol de 2014.

Un esforç total és una victòria completa

M. Ghandi

Acknowledgments

First and the most important I would like to thank my supervisors Dr. Josep Calbó and Dr. Josep-Abel González for giving me the opportunity to begin my research career with them, which has led to this doctoral thesis, and for their guidance and support during these years.

I am grateful to Ministry of Science and Innovation of the Spanish Government, currently Ministry of Economy and Competitiveness, for the FPI fellowship (Researcher Staff Formation, FPI BES-2008-003129). And for the two brief stay grants (EEBB-2011-44092 and EEBB-I-12 03669) which made possible the two training brief stays: in the Pacific Northwest National Laboratory (PNNL, Richland, WA, USA) in 2011, and in Vaisala Oyj. (Vantaa, Helsinki, Finland) in 2012.

This thesis has also been possible thanks to Ministry of Science and Innovation which funded the research Projects: “Clouds and climate change: trends and variability of cloudiness and sunshine duration in the Iberian peninsula, and measurement and modeling of cloud radiative effects at the surface (NUCLIEREX)” (CGL2007-62664/CLI), and “Clouds and their effect on radiation: from studies of conditions at the local scale to climatological analyses of global extent. Interactions with the atmospheric aerosol (NUCLIERSOL)” (CGL2010-18546).

I want to thank the Spanish Meteorological State Agency (AEMET) which kindly provided visual observations of cloudiness used for comparison in this thesis. Likewise, acknowledgements to the Atmospheric Measurements Research (ARM) Program Research facility (sponsored by the U.S. Department of Energy) for providing valuable long periods of data (ARSCL) and TSI animations from the Southern Great Plains (OK, USA). Also, acknowledgements to National Oceanic and Atmospheric Administration (NOAA) Comprehensive Large Array-data stewardship system (CLASS) to provide GOES images for research use.

My sincere acknowledgments to the members of the projects: Dr. Javier Martín-Vide, especially because without his support regarding statistical analysis the thesis would have remained incomplete; Dr. Arturo Sanchez-Lorenzo, for being the fastest paper sender ever and for sharing his experiences with me; Dr. Antoni Viúdez, for his wise tips while we were sharing the office; and Dr. Jordi Badosa. To my brief stay advisors and mentors: Dr. Charles N. Long, for their high value contributions and comments to my manuscripts, and Victor Morris (from PNNL); Atte Salmi and Christopher Munkel (from Vaisala). And to Dr. Lydia Dimitrieva-Arago for her explanations and interesting discussions while visiting the University of Girona in the frame of the UE Project CLIMSEAS (FP7-PEOPLE-2009-IRSES Proposal N. 247512).

I also want to thank all my colleagues, Doctors and Professors, of the Department of Physics in the University of Girona, and specially my fellow Ph.D. students, for the friendship and good times: Dr. Dolors Pujol, Dr. Cristina Miàs, Dr. Jordi Colomer, Dr. Teresa Serra, Dr. Marianna Soler, Dr. Bruna Comas, Sandra Ricart, Nazha ElAlloui, Roger Arbusé, Lluís Calderer, Nitin Bharadwaj, Àlex Sànchez, Aaron Enríquez, Àlex Ros and Conxi Pau. Without forgetting the Service and Administration Personal (PAS) of the Department of Physics: Anna Espígol, Xevi Baca, Xicu Gómez, Marc Rodríguez, and Quico Pazo, as well as Natàlia Adell from UdG Technical Research Services.

I would like to express my gratitude to reviewers for the valuable suggestions that allowed improving the published papers.

And last but not least, I owe my deepest gratitude to all my family and friends who have given me their support in my choice of career and while preparing and writing this thesis. In particular, I want to thank Jaume Costa for his immensurable support and Xus López for his unconditional love, understanding and patience.

There would be many other names worth mentioning here. I just hope I have been able to show my sincere gratitude because a part of this thesis belongs to them, and it wouldn't be like this without them.

Contents

Publications and communications related to the thesis	xiii
List of acronyms and abbreviations.....	xv
List of figures	xxiii
List of tables.....	xxix
Abstract	xxxix
Resum	xxxiii
Resumen	xxxv
1. Introduction.....	1
1.1. Clouds and their classification.....	1
1.2. Current interest in clouds.....	14
1.3. Macroscopic detection, quantification and geometric characterization of clouds	21
2. Goals	27
3. Instruments, data and methodology.....	31
3.1. Cloud cover and cloud base height	31
3.1.1. Human observations	31
3.1.2. Sky cameras	34
3.1.3. LIDAR technology and ceilometer measurements	38
3.1.4. Surface radiometry.....	43
3.1.5. Satellite observations	50
3.2. Cloud vertical structure	55
3.2.1. Remote sensing by active ground-based systems and value added products (ARSL).....	56
3.2.2. Satellite observations (the A-train)	63
3.2.3. Aircraft in situ measurements	66
3.2.4. Radiosoundings	67
3.3 Methodology	74
3.3.1 Cloud cover and cloud base height from ceilometer measurements (Girona).....	74
3.3.2. Cloud vertical structure from radiosoundings and ARSL (Southern Great Plains)	77
3.3.2-a. Selecting suitable cases (horizontal displacement of the radiosonde and GOES images)	78

3.3.2-b. Radiosounding methods for cloud vertical structure estimation.....	81
3.3.2-c. Classification of the situations	90
4. Results and discussion	93
4.1. Cloud occurrence as cloud cover estimator.....	93
4.2. Cloud base height from ceilometer measurements	97
4.2.1. Cloud layers and CBH distributions.....	97
4.2.2. Yearly evolution of the CBH distribution	102
4.2.3. CBH behavior during some atmospheric situations.....	106
4.2.3-a. Winter low pressure systems.....	107
4.2.3-b. Summer conditions.....	109
4.3. Cloud vertical structure from atmospheric profiles and surface measurements.....	113
4.3.1. CVS behavior during some atmospheric conditions	114
4.3.2. General comparison of methods	122
4.3.3. ZHA10 tests and improvements.....	126
4.3.4. ZHA10i application example	131
5. Conclusions	135
BIBLIOGRAPHY	141
ANNEX 1: Synoptic maps of sea level pressure, temperature, and geopotential height at 500hPa and 850hPa; and Meteosat images; for some atmospheric situations (see section 4.2.3).....	155
ANNEX 2: Website summary.....	159

Publications and communications related to the thesis

Peer-reviewed papers (published/accepted):

- Title: "Comparing the cloud vertical structure derived from several methods based on radiosonde profiles and ground-based remote sensing measurements". Authors: **Montse Costa-Surós**; Josep Calbó, Ph.D.; Josep-Abel González, Ph.D.; Charles N. Long, Ph.D. Journal: *Atmospheric Measurement Techniques* (Impact factor 3.205, journal 15 of 74, 1st Quartile of Meteorology and Atmospheric Sciences category).
- Title: "Behavior of cloud base height from ceilometer measurements". Authors: **Montse Costa-Surós**; Josep Calbó, Ph.D.; Josep-Abel González, Ph.D.; Javier Martin-Vide, Ph.D. Journal: *Atmospheric Research* (Impact factor 1.911, journal 32 of 71, 2nd Quartile of Meteorology and Atmospheric Sciences category). Volume 127, June 2013, pages 64-76. DOI: 10.1016/j.atmosres.2013.02.005

Peer-reviewed paper (under revision):

- Title: "Modeling Atmospheric Longwave Radiation at the Surface during Overcast Skies: The Role of Cloud Base Height". Authors: Antoni Viúdez-Mora, Ph.D.; **Montse Costa-Surós**; Josep Calbó, Ph.D.; Josep-Abel González, Ph.D. Journal: *Journal of Geophysical Research - Atmospheres* (Impact factor 3.174, journal 23 of 172, 1st Quartile of Geosciences, Multidisciplinary category).

Communication Posters:

- Title: "Comparing the Cloud Vertical Structure derived from several methods based on atmospheric profiles and surface measurements" Conference: 16th International Conference on Clouds and Precipitation (ICCP 2012) in Leipzig (Germany). Authors: **Costa-Surós, M.**; Calbó, J.; González, J.A.; Long, C.N. Year: 2012

- Title: "How ceilometer detects some specific meteorological conditions?"
Conference: European Geosciences Union. General Assembly (EGU2012) in Vienna (Austria). Authors: **Costa-Surós, M.**; Calbó, J.; González, J.A.; Martin-Vide, J. Year: 2012
- Title: "Evaluation of Infrared Sky Imagers at the ARM Southern Great Plains Site"
Conference: II Science Team Meeting of the Atmospheric System Research (ASR) in San Antonio (TX, USA). Authors: Morris, V.; Klebe, D.; **Costa-Surós, M.** Year: 2011
- Title: "Monthly distributions of cloud base height determined with a ceilometer"
Conference: European Geosciences Union. General Assembly (EGU2010) in Vienna (Austria). Authors: **Costa-Surós, M.**; Calbó, J.; González, J.A. Year: 2010
- Title: "Caracterització de la nuvolositat mitjançant un ceilòmetre i una càmera hemisfèrica d'observació del cel a Girona"
Conference: Segones Jornades de Meteorologia i Climatologia de la Mediterrània Occidental (JMCMO) in Valencia (Spain). Authors: **Costa-Surós, M.**; Calbó, J.; González, J.A. Year: 2010
- Title: "Altura de la base dels núvols mesurada amb ceilòmetre: anàlisi d'un any i mig de mesures a Girona"
Conference: Primeres Jornades de Meteorologia i Climatologia de la Mediterrània Occidental in Barcelona (Spain) Authors: **Costa-Surós, M.**; Calbó, J.; González, J. A. Year: 2008

Chapter in book:

- Chapter title: "Estudi de la distribució de l'altura de la base dels núvols. Aplicació a Girona". Author: Costa-Surós, M. Book title: "Recerques en Medi Ambient Màster Universitari en Medi Ambient 2006/2010". Pag 39-46. Coord.: Pintó, J. Ed.: Documenta universitària. Year: 2011. ISBN: 978-84-8458-362-2.

List of acronyms and abbreviations

AATSR: Advanced Along Track Scanning Radiometer

ACARS: Aircraft Communications, Addressing, and Reporting Systems

ACRF: ARM Climate Research Facility

AIRIS: Atmospheric Infrared Sounder

ALOS: Advanced Land Observation Satellite

AMF: ARM Mobile Facility

AMSRE: Advanced Microwave Scanning Radiometer for EOS

AMSU: Advanced Microwave Sounding Unit

APCADA: Automatic Partial Cloud Amount Detection Algorithm

ARM: Atmospheric Radiation Measurement

ARSL: Active Remote Sensing of Clouds

ASAP: Automated Shipboard Aerological Program

ASIVA: All Sky Infrared Visible Analyzer

ASOS: Automated Surface Observing System

ASTEX: Atlantic Stratocumulus Transition Experiment

ATSR: Along-Track Scanning Radiometer

AVHRR: Advanced Very High Resolution Radiometer

AVNIR: Advanced Visible and Near Infrared Radiometer

BBC: BALTEX Bridge Campaigns

BSRN: Baseline Surface Radiation Network

CALIOP: Cloud-Aerosol Lidar with Orthogonal Polarization

CALIPSO: Cloud-Aerosol Lidar and Infrared Pathfinder Satellite Observation

CART: Cloud and Radiation Testbed

CBBE: Cloud Base Best Estimate

CBH: Cloud Base Height

CC: Cloud Cover

CCD: Color Charge-coupled device

CDT: Central Daylight Time

CERES: Clouds and Earth's Radiant Energy System

CLTC: Cloud Layer Thickness Climatology

CMIP: Coupled Model Intercomparison Project

CMOS: Complementary Metal–Oxide–Semiconductor

CNES: Centre National d'Etudes Spatiales

COMS: Communication, Ocean and Meteorological Satellite

CPR: Cloud Profiling Radar

CRM: Cloud-Resolving Models

CRU: Climate Research Unit

CTH: Cloud Top Height

CVS: Cloud Vertical Structure

C&C: CloudSat and CALIPSO

DMSP: Defense Meteorological Satellite Program

DOE: Department of Energy

ECMWF: European Center for Medium range Weather Forecast

EECRA: Extended Edited Cloud Report Archive

EOS: Earth Observation System

ERA: ECMWF Re-Analyses data

ERBE: Earth Radiation Budget Experiment

ERS: European Remote Sensing (satellite)

ETM+: Enhanced Thematic Mapper plus

FOV: Field Of View

FY: FengYun (satellites)

GAW: Global Atmospheric Watch

GCM: General Circulation Model

GCOS: Global Climate Observing System

GEWEX: Global Energy and Water Experiment

GOES: Geostationary Operational Environmental Satellite

GOMS: Geostationary Operational Meteorological Satellite

GPS: Global Positioning System

GSD: Ground Sample Distance

GTS: Global Telecommunication System

IASI: Infrared Atmospheric Sounding Interferometer

ICI: Infrared Cloud Imager

ICSU: International Council for Science

IFOV: Incidence Field Of View

IIR: Imaging Infrared Radiometer

IOC: Intergovernmental Oceanographic Commission

IPCC: Intergovernmental Panel on Climate Change

IR: Infrared Radiation

IRAS: InfraRed Atmospheric Sounder

IRR: IR Radiometer

ISCCP: International Satellite Cloud Climatology Project

KOMPSAT: Korea Multi-Purpose Satellite

LIDAR: Light Detection And Ranging

LW: LongWave

LW↓: LongWave irradiance downward

MERIS: Medium Resolution Imaging Spectrometer

METAR: METeorological Aerodrome Report

MFR7: Multi-Filter Radiometer

MFRSR: Multi-Filter-Rotating Shadowband Radiometer

MISR: Multi-angle Imaging Spectroradiometer

MMCR: Milli-Meter wavelength Cloud Radar

MODIS: Moderate Resolution Imaging Spectroradiometer

MOS: Marine Observation Satellite

MPL: Micro Pulse Lidar

MS: Microwave Sounder

MTSAT: Multifunctional Transport Satellites

MW: MicroWave

MWRI: Micro Wave Radiometer Imager

N7GCC: Nimbus-7 Global Cloud Climatology

NASA: National Aeronautics and Space Administration

NCAR: National Center for Atmospheric Research

NIR: Near InfraRed

NOAA: National Oceanic and Atmospheric Administration

NSA: North Slope Alaska

OMI: Ozone Monitoring Instrument

PNNL: Pacific Northwest National Laboratory

POES: Polar Operational Environmental Satellite

POLDER: Polarization and Directionality of the Earth's Reflectances

PR: Precipitation Radar

RAOBS: RAwinsonde OBServations

RBC: Rotating Beam Ceilometer

RH: Relative Humidity

RL: Raman Lidar

RS: RadioSonde

RTM: Radiative Transfer Model

SEVIRI: Spinning Enhanced Visible and Infrared Imager

SGP: Southern Great Plains

SMC: Servei Meteorologic de Catalunya

SMS: Synchronous Meteorological Satellites

SOBS: Surface OBSservation

SSR: Surface Solar Radiation

SST: Sea-Surface Temperature

SURFRAD: NOAA's Surface Radiation Network

SW: ShortWave

SYNOP: Surface Synoptic Observations

TCC: Total Cloud Cover

TIROS: Television Infrared Observation Satellite

TMI: TRMM Microwave Imager

TOA: Top Of the Atmosphere

TRMM: Tropical Rainfall Measuring Mission

TSI: Total Sky Imager

TWP: Tropical Western Pacific

UTC: Coordinated Universal Time

UV: UltraViolet

VCEIL: Vaisala CEILometer

VHRR: Very High Resolution Radiometer

VIRS: Visible InfraRed Scanner

VIS: VISible

VISSR: Visible and Infrared Spin Scan Radiometer

VTIR: Visible and Thermal Infrared Radiometer

WCRP: World Climate Research Programme

WFC: Wide Field Camera

WMO: World Meteorological Organization

WRDC: World Radiation Data Center

WSC: Whole Sky Camera

WSI: Whole Sky Imager

WV: Water Vapor

YES: Yankee Environmental Systems Inc.

Acronyms related with the most cited references and with the methodology:

PWR95: 'Poore, Wang and Rossow, 1995' method/dataset

WR95: 'Wang and Rossow, 1995' method/dataset

CE96: 'Chernyk and Eskridge, 1996' method

DS99: 'Dimitrieva-Arragó and Shatunova, 1999' method

MNS05: 'Minnis et al., 2005' method

WRZ00: 'Wang, Rossow and Zhang, 2000'

WRUR99: 'Wang, Rossow, Uttal and Rozendaal, 1999'

ZHA10: 'Zhang et al., 2010' method

ZHA10i: 'Zhang et al., 2010' improved method

ZHA10iLR: 'Zhang et al., 2010' improved Low Resolution method

ARSClv: values of cloud bases and tops according to visual inspection of the ARSCL data and RS trajectory (only vertical position considered), which are graphically superposed.

ARSCLm: mean values of ARSCL cloud bases and tops calculated between the time of when the RS launch and half an hour later.

CBH-ZHA10i: cloud base height as derived from ZHA10i method estimation from RS vertical profile measurements

CBH-CL31: cloud base height obtained from ceilometer CL-31

CBH-ARSCL: cloud base height from ARSCL instruments

Other abbreviations:

Ci: *Cirrus*

Cc: *Cirrocumulus*

Cs: *Cirrostratus*

Ac: *Alto cumulus*

As: *Altostratus*

St: *Stratus*

Sc: *Stratocumulus*

Cu: *Cumulus*

Cb: *Cumulunimbus*

N_s : *Nimbustratus*

C_L : Low Clouds

C_M : Middle Clouds

C_H : High Clouds

ΔT_d : dewpoint depression

T_{dew} : dewpoint temperature

T_{dry} : dry air temperature

P: pressure

T: temperature

z: height

asl: above sea level

agl: above ground level

T'' : second derivative of temperature

RH'' : second derivative of relative humidity

P_{clid} : probability of cloud occurrence (in DS99 method)

maxRH: relative humidity maximum threshold

minRH: relative humidity minimum threshold

interRH: relative humidity inter threshold

RH_{ice} : relative humidity relative to ice

RH_{water} : relative humidity relative to water

CI_m : confidence interval of each method

d_m : dispersion of each method

PA_m : number of cases of 'Perfect Agreement' for each method

n : total number of cases

List of figures

Figure	Page
Figure 1. Visual representation of the ten main cloud types (with the deliberately permission of reproduction by the Cloud Appreciation Society, www.cloudappreciationsociety.org)	12
Figure 2. The global annual mean energy budget of Earth for the approximate period 2000-2010. All fluxes are in Wm^{-2} . Solar fluxes are in yellow and infrared fluxes in pink. The four flux quantities in purple-shaded boxes represent the principal components of the atmospheric energy balance (Stephens et al., 2012).	15
Figure 3. Robust cloud responses to greenhouse warming (those simulated by most models and possessing some kind of independent support or understanding). The tropopause and melting level are shown by the thick solid and thin grey dashed lines, respectively. Changes anticipated in a warmer climate are shown by arrows, with red color indicating those making a robust positive feedback contribution and grey indicating those where the feedback contribution is small and/or highly uncertain. No robust mechanisms contribute as negative feedback (Boucher et al., 2013).	17
Figure 4. Schematic representation of dimming (a) and brightening (b) periods over land surfaces. Values denote best estimates of overall changes in surface energy fluxes over both periods in W m^{-2} (ranges of literature estimates for SSR dimming/brightening in parentheses). Positive (negative) numbers, shown in red (blue), denote increasing (decreasing) magnitudes of the energy fluxes in the direction indicated by the arrows. Changes in ground heat flux (GH) and sensible heat flux (SH) are considered small compared to the above mentioned flux changes (figure from Wild, 2012).	18
Figure 5. A weather log of human observations of clouds taken in Girona Airport in January of 1994. The first column are the days of the month, next columns are the genera of low clouds and its cover, then the medium and high clouds genera and finally the total cloud cover. These notes are taken three times per day (at 7h, 13h and 18h).	32
Figure 6. Table to guide the observations: symbols used in plotting a report. Left, symbols to represent total cloud cover. Right, symbols (and numbering codes) for cloud types corresponding to the three <i>étages</i> : low CL, middle CM, and high CH (Ahrens, 2009; aviation magazine: http://avstop.com/ac/5-7.html)	33
Figure 7. a) Whole Sky Camera (WSC) designed by the University of Girona and installed over a sun-tracker and with a sun-blocker at Girona (Spain); b) WSC image of a clear sky situation at Girona on July 6th, 2009; c) WSC image showing altocumulus and cirrus clouds, taken at Girona on July 19th, 2009.	37
Figure 8. a) The Total Sky Imager (TSI by YES) installed at PNNL, Richland, WA; b) TSI image with low clouds acquired by the TSI on October 1st, 2009 at SGP (OK); c) TSI image of an overcast cloud situation on July 5th, 2009 at SGP (OK) (source of TSI images: ARM data Archive).	37
Figure 9. Three possible alignment arrangements of a lidar's transmitted beam and receiver field of view (based on Argall and Sica, 2003).	38

Figure 10. Different brands and models of ceilometers: a) Belfort Laser Ceilometer 7013C (U.S. DOE's ARM Program), b) 80171 Cloud Ceilometer (Belfort Instruments website), c) Vaisala CT12K Laser Ceilometer, d) Vaisala CT25K (U.S. DOE's ARM Program), e) Vaisala CT75K (British atmosphere datacenter website), f) Vaisala CL-31 (Vaisala website), g) Vaisala CL-51 (Vaisala website), h) Jenoptik CHM15K (Jenoptik website), i) Eliasson CBME80 ceilometers (Eliasson Engineering website), and j) ceilometer 8200-CHS (MTECH systems website).	40
Figure 11. Ceilometer's typical measurement signal. Generally, particles at all heights backscatter light, and so the actual return signal may look like that shown in the figure. The instantaneous magnitude of the return signal will provide information on the backscatter properties of the atmosphere at a certain height. Information about fog and precipitation, as well as clouds, can be derived from the return signal. Since fog and precipitation attenuate the light pulse, the cloud base signal will appear lower in magnitude in the return echo. However, the fog and precipitation information also provides data for estimating this attenuation and computing the necessary compensation, up to a limit (Vaisala Oyj., 2006).	41
Figure 12. a) Kipp & Zonen CM11 solar diffuse pyranometer (spectral response between 0.28 - 2.8 μm) over a sun tracker and blocker; b) Kipp & Zonen CH1 pyrliometer (spectral response between 0.2- 4 μm and FOV 5 $^\circ$) and c) CG1 Kipp & Zonen pyrgeometer (measuring in the longwave spectrum of 4 to 40 μm and IFOV of 150 $^\circ$) with a sun blocker; and all three over a sun-tracker (Girona, Spain); d) A similar assembly, but with Eppley radiometers, over a sun-tracker in PNNL (Richland, WA).	44
Figure 13. Kipp & Zonen CM11 (a) and Li-Cor LI200SA (b) pyranometers which measure the global solar irradiance. The first one has spectral response between 0.28 - 2.8 μm ; the second has a spectral response between 0.4 - 1.1 μm . They are both installed at Girona, Spain	45
Figure 14. CG1 Kipp & Zonen pyrgeometer, which is mounted over a sun-tracker (Kipp & Zonen 2AP) with a sunblocker. It measures the infrared irradiance (spectral response between 0.3-2.2 μm) and has an incidence field of view (IFOV) of 150 $^\circ$. This instrument is installed in Girona, Spain.	45
Figure 15. a) CIR-4 and b) CIR-13 (from: Atmos Company website)	48
Figure 16. Nubiscope (from: Nubiscope website)	48
Figure 17. Multi-Filter-Rotating Shadowband Radiometers (MFRSR) installed at PNNL (Richland, WA)	49
Figure 18. Raman Lidar (ARM webpage and Newsom, 2009)	60
Figure 19. a) Ceilometer CT25K b) Micro Pulse Lidar (MPL), c) Milli-Meter wavelength Cloud Radar (MMCR) (ARM website).	60
Figure 20. A thermodynamic diagram build from data collected by a radiosonde in Southern Great Plains on 8 June 2011 at 05:27h (Skew-T, Log(P) Diagram).	68
Figure 21. Most used worldwide radiosonde models: a) Vaisala RS-80 (public domain, Wikimedia commons); b) Vaisala RS-9 (Vaisala website); c) Vaisala RS41 radiosonde (Vaisala website); d) GPS Mark II Microsonde (Sippican website); e) M2K2-DC (Meteo Modem website); f) M10 GPSONde (Meteo Modem website); g) RS-06G GPS radiosonde from MEISEI (Japan); h) DFM-09 radiosonde (Graw website); i) Inside view of SRS-C34 radiosonde (Meteolabor website).	70

Figure 22. a) Vaisala CL-31 ceilometer and b) CL-View, the ceilometer's software (Girona, Spain)	77
Figure 23. The boxplot shows the horizontal displacement, every 500 m height, of the 259 radiosondes launched from SGP (the boxplot shows the minimum, the first quartile, the median, the third quartile, the maximum and, if any, observations that might be considered outliers (plus symbols). The inset shows the horizontal projection vision of the RS position with respect to the launch point when they reach 15 km. The semi-circle represents the median of all displacements (79 km).	80
Figure 24. The ARM Mobile Facility (AMF, from ARM website)	82
Figure 25. Simplified representation, or flowchart, of PWR95 method, as it has been applied. Red ovals are variables (measured from radiosonde or calculated by the methodology); blue rectangles are the method procedures.	84
Figure 26. (a) Monthly cloud occurrence for the period 2007-2010, as derived from ceilometer data. Error bars indicate \pm one standard deviation of the original data. (b) Averaged monthly cloud occurrence as detected by the ceilometer for the period 2007-2010 and averaged cloud cover from visual observations at Girona Airport for the period 1973-2003. Error bars indicate \pm one standard deviation, as an estimation of the interannual variability. (c) Seasonal cloud cover in the Iberian Peninsula, series from the ISCCP, CRU and ERA datasets (several periods, see Calbó and Sanchez-Lorenzo, 2009) and seasonal averages of cloud occurrence from ceilometer data (December, January and February are considered as 'Winter'; March, April and May are 'Spring'; June, July and August are 'Summer'; and September, October and November are 'Autumn').	95
Figure 27. (a) Frequency distribution of CBH for all found layers aggregated, and when a single layer is detected. (b) Distribution of the CBH for the lower and higher layer when 2 layers are detected. (c) Distribution of the CBH for the lower, middle and higher layer when 3 layers are detected.	99
Figure 28. Frequency distribution of the distance between consecutive CBH detected by the ceilometer in multilayered cloud systems.	102
Figure 29. Standardized single layer CBH frequencies for some months, representative of each season, of the studied period.	103
Figure 30. (a) July of 2008 histogram fits a Burr distribution; (b) November of 2009 histogram fits a uniform distribution.	104
Figure 31. (a) January and July cumulative frequencies for the CBH of single layer cases; (b) April and October cumulative frequencies for the CBH of single layer cases; (c) Mean for the four years (2007-2010) cumulative frequencies for the CBH of single layer cases for January, April, July and October.	105
Figure 32. (a) Skewness (asymmetry) correlation with CBH mean; (b) skewness correlation with kurtosis.	106

Figure 33. (a) Evolution of the ceilometer detected CBH in December 2009 (first CBH in blue, second CBH in green, third CBH in red). (b) A detail for 25-26 December 2009, including (dashed lines) the periods of rain, detected by the ceilometer itself and by the rain gauge and the sky camera. (i) Clear sky seen from the whole sky image from December, 25 at 12.00h. (ii) <i>Stratocumulus</i> clouds on December 25 at 12.45h. (iii) Sky image from December 26 at 12.06h where <i>Stratus</i> clouds cover all the sky and leave some precipitation.	108
Figure 34. Frequency distributions of CBH for two different periods of December 2009.	109
Figure 35. (a) Idem Figure 33 but for July 2009. (b) A detail for 6-7 July 2009, including (dashed lines) the periods of rain. (i) Whole sky image from July 7 at 7.30h where several cloud types in different layers can be seen and (ii) at 13.15h with <i>Stratus</i> that cover the sky (c) A detail for 18-19 July 2009. (iii) Whole sky image from July 19 at 11.30h, with <i>Cumulus humilis</i> clouds produced by convection; (iv) the image taken at 12.30h where clouds are disappearing.	111
Figure 36. Frequency distributions of CBH for two different periods of July 2009.	112
Figure 37. Temperature (T_{dry} (°C), in red) and relative humidity with respect to water (RH (%), in blue) profiles above ground level from the radiosonde on October 5 of 2009 at 23.23h at SGP. Blue shading represents the cloud layers as detected by ARSCL. The values (on the right) related to every cloud layer boundary indicate the sonde horizontal distance from ARSCL site in kilometers when it reached those altitudes.	113
Figure 38. Case 1: 15 April 2009, No clouds. (a) Vertical position of the radiosounding depending on the time and the ARSCL products around the RS launch time (11:21 h UTC). (b) Cloud layers as detected by ARSCL (ARSCLm and ARSCLv), and as found by the explained methods (PWR95, WR95, CE96, DS99, MNS05 and ZHA10). (c) GOES image in the infrared channel at 12:00 UTC (approximately 25-45 min from the launch time). Dots indicate the horizontal position of the RS every 3 km height.	117
Figure 39. Idem as Figure 38, but for Case 2: 15 October 2009, Low clouds. RS launch time: 5:23 h UTC. GOES infrared image at 06:00 UTC.	118
Figure 40. Idem as Figure 38, but for Case 3: 10 July 2009, Middle clouds. RS launch time: 11:30 h UTC). GOES infrared image at 12:00 UTC.	119
Figure 41. Idem as Figure 38, but for Case 4: 20 January 2009, High clouds. RS launch time: 11:34 h UTC. GOES infrared image at 12:00 UTC.	120
Figure 42. Idem as Figure 38, but for Case 5: 5 October 2009, 2 layers of clouds: low and high clouds. RS launch time: 23:28 h UTC. GOES infrared image at 00:15 UTC (6 October 2009).	121
Figure 43. Comparison of cloud base height as derived from ZHA10 and ZHA10i methods estimation from RS vertical profile measurements against the cloud base height from ARSCL measurements (CBH-ARSCL) in SGP. The black diagonal is the line of the perfect agreement.	127
Figure 44. Downwelling longwave irradiance from pyrgeometer measurements against cloud base height measured with the ceilometer. Both values are ten minute averages. Lines correspond to the linear regression for each subset of points (Viúdez-Mora et al., 2014).	132

Figure 45. Comparison of cloud base height as derived from vertical profile (CBH-ZHA) against the cloud base height from ceilometer measurements (CBH-CL31). The diagonal is the line of the perfect agreement. Two outliers (CBH-ZHA ~ 9 km) are not shown (Viúdez-Mora et al., 2014). 133

Figure 46. Comparison between calculated and measured $LW\downarrow$ at Girona, during overcast conditions and for the RTM results when using CBH measured by ceilometer (left) and for the ZHA10i results. See text for definition of tests. Warm season data (red) and cold season data (blue) are distinguished in the plots. Equally, the linear regression lines are given for both subsets of data (Viúdez-Mora et al., 2014). 134

List of tables

Table	Page
Table 1. Characteristic size, concentration, and terminal velocity of particles involved in condensation and precipitation processes, including condensation nuclei and cloud droplets (adapted from Ahrens, 2009; Shuttleworth, 2012; Stull, 1995; Wallace and Hobbs, 1977).	4
Table 2. Latin basic cloud form names and their meaning.	10
Table 3. The three atmospheric <i>étages</i> according to the World Meteorological Organization (1975).	11
Table 4. Characteristics of instruments used as the basis of ARSCL value added product and, for comparison, the characteristics of the most used ceilometer (Vaisala CL-31, also used in Girona site) (extracted from the corresponding Handbooks from ARM Climate Research Facility).	62
Table 5. The most interesting instruments, related to cloud characteristics, in the A-Train constellation and their primary purpose (adapted from L'Ecuyer and Jiang, 2010).	66
Table 6. Currently used radiosondes (radiosonde brand websites; Nash et al., 2011).	73
Table 7. Summary of the applied RS methods.	85
Table 8. Summary of the values for min-RH, inter-RH and max-RH, from Zhang et al. (2010).	89
Table 9. Behavior of the six RS methods for cloud detection compared to ARSCL observations. Data in bold account for 'Perfect agreement' cases; data in italic account for 'Approximate agreement' cases.	124
Table 10. Seasonal values of perfect agreement (in parentheses the total number of cases) and its maximum difference for each method (W: winter, Sp: Spring, Su: Summer and A: autumn).	125
Table 11. Behavior of the tests performed on ZHA10 method compared to ARSCL observations. Data in bold account for 'Perfect agreement' cases; data in italic account for 'Approximate agreement' cases.	129
Table 12. Summary of the values for max-RH, from Zhang et al. (2010) and the new max-RH thresholds suggested for the low resolution test.	130

Abstract

Given the importance of clouds in the climate, and the difficulty in determining their behavior and their contribution to climate change, there is a need to improve methods for automatic and continuous description of cloud characteristics. The cloud vertical distribution and, in particular, the cloud base height, which are linked to cloud type, are both important characteristics for describing the impact clouds have on the climate.

This dissertation presents a complete study of cloudiness above Girona (Spain), and which has been measured with a ceilometer because ceilometers constitute, a priori, a reliable instrumental method for sounding the atmosphere and describing cloudiness, specifically cloud base height (CBH), cloud cover, and even cloud vertical structure (CVS). In addition, and in order to better describe the cloud vertical structure, a comparison of the CVS obtained from methods based on radiosonde profiles with estimations produced by ground-based active instruments (that is, the Active Remote Sensing of Clouds –ARSCl– cloud base and top heights) over Southern Great Plains (SGP, OK, USA) is presented.

Specifically, the first study covers a four year period (2007-2010) of high resolution ceilometer measurements (in both time and the vertical direction). The cloud occurrence and CBH distributions of the whole data set are analyzed, and furthermore the behavior of CBH on different time scales is investigated, including a detailed statistical analysis of the CBH frequency distributions, which have been carried out on a monthly and seasonal basis. These distributions are compared with previous results concerning CBH behavior that can be found in the literature. Moreover, some specific atmospheric situations are described, thus adding further insight into the behavior of CBH.

Several conclusions are derived from this study in Girona, namely ceilometer measurements reveal a seasonal cycle, with significant differences between the "extreme" seasons (winter and summer) and the "transition" seasons (spring and autumn). Summer months in general and July in particular behave quite differently to other periods in the year, both in terms of cloud presence (with a minimum cloud occurrence of about 20-30%) and in the distribution of CBH (with more than 25% of clouds having CBH around 1400 m and 80% of clouds with CBH lower than 3000 m). The distributions of CBH are explained by certain atmospheric situations that generate clouds, in particular conditions that produce the large number of low level clouds are found.

In a second study, several methods for estimating the CVS based on atmospheric sounding profiles are compared with each other and with a ground-based system, the ARSCL, which is taken as a reference. Specifically, the cloud vertical structures from 193 radiosonde profiles acquired at the ARM SGP site are analyzed. These profiles cover the year 2009, with all the seasons being represented, and four specific case studies are described in detail. This study extends previous comparison studies on radiosounding methods used to obtain CVS, as it considers even more methods and accurately compares retrievals against a reliable reference (ARSCL) and for an accurately selected set of cases.

The general results of the comparison on an annual and seasonal basis are given, and some modifications to one method are tested. Also, some improvements for one particular method are proposed, specifically a technique for low resolution profiles. The analyses made at SGP reveal the methods' strengths and weaknesses. Thus, the perfect agreement (i.e. when the whole CVS is correctly estimated) for the original methods ranges between 26-64%; the methods show additional approximate agreement (i.e. when at least one cloud layer is correctly assessed) of 15-41%. The perfect agreement, even when using low resolution profiles, can be improved by up to 67% (in addition to 25% of the approximate agreement). It would appear that one method, provided that is conveniently modified, may be successfully applied to lower resolution profiles such as the WMO's Global Telecommunication System (GTS) vertical profiles or to the reanalysis temperature and humidity products. An application of a radiosounding method in a modeling study of the ground-level infrared irradiance under overcast conditions is also summarized.

Resum

Donada la importància que tenen els núvols en el clima, i la dificultat en determinar el seu comportament i la seva contribució al canvi climàtic, cal millorar els mètodes per una descripció automàtica i contínua de les característiques dels núvols. La distribució vertical dels núvols, i especialment l'altura de la base, que va vinculada al tipus de núvol, és una característica important per tal de descriure el seu impacte climàtic.

Aquest treball presenta un estudi complet de la nuvolositat mesurada amb un ceilòmetre a Girona (Espanya), ja que els ceilòmetres són, a priori, una metodologia instrumental fiable a l'hora de sondejar l'atmosfera i descriure la nuvolositat, especialment l'altura de la base dels núvols (CBH), la cobertura de núvols, i fins hi tot l'estructura vertical dels núvols (CVS). Per altra banda, i amb l'objectiu de descriure millor l'estructura vertical, s'ha fet una comparació de la CVS obtinguda a partir de mètodes basats en perfils de radiosondatges amb estimacions obtingudes d'instruments actius en superfície (això és, les altures de les bases i cims dels núvols obtingudes a partir del Active Remote Sensing of Clouds, ARSCL) sobre Southern Great Plains (SGP, OK, EUA) per tal de trobar la millor aproximació a l'estructura vertical real i revelar les fortaleses i febleses dels mètodes utilitzats.

Concretament, s'ha estudiat quatre anys (2007-2010) de mesures del ceilòmetre en alta resolució (tant temporal com espacial, en direcció vertical). La probabilitat de presència de núvol (ocurrència) i les distribucions de la CBH de tota la base de dades han estat analitzades, juntament amb el comportament de la CBH a diferents escales temporals, incloent l'anàlisi estadística de la distribució de freqüència de la CBH a escala mensual i estacional. Aquestes distribucions han estat comparades amb resultats trobats a la literatura referents al comportament de la CBH. A més, s'han descrit algunes situacions atmosfèriques concretes per tal d'aportar un coneixement més profund de les distribucions de freqüència de la CBH.

Varies conclusions s'han derivat de l'estudi a Girona: les mesures del ceilòmetre revelen un cicle estacional, amb diferències importants entre les estacions "extremes" (hivern i estiu) i les de "transició" (primavera i tardor). Els mesos d'estiu en general i el juliol en particular presenten característiques bastant diferents dels altres períodes de l'any, tant pel que fa a la presència de núvols (amb un mínim d'ocurrència d'un 20-30%) com pel que fa a la distribució de la CBH (amb més d'un 25% de núvols que tenen la base al voltant de 1400 m i un 80% dels núvols amb la base per sota de 3000 m). Les distribucions de la CBH s'expliquen a partir de situacions atmosfèriques

concretes que generen núvols, en particular condicions que produeixen una gran quantitat de núvols baixos.

En un segon estudi s'ha comparat diversos mètodes d'estimació de la CVS basats en perfils de sondatge atmosfèrics, entre ells i amb un sistema de mesura en superfície, l'ARSCL, el qual s'ha pres com a referència. Concretament s'ha estudiat l'estructura vertical de la nuvolositat obtinguda de 193 perfils de radiosondatges adquirits a la localització de l'ARM SGP. Aquests perfils cobreixen tot l'any 2009, totes les estacions hi són representades, i a més quatre casos en particulars han estat estudiats i descrits amb detall. Aquest estudi estén les comparacions publicades anteriorment de mètodes d'obtenció de la CVS a partir de radiosondatges, ja que aquí es consideren més mètodes i es compara amb precisió els resultats amb una referència fiable (ARSCL) i per un conjunt de casos seleccionats acuradament.

Es presenta els resultats generals de la comparació, a escala anual i estacional. Per un mètode determinat es presenta els resultats d'algunes modificacions i es proposa algunes millores, en particular per perfils de baixa resolució. Les anàlisis revelen els punts forts i febles dels mètodes. Així, l'acord perfecte (quan tota la CVS és estimada correctament) pels mètodes originals es troba entre el 26 i el 64%; els mètodes mostren acord aproximat (quan al menys una capa de núvols és estimada correctament) entre el 15 i el 41% dels casos. L'acord perfecte pot ser millorat fins el 67% (més un 25% d'acord aproximat), fins i tot emprant perfils de baixa resolució. Un dels mètodes, un cop modificat convenientment, pot ser aplicat a perfils de baixa resolució com els del *WMO's Global Telecommunications System*, o a productes de reanàlisi de temperatura i humitat. Es resumeix també una aplicació a un estudi de modelització de la irradiància infraroja incident en superfície en condicions de cel ennuvolat.

Resumen

Dada la importancia que tienen las nubes en el clima, y la dificultad para determinar su comportamiento y su contribución al cambio climático, existe la necesidad de mejorar los métodos para una descripción automática y continua de las características de las nubes. La distribución vertical de las nubes, y especialmente la altura de la base, que está vinculada al tipo de nube, es una característica importante para describir su impacto climático.

Este trabajo presenta un estudio completo de la nubosidad medida con un ceilómetro en Girona (España), ya que los ceilómetros son, a priori, una metodología instrumental fiable para sondear la atmosfera y describir la nubosidad, especialmente la altura de la base de las nubes (CBH), la cobertura nubosa, e incluso la estructura vertical de las nubes (CVS). Por otra parte, y para mejorar la descripción de la estructura vertical se ha realizado una comparación de la CVS obtenida a partir de métodos basados en perfiles de radiosondeos con estimaciones obtenidas de instrumentos activos en superficie (es decir, las alturas de las bases y cimas de las nubes obtenidas a partir del Active Remote Sensing of Clouds, ARSCL) sobre Southern Great Plains (SGP, OK, EUA) para encontrar la mejor aproximación a la CVS real y revelar los puntos fuertes y débiles de los métodos utilizados.

Concretamente, se ha estudiado cuatro años (2007-2009) de medidas del ceilómetro en alta resolución (tanto temporal como espacial, en dirección vertical). La probabilidad de presencia de nube (ocurrencia) y las distribuciones de la CBH de toda la base de datos han sido analizadas, además del comportamiento de la CBH a diferentes escalas temporales, incluyendo el análisis estadístico de las distribuciones de frecuencia de la CBH a escala mensual y estacional. Estas distribuciones han sido comparadas con los resultados de la literatura referentes al comportamiento de la CBH. Asimismo se ha descrito algunas situaciones atmosféricas concretas, lo que ha llevado a un conocimiento más profundo de las distribuciones de frecuencia de la CBH.

Varias conclusiones se han derivado del estudio en Girona: las medidas del ceilómetro rebelan un ciclo estacional, con diferencias importantes entre las estaciones “extremas” (invierno y verano) y las de “transición” (primavera y otoño). Los meses de verano en general y Julio en particular presentan características bastante diferentes de los otros periodos del año, tanto por lo que se refiere a la presencia de nubes (con un mínimo de ocurrencia de nubes de un 20-30%) como a la distribución de la CBH (con más de un 25% de nubes que tienen la base alrededor de los 1400 m y un 80% de las nubes con la base por debajo los 3000 m). Las distribuciones de la

CBH se explican a partir de situaciones atmosféricas concretas que generen nubes, en particular condiciones que producen una gran cantidad de nubes bajas.

En un segundo estudio se ha comparado diversos métodos de estimación de la CVS basados en perfiles de sondeos atmosféricos, han estado comparados entre ellos y con un sistema de medida en superficie, ARSCL, que se ha tomado como referencia. Concretamente se ha estudiado la estructura vertical de la nubosidad obtenida de 193 perfiles de radiosondeos adquiridos en la localización del ARM SGP. Estos perfiles cubren todo el año 2009, todas las estaciones se encuentran representadas, y además cuatro casos en particular han sido estudiados y descritos con mayor detalle. Este estudio extiende las comparaciones publicadas anteriormente entre métodos de obtención de la CVS a partir de radiosondeos, ya que aquí se consideran más métodos y se compara con precisión los resultados con una referencia fiable (ARSCL) y para un conjunto de casos seleccionados cuidadosamente.

Se presenta los resultados generales de la comparación, a escala anual y estacional. Para un método determinado se presenta los resultados de algunas modificaciones y se propone algunas mejoras, en particular para perfiles de baja resolución. Los análisis revelan los puntos fuertes y débiles de los métodos. Así, el acuerdo perfecto (cuando toda la CVS es estimada correctamente) se encuentra entre el 26 y 64% para los métodos originales; los métodos muestran acuerdo aproximado (cuando al menos una capa de nubes es estimada correctamente) entre el 15 i el 41% de los casos. Se puede mejorar el acuerdo perfecto hasta el 67% (más un 25% de acuerdo aproximado), incluso usando perfiles de baja resolución. Uno de los métodos, una vez modificado convenientemente, puede ser aplicado a perfiles de baja resolución como los del WMO's Global Telecommunications System, o a productos de reanálisis de temperatura y humedad. Se resume también una aplicación a un estudio de modelización de la irradiancia infrarroja incidente en superficie en condiciones de cielo nublado.

1. Introduction

1.1. Clouds and their classification

According to the World Meteorological Organization (WMO, 1975) a cloud “is a hydrometeor consisting of minute particles of liquid water or ice, or of both, suspended in the free air and usually not touching the ground. A cloud may also include larger particles of liquid water or ice as well as non-aqueous liquid or solid particles such as those present in fumes, smoke or dust”. Today, there is an ongoing discussion in the scientific community if the term ‘cloud’ should also include those that are nearly invisible to the human eye, but are readily detectable in satellite thermal imagery (Rangno, 2003; Tapakis and Charalambides, 2012). In fact, Rangno (2003) specifies that water particles must be present in sufficient concentration to be visible to the naked eye to be considered as cloud. It is worth commenting that there are important efforts to differentiate between water droplets, ice crystals, and aerosol particles, which all produce a decrease in visibility but have different physical and radiative properties.

Clouds are tenuous and transitory; no single cloud exists for more than a few hours, and most small clouds in the lower atmosphere exist for only a few minutes. In precise terms, the demarcation between a cloud and clear air is hard to define: it is not clear how many cloud droplets or ice crystals per unit volume constitute a cloud, or when cloud droplets are large enough to be considered raindrops, or when ice particles and snow constitute precipitation. There is no unanimity between scientists because the distinction between cloud particles and precipitation particles, for example, is not black and white, rather they represent a continuum of sizes. For some scientists, a droplet of 50 μm diameter represents a ‘drizzle’ drop because it must have formed from collisions and coalescence with other droplets, whereas for others it may be termed a ‘cloud’ droplet because it falls too slowly. Also, the farther an observer is from falling precipitation, the more it appears to be a cloud due to perspective. For example, many of the higher clouds above us, such as *cirrus* and *altostratus*, are composed mainly of ice crystals and snowflakes that are settling toward the Earth, and would not be considered a cloud by an observer inside them, but rather a light snowfall (Rangno, 2003).

Clouds form when the water vapor in the air reaches saturation and condenses into droplets or crystals. This can be produced either by a decrease in the air temperature (this is the most frequent case) or by an increase in the water vapor content (by addition or mixing). Often the cooling process results from the ascent of an air parcel and its corresponding expansion, a

process that can be considered adiabatic (or pseudoadiabatic, given the latent heat released when saturation has been reached). The major mechanisms responsible for the formation and development of clouds are summarized next (Ahrens, 2009; Cuadrat and Pita, 2009; Di Franco, 1984; Moran and Morgan, 1995):

1. Free convection: the development of a thermal, a rising bubble of air that carries heat energy (taken from surface heating) upwards by convection. With the ascent, the expansion cools the air down, which often reaches saturation. This process usually produces cumuliform clouds.
2. Uplift upon topography: the so-called orographic clouds are formed when the wind blows over hills or mountains and the air is forced to rise up producing a subsequent cooling.
3. Widespread ascent due to convergence of surface air (sometimes associated to atmospheric depressions) and uplift along weather fronts: linked to cold fronts (*cumulonimbus*) or with the passing of a warm front: *cirrus*, *cirrostratus*, *altostratus*, *cumulus*, *nimbostratus*, and *stratus*.
4. Other cloud formation processes include non-adiabatic cooling and/or water addition and mixing:
 - a. Advection: Progressive cooling of warm and wet air above cool regions (usually forming stratiform clouds). For example, advection fog: cooling of surface air up to its saturation point may be accomplished when warm moist air moves over a cold surface. The surface must be sufficiently cooler than the air above thus allowing a significant transfer of heat from air to surface.
 - b. Radiative cooling: At night the air near the surface may cool through emission of infrared radiation up to the saturation point and resulting in fog.
 - c. Rain and snow falling from high clouds may cool down (through evaporation) the air under them, producing stratiform clouds.
 - d. Evaporation (mixing) fog: water vapor is added to the air through evaporation from a water (or wet) surface. Then, the moist air may eventually mix with relatively dry air and produce fog.
 - e. Anthropogenic clouds (anthropoclouds): clouds formed due to human activities that inject water vapor, aerosols and hot air into the atmosphere, which under certain conditions may enhance cloud formation (e.g. contrails) (Mazón et al., 2012).

Actually, the condensation process that produces clouds is not quite so simple. There must be airborne particles (aerosol) onto which water vapor can condense to produce cloud droplets (heterogeneous nucleation). In other words, homogeneous (pure water) condensation is almost impossible in the atmosphere: relative humidity of several hundred percent would be required before condensation could begin in a homogeneous nucleation. Some concentration of particles, specifically those called condensation nuclei are indispensable for cloud formation. A condensation nuclei is a minute (diameter $< 10 \mu\text{m}$) and hygroscopic particle, such as those contained in dust, volcano ashes, factory smoke, forest fire smoke, ocean spray (i.e. salt particles), or even sulfate particles emitted by phytoplankton in the oceans (Ahrens, 2009; Di Franco, 1984; Moran and Morgan, 1995). The condensation nuclei most favorable for producing clouds have radii of $0.1 \mu\text{m}$ or more. Usually, between 100 and 1000 nuclei close to this size exist in a cubic centimeter of air. Their number decreases in clear “country” air and over the oceans, where concentrations may dwindle to only a few nuclei per cubic centimeter. Over industrial cities condensation nuclei are most abundant, therefore highly polluted air may contain nearly 1 million particles per cubic centimeter (Ahrens, 2009). Condensation nuclei are extremely light (many have a mass less than one-trillionth of a gram), so they can remain suspended in the air for many days. Note in Table 1, that their terminal velocity is very small (of the order of $\mu\text{m/s}$) in comparison to cloud droplets (cm/s) and to typical raindrops (m/s). The terminal velocity is the final, constant speed at which drops and particles would fall within the atmosphere if air was quiet. It is the velocity at which the upward pull of air drag and downward pull of gravity are in equilibrium so that a falling object is no longer accelerating. Because weight is dependent on mass (and consequently on the particle volume) and air resistance is proportional to the cross-sectional area of an object, terminal velocity is dependent on the particle’s mass and size: larger particles fall faster than small particles. In Table 1 condensation nuclei and cloud droplets are classified according to their characteristic size, concentration, and terminal velocity.

Water condensation is a continuous process that begins on hygroscopic nuclei, sometimes at relative humidity as low as 75%. As the relative humidity increases and gradually approaches 100% the droplets grow larger, and condensation begins on the less-active nuclei. So a large fraction of the available nuclei have water condensing on them, until eventually the droplets’ suspension become visible to the naked eye. Therefore, cloud formation does not necessarily need relative humidity reaches 100%. Despite this, for certain conditions (in particular, if there are not enough nuclei), air may contain more vapor than the vapor necessary to become saturated; this is called ‘supersaturated air’. Of course, this whole process depends totally on the temperature, because the saturation (specifically, the equilibrium vapor pressure or saturation

vapor pressure) depends strongly on temperature according to the Clausius-Clapeyron equation (Ahrens, 2009).

Table 1. Characteristic size, concentration, and terminal velocity of particles involved in condensation and precipitation processes, including condensation nuclei and cloud droplets (adapted from Ahrens, 2009; Shuttleworth, 2012; Stull, 1995; Wallace and Hobbs, 1977).

Type of particle	Approximate radius (μm)	Number of particles (per cm^3)		Terminal velocity (m/s)
		Range	Typical	
Small (Aitken) condensation nuclei	<0.2	1000 to 10,000	1000	10^{-7} to 10^{-6}
Large condensation nuclei	0.2 to 1.0	1 to 1000	100	10^{-6} to 10^{-4}
Giant condensation nuclei	>1.0	<1 to 10	1	1.2×10^{-4} to 4.8×10^{-4}
Fog and cloud droplets	>2.0	10 to 1000	300	0.01 (for a typical cloud droplet of 10 μm radii)
Typical raindrop	1000	-	10^{-3}	6.5 to 7

In conclusion, without aerosol particles cloud formation in the atmosphere would not occur at the temperatures and relative humidities at which clouds are observed to exist. Pure water droplets can form from the vapor phase only at very high supersaturations, that is, at partial pressures well above the equilibrium vapor pressure for water at a given temperature. The presence of aerosol in the atmosphere provides nuclei onto which water vapor can condensate in a liquid or ice phase at much lower partial pressures, initiating droplet formation and eventually causing the nuclei to grow into sizes recognized as cloud particles. At the same time, incorporation into cloud water and precipitation is the main mechanism by which small particles

are removed from the atmosphere (this process is called wet deposition). Thus, to some extent aerosol particles can affect their own atmospheric removal rates, by influencing the conditions for cloud formation and the properties of the clouds into which they become incorporated (Kreidenweis, 2003). A schematic representation of the multiphase cloud-particle-trace gas system in the atmosphere can be seen in Figure 1 of the article by Collett and Herckes (2003), including the following processes: dry and wet deposition, particle and gas scavenging by cloud drops, chemical reaction, and precipitation formation in a mixed-phase (ice-liquid water) cloud.

Human interest in clouds is not new. In fact, looking back over the past, it began with the study of the alternation of the seasons to perform some sort of weather forecast. This practice is as old as hunting, fishing and gathering berries. Knowledge of climatic regularities is vital, literally, because it allows the weather to be anticipated and forecast; for instance short term local forecasts can be obtained through cloud observation. The presence of a particular cloud in a determined place in the sky explains where the water is condensing, while, the cloud dimension and height indicates which processes are driving the formation of the cloud (Di Franco, 1984). In this sense, even in very early times, weather forecasting, meteorology and climatology were practiced; albeit in an informal and fairly scientific way.

The ancient Greeks laid down important foundations for today's modern physics, and meteorology was close to the heart of their science. The effects of climate on human beings were of interest for philosophers such as Aristotle (384 - 322 B.C.), and historians such as Thucydides (ca. 460 - ca. 395 B.C.) and Herodotus (ca. 484 - ca. 425 B.C.) (Ogilvie, 2010). Aristotle wrote *Meteorologica* (meaning 'a study of things that fall from the sky') in about 340 B.C., which was the first-ever comprehensive book on meteorology. This volume would define the subject itself and would be the source of inspiration that led to development of meteorological thinking (Roulstone and Norbury, 2013). Climatologists consider this treatise as distant roots of scientific research, but interestingly, Aristotle addressed the issue as a philosopher as for him, it was important to overcome the contradictions into which pre-Socratic conceptions had fallen (Acot, 2005). Another great scholar of this ancient Greek tradition was Archimedes of Syracuse who discovered fundamental laws of physics, together with some ground-breaking mathematics. In contrast to Aristotle, his contributions should certainly be classified under the heading of "exact science". He discovered the basic principles of hydrostatics, the principle of buoyancy, a principle we see in action every time clouds form and remain above us, and provided the first clues to answering some basic questions about the way air circulates around the Earth (Roulstone and Norbury, 2013). See Acot (2005) for an extensive history of climate science.

Throughout the centuries, there have been many attempts to objectify atmospheric processes by means of measurements and to discover hidden regularities including laws which would eventually drive climate science. Grand Duke Fernando II de Medici (1610-1670) created a network of observers in 1653 equipped with standardized instruments and an academy ('Academia del Cimento', founded in 1657) to centralize the data collected. This was certainly the first academy of sciences of history. The standardization of instruments was a very important stage, as only when thermometers, barometers, anemometers, hygrometers, and rain gauges were both reliable and relatively accurate would the material conditions be established for the scientific study of weather and climate. The study of climate (or climates) was also possible, or at least enriched, when other precision instruments (especially timers) allowed long safe voyages during the eighteenth century. Thanks to precise timers, which allow geographical longitude to be measured accurately, was it possible to trace secure bearings. While at that same period of time how to calculate latitude, by measuring the height of the sun at noon was albeit already well-known, precision was an issue, because an error of only one degree corresponds to an error in the order of 100 km. Therefore, along with mapping improvements and more importantly, the first reliable chronometer (built in 1761 by Englishman John Harrison (1693-1776)), physicists who were engaged in climatology were able to discover, observe and quantify more easily than ever before the different climates of the globe which in turn opened the way to a "planetary" or "global" vision of the weather and climate. In fact, the history of technology has a lot to do with the general history of science, especially in the progress of weather science (Acot, 2005).

The interest in historical climate reconstruction did not begin until the eighteenth and nineteenth centuries, with the use of diverse documentary evidence as an aid, and the founding of climatology as a science came about in the early twentieth century. In the 1970s and 1980s, the involvement of historians, as well as meteorologists, in the reconstruction of past climates based on documentary evidence, ushered in a new era for the discipline of historical climatology. In due course, the development of sophisticated methods of data calibration and statistical techniques led to the reconstruction of climate indices for many countries and regions, that were based on many different types of historical data such as medieval annals and chronicles, a variety of secular and ecclesiastical records, weather diaries, personal and official correspondence, early newspapers, a variety of recorded phenological data (e.g. the dates of flowering of plants and crop yields), and ships' log books. However, little information about clouds was recorded (Ogilvie, 2010). The problem with the historical documentary information is that it tends to emphasize extreme conditions since these were generally the most important phenomena that deserved recording. Information from different observers may be further

biased as the qualitative standards used to reflect weather conditions are likely to be observer-dependent (Jones, 2008). An extensive review of the subject which emphasizes studies from Europe is provided by Brazdil et al. (2005). Historical climatology has made a great deal of progress since 1990, due to an important extension of its research possibilities.

However, most climate studies focus on temperatures and precipitation, the most noticeable example being the widely used Köppen climate classification index (established in 1884) (see the translated and edited version of the original paper in Volken and Brönnimann, 2011) which is based on the concept that native vegetation is the best expression of climate and combines average annual and monthly temperatures and precipitation, and the seasonality of precipitation (Peel et al., 2007). Other example are climographs, which represent the yearly evolution of temperature along with precipitation (usually on a scale 1:2 or 1:3), and allow the type of climate in the region to be easily distinguished and whether or not it has hydric deficit or excess in some particular months or seasons. But there are other important meteorological variables such as wind, humidity, pressure, insolation or cloudiness, which have scarcely been treated because they are more difficult to quantify and have a secondary impact on landscape, ecosystems, and economies. There is a lack of climatic studies into cloudiness and so this dissertation addresses this by making a contribution towards filling this gap, by studying the behavior and characteristics of clouds in some specific climates, and by using objective methods to characterize the cloud field from a macroscopic point of view.

Cloud climatologies are used to determine the radiative effects of clouds on climate and to determine the extent to which interannual and multidecadal changes in the Earth's radiation budget can be attributed to changes in clouds. Cloud climatologies are also important in assessing the prediction of clouds by climate models, in studying the significance of chemical reactions in clouds, in quantifying climatic feedbacks involving clouds, in estimating the radiative forcing by anthropogenic aerosols, in selecting sites for astronomical observatories and atmospheric field experiments, and in assessing the potential for solar energy development. As far as climate is concerned, the most important properties of clouds are those that affect radiation and precipitation, namely, cloud height, thickness, horizontal extent and horizontal variability, water content, phase (liquid or ice), and droplet and crystal sizes. Many of these properties define what is known as 'cloud type' so we can say that it is important to distinguish the different cloud types. The climatic effects of clouds further depend on the geographical location, the albedo and temperature of the underlying surface, as well as the season of the year and time of day. Locally, the effect of clouds on the Earth's radiation budget is generally negative

in the daytime but positive at night (that is, clouds cool the surface in the day but warm the surface at night), so an accurate determination of the diurnal cycle of each cloud type is an important component of any cloud climatology (Warren and Hahn, 2003). On a global scale, the net mean cloud radiative effect is of approximately -20 Wm^{-2} due to the strong shortwave negative effect (by enhancing planetary albedo) that is only partly compensated by the longwave positive (i.e. greenhouse) effect (Boucher et al., 2013).

The interest of scientists in classifying clouds also started in the past two centuries. The process of objectively classifying the many shapes and sizes of something as ephemeral as a cloud was first attempted at the beginning of the nineteenth century by Jean Baptiste Lamarck, a French naturalist who suggested a classification in 1802. The suggested descriptions tried to resemble much of what people see when watching clouds. In 1803, an English chemist, Luke Howard, proposed Latin terminology for Lamarck's classification (note that Latin descriptors were already used by scientists in other fields). For this reason and because he published his results in a relatively widely disseminated journal, *Tilloch's Philosophical Magazine*, Howard's system became accepted and was reproduced in books and encyclopedias during the ensuing years (Rangno, 2003; WMO, 1975). Thus, Lamarck's classification and Howard's terminology are the basis for the cloud classification still universally accepted today.

Later, the use of theodolites and photogrammetry in Uppsala (Sweden), as well as at sites in Germany and in the US in the 1880s, gave the first measurements of cloud heights, which eventually led to the concept of low, middle, and high cloud groupings into which Howard's cloud types were more systematically placed by H. Hidebrandsson and R. Abercromby in their 1887 classification. Hidebrandsson was the Director of the Uppsala Observatory and the first to use photography in the study and classification of cloud forms. In response to the enthusiasm that the question of clouds and their types generated among naturalists in the nineteenth century R. Abercromby, a member of the British Royal Meteorological Society, made two voyages around the world to make sure that no cloud type had been overlooked. Also by then *cumulus* and *cumulonimbus* clouds had become a fourth distinct category representing 'convective' clouds, those with appreciable upcurrents. Howard's modified classification system was reexamined at the International Meteorological Conference held in Munich in 1891 and was expressly recommended for consideration and publication with illustrations in atlas form. The first edition of a color cloud atlas was printed in 1896. This atlas was reprinted in 1910 and over the following decades, without any substantial amendments (Di Franco, 1984; Rangno, 2003; WMO, 1975).

In the 1920s, observations were standardized between the different nations, so while the pertinent international committees added several minor modifications to the cloud classification system, they were only modifications that were deemed necessary to dissipate misunderstandings and further the uniformity of observations. As a result, the *International Atlas of Clouds and Study of the Sky, Volume I, General Atlas* was published in 1932 by the International Commission for the Study of Clouds, created in 1921. The contribution of a Catalonian Maecenas, Rafael Patxot, is remarkable as it was he who made the printing of 1000 free copies of the complete Atlas possible (hence the 1932 Atlas edition is available in Catalan as well as English and French). A modified edition of the same work appeared in 1939, under the title *International Atlas of Clouds and of Types of Skies, Volume I, General Atlas*. At this point, the definitions of cloud types had nearly reached their modern forms. This Atlas, which is the most comprehensive version of the classification system, was revisited by the WMO in 1956, and again in 1975. Later, in 1987, an updated version of *Volume II* was published, with the introduction of photographs from more disparate locations than in the previous versions (Di Franco, 1984; Rangno, 2003; WMO, 1975).

In conclusion, the modern classification scheme is based ultimately on Howard's system. Howard observed, as had Lamarck, that there were three basic cloud types: cirrus (fibrous and wispy clouds), stratus (sheet-like laminar clouds that covered much or all of the sky) and cumulus (clouds that were less pervasive but had a strong vertical architecture). Howard used an additional Latin term, nimbus, to refer to a cloud or system of clouds from which precipitation falls (nowadays, nimbus is used as a suffix or prefix and not as a cloud type itself) (Rangno, 2003). In fact, the four basic Latin cloud form names have a very intuitive meaning (Table 2), and clouds can be described by combining the basic types (Ahrens, 2009). The International Cloud Atlas remarks that the appearance of a cloud depends, on besides the nature, sizes, number and distribution in space of its constituent particles, on the intensity and color of the light received by the cloud and on the relative positions of the observer and source of light with respect to the cloud. The Atlas gives some guidelines to be considered in terms of the dimensions, shape, structure, texture, luminance and color for each of the cloud forms (for more information see WMO, 1975, 1987). Similarly, some attributes that may be important when identifying clouds are given by Rangno (2003), as well as a series of questions that could help in the categorization of clouds and in automatizing the surface observation in the so-called 'SYNOP' coding (surface synoptic observations): "Is sky covered by clouds?", "Is the Sun's disk obscured?", "Is the Sun's position visible? and if so, is it sharply defined or diffuse?", "Is there any particular cloud pattern: small cloud elements, rows, billows, undulations?", "Is it raining or snowing?", and if so, "Is the

rain or snow falling from it concentrated in a narrow shaft, suggesting heaped cloud tops above”, or “Is the precipitation widespread with little gradation, a characteristic that suggests uniform cloud tops?”.

Table 2. Latin basic cloud form names and their meaning.

Latin denomination	Meaning
<i>stratus</i>	layer / flat
<i>cumulus</i>	heap / heaped up
<i>cirrus</i>	curl of hair
<i>nimbus</i>	violent rain

As already mentioned, clouds are continuously changing therefore and appear in an infinite variety of forms. It is possible, however, to define a limited number of (1) genera, that is the main characteristic form of a cloud, by combining the four principal denominations and then to add further details in a hierarchical manner: (2) species, that depend on the peculiarities in shape and differences in the internal structure of a cloud, (3) varieties, that define the special characteristics of the arrangement and transparency of a cloud, (4) supplementary features and accessory clouds, where minor cloud forms are attached to the main part of the cloud, and (5) mother cloud, that defines the origin of a cloud, in the cases where the cloud was formed from another cloud (Ahrens, 2009). Moreover, the International Cloud Atlas also presents another group of clouds, rarely or only occasionally observed. Some of these so-called ‘special clouds’ consist, for the greater part or in their entirety, of non-aqueous liquid or solid particles. The definition of a cloud given previously is therefore not applicable to all special clouds. Special clouds include: noctilucent clouds, anthropogenic clouds (e.g. condensation trails, clouds resulting from industry and clouds resulting from explosions), clouds from waterfalls, clouds from fires (e.g. *pyrocumulus*), and clouds from volcanic eruptions (Mazón et al., 2012; WMO, 1975).

In addition to the standardized genus-species system, the WMO also classifies clouds by the altitude of their bases (the cloud base height, CBH) and divides the troposphere vertically into three levels (or *étages*): high, middle and low. It must be taken into account that the atmospheric *étages* overlap and their limits vary with latitude (Table 3) (WMO, 1975). Hence, the boundaries between *étages* should be considered somewhat flexible. Note that, what is classified as an *altocumulus* layer when seen from sea level could be termed a *stratocumulus* layer when seen by an observer at the top of a high mountain (Rangno, 2003). In this sense, there are specific instructions in the International Cloud Atlas (WMO, 1975) for the observation of clouds from mountain stations.

The ten cloud genera (that are mutually exclusive), and in relation to the corresponding *étages* are presented next (see also Figure 1):

- *Cirrus* (Ci), *Cirrocumulus* (Cc) and *Cirrostratus* (Cs) for the high *étage* (high level clouds)
- *Altostratus* (As) for the middle *étage* (middle level clouds)
- *Stratus* (St), *Stratocumulus* (Sc) for the low *étage* (low level clouds)
- *Altostratus* (As) is usually found in the middle *étage*, but it sometimes extends to higher levels
- *Nimbostratus* (Ns) is almost invariably found in the middle *étage* but it sometimes extends into the other *étages*
- *Cumulus* (Cu) and *Cumulunimbus* (Cb) usually have their bases in the low *étage*, but their vertical extent is often so great that their tops may reach into the middle and even high *étages* (known as ‘convective’ clouds)

Table 3. The three atmospheric *étages* according to the World Meteorological Organization (1975).

Étages	Polar Regions	Temperate Regions	Tropical Regions
High	3-8 km	5-13 km	6-18 km
Middle	2-4 km	2-7 km	2-8 km
Low	From the Earth’s surface to 2 km		



Figure 1. Visual representation of the ten main cloud types (with the deliberately permission of reproduction by the Cloud Appreciation Society, www.cloudappreciationsociety.org)

An alternative classification of clouds takes into account their phase composition. Water clouds are composed entirely of water droplets (ordinary and/or supercooled), while ice-crystal clouds are composed entirely of ice crystals, and mixed clouds contain a combination of both water phases. The phase composition of clouds depends, obviously, on ambient temperature, which depends on height level, season, and latitude. Within the high cloud family, *cirrostratus* and *cirrus* are always ice-crystal clouds, while *cirrocumulus* may be mixed. These clouds are typically thin and white in appearance, but can appear in a magnificent array of colors when the sun is low on the horizon. Mid-level clouds are composed primarily of water droplets; however, they can also be composed of ice crystals when temperatures are low enough. Low-level clouds are usually composed of water droplets and occasionally they are mixed. Cumulonimbus are always mixed-phase clouds, since they extend through almost the whole troposphere (Ahrens, 2009; Tapakis and Charalambides, 2012; WMO, 1975).

Cloud surface observations are coded into weather reports using the 'synoptic code' of the WMO, which is used worldwide. The synoptic code was defined in 1929 but was changed in 1949; the reporting procedures were adopted worldwide in the early 1950s. The information

about clouds in the synoptic weather reports consists of total cloud cover, low or middle cloud amount, low cloud type, middle cloud type, high cloud type, present weather, and base height of the lowest cloud. About 6500 land stations routinely report cloud observations in the synoptic code. Usually they report every three hours beginning at 0000 UTC, but about one-quarter of them report only every six hours. About 20% of the stations do not make observations at night. The average spacing of land stations is about 180 km, but this is far from uniform. Europe has more stations than are strictly needed for cloud climatology, whereas the Antarctica has too few. Some parts of the Sahara Desert and Western Australia are also inadequately sampled. Besides land stations, weather (and cloud) observations are also performed from ships crossing the oceans. Most ships make weather observations four times per day; the observations are recorded in logbooks and also transmitted by radio to world meteorological centers. In a recent typical year, daily reports from an average of 1150 ships are received at 0000, 0600, 1200, 1800 UT and from 160 ships at 0300, 0900, 1500, 2100 UT as well. The average spacing of ships that report clouds is 600 km, much greater than for weather stations on land, but since the ships are moving they sample most parts of the ocean. However, for many parts of the ocean the accuracy of computed mean cloud amounts is limited by the scarcity of observations. This is not the case on land, where the random error due to inadequate temporal sampling is very small (Warren and Hahn, 2003). This dataset, called the Extended Edited Cloud Report Archive (EECRA) dataset has put together synoptic observations for all oceans since 1952 and for all continents since 1971: it contains about 81 million cloud observations from ships and 380 million from land stations (information updated in 2012, available at: <http://cdiac.ornl.gov/epubs/ndp/ndp026c/ndp026c.html>). In an extensive analysis of this data, EECRA land reports were averaged at each of the 5388 chosen stations over monthly and seasonal time spans for each year from 1971 through 2009 (Eastman and Warren, 2013).

Besides human observations from the ground, nowadays there are other techniques for cloud observation, such as surface instruments: lidar, radar and sky cameras, and satellite measurements. Clouds can also be detected by in situ atmospheric profiles obtained from radiosoundings or aircraft. In section 3, extended information is given about all of these techniques. However, preceding this, in the following section, the importance of clouds from a scientific point of view, will be examined, in particular for the understanding and modeling of atmospheric dynamics and the Earth's climate.

1.2. Current interest in clouds

Clouds are an important component of the Earth's climate system. At any given time clouds cover between 60% and 70% of the globe and they exert various influences on the Earth-atmosphere system, of which the most important are detailed next (Jakob and Miller, 2003; Warren and Hahn, 2003):

- In radiative processes: clouds reflect solar radiation back to space and absorb thermal infrared radiation (IR) emitted from below. Each of the shortwave and longwave components of cloud forcing is about ten times as large as those for a carbon dioxide doubling. However, they are in a delicately balanced state and the warming effect of the longwave cloud forcing is nearly canceled by a correspondingly large cooling shortwave cloud forcing, and the finally observed net cloud forcing is only about four times as large as the expected value of radiative forcing from a carbon dioxide doubling (Fu, 2003; Houghton, 1997; Ramanathan et al., 1989; Salazar and Poveda, 2009).
- In the hydrological cycle: clouds produce rain and snow (see extended review of the hydrological cycle amplification of external radiative forcings: Stevens and Bony, 2013);
- In the release and consumption of latent heat related to phase changes of water either directly inside the clouds or in precipitation generated in them (Jakob and Miller, 2003);
- In the transport of heat, moisture, momentum and atmospheric trace constituents over large distances in the vertical in convectively generated clouds (Jakob and Miller, 2003).

Regarding the radiative processes, the global mean energy budget of the Earth (2000-2010) is presented in Figure 2 (Stephens et al., 2012). The surface radiative fluxes summarized in the figure are an average of five different estimates that use mixtures of global satellite data, surface measurements and atmospheric-state information from global weather analysis products. The quantities correspond to flux densities, expressed in Wm^{-2} , and contain error estimates. The observed energy flux incoming at the top of the atmosphere (TOA) is 340.2 ± 0.1 (shortwave, SW), and the flux outgoing at TOA is 100.0 ± 2 (SW) plus 239.7 ± 3.3 (longwave, LW), so according to this recent data, there is an imbalance of 0.6 ± 0.4 . On the surface a balance is established among these fluxes: 188 ± 6 (SW downward), 23 ± 3 (SW upward), 24 ± 7 (sensible heat flux upward), 88 ± 10 (latent heat flux upward), 398 ± 5 (LW upward), and 345.6 ± 9 (LW downward), which produces an insignificant imbalance of 0.6 Wm^{-2} given the error estimate of 17 Wm^{-2} . The cloud effect on the SW (albedo effect) is $47.5 \pm 3 \text{ W/m}^{-2}$, whereas clouds reduce the outgoing longwave flux relative to clear skies by approximately $26.7 \pm 5 \text{ W/m}^{-2}$ (a measure of their greenhouse effect). This gives a net loss of radiation of $21 \pm 6 \text{ W/m}^{-2}$ from the Earth by clouds, mostly by

reflection of sunlight from clouds in the mid-latitude summer hemisphere. In fact, low, highly reflective clouds tend to cool the surface, whereas high, semitransparent clouds tend to warm it because they let much of the shortwave radiation through but are opaque to the longwave radiation (Houghton, 1997); as previously stated, the overall combined effect according to (Stephens et al., 2012) is cooling.

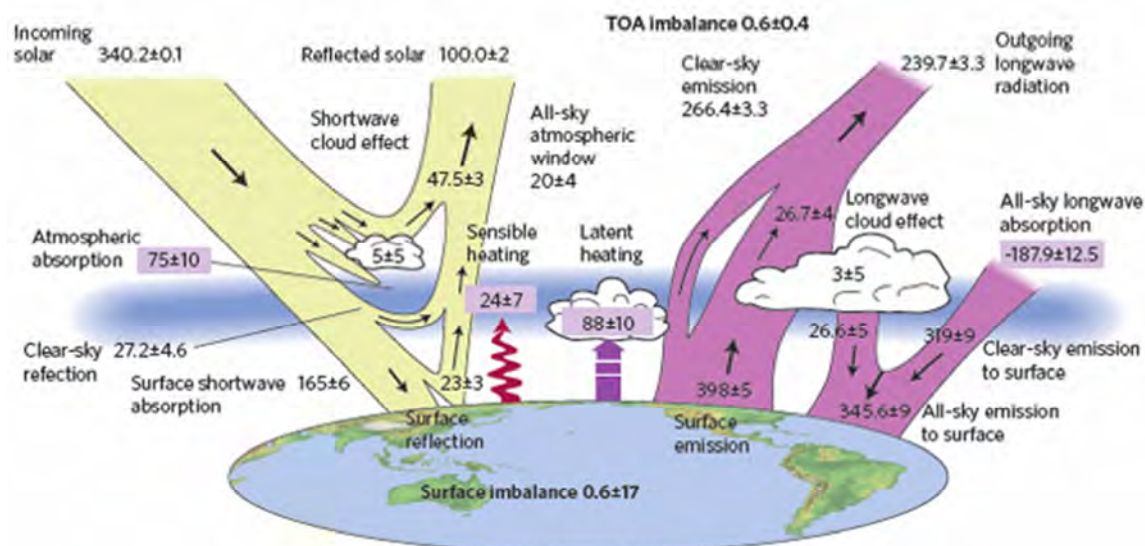


Figure 2. The global annual mean energy budget of Earth for the approximate period 2000-2010. All fluxes are in Wm^{-2} . Solar fluxes are in yellow and infrared fluxes in pink. The four flux quantities in purple-shaded boxes represent the principal components of the atmospheric energy balance (Stephens et al., 2012).

So, clouds are a key factor among the components that drive the climate and play a significant role in the climate feedback mechanisms. But even the direct impact of cloudiness on the Earth is not yet well understood by the scientific community. In particular, further research is needed into the effects of the cloud vertical structure (CVS) in the atmospheric circulation and the complex role of cloudiness and specifically of the CVS in the Earth's radiative budget. The description of the cloud vertical structure, or at least of cloud type, is very important because, as previously mentioned, the overall impact of clouds on the Earth's energy budget involves two opposing effects depending on cloud height (Naud et al., 2003) and also on the particular radiation band (shortwave or longwave). In addition, the CVS affects the atmospheric circulation directly by modifying the radiative cooling profile and the atmospheric stability. The effects of CVS on atmospheric circulation have been described through the use of atmospheric models by

many authors such as Wang and Rossow (1998). On the other hand, a single cloud has a different effect on solar irradiance compared to multiple clouds or overcast skies, since the reduction of the irradiance depends on whether the cloud obscures the sun or not and on cloud coverage. Moreover, Crewell et al. (2004) underlined the importance of clouds in multiple scattering and absorption sunlight processes which, at the same time, have a significant impact on the atmospheric diabatic heating. Given the complexity of all these phenomena, they are not yet fully understood and are subject to considerable uncertainties. The well-known difficulties in determining how clouds contribute to climate change, due to the complexity of the processes involved, and the uncertainties associated with the available data (linked to the vast amount of information needed, including spatial distribution) are addressed in several studies (Wielicki et al., 1995; Solomon et al., 2007; Heintzenberg and Charlson, 2009; Boucher et al., 2013).

Recently, studies based on observations and modeling have concluded that the greatest uncertainty in the top of the atmosphere fluxes comes from the cloud feedback (Dessler, 2013). Several cloud feedback mechanisms now appear consistently in global circulation models (GCMs), as summarized in Figure 3 (Boucher et al., 2013). In response to global warming, nearly all feedback acts in a positive direction as it results in a further temperature increase. First, high clouds are expected to rise in altitude and thereby exert a stronger greenhouse effect on warmer climates. This altitude feedback mechanism is well understood, has theoretical and observational support, occurs consistently in GCMs and cloud-resolving models (CRMs), and explains about half of the mean positive cloud feedback in GCMs. Second, middle and high-level cloud cover tends to decrease in warmer climates even within the tropics, although this feedback effect is ambiguous and as yet cannot be tested observationally. Third, observations and most models suggest that storm tracks shift poleward in a warmer climate, drying the subtropics and moistening the high latitudes, which causes further positive feedback via a net shift of cloud cover to latitudes that receive less sunshine. Finally, most GCMs also predict that low cloud amount decreases, especially in the subtropics, another source of positive feedback though one that differs significantly among models and lacks a well-accepted theoretical basis. Over middle and high latitudes, GCMs suggest that warming-induced transitions from ice to water clouds may cause clouds to become more opaque, but this appears to have a little systematic net radiative effect in models, possibly because it is offset by cloud altitude changes (Boucher et al., 2013).

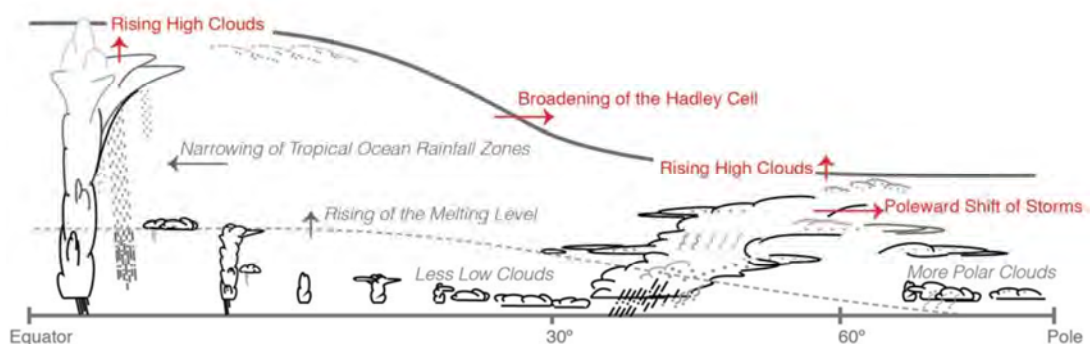


Figure 3. Robust cloud responses to greenhouse warming (those simulated by most models and possessing some kind of independent support or understanding). The tropopause and melting level are shown by the thick solid and thin grey dashed lines, respectively. Changes anticipated in a warmer climate are shown by arrows, with red color indicating those making a robust positive feedback contribution and grey indicating those where the feedback contribution is small and/or highly uncertain. No robust mechanisms contribute as negative feedback (Boucher et al., 2013).

Observational evidence, mostly obtained from the surface (worldwide networks of pyranometers) and also verified by satellite observations and proxy data, suggests that substantial changes in surface solar radiation (SSR; also known as global radiation) occur over time and may profoundly affect the environment. Early studies carried out in the 1990s pointed to a remarkable decline of SSR at selected observation stations between the 1950s and the 1980s. This decline is now confirmed by extensive literature in many places around the globe. This phenomenon is popularly described as ‘global dimming’ (Figure 4a); although ‘global’ originally referred to ‘global radiation’, a synonym for SSR, rather than to a global scale dimension of the phenomenon. More recent studies using SSR records, updated to the year 2000 and later have found, however, a trend reversal and partial recovery at many of the sites since the 1980s. The term ‘brightening’ was thereby coined to emphasize that the decline in SSR no longer continued after the 1980s (Figure 4b). On the other hand, the longest observational records, which go back to the 1920s and 1930s at a few sites in Europe, further indicate some brightening tendencies during the first half of the twentieth century, known as ‘early brightening’. Finally, the latest updates on developments beyond the year 2000 show mixed tendencies (Wild, 2009, 2012). The brightening is somewhat less coherent than the preceding dimming, with trend reversals found at widespread locations, although some regions are still with continued decrease (e.g. India). Note that observed brightening has not fully compensated the prior dimming, so that insolation levels at the turn of the millennium were still below those in the 1950s. (Wild, 2009, 2012). The causes of dimming and brightening cannot be explained by

changes in the luminosity of the sun, but rather must have their origins in alterations in the transparency of the atmosphere, which depends on the presence of clouds, aerosols, and radiatively active gases. Cloud cover changes effectively modulate SSR on an interannual basis, but their contribution to the detected longer-term (decadal) SSR trends is not always obvious. In addition, even if only SSR for cloudless days is analyzed, dimming and brightening trends are found. Currently, it has been suggested that dimming and brightening has a strong link with aerosol-cloud interactions. However, a number of issues related to dimming/brightening are not well established and still under debate, such as the quality and representativeness of the underlying observational data as well as the large-scale significance of the phenomenon (Wild, 2012).

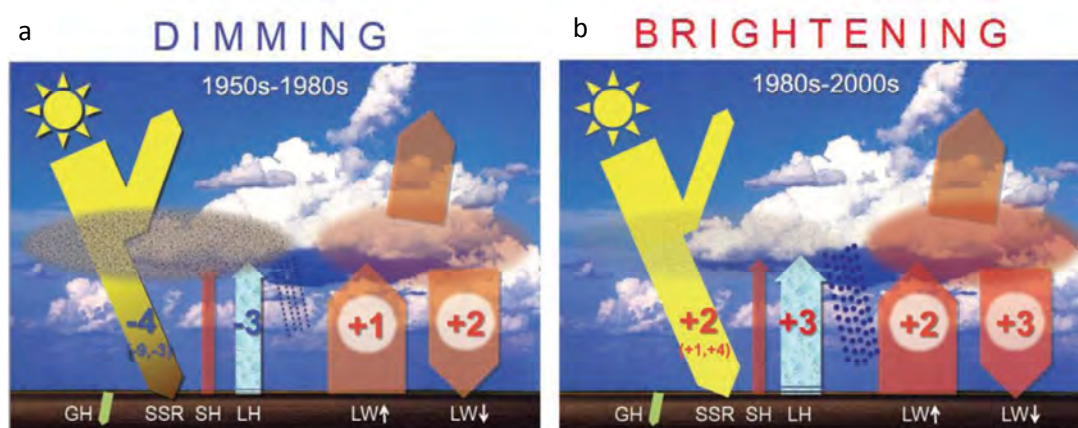


Figure 4. Schematic representation of dimming (a) and brightening (b) periods over land surfaces. Values denote best estimates of overall changes in surface energy fluxes over both periods in $W m^{-2}$ (ranges of literature estimates for SSR dimming/brightening in parentheses). Positive (negative) numbers, shown in red (blue), denote increasing (decreasing) magnitudes of the energy fluxes in the direction indicated by the arrows. Changes in ground heat flux (GH) and sensible heat flux (SH) are considered small compared to the above mentioned flux changes (figure from Wild, 2012).

Modeling, in other words the description of a system using mathematical concepts and language, constitutes a useful way to gain insight into the knowledge of phenomena. A model may help to explain a system, to study the effects of different components, and to make predictions about the system's behavior. An atmospheric model is constructed around the full

set of primitive dynamical equations which govern atmospheric motions. It can supplement these equations with parameterizations for moist processes (clouds and precipitation), among others, (turbulent diffusion, radiation, heat exchange, soil, vegetation, surface water, etc.). There are two kinds of atmospheric models: weather forecast models (used to predict microscale phenomena such as tornadoes, boundary layer eddies, synoptic flows, etc., besides the usual application for routine weather forecast) and climate models (capable of replicating climate regimes of past millennia and projecting the future of the Earth's climates) (Lynch, 2008). The mathematical equations for the physics and dynamics of the atmosphere are nonlinear and impossible to solve exactly; therefore, numerical methods obtain approximate solutions. Various numerical techniques can be applied to achieve this goal, but all of them ultimately involve splitting the area over which the model is applied into "boxes" or "cells" of finite size in both the horizontal and the vertical.

The equations that serve as the basis for most numerical weather and climate prediction models (e.g. the momentum equations for a spherical Earth, the thermodynamic energy equation, the continuity equation for total mass, or the ideal gas law) are introduced into models to produce (prognostize) variables such as temperature, precipitation, or wind, in each of the grid cells. Parameterization involves the representation of a process in terms of its known relationship with variables resolved on the model grid. Parameterizations (i.e. diagnostic equations) are used to treat clouds and radiation in weather and climate models, among other weather characteristics (Warner, 2011). Given the importance of the various influences that clouds (and therefore their composition, geometry and distribution) exert on the evolution of both the atmosphere and the surface, it is immediately obvious that those effects need to be included in the atmospheric models. To describe the main effects clouds have on the atmosphere as outlined above, at least the horizontal coverage of clouds, normally referred to as cloud fraction, and the vertical extent and distribution of the clouds (Jakob and Miller, 2003), already referred to as CVS, need to be resolved to be the applied parameterization. Then, the radiative effect of clouds is also parameterized by modifying the bulk emissivity depending on the cloud fraction and/or type. The assumed or computed vertical structure of cloud occurrence in general circulation models (GCMs) is one of the main reasons why the different models predict a wide range of future climates. For example, most GCMs underestimate the cloud cover while only a few overestimate it (Xi et al., 2010). Therefore, to improve the understanding of cloud-related processes and to increase the predictive capabilities of global circulation models, there is a need for better and more accurate observations of global cloud amounts and, in particular, of the

vertical distributions of clouds. At the same time, this would allow a better adjustment of the parameterizations. Overall, this thesis is a contribution towards addressing this need.

Large-scale models are usually initialized using METAR (METeorological Aerodrome Report) or SYNOP reports, which include the typical meteorological characteristic annotations. These reports contain observations from a variety of methods: regular radiosonde observations, near-surface weather stations, commercial aircraft or ship reports, Doppler radar/lidar and satellite data, etc. (Lynch, 2008; Warner, 2011). Radiosoundings are a primary source of information since they still are the only generally available, and somewhat spatially and temporally regular, sources of three-dimensional atmospheric data over land. Unfortunately, these profilers are many hundreds of kilometers apart, so a typical situation is one in which synoptic-scale processes may be represented reasonably, but those on the mesoscale are not. Even though there are currently many other sources of observational data from satellites, radars, commercial aircrafts, etc. the reliance on radiosondes explains why operational forecast models still use 0000 UTC and 1200 UTC as two of the times when forecasts are initiated daily (most operational models employ four cycles per day, initialized at 0000, 0600, 1200 and 1800 UTC) (Warner, 2011).

Willén et al. (2005) tested several large-scale models and found that they overestimate the occurrences of small cloud fractions and underestimate the occurrences of clear-sky and overcast. In fact, clouds occur more frequently in the models, but with smaller amounts when present. In addition, models tend to produce lower cloud base heights when compared with measurements by lidars. For example, van Lipzig et al. (2006) and Schroeder et al. (2006) comment on the BALTEX Bridge Campaigns (BBC) measurements and state that this data can be used to investigate whether 'state-of-the-art' atmospheric models are capable of adequately representing clouds. Moreover, Hogan et al. (2009) found that models tend to be least skillful at predicting the timing and placement of boundary-layer clouds and most skillful at predicting mid-level clouds. Probst et al. (2012) compared global and zonal cloud cover fraction for total cloudiness from the ISCCP D2 dataset to the same quantities produced by 21 climate models from the World Climate Research Programme's (WCRP's) Coupled Model Intercomparison Project phase 3 (CMIP3), and found that most models underestimate the yearly averaged values of cloudiness over all the analyzed areas. Similarly, an assessment of models based on ground based instruments is addressed by the Cloudnet Project. Specifically, the aim of this project is to provide a systematic evaluation of clouds in forecast models (Illingworth et al., 2007) by comparing it with the cloud fraction (among other secondary cloud characteristics) derived from

long-term radar, lidar and microwave radiometer. Recently, studies are being developed that analyze the cloudiness behavior in the Coupled Model Intercomparison Project Phase 5 (CMIP5) as compared with several references, including satellite data and reanalysis (Enriquez et al., 2013).

Therefore, there is consensus that continuous observation of cloudiness is essential to study climate change and variability. For instance, 'cloud properties' is regarded as an Essential Climate Variable (ECV) in the Global Climate Observing System (GCOS) (<http://gosc.org/ios/MATRICES/ECV/ECV-matrix.htm>). Working Group I's contribution to the Intergovernmental Panel on Climate Change (IPCC) fifth assessment report (Boucher et al., 2013) remarked that the quantification of clouds in models, among others, continues to be a challenge. Other authors such as Ramanathan et al. (1989) and Zelinka and Hartmann (2010) state that in order to describe the impact of clouds on climate cloud base and top heights (which are linked to cloud type) are important characteristics, besides the temporal and spatial distribution of cloudiness. Consequently, there is a general need for improvement of automatic cloud observation and continuous cloud description for climatological issues. Specifically, more quantitative information is needed about cloud characteristics, behavior, interaction, and processes in which clouds take part.

This dissertation treats the variables describing the clouds from a macroscopic geometrical point of view (CBH, CVS, Cloud fraction), which are prioritized over the microphysical characteristics such as liquid water path or the size distribution of drops.

1.3. Macroscopic detection, quantification and geometric characterization of clouds

As mentioned earlier, observations and measurements are fundamental to acquire insight into cloud processes and specifically to obtain the cloud cover, the CBH and the CVS. Several approaches are possible for investigating such characteristics, including ground based instrumentation and observation, satellite-based observation, and/or meteorological model simulation. For some of these methods, the problem of overlapping cloud layers that hide each other is noticeable. Surface observers can see most of the low clouds with or without higher clouds above them, while satellites can observe most of the high clouds with or without the lower clouds beneath them. These limitations have hindered the development of reliable quantitative information about cloud overlapping and, in general, about the vertical distributions of cloud fractions and cloud occurrence. Further discussion on the advantages and

limitations of satellite and surface observations of the cloudiness can be found in Warren and Hahn (2003).

In fact, the high temporal and spatial variability of clouds create difficulties for their quantitative observation. In general, surface weather observations provide total cloud cover and cloud amount by morphological type, so frequency distributions of occurrence and co-occurrence of different cloud types may be derived. It is usually accepted that cloud characteristics obtained from satellite and from the ground (either subjective or instrumental observations) are complementary to each other in order to acquire a comprehensive understanding of extension, height, and structure of clouds (Ebell et al., 2011).

Several instruments, devices and platforms devoted to cloud observation and quantitative measurements of cloud macroscopic characteristics are explained in section 3. The advantages and disadvantages of the different instrumentation are briefly presented in this subsection, as well as the limitations of the instruments used by researchers to develop different approaches for distinguishing and classifying clouds. More detail on the different equipment and methodologies used specifically to determine cloud cover, cloud base height (CBH) and cloud vertical structure (CVS) is given in section 3.

Usually the instruments that measure cloud characteristics from the ground have been divided into column (e.g. ceilometers) and hemispheric (e.g. radiometers and sky cameras). Radiometers such as pyranometers or pyrgeometers are very simple to operate, although in order to be used for cloud detection they require great accuracy and appropriate maintenance, especially in dusty areas. Long et al. (2006a) provide a cloud fraction estimation from the shortwave cloud effect by using the Long and Ackerman (2000) methodology for estimating the clear-sky total and diffuse solar radiation, based on high resolution measurements (1-5 minutes) of total and diffuse (or direct) solar radiation. By combining global and diffuse solar irradiance measurements, an estimation of cloud cover and even of cloud type can be provided (Calbó et al., 2001). In addition, from longwave radiation measurements it is possible to estimate the cloud base temperature, and then to evaluate the CBH (Durr and Philipona, 2004). On the other hand, cameras provide high resolution images, although their FOV (field of view) is limited by the lens used; even all-sky cameras provided with fish-eye lenses have limits to the visual range (i.e. to the viewing area) depending on visibility conditions. Furthermore, the resolution of all-sky cameras becomes poorer and towards the horizon perspective issues arise. As for column methods, lidars and ceilometers have a very limited FOV, partially compensated by the high time resolution and their precision. Lately, ceilometers have been becoming more popular and in a

recent assessment the number of ceilometers deployed worldwide rose to more than 1000 (Werner, 2012). Finally, radars have very high resolution and accuracy in detecting clouds, distinguishing them from sky, and especially in detecting microphysical characteristics, but they cannot be used independently for cloud classification (Illingworth et al., 2007; Tapakis and Charalambides, 2012). The integration of all the ground based equipment in one location provides the maximum cloud information available for a comprehensive description. Unfortunately, there are very few locations worldwide with this huge amount of information from different ground-based instruments. However, three ARM (Atmospheric Radiation Measurement program, <http://www.arm.gov/>) permanent sites do exist: in North Slope Alaska (USA), Southern Great Plains (USA), and Tropical Western Pacific (Papua New Guinea), plus the mobile facility; and nine sites from Cloudnet (www.cloud-net.org) in Cabauw (the Netherlands), Palaiseau (France), Chilbolton (United Kingdom), Mace Head (Ireland), Potenza (Italy), Sodankyla (Finland), Lindenberg, Juelich and Leipzig (Germany);.

Radiosondes (RS) may be considered a column ground-based in-situ method because the balloon is constantly moving upwards and the measurements are allocated to every height at the precise time when they were recorded. However, apart from their limited time/spatial distribution (hours/hundreds of km) radiosonde launches cannot be used for continuous, sequential measurements over a specific desired site since the ascent of the sonde is not totally vertical over the site, and the ascent rate is neither constant nor equal between different RS launches. Furthermore, the preparation of the release of the meteorological balloon usually has to be done manually, limiting the automation of the method. In spite of that, there are some automatic sounding systems available: e.g. Vaisala DigiCora Unmanned Sounding System AUTOSONDE, which, since 1998, has been able to launch 24 radiosondes by remote control, (see Vaisala webpage); or a recently installed system at the University of Barcelona by the Catalan Meteorological Service (SMC) with autonomy of 6 days (12 RS). Although radiosondes have the advantage of providing real-time, reliable measurements which are useful to derive cloud properties over multiple atmosphere layers, cost may limit the use of RS in continuous operation or in research campaigns. Conclusions extracted from this dissertation might be of importance because of the large amount of every day radiosounding launches around the world. There are between 700 (according to Oolman, 2013, personal communication) and 1500 sites (according to Xavier Soler, 2014, personal communication) where RS are launched every 12h. WMO (2007) mentions 960 sites around the world where RS are usually launched 2 to 4 times a day. However, deficits in spatial (i.e. lack of data of some parts of the world) and temporal (i.e. soundings are

usually launched twice a day) hinder the broad use of the obtained vertical profiles for climatic studies of cloud vertical structure (Nowak et al., 2008; Poore et al., 1995).

In general, the most important advantage of ground based equipment (e.g., radiometers, sky cameras, lidars, cloud radars and radiosondes) is that they provide on-site, real-time measurements continually and at very high temporal resolution. Most ground based instruments have a relatively low purchase cost, providing long term and low cost measurements. Additionally, weather reports of clouds (derived from visual observations with low resolution) have been available at official observing institutions for several decades and at no charge, so interdecadal variations and trends can be studied. The cost of the equipment is an important factor in cloud measurements, since the use of satellites is much more expensive than most ground instruments. Yet, some specialized ground meteorological observing systems such as RADARs may be as equally expensive as satellite-borne devices (Clothiaux et al., 1999, 2000; Tapakis and Charalambides, 2012; Warren and Hahn, 2003). The major disadvantage of ground equipment is its small viewing range area, limiting the ability of monitoring the formation of clouds and their movement over a large sky area. Nevertheless, since the state of the sky is measured on-site, they do provide sufficient accuracy for local cloudiness. On the other hand, satellites provide large-scale cloud information and measurements from different sensors that cover several bands (microwave –MW-, infrared –IR-, visible –VIS-) although the provided data is in low spatial (and sometimes temporal) resolution and may contain significant errors; small clouds are often overlooked due to the limited analysis and low or thin clouds are frequently not distinguished from land. Other clouds, such as those over snow or low clouds at night are difficult to detect from satellites because they provide little contrast in albedo or temperature with the underlying surface. To the contrary, surface observers are close to the clouds, so they can identify clouds by type, including clouds smaller than a satellite's pixel size, which is typically at least 1 km (Heinle et al., 2010; Tapakis and Charalambides, 2012; Warren and Hahn, 2003).

On the other hand, the major advantage of satellites is that they can view a large area, which enables them to provide large scale cloud information. Furthermore, the satellites' aerial view does not include the sun, overcoming one of the major disadvantages of ground-based cameras. Moreover, geostationary satellites have the ability to collect continuous data of the same region and develop a database of the landmark over time to be used for comparison with future views and cloud detection. There are enough geostationary satellites in the equatorial orbit to cover the entire globe, but the major disadvantage of these satellites results precisely from the orbit: this produces a non-perpendicular (i.e. tangential) vision of middle and high latitude regions. A

further problem can appear when merging images taken from different satellites because of their different calibration, resolution or any other peculiar characteristics that each satellite and its onboard sensors may have. Non-geostationary satellites are not constantly over the same area, so they cannot provide continuous measurements, while on the contrary, they can measure correctly over Polar latitudes. The satellite's second major disadvantage is their low spatial and temporal resolution, as mentioned above, compared to most ground based instruments, so their cloud detection capability is limited to large clouds. Spatial resolution refers to the satellite sensor's ability to effectively capture a portion of the Earth's surface in a single pixel and is typically expressed in terms of Ground Sample Distance (GSD). The resolution of weather satellite images varies depending on the instrument used and the altitude of the satellite's orbit. Currently, several geostationary and polar satellites devoted to atmospheric observations offer resolutions of about 1-5 km (<http://www.nrcan.gc.ca/earth-sciences/geomatics/satellite-imagery-air-photos/satellite-imagery-products/educational-resources/9387>). In the case of temporal resolution, non-geostationary satellites record one set of measurements per orbit, while geostationary satellites have highest temporal resolution (intervals between measurements are in the order of minutes) (Ahrens, 2009; Tapakis and Charalambides, 2012).

In summary, clouds can be macroscopically detected, quantified and characterized by human observation, which is the simplest and most immediate way and was the most widely-used method of the past. Later, along with the development in technology, lots of surface and remote sensing instruments have been developed and data obtained with some of these reliable instruments are studied in this dissertation. Specifically, the horizontal cloud cover is found through visual human observation, sky-camera, ceilometer, and satellite images; the cloud base height and the cloud vertical structure is derived mainly from ceilometer measurements and radiosounding profiles, although other instruments (cloud radar and micropulse lidar) are also used as complementary devices.

2. Goals

Detailed studies of the behavior of cloudiness in general and of the macroscopic horizontal and vertical characteristics of clouds in particular may contribute to the appropriate classification of clouds, which is an important issue as noted in section 1. Knowledge of the global climatology of cloud types and cloud vertical structure is a key factor for fully understanding the role of clouds in the atmospheric circulation and their effects and feedbacks on the Earth's radiative budget. Accurate observations of local vertical distributions of clouds are needed to improve the overall understanding of cloud-related processes and to increase the predictive capabilities of atmospheric models.

Consequently, the general objective of this doctoral thesis is to contribute to a broader exploitation of the large amount of experimental information (already in existence and being continuously extended) that can be used to characterize cloudiness from a geometrical point of view. This information is obtained from widely deployed instruments which are basically ceilometers and radio-soundings. The retrievals of either horizontal or vertical distributions of the cloud field are studied by specifically analyzing the cloud cover, the cloud base height and the cloud vertical structure derived from these devices. Within the frame of this general goal, several specific objectives are also addressed:

- To evaluate the cloud cover estimations derived from ceilometer measurements, and to compare them with human observations at monthly temporal resolution.
- To acquire a deeper knowledge about the cloud base height (CBH), and to describe its behavior, including different time scales, measurements from the surface with a ceilometer, and comparisons with other kind of estimations (human observations, radiosoundings, etc.).
- To test several methods to obtain the cloud vertical structure (CVS) based on radiosonde profiles available in the literature and to make a detailed comparison of the CVS obtained with the best estimated CVS, as represented by a conjunction of three ground-based instruments: ceilometer, micro-pulse lidar and cloud radar (the ARSCL product, Active Remote Sensing of Clouds), in order to reveal the methods' strengths and weaknesses.

- To propose improvements to the previously tested methods to obtain the CVS based on radiosonde profiles.
- To analyze the effect on the agreement with the ARSCL estimate of lowering the vertical resolution of the vertical profiles in order to derive a method potentially useful to be applied to lower resolution vertical profiles such as those transmitted through the WMO's Global Telecommunication System (GTS); or to the reanalysis temperature and humidity products.

Related to the latter specific objectives, this study extends previous comparison studies on RS methods used to obtain CVS, since it considers even more methods and accurately compares retrievals against a reliable reference (ARSCL) and for an accurately selected set of cases.

The results of this dissertation have been partially published. First, the cloud base height and the cloud cover long-term behavior have been studied in detail over Girona and their climatic behavior has been evaluated through a ceilometer. Moreover, some specific atmospheric situations are described, adding some insight into the frequency distributions of CBH. These studies correspond to subsections 4.1 and 4.2 and were entitled "Behavior of cloud base height from ceilometer measurements" and published in June 2013 in *Atmospheric Research*. Secondly, subsections 4.3.1, 4.3.2 and 4.3.3 have been accepted to be published under the title "Comparing the cloud vertical structure derived from several methods based on radiosonde profiles and ground-based remote sensing measurements" in the journal *Atmospheric Measurement Techniques*. The site chosen for this latter research was the Southern Great Plains (OK, USA), because of the availability of a great amount of instrumentation: ARSCL product (from ceilometer, micro-pulse lidar and cloud radar) and radiosounding measurements. Some improvements for the methods are proposed, in particular a method for low resolution profiles. An application of the best method found (subsection 4.4) has been submitted as a paper and is under revision in the *Journal Geophysical Research – Atmospheres*.

This research has been possible thanks to a predoctoral scholarship grant from the former Spanish Ministry of Science and Innovation (currently the Ministry of Economy and Competitiveness). This research was conducted under the umbrella of the NUCLIEREX and NUCLIER SOL projects, also funded by the former Spanish Ministry of Science and Innovation and developed at the Department of Physics of the University of Girona. The overall aim of these projects is to contribute to reducing uncertainties associated to clouds in the radiation models used in the description of climate and in studies of climate change. Specifically, this thesis is

involved with tasks aimed at improving the knowledge of cloudiness behavior through the study of cloud cover, the CBH and the CVS by means of ground-based observations, instruments, and methodologies.

Data used for this research was provided by two sites equipped with suitable experimental facilities: Girona (in the NE of the Iberian Peninsula) and the Southern Great Plains (SGP, OK, USA). Data from Girona comes from the station owned by the University of Girona and run by the research group where this thesis has been developed. Data from the SGP has been supplied by the Atmospheric Radiation Measurement (ARM) Program Climate Research Facility, which is sponsored by the U.S. Department of Energy (DOE). The author enjoyed a brief research stay in 2011 at the Pacific Northwest National Laboratory (PNNL, WA, EUA) which is one of the United States' DOE National Laboratories in charge of running the ARM program. She also took advantage of a second stay, this time at the company Vaisala (Finland), as part of her PhD programme development. Both stays were funded by grants from the former Spanish Ministry of Science and Innovation (currently the Ministry of Economy and Competitiveness).

3. Instruments, data and methodology

Besides surface visual observations, a lot of instruments are deployed worldwide to analyze the atmosphere in general and characterize clouds in particular. Instruments can be divided into in-situ (aircrafts and radiosondes) and remote sensing (from the surface or onboard satellites). In situ instruments obtain direct measurements of most relevant variables (temperature, vapor and water content, pressure,...) and even of microphysical properties of clouds (droplet size, ice crystals shapes,...). A primary challenge when analyzing remote sensing measurement is deriving useful data at low signal-to-noise ratios, because atmospheric quantities and constituents (winds, temperature, humidity, trace gases, etc.) interact with electromagnetic and acoustic radiation in different ways, but always in a weakly manner (except for some high absorption bands). The only notable exception is clouds, which present strong interactions with electromagnetic radiation at different wavelengths. Moreover, when talking about remote sensing instruments, two major categories exist: active and passive. Active instruments emit electromagnetic or acoustic radiation and detect the portion of that radiation returned from the target volume of the atmosphere (e.g., radar, lidar, and sodar). Passive instruments, on the other hand, detect radiation from natural sources that is scattered or modified by the atmosphere (e.g., radiometers).

In this section, a number of instruments and methods that can be used to measure clouds and to determine its horizontal and vertical extent are reviewed, although only part of this instrumentation was used in this work. A distinction is made between those instruments that measure cloud cover and cloud base height (3.1) from those that determine the cloud vertical structure (3.2). The instruments used in the present research and the sites where they are deployed are described in more detail in the last subsection (3.3).

3.1. Cloud cover and cloud base height

3.1.1. Human observations

Until the end of the last century, the determination of cloud coverage and estimations of cloud heights were mainly performed by human observers. Actually, for many years classic human observations have been recording the cloud cover (in octas or in tenths), the amount of the lowest clouds, and the cloud genera around the world and usually three times per day. With this

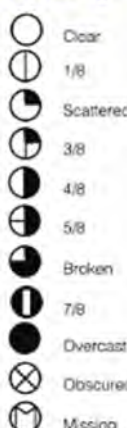
information one is capable to approximately infer the CBH, or at least the range of heights where the cloud is formed, because this is closely related to the cloud genera. Of course, this does not constitute an exact measurement, but gives an approximation that has been useful historically. So, each *étage* is defined by the range of levels at which clouds of certain genera (defined in the introduction) occur most frequently. Sometimes clouds are identified with the codes C_L, C_M and C_H plus a number from 1 to 9, providing a convenient way of describing clouds in meteorological reports by means of figures selected from tables of specifications as presented in the International Cloud Atlas (WMO, 1975). Other times the codification is associated to the height of the CBH observed (e.g. Ator, 2002).

A basic cloud observation log (Figure 5) must have at least this information (ideally taken two or three times a day at the same hours every day): date, hour, whether the sun is above the horizon or not, low clouds genera, low clouds cover, middle clouds genera, high clouds genera, total cloud cover, whether the sun is visible or not, and other observations as cloud species or varieties, supplementary features and accessory clouds, etc. Standard symbols that are used to take notes by human observers are shown in Figure 6.

DIA	NUBOSIDAD - CLASE Y CANTIDAD EN OCTAVOS DE CIELO CUBIERTO														
	07 HORAS					13 HORAS					18 HORAS				
	BAJAS CL CL	N B	MEDIAS CL CL	ALTAS CL CL	N T	BAJAS CL CL	N B	MEDIAS CL CL	ALTAS CL CL	N T	BAJAS CL CL	N B	MEDIAS CL CL	ALTAS CL CL	N T
1	-	0		ci	1	cu, se	1			1	cu, se	1			1
2	cu, se	3	ac	ci	6	se	2	ac	ci	7	se	3	ac	ci	7
3	cu, se	2			2		0		ci	2		0	ac		1
4	cu, se	5	ac, ay		8	cu, se	4	ac	ci, ci	6	cu, se	2	ac		3
5	DESP	0			0	cu, se	1	ac	ci	7	cu, se	1	ac	ci	7
6	se	2	ac, ay		7	se	5	ay		8	se	6	ay		8
7	cu, se	6	ay		8	cu, se	4	ac		5	se	3	ac		5
8	DESP	0			0	DESP	0			0	DESP	0			0
9	DESP	0			0		0		ci	1		0		ci	2
10	cu, se	5	ac		7	cu, se	2	ac		5	cu, se	3	ac, ay		7
		23	← SUMA →		39		19	← SUMA →		42		19	← SUMA →		41

Figure 5. A weather log of human observations of clouds taken in Girona Airport in January of 1994. The first column are the days of the month, next columns are the genera of low clouds and its cover, then the medium and high clouds genera and finally the total cloud cover. These notes are taken three times per day (at 7h, 13h and 18h).

Cloud Coverage



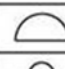
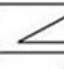
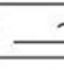

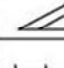
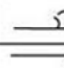


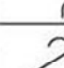
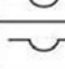
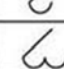
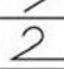
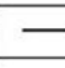
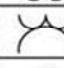
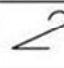

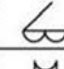
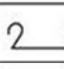

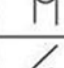
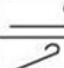
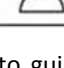

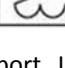
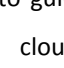
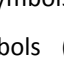
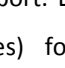
C_L	DESCRIPTION (Abridged from W.M.O. Code)	C_M	DESCRIPTION (Abridged from W.M.O. Code)	C_H	DESCRIPTION (Abridged from W.M.O. Code)
1	 Cu, fair weather, little vertical development & flattened	1	 Thin As (most of cloud layer semitransparent)	1	 Filaments of Ci, or "mares tails", scattered and not increasing
2	 Cu, considerable development, towering with or without other Cu or SC bases at same level	2	 Thick As, greater part sufficiently dense to hide sun (or moon), or Ns	2	 Dense Ci in patches or twisted sheaves, usually not increasing, sometimes like remains of Cb, or towers tufts
3	 Cb with tops lacking clear-cut outlines, but distinctly not cirriform or anvil shaped, with or without Cu, Sc, St	3	 Thin Ac, mostly semi-transparent, cloud elements not changing much at a single level	3	 Dense Ci, often anvil-shaped derived from associated Cb
4	 Sc formed by spreading out of Cu; Cu often present also	4	 Thin Ac in patches; cloud elements continually changing and/or occurring at more than one level	4	 Ci, often hook-shaped gradually spreading over the sky and usually thickening as a whole
5	 Sc not formed by spreading out of Cu	5	 Thin Ac in bands or in a layer gradually spreading over sky and usually thickening as a whole	5	 Ci and Cs, often in converging bands or Cs alone; generally overspreading and growing denser, the continuous layer not reaching 45 altitude
6	 St or Fs or both, but no Fs of bad weather	6	 Ac formed by the spreading out of Cu	6	 Ci and Cs, often in converging bands or Cs alone; generally overspreading and growing denser, the continuous layer exceeding 45 altitude
7	 Fs and/or Fc of bad weather (scud)	7	 Double-layered Ac, or a thick layer of Ac, not increasing; or Ac with As and/or Ns	7	 Veil of Cs covering the entire sky
8	 Cu and Sc (not formed by spreading out of Cu) with bases at different levels	8	 Ac in the form of Cu-shaped tufts or Ac with turrets	8	 Cs not increasing and not covering entire sky
9	 Cb having a clearly fibrous (cirriform) top, often anvil-shaped, with or without Cu, Sc, ST or scud	9	 Ac of a chaotic sky, usually at different levels; patches of dense Ci are usually present	9	 Cc alone or Cc with some Ci or Cs but the Cc being the main cirriform cloud

Figure 6. Table to guide the observations: symbols used in plotting a report. Left, symbols to represent total cloud cover. Right, symbols (and numbering codes) for cloud types corresponding to the three étages: low C_L, middle C_M, and high C_H (Ahrens, 2009; aviation magazine: <http://avstop.com/ac/5-7.html>).

Observers have often difficulties to distinguish between some cloud types. For example, identifying altostratus/altocumulus and cirrus clouds reliably, particularly at night or when lower clouds are present, is quite complicated. In addition, surface observations do not provide any information on cloud-top height or optical thickness (Poore et al., 1995). These and other difficulties result in a limited number of climatic studies of cloudiness based on classical surface observations, especially when compared with studies of other variables such as temperature or precipitation. There are, however, a number of notable exceptions: for example, Warren et al. (2007) developed a global climatology of clouds; and at continental scale we can mention the works by Henderson-Sellers (1992) for Europe, Dai et al. (2006) for the USA, Kaiser (2000) for China, and Sun and Groisman (2000) for the former Soviet Union; finally Calbó and Sanchez-Lorenzo (2009) presented a cloud climatology for the Iberian Peninsula.

3.1.2. Sky cameras

Sky camera developers attempt to substitute human observations with the aim of getting a major number of observations, giving them more objectivity, and reducing costs at the same time. So, for example, cameras tend to have the same sensibility to light as the human eye. In general, they have similar limitations and advantages of human observations. On the one hand, both have a 180° view of the sky and both can record the sky in color during the day (further, IR cameras can observe clouds at night). On the other hand, the major disadvantage of camera-based techniques is that they have systematic detection errors such as misdetection of thin clouds and limitations in distinguishing cloud types (Calbó and Sabburg, 2008).

A ground-based all-sky camera is an automated imaging system for sky observations and estimation of the cloud coverage that covers a 180° view of the sky (Calbó and Sabburg, 2008; Cazorla et al., 2008; Cazorla Cabrera, 2010; Heinle et al., 2010; Kassianov et al., 2005a; Kreuter et al., 2009; Long et al., 2006b; Schade et al., 2009; Shields et al., 1991, 2013), or part of the sky (Janeiro et al., 2010; Souza-Echer et al., 2006) at scheduled time intervals. A typical all-sky camera has two major components: the first component is a weather proof box with the optical assembly and the second is the computer control devices (Pfister et al., 2003). At the heart of the optical assembly is a color charge-coupled device (CCD) or Complementary Metal Oxide Semiconductor (CMOS) array, although some versions of all-sky cameras use monochromatic sensors. Typically, the optical assembly consists of a fisheye lens positioned on top the camera and pointing upwards to mirror the whole sky, a hemispherical glass optical dome for environmental protection, and a sun blocker. For example, the Whole Sky Camera (WSC) developed at the UdG (more information and live images in: <http://www.udg.edu/Fisicaambiental/Estaciometeorologica/tabid/14749/Default.aspx>), is mounted on a Sun tracker with a shadowing system (Figure 7), and is an example of a cost-effective alternative camera. In fact, several research groups and institutions have developed non-commercial sky cameras for their own requirements. However, other cameras are developed without any sun occultator such as that by Heinle et al. (2010) by means of using large dynamic range sensors that do not become saturated for the direct sunlight; still other cameras use neutral density or spectral filters to block the sun's intense direct-normal radiation (e.g. Cazorla et al., 2009; Pfister et al., 2003).

An alternative arrangement of the all-sky camera consists of the camera pointing downwards to a convex mirror which allows projecting a 180° image of the sky onto the camera sensor. This is in fact the solution applied to the most broadly deployed camera worldwide, i.e. the Total Sky

Imager (TSI) by Yankee Environmental Systems (YES) Inc. Additional features include a heated glass and an optional solar tracking occultator used to hide the sun spot, to prevent camera blooming and the production of artifacts in the image (Calbó and Sabburg, 2008; Long et al., 2006b; Pfister et al., 2003) (Figure 8). This camera comes with a piece of software that estimates cloud cover, including distinction between opaque and thin clouds (Long et al., 2006b; Kassianov et al. (2005b)). Likewise, both commercial models and non-commercial prototypes in general include an image processing algorithm that runs on a computer workstation and captures and saves images at user-defined intervals. Most algorithms for processing images from sky cameras use a “color ratio threshold” to distinguish whether a pixel represents a clear or cloudy portion of the sky image (Calbó and Sabburg, 2008; Cazorla et al., 2008).

Cameras can photograph the state of the sky in the visible and/or in the IR band (Feister and Shields, 2005; Feister et al., 2010; Seiz et al., 2007; Shields et al., 1991, 2013). Visible spectrum cameras (Calbó and Sabburg, 2008; Cazorla et al., 2008; Long et al., 2006b; Schade et al., 2009) detect and classify clouds based on the differences in the color and intensity between the different cloud types and the sky. For example, Calbó and Sabburg (2008) derived cloudiness and cloud type: several features (statistical measurements of image texture, some based on the Fourier transform and some computed from the image where cloudy pixels are distinguished from clear-sky pixels) that could be useful for cloud-type classification were extracted from digital images of the sky. The use of the most suitable features in an automatic classification algorithm was also shown and discussed. IR cameras’ classification scheme is based on the difference of emitted thermal IR radiation from the different types of clouds and the sky (Klebe et al., 2014; Liu et al., 2011, 2013; Smith and Toumi, 2008). Thus, clouds are in general “warmer” (i.e. emit more thermal IR radiation) than the background sky. In summary, visible spectrum cameras can only measure in daytime, but in three wavelength channels, while on the contrary IR cameras can take measurements both on daytime and nighttime. For this reason some authors are developing hybrid cameras that use VIS and IR techniques and take advantage of both types of instruments.

Besides estimating cloud cover and cloud type, an approximation to estimate the CBH was tested in Kassianov et al. (2005a) from paired ground-based hemispherical observations. They used two TSI separated 0.5 km from each other to infer the CBH. The basis of this method is formed by the overlapping area of the two adjusted images. Their results suggested that, at least for single-layer cloud fields, moderately accurate (within 0.35 km) CBH retrieval is possible. Other recent developments make use of the polarizing properties of the atmosphere: Kreuter et

al. (2009) presented a simple and inexpensive fully automated all-sky imaging system based on a commercial digital camera with a fish-eye lens and a rotating polarizer. The system is characterized and two examples of applications in atmospheric physics are given: polarization maps and cloud detection. All-sky polarization maps are obtained by acquiring images at different polarizer angles and computing Stokes vectors. The polarization in the principal plane, a vertical cut through the sky containing the Sun, is compared to measurements of a well-characterized spectroradiometer with polarized radiance optics to validate the method. The images are further used for automated cloud detection using a simple color-ratio algorithm.

Some commercial or broadly deployed sky cameras are listed next:

- The Total Sky Imager (TSI) 880 built by Yankee Environmental Systems, Inc. It is an automatic, full-color sky imager system that provides real-time processing and display of daytime sky conditions (Yankee Environmental Systems Inc. website, Calbó and Sabburg, 2008; Long et al., 2001, 2006b; Pfister et al., 2003) (Figure 8).
- The Infrared Cloud Imager (ICI) is comprised by an IR camera, one or two blackbody calibration sources, a gold-plated beam-steering mirror, and control electronics. The ICI system records radiometrically calibrated images of the sky in the thermal IR window band of 8000–14,000 nm at a field of view of approximately $18^\circ \times 13.5^\circ$ (Smith and Toumi, 2008).
- The hybrid VIS/IR Whole Sky Imager (WSI) is a passive automated digital imaging system manufactured at the University of California San Diego, that obtains both visual and Near IR (NIR) images of the sky at a 180° FOV under both day and night conditions, in order to assess cloud fraction, cloud morphology, and radiance (Feister and Shields, 2005; Feister et al., 2010; Seiz et al., 2007; Shields et al., 1991, 1993, 2013). It is a modification of a former all-sky camera, which uses additional spectrum and neutral density filters on a mechanical filter changer.
- The Solmirus All-Sky Infrared Visible Analyzer (ASIVA) is another hybrid camera used for cloud detection and classification that provides measurements from two cameras, one in the VIS and the other in the IR (8000–13000 nm). The VIS camera consists of a CCD or CMOS sensor and a 180° fish eye lens. The IR camera consists of a microbolometer IR sensor, a filter wheel, a blackbody calibration source and a 180° fish eye diamond coated lens (Klebe et al., 2014; Morris and Klebe, 2010; Morris et al., 2011; Solmirus website).
- The Automatic Cloudiness Detection System SONA developed by Sieltec Canarias S.L in collaboration with the Izaña Atmospheric Research Center (managed by the

Meteorological State Agency of Spain) in the Canary Islands provides hemispherical images of the sky which are processed and analyzed in real time providing an objective and accurate value of cloud cover percentage using nonlinear multilayer neural networks for image pattern recognition. The system consists on a 640x480 pixel resolution CCD camera with an infrared filter. (Gonzalez et al., 2012) (<http://sonaspecs.zohosites.com/>, http://izana.aemet.es/index.php?option=com_content&view=article&id=180&Itemid=157&lang=es).

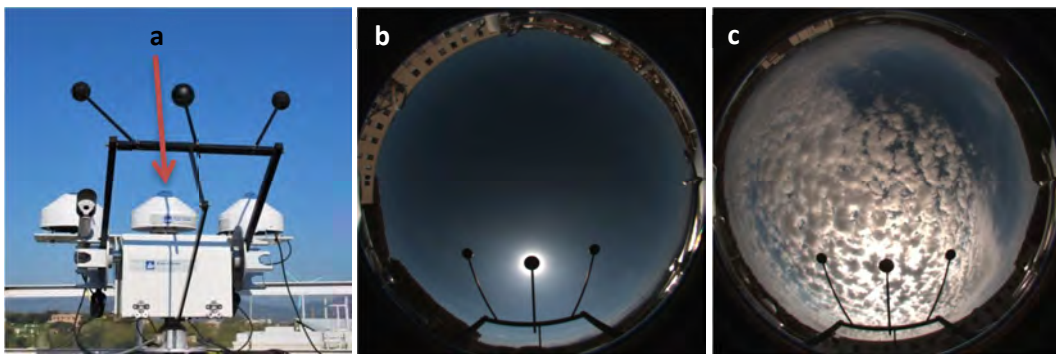


Figure 7. a) Whole Sky Camera (WSC) designed by the University of Girona and installed over a sun-tracker and with a sun-blocker at Girona (Spain); b) WSC image of a clear sky situation at Girona on July 6th, 2009; c) WSC image showing altocumulus and cirrus clouds, taken at Girona on July 19th, 2009.

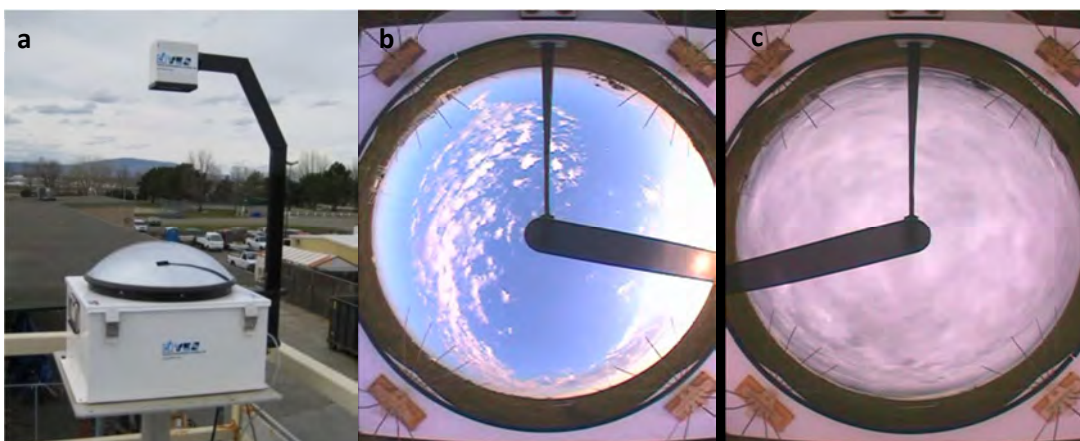


Figure 8. a) The Total Sky Imager (TSI by YES) installed at PNNL, Richland, WA; b) TSI image with low clouds acquired by the TSI on October 1st, 2009 at SGP (OK); c) TSI image of an overcast cloud situation on July 5th, 2009 at SGP (OK) (source of TSI images: ARM data Archive).

3.1.3. LIDAR technology and ceilometer measurements

As far as ground-based instrumentation is concerned, lidars and ceilometers (in particular) are the most commonly used active remote sensing measuring instrumentation devoted to estimate CBH. The principle of lidar (Light Detection And Ranging) is the determination of clouds by analyzing the atmospheric density profiles of the returning signal from a beam of light projected into the atmosphere. One of the first proposals in this sense suggested an anti-aircraft searchlight as the source of the beam and a distant large telescope as the receiver. In this configuration, now known as bistatic (Figure 9), the range of the scattering can be determined by geometry. In the bistatic configuration, the FOV of the receiver is scanned along the transmitted beam in order to obtain an altitude profile of the scattered light. Typically, modern lidar systems are monostatic in configuration, with collocated transmitter and receiver. Monostatic systems can be subdivided into two categories: coaxial systems, where the light beam is transmitted coaxially with the receiver's FOV, and biaxial systems, where the transmitter and receiver are located adjacent to each other. Current monostatic lidar systems use pulsed laser sources, thereby enabling the range at which scattering occurs to be determined from the round-trip time of the scattered light (Argall and Sica, 2003).

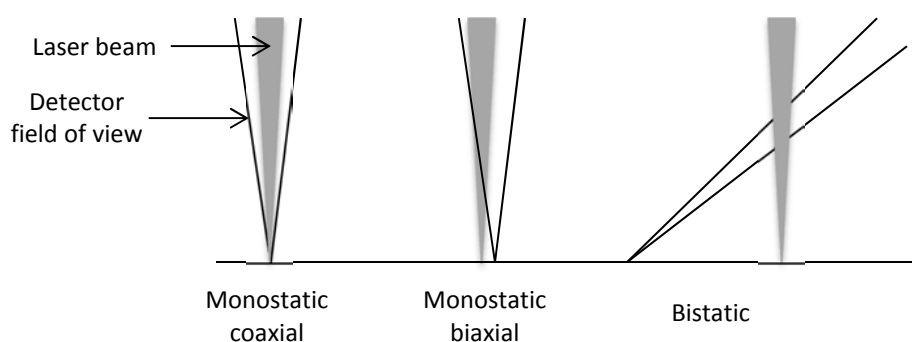


Figure 9. Three possible alignment arrangements of a lidar's transmitted beam and receiver field of view (based on Argall and Sica, 2003).

A former precursor of the current ceilometers based on lidar technology is the so-called rotating-beam ceilometer (RBC), which for many years provided information on cloud ceiling, especially at airports. Rotating beam ceilometer use optical triangulation to measure the CBH. The transmitter emits a narrow light beam of a 2° divergence. The light beam is swept in a

vertical arc extending typically from 8 to 85°. The receiving unit is pointed directly upwards, positioned at a known distance from the transmitter, and comprises a photoelectric cell and an angle-of-view restrictor; the restrictor ensures that only light vertically downwards can reach the photoelectric cell. A pen in the recording unit, moving simultaneously with the transmitter beam, records when a cloud signal is received (Eberhard, 1986; WMO, 2008). The angle at which the reflection from a cloud is detected along with the distance between receiver and transmitter allow determining the CBH. But RBCs are very sensitive to the presence of precipitation: in moderate or heavy precipitation, the instrument can either indicate low cloud erroneously or fail to detect clouds at all. In foggy conditions, the light beam may be dissipated at a low level and the ceilometer can fail to give any useful indication of clouds, even when a low cloud sheet is present (WMO, 2008). Nowadays, most of the rotating-beam ceilometers have been phased out and replaced with vertically pointing laser-beam ceilometers (Ahrens, 2009).

The first lidar was built in the 1960s soon after the invention of the laser, and extensive work went into developing lidar remote sensing techniques. In the 1970s and 1980s, with the advent of lasers that could be tuned over a wide range of wavelengths, the application of lidar in atmospheric remote sensing became more widespread. In the 1990s, it began a trend towards more compact and robust lidar systems and an increased use of solid state lasers as lidar transmitters. Lidars that are in use today operate at wavelengths from the near ultraviolet to the far infrared regions of the electromagnetic spectrum (Angevine et al., 2003) with some aims: pollution and atmospheric particles control, boundary layer and mixing-layer height monitoring, etc., both in atmospheric research programs and routinely at some particular sites. Other, more modern types of lidars, such as micropulse lidars (MPL) and the Raman lidar (RL) will be explained in section 3.2.1.

A modern ceilometer (Figure 10) is a specific type of lidar devoted to determining the cloud base height (CBH). Current ceilometers make use of the elastic lidar principle: they emit signals vertically in the atmosphere and measure the profile of the backscattered light from clouds and precipitation with a receiver telescope (Ahrens, 2009; Boers et al., 2010; Haij et al., 2006; Martucci et al., 2010). Besides CBH, other information can be derived from the backscatter signal such as the convective mixing height (Emeis et al., 2008a, 2008b; Muenkel, 2007; Muenkel et al., 2004). There are at least several hundred units in existence today worldwide, since these instruments are notably compact, can work unattended, and can measure routinely at least the first CBH and locate the lower three clouds in one pulse (Angevine et al., 2003; Costa-Surós et al., 2013; Emeis et al., 2004; Nowak et al., 2008). Traditionally their importance has always been

closely linked to the needs of aviation (Holejko and Nowak, 2000). Thus, development of an automated ceilometer system for measuring cloud amounts and CBH was required to meet the needs of the increasing volume of aviation traffic and to replace systems based on visual observations (Mancuso et al., 1971). This instrument, in fact, has become a standard both for operational purposes (in particular at airports) and for research goals (it is a common instrument at ARM and Baseline Surface Radiation Network measurement sites).



Figure 10. Different brands and models of ceilometers: a) Belfort Laser Ceilometer 7013C (U.S. DOE's ARM Program), b) 80171 Cloud Ceilometer (Belfort Instruments website), c) Vaisala CT12K Laser Ceilometer, d) Vaisala CT25K (U.S. DOE's ARM Program), e) Vaisala CT75K (British atmosphere datacenter website), f) Vaisala CL-31 (Vaisala website), g) Vaisala CL-51 (Vaisala website), h) Jenoptik CHM15K (Jenoptik website), i) Eliasson CBME80 ceilometers (Eliasson Engineering website), and j) ceilometer 8200-CHS (MTECH systems website).

As already commented, the vertical profile of the backscattered light allows determining the CBH. Usually, CBH is defined as the height at which the ceilometer signal returns its maximum value (Eberhard, 1986) but sometimes the highest backscatter signal is not coming from the base of the cloud (e.g. when there is precipitation) and then the newer ceilometer's software uses more complex algorithms to guess the CBH likewise (Vaisala Oyj., 2006) (Figure 11). In general terms the ceilometer software operation is based on using some confidential threshold values to the backscatter signal to find the cloud base identification and vertical visibility calculation. Regarding one on these thresholds, Van Tricht et al. (2014) mention that the standard cloud-base detection algorithms of ceilometers are designed to detect optically thick liquid-containing clouds, and propose a new algorithm that uses a backscatter threshold to detect optically thin hydrometeors at polar latitudes. The optimal attenuated backscatter threshold of $3 \times 10^{-4} \text{ km}^{-1} \text{ sr}^{-1}$ was determined by a sensitivity analysis on all available cases for the stations they studied in the Antarctica and in Greenland.

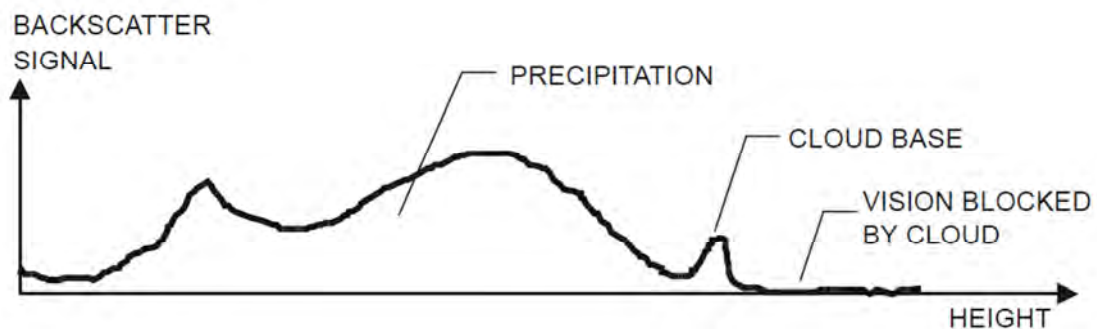


Figure 11. Ceilometer's typical measurement signal. Generally, particles at all heights backscatter light, and so the actual return signal may look like that shown in the figure. The instantaneous magnitude of the return signal will provide information on the backscatter properties of the atmosphere at a certain height. Information about fog and precipitation, as well as clouds, can be derived from the return signal. Since fog and precipitation attenuate the light pulse, the cloud base signal will appear lower in magnitude in the return echo. However, the fog and precipitation information also provides data for estimating this attenuation and computing the necessary compensation, up to a limit (Vaisala Oyj., 2006).

Although these vertically pointing instruments (lidars and ceilometers) are mainly used for measuring the CBH, time series analysis are used to calculate the fraction of the total time that cloud elements are detected by the observing instrument. This 'cloud time fraction' (in this thesis specifically named 'cloud occurrence', see section 3.2) is then assumed to represent the nadir projected area cloud fraction, i.e., the portion of the surface that is shaded if the clouds

are illuminated from directly above. It has been noted, for example by Kassianov et al. (2005a), that these two quantities, fractional sky cover and nadir projected cloud fraction, are inherently different but related quantities. A hemispheric method simulates the observer better than a column method, as it will ingest data from the same sky view as the observer. While this is true in a general sense, it much depends on the procedure to convert the instrumental output to equivalent cloudiness values (Boers et al., 2010). Actually, the Automated Surface Observing System (ASOS, which is a suite of automated sensors that are designed to serve meteorological and aviation observing needs, and that serves as a primary climatological observing network – there are currently more than 900 ASOS sites in the US) uses a laser beam ceilometer to measure cloud height and then infers the amount of cloud cover by averaging the amount of clouds that have passed over the sensor during 30 minutes, and so does Vaisala's algorithm (see section 3.1.6).

The WMO recognizes that, using current technology, laser ceilometers provide the most accurate, reliable and efficient means of measuring CBH from the ground when compared with alternative equipment (WMO, 2008). Inter-comparison studies of measurements by laser ceilometers from different manufacturers have been carried out several times. For example, during the WMO International Ceilometer Intercomparison (Jones et al., 1988) several designs of ceilometers were inter-compared and also other tests were made by comparing with RBC and pilot-balloon observations. Some early comparisons between RBC and newly developed laser ceilometers indicated that RBC had a superior performance during moderate rain.

Martucci et al. (2010) studied twelve cases of multilayer CBH retrievals from two ceilometers (Vaisala CL31 and Jenoptik CHM15K) from September to December 2008 in Ireland and they suggested applying an independent algorithm to both ceilometer backscatter signals to provide more accurate estimates of the CBH in both simple and complex cloud patterns. Other works have also suggested improvements to the basic algorithm or new values for the thresholds (Shupe et al., 2011; Van Tricht et al., 2014).

Other studies compare ceilometers against other remote sensing ground-based instruments intended to retrieve cloud properties, or even combine measurements from different instruments to obtain a better description of clouds. Kalb et al. (2005) compared an MPL, a Belfort Laser Ceilometer, a Vaisala Ceilometer and a MMCR at Larmont and Blackwell (OK, USA) ARM sites. This comparison revealed that the MPL is superior to both the Belfort Laser and the VCEIL in reporting the presence of cirrus cloud bases, but inferior in detecting low clouds. Garrett and Zhao (2013) measured cloud properties in the Arctic using a combination of active

and passive remote sensors including the Vaisala 25K Laser Ceilometer. They found that the ceilometer occasionally detects the base of a thin cloud that is invisible to the radar; or, if the cloud precipitates, that the radar cloud top lies below the ceilometer cloud base.

Some current commercial ceilometers are listed next:

- Belfort 80171 Cloud Ceilometer (Figure 10b) can estimate the heights of up to 5 cloud bases, ranging from 0 to 7.5km with 10 m resolution (Belfort Instrument Website)
- Vaisala ceilometers estimate up to 3 layers of clouds and use 0.91 μm laser beam wavelength. Nowadays, two models are available: CL-31 model (Figure 10f) which measurement range is 0-7.6 km and reporting resolution 5 m (selectable); and CL-51 (Figure 10g) which can reach clouds up to 13 km with a reporting resolution of 10 m (Vaisala website)
- Jenoptik CHM15K (Figure 10h) has an operating range of up to 15 km (Jenoptik website)
- Eliasson CBME80 ceilometer (Figure 10j) reaches 7620 m (Eliasson Engineering website)
- MTECH Ceilometer 8200-CHS (Figure 10k) reaches 8000 m and is capable to retrieve up to 4 cloud layers (MTECH systems website)

3.1.4. Surface radiometry

Radiometers include passive equipment that measures natural radiation (either irradiance or radiance) received on a particular site. These instruments are not initially intended to observe clouds, but there are several methodologies to derive the cloud cover from these instruments primarily developed for radiation measurement. Radiometers measure in shortwave and/or longwave; in narrow, wide, or specific spectral wavelengths; with different FOV (hemispheric, unidirectional, etc.); and even with a sun blocker in order to measure only the diffuse radiation. Furthermore, spectroradiometers are automated radiometer systems that scan at a pre-specified spectral range, at predefined scanning steps allowing measurements at multiple wavelengths using only one instrument. This subsection is devoted only to ground based devices, such as the broadly deployed pirgeometers and pyranometers, however it is interesting to remind that this kind of instruments (radiometers and spectroradiometers) are also used onboard of satellites.

Specifically, a pyranometer (Figure 12a, Figure 13a and b) is an instrument for measuring the total global shortwave radiation (0.3 to 3 μm approximately)(WMO, 2008). The same instrument may be used to measure the diffuse component of solar radiation if installed in conjunction with

a sun blocker. These instruments provide a measurement of the incident solar irradiance, indicating the effect of intervening clouds along the solar beam path from the sun to the sensor, thus providing a time series of global irradiance eventually affected by clouds (Calbó et al., 2001). Thus, Calbó et al. (2001) suggested a method for automatic recognition of sky condition based on ground measurements of broadband global and diffuse solar radiation. Few other works dealing with similar research have been found so far. For example, Long and Ackerman (2000) used measurements of the downwelling global and diffuse shortwave radiation to identify periods of clear skies. Subsequently, Long et al. (2006b) estimated the fractional sky cover from broadband shortwave radiometer measurements.

Pyrgeometers (Figure 12c and Figure 14) measure in the longwave spectrum (between 4 and 40 μm). APCADA is the acronym for “The Automatic Partial Cloud Amount Detection Algorithm” (Boers et al., 2010; Durr and Philipona, 2004) and is a system developed for estimating the actual sky cloud cover from surface measurements of longwave downward radiation, temperature, and relative humidity, every 10 minutes. The authors recognize that thin high clouds (cirrus clouds) cannot be detected by APCADA. Thus, only total cloud amount without cirrus clouds is estimated by APCADA (that is why the algorithm mentions “partial” cloud amount).

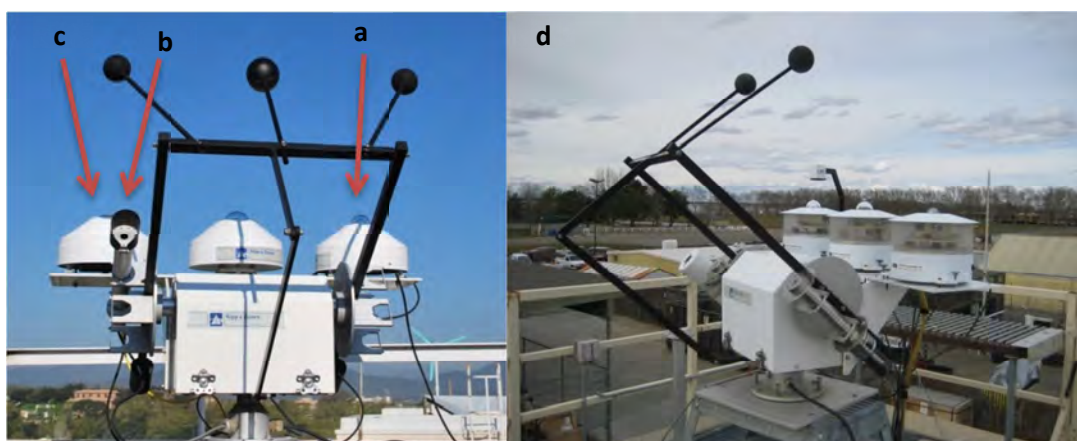


Figure 12. a) Kipp & Zonen CM11 solar diffuse pyranometer (spectral response between 0.28 - 2.8 μm) over a sun tracker and blocker; b) Kipp & Zonen CH1 pyrliometer (spectral response between 0.2- 4 μm and FOV 5 $^\circ$) and c) CG1 Kipp & Zonen pyrgeometer (measuring in the longwave spectrum of 4 to 40 μm and IFOV of 150 $^\circ$) with a sun blocker; and all three over a sun-tracker (Girona, Spain); d) A similar assembly, but with Eppley radiometers, over a sun-tracker in PNNL (Richland, WA).

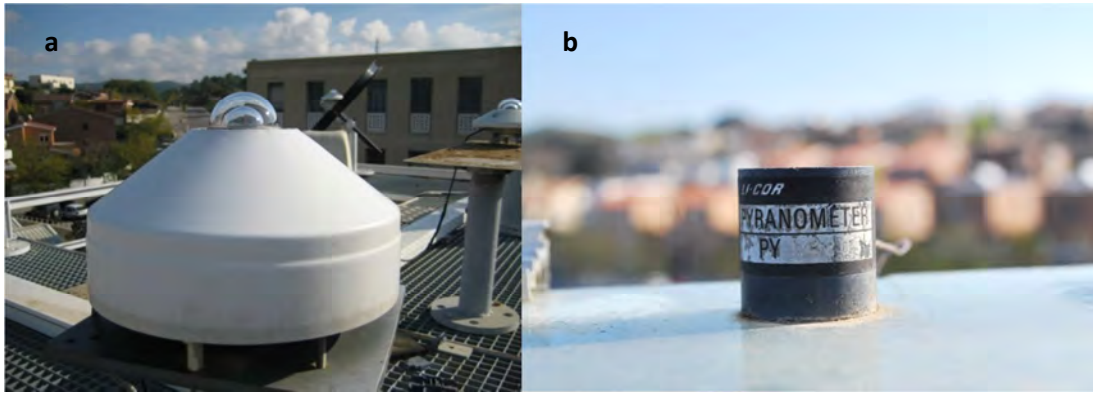


Figure 13. Kipp & Zonen CM11 (a) and Li-Cor LI200SA (b) pyranometers which measure the global solar irradiance. The first one has spectral response between 0.28 - 2.8 μm ; the second has a spectral response between 0.4 - 1.1 μm . They are both installed at Girona, Spain.



Figure 14. CG1 Kipp & Zonen pyrgeometer, which is mounted over a sun-tracker (Kipp & Zonen 2AP) with a sunblocker. It measures the infrared irradiance (spectral response between 0.3-2.2 μm) and has an incidence field of view (IFOV) of 150°. This instrument is installed in Girona, Spain.

Some measurement programs and networks around the world which use surface radiometers (pyranometers and pyrgeometers) which could be useful to derive information on cloudiness, are summarized next:

- Atmospheric Radiation Measurement (ARM) Program: created in 1989 by U.S. Department of Energy, it is a scientific program that provides data from strategically located in situ and remote sensing observatories around the world. It have several highly instrumented ground stations to study cloud formation processes and their influence on radiative transfer. Currently, this scientific infrastructure also includes two mobile facilities, an aerial facility, and a data archive available for use by scientists worldwide

through the ARM Climate Research Facility. ARM is a multi-laboratory, interagency program, and is a key contributor to national and international research efforts related to global climate change, in particular in all cloud-related effects and feedbacks. Thus, a primary objective of the facility is to improve scientific understanding of the fundamental physics related to interactions between clouds and radiative feedback processes in the atmosphere. ARM focuses on obtaining continuous field measurements and providing data products that promote the advancement of climate models (<http://www.arm.gov/>).

- Baseline Surface Radiation Network (BSRN): conceived in the late 1980s by the World Climate Research Program (WCRP, sponsored by WMO, ICSU, and IOC) provides near-continuous, long-term, in situ-observed, Earth-surface, broadband irradiances (solar and thermal infrared) and certain related parameters from a network of more than 50 globally diverse sites. The collected data is intended to be utilized for climate research applications, in particular satellite product validation, climate model comparisons, and establishment of regional radiation climatologies, all in support of Earth radiation budget studies. In the mid 1990s, BSRN was included under the WCRP program called the Global Energy and Water Experiment (GEWEX). By the late 1990s, BSRN was designated as a contributing network to the WMO Global Atmospheric Watch (GAW) program and in the early 2000s was designated as the Global Baseline Surface Radiation Network of the Global Climate Observing System (GCOS) (<http://www.ndsc.ncep.noaa.gov/coop/bsrn/>).
- World Radiation Data Center (WRDC): established in 1964 and located at the Main Geophysical Observatory in St. Petersburg (Russia) serves as a central repository for solar radiation data collected at over 1000 measurement sites throughout the world. The WRDC centrally collects, archives and publishes radiometric data from the world to ensure the availability of these data for research by the international scientific community. The WRDC archive contains the following measurements (not all observations are made at all sites): global solar radiation, diffuse solar radiation, downward atmospheric radiation, sunshine duration, direct solar radiation, net total radiation, net terrestrial surface radiation (upward), terrestrial surface radiation, reflected solar radiation, spectral radiation components (instantaneous fluxes)(<http://wrdc-mgo.nrel.gov/>).
- NOAA's Surface Radiation Network (SURFRAD): was established in 1993 through the support of NOAA's Office of Global Programs. Its primary objective is to support climate research with accurate, continuous, long-term measurements of the surface radiation

budget over the United States. This differs from ARM sites, where surface radiation budget measurements are also being made, in that ARM uses clustered measurements over a limited area for process-oriented studies. Currently seven SURFRAD stations are operating in climatologically diverse regions: Montana, Colorado, Illinois, Mississippi, Pennsylvania, Nevada and South Dakota. This represents the first time that a full surface radiation budget network has operated across the U. S. Independent measures of upwelling and downwelling, solar and infrared are the primary measurements; ancillary observations include direct and diffuse solar, photosynthetically active radiation, UVB, spectral solar, and meteorological parameters. Observations from SURFRAD have been used for evaluating satellite-based estimates of surface radiation, and for validating hydrologic, weather prediction, and climate models (<http://www.esrl.noaa.gov/gmd/grad/surfrad/>).

Besides the common instruments described above, there are also some commercial irradiance meters specifically intended for cloud description. Some of these instruments are detailed next (see Tapakis and Charalambides, 2012 for an extended revision):

- The Infrared Pyrometer CIR-7 (known as Nephelo) is a ground-based instrument designed and assembled by Atmos SARL in France for day and night cloud cover imaging. It comprises 7 IR pyrometers in the spectral range of 9–14 μm , each with a 12° field of view. CIR-4 and CIR-13 (Figure 15) are different versions of CIR-7, based on the same principles, consisting of 4 and 13 IR sensors respectively.
- The Nubiscope (Figure 16) is an instrument that consists of an IR pyrometer that receives IR radiation emitted from the atmosphere in the spectral region of 8-14 μm with a full viewing angle of 3° (Boers et al., 2010). It provides the cloud fraction of the sky for three different levels of the sky in order to classify low, medium and high clouds. Moreover the algorithm calculates the Cloud Base Height (CBH) and a rough cloud description such as clear sky, overcast, broken clouds, cirrus and fog. A further development of the instrument provides even more types of clouds such as transparent clouds, low transparent clouds and heavy precipitation (Feister et al., 2010).

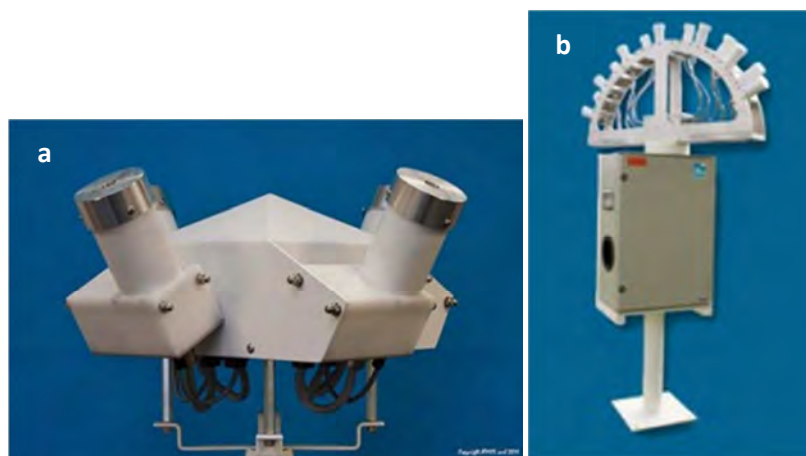


Figure 15. a) CIR-4 and b) CIR-13 (from: Atmos Company website).



Figure 16. Nubiscope (from: Nubiscope website).

Boers et al. (2010) performed an integrated assessment of five different observational methods to derive the fractional cloudiness. The five methods were based on either active or passive systems and use either a hemispheric (nubiscope, TSI and APCADA) or column remote sensing techniques (ceilometer and radar) and also a 30 year climatology of human observation to be used as reference. They found that column methods report lower frequency of occurrence of cloudiness, at least for the intermediate 2-6 octas range. Another comparison between different types of ground-based sensors used to derive macroscopic cloud data such as cloud cover and CBH is presented in Feister et al. (2010). Specifically, four instruments are compared: a Nubiscope (an infrared sky scanner), a Daylight VIS/NIR WSI, a ceilometer LD-40 (measuring in the near infrared region) and a ka band cloud radar (microwave band region, extremely high frequency).

Finally, other radiometers which could potentially offer some cloud information but which still do not have any methodology associated to obtain the cloud cover or the CBH are:

- UV radiometers that measure the UV radiation from the Sun spectrum. Any differences in the measured UV irradiance compared to clear sky conditions may be considered to occur due to the presence of clouds. There are several commercial UV radiometer models, either measuring UV total irradiance (0.28 to 0.4 μm), only parts of it: UV-A (0.32 to 0.4 μm) or UV-B (0.28 to 0.32 μm), or spectrally weighted irradiances (as erythemal irradiance).
- The pyrheliumeter (Figure 12b) is used for measuring the direct normal irradiance (0.2 to 4 μm) with typically 5° FOV (WMO, 2008). Of course a cloud that blocks the solar beam modifies notably the measurements of a pyrheliumeter.
- The sun photometer (or sun radiometer) is a photometer that is turned towards the sun measuring the intensity of direct sunlight. There are many variations of sun photometers that use different filters for measuring one or more spectral bands, stationary or portable, with tracker or without moving parts. The Multi-Filter-Rotating Shadowband Radiometer (MFRSR) (Figure 17) is a sun photometer that collects sky radiation through a horizontal diffuser and uses a rotating shadow band to separately measure the global and diffuse components of the radiative field; the direct component is derived as the difference between the two measurements. The commercial model MFR-7 has a channel for the total shortwave radiation (0.3 to 3 μm), and six more spectral channels. It uses the IR/WV (water vapor) (0.94 μm band) to estimate the water vapor column and the other channels to derive the aerosol optical thickness. The same principles as the MFRSR apply to the Rotating Shadowband Spectroradiometer (RSS) but in the spectral range of 0.36 to 1.05 μm . (Min and Harrison, 1996; Min et al., 2004).



Figure 17. Multi-Filter-Rotating Shadowband Radiometers (MFRSR) installed at PNNL (Richland, WA).

3.1.5. Satellite observations

There are numerous satellites orbiting the Earth which serve different purposes. Some are geostationary (e.g.: Meteosat and GOES –Geostationary Operational Environmental Satellite series–), i.e. they circle the earth in a geosynchronous orbit, scanning always the same area and allowing a continuous monitoring of a specific region. Geostationary satellites are important because they use a “real time” data system, meaning that the satellites transmit images to the receiving system on the ground as soon as the camera takes the picture; this information is a great help in forecasting the progress of large weather systems (Ahrens, 2009). Other satellites follow polar orbits (for example, the US Air Force surveillance satellites of the Defense Meteorological Satellite Program –DMSP– series), i.e. they pass over both poles of the earth during each orbit. The polar orbiting satellites, which closely parallel the earth’s meridian lines, at each pass monitor an area to the west of the previous pass as the earth rotates to the east beneath the satellite, and eventually, the satellite covers the entire earth (Ahrens, 2009). Polar-orbiting satellites have the advantage of photographing clouds directly beneath them but the inconvenience that no one spot on the Earth's surface can be continuously sensed from a satellite in a polar orbit. Thus, they provide sharp pictures in Polar regions, where photographs from a geostationary satellite are distorted because of the low angle at which the satellite “sees” this region. Polar orbiters also circle the earth at a much lower altitude (about 850 km) than geostationary satellites (nearly 36,000 km). A sun synchronous orbit satellite (e.g.: NOAA, ERS series (European Remote Sensing satellites); the A-Train constellation, which include four satellites: Aura, CALIPSO, CloudSat, and Aqua) is a polar orbit satellite that passes over the same location at the same time every day (L’Ecuyer and Jiang, 2010; Tapakis and Charalambides, 2012). The surface illumination angle is nearly the same in every revolution, and this consistent lightening is a useful characteristic for satellites that image the Earth surface in VIS or IR wavelengths (weather and spy satellites) and for other remote sensing satellites (ocean and atmosphere remote sensing instruments that require sunlight).

To date, meteorological satellites have recorded information over the Earth at a limited number of wavelengths through the use of specially designed radiometers. These radiometers incorporate filters that allow radiation only over a very narrow wavelength range to pass through towards the detectors. Such narrowband wavelengths are typically chosen in atmospheric “windows”, where the atmospheric constituents such as water vapor and carbon dioxide least attenuate the energy along the path from the surface, through the atmosphere, and finally to the satellite. Typically, operational satellites record images at visible (VIS)

wavelength (e.g., 0.65 μm), near-infrared (NIR) wavelength (3.82 μm) and infrared (IR) wavelength (11 μm). Radiances at visible and near-infrared wavelengths are often converted to reflectances whose values range from 0 to 1. Infrared radiances are often converted to brightness temperatures through application of the Planck function.

Weather satellites, thanks to their on-board imager, provide extremely valuable cloud photographs of areas where there are no ground-based observations (Ahrens, 2009). At visible wavelengths cloudy scenes appear brighter than cloud-free scenes when viewed from above. Thick clouds appear brighter in the photographs because they have higher reflectivity (higher albedo) than thin clouds. Clouds are usually colder than the underlying surface, so the emission of thermal-infrared radiation to space is less than for clear scenes. During the daytime clouds can be detected in both wavelength regions, but at night only in the thermal infrared.

Global cloud observations based on satellite measurements serve in numerical weather models, where the time scale of interest is on the order of hours to days. Specifically, satellite-derived cloud and clear-sky properties from the geostationary satellites serve as initial conditions for models, that is, to describe cloud distribution at a given time. Satellite-derived cloud properties are also useful for developing and testing global climate models where the time scale of interest is months to years. Moreover, Forsythe et al. (2000) and references therein summarize the research oriented to retrieve cloud type and cloud base height, specifically their study describes how the combination of a (visible and infrared) satellite-derived cloud classification (GOES-8) with surface observations can improve analysis of CBH. New generation satellites (e.g. CALIPSO and CloudSat) will allow increasing and improving cloud climatologies (see section 3.2.2).

Several satellite projects have been providing useful data to build cloud climatologies. As explained, cloud climatologies could be developed using visual observations of clouds from the Earth's surface (as coded in weather reports on land and ships in the ocean); or using radiances measured by satellites in polar and geostationary orbits. Measurements from satellites can be used to produce a cloud climatology if the following criteria are satisfied: pixel size is at most a few kilometers, temporal sampling is conducted at regular intervals throughout the day and night, the coverage is global; and a long period of record (many years) is maintained. To satisfy these requirements, the International Satellite Cloud Climatology Project (ISCCP) uses five geostationary satellites that hover over the Equator at five longitudinal locations, and two polar orbiting satellites. This project began in 1983 and continues to 2009 (Warren and Hahn, 2003; ISCCP website). And, at least, to 2013 has been continued with equivalent data named "CERES ISCCP-D2like Product" (<http://ceres.larc.nasa.gov/products.php?product=ISCCP-D2>). ISCCP

reports global distributions of cloud amount, cloud-top temperature/pressure, and optical thickness, among other variables (Rossow and Schiffer, 1991). Specifically, the current ISCCP satellites are: NOAA-# (National Oceanic and Atmospheric Administration), Meteosat-# (EUMESAT), GOES-EAST-# (Meteorological Service of Canada), GOES-WEST-# (Colorado State University), and GMS-# (Japan Meteorology Agency and Meteorological Satellite Center), where # denotes the series number (ISCCP website).

On the other hand, the Nimbus-7 cloud climatology (N7GCC) was formed by National Aeronautics and Space Administration (NASA) in late 1982 and provides information on cloud altitude distributions and cloud amount (Hwang et al., 1988; Stowe et al., 1989). The basic measurements were made by the Temperature Humidity Infrared Radiometer (THIR), onboard Nimbus-6 (similar instruments flown on Nimbus 4, 5 and 7), and the Total Ozone Mapping Spectrometer (TOMS), onboard Nimbus-7 satellite (nssdc.gsfc.nasa.gov/nmc/spacecraftDisplay.do?id=1978-098A).

The NOAA-# series is the Polar Operational Environmental Satellite (POES) group of satellites for weather purposes launched by NOAA. The former versions of the NOAA-# series were the Television Infrared Observation Satellite (TIROS-#) series. The main imager of the NOAA-# satellites is the Advanced Very High Resolution Radiometer (AVHRR), which is a radiation-detection imager used for remotely determining cloud cover and the surface temperature (note that the term surface can mean the surface of the Earth, the upper surfaces of clouds, or the surface of a body of water) (noaasis.noaa.gov/NOAASIS/ml/avhrr.html).

As far as geosynchronous satellites are concerned, the following are the most known for cloud measuring purposes: Synchronous Meteorological Satellites (SMSs) is the name for the first three GOES (Geostationary Operational Environmental Satellite series). The GOES-# satellites have on board the GOES I-M Imager, a five channel (one visible, four IR) imaging radiometer measuring at a wavelength range from 0.65 μm to 12 μm . (www.noaa.gov, www.oso.noaa.gov). The Meteosat series of satellites are operated by EUMETSAT. The imager of the Meteosat satellite series is the Spinning Enhanced Visible and Infrared Imager (SEVIRI) instrument. SEVIRI is a line-by-line scanning radiometer, which provides image data in four Visible and Near-Infrared (NIR) channels and eight IR channels. A key feature of this instrument is its continuous imaging of the earth with a baseline repeat cycle of 15 minutes (www.eumetsat.int). Geostationary Meteorological Satellite (GMS-#) series, better known as Himawari, were operated by the Japan Meteorological Agency. The successor series is called Multifunctional Transport Satellites (MTSAT-#) and consists of MTSAT-1 and MTSAT-2. MTSAT-2, known as

Himawari-7, carries an imaging telescope of five channels: one visible, two IR, one IR/WV and one NIR (www.jma.go.jp/jma/indexe.html).

Other satellites that report some cloud characteristics are briefly described next:

- The Defense Meteorological Satellite Program (DMSP) consists of a series of sun synchronous satellites that provide global VIS and IR meteorological, oceanographic and solar-geophysical data, used for defense operations. Among other imagers, they carry onboard the Special Sensor Microwave Imager (SSM/I), which is a seven-channel passive MW radiometric system that measures brightness temperatures (National Snow and Ice Data Center: <http://nsidc.org/>)
- The Tropical Rainfall Measuring Mission (TRMM) satellite was launched in 1997 in a non-sun-synchronous orbit at a low altitude height of 350 km, with the ultimate objective of measuring rainfall over earth. Among other imagers, it carries onboard the Precipitation Radar (PR), the TRMM Microwave Imager (TMI), the Visible InfraRed Scanner (VIRS), and the Clouds and Earth's Radiant Energy System (CERES). CERES products include both solar-reflected and Earth-emitted radiation from the top of the atmosphere to the Earth's surface. Cloud properties are determined using simultaneous measurements by other Earth Observation System (EOS) and instruments such as the Moderate Resolution Imaging Spectroradiometer (MODIS) and the Visible and Infrared Sounder (VIRS). Analyses using CERES data, built upon the foundation laid by previous missions such as NASA Langley's Earth Radiation Budget Experiment (ERBE), are leading to a better understanding of the role of clouds and the energy cycle in global climate change (<http://trmm.gsfc.nasa.gov/>, <http://ceres.larc.nasa.gov/>).
- The European Remote Sensing (ERS-#) satellite series consists of the sun-synchronous satellites ERS-1 and ERS-2. The ERS-1 mission ended on March 2000 and ERS-2 was retired on September 2011 (<https://earth.esa.int/web/guest/missions/esa-operational-eo-missions/ers>). Among other instruments, ERS-2 had on-board the Microwave Radiometer which main objective was the measurement of the integrated atmospheric water vapour column and cloud liquid water content; the Along-Track Scanning Radiometer (ATSR) which consisted in a IR Radiometer (IRR) and a Microwave Sounder (MS), providing four IR channels, three VIS channels and two passive MW channels for measuring Sea-Surface Temperature (SST) and cloud-top temperatures, among other variables (www.eumetsat.int, www.esa.int/ESA). The successor of ERS-2 is Envisat, which is operational since 2002 and has the improved versions of the imagers of the ERS series such as the Advanced Along Track Scanning Radiometer (AATSR) and the

Medium Resolution Imaging Spectrometer (MERIS) consisting of 15 channels across the 0.390 μm to 1.04 μm spectral range (earth.esa.int/web/guest/missions/esa-operational-eo-missions/envisat).

- The MetOp is the polar orbiting European satellite series equivalent to NOAA-# (US). The first satellite of this group was launched in 2006. Like the NOAAs, MetOp carries onboard the AVHRR (Advanced Very High Resolution Radiometer) and AMSU (Advanced Microwave Sounding Unit) imagers. Furthermore, it flies the Infrared Atmospheric Sounding Interferometer (IASI) that is used for temperature and humidity measurements (http://www.esa.int/Our_Activities/Observing_the_Earth/The_Living_Planet_Programme/Meteorological_missions/MetOp).
- The Landsat-# program started in 1972 with Landsat-1 at first under NASA and then under NOAA responsibility and consists of seven sun-synchronous satellites. The imagers on-board Landsat-7 are the Enhanced Thematic Mapper plus (ETM+), that has eight channels (three VIS, four IR and one panchromatic), and the Multispectral Scanner with five channels in the range of 0.5–1.1 μm (<http://landsat.gsfc.nasa.gov/>).

Besides the US and Europe, other countries have more recently developed satellites with the same characteristics as the described above. Similar products could be obtained from these satellites because they have similar sensors, however no routinely cloud products have been generated so far. Some examples are:

- Fengyun (FY-##) is the name of China's weather satellites (Hong Kong Observatory). The FY-2C carries the Visible and Infrared Spin Scan Radiometer (VISSR) that was used in the SMS satellites, which has five channels in five different spectral bands measuring from 0.550 to 12.500 μm . FY-1 and FY-3 series are in sun-synchronous orbits. FY-3A is the successor of the FY-1 series and was launched in 2008 in order to make global observations of the earth's land, oceans, atmosphere and other parameters in real time (http://www.hko.gov.hk/wxinfo/intersat/fy2e/satpics_vis.shtml). The 11 instruments onboard both platforms (FY-3A/B) include: 1) the Visible and Infrared Radiometer (VIRR); 2) Medium Resolution Imager (MERSI); 3) Infrared Atmospheric Sounder (IRAS); 4) Microwave Temperature Sounder (MWTS); 5) Microwave Humidity Sounder (MWS); 6) Microwave Radiation Imager (MWRI); 7) Solar Backscatter Ultraviolet Sounder; 8) Total Ozone Mapping Unit (TOU); 9) Earth Radiation Measurer; 10) Solar Irradiation Monitor (SIM); and 11) Space Environment Monitor (SEM) (Weng et al., 2012).

- Kaplana-1 known as MetSat-1 is a geostationary meteorological satellite launched by the Indian Space Research Organization on 2002. Kaplana's imager is the Very High Resolution Radiometer (VHRR) which has three channels: the VIS channel (0.550–0.750 μm), the IR channel (10.500–12.500 μm) and the IR/WV channel (5.700–7.100 μm) (www.webcitation.org/5kf22DF7y).
- The Marine Observation Satellite 1 (MOS-1) also called Momo-1 (http://www.jaxa.jp/projects/sat/mos1/index_e.html) and the Advanced Land Observation Satellite (ALOS), also called Daichi, are Japanese satellites (<http://www.jma.go.jp/jma/indexe.html>). MOS-1 is a polar orbiting satellite and ALOS is a low earth orbiting satellite. Both of them have three different operational sensors. ALOS has the most advanced imager from Japan's satellites: the Advanced Visible and Near Infrared Radiometer type 2 (AVNIR-2) comprised of four channels from 0.420 μm to 0.890 μm . MOS-1 has the older Visible and Thermal Infrared Radiometer (VTIR), but cannot provide enough information to distinguish clouds from ice over land or sea (http://www.jaxa.jp/index_e.html).
- Russia's space agency (Roscosmos) launched Elektro-L no.1, also known as Geostationary Operational Meteorological Satellite No.2 (GOMS No.2), which is a meteorological satellite which works in geostationary orbit (<http://www.russianspaceweb.com/elektro.html>).
- KOMPSAT-1 (Korea Multi-Purpose Satellite-1) is a high resolution optical mission from South Korea launched in 1999 (<https://earth.esa.int/web/guest/missions/3rd-party-missions/historical-missions/kompsat-1>), while COMS (Communication, Ocean and Meteorological Satellite) is another Korean satellite with a multi-spectral channel imager capable of providing imagery and radiometric information of the Earth's surface and cloud cover over 5-channels (one visible and 4 infrared channels) (https://www.eumetsat.int/cs/idcplg?IdcService=GET_FILE&dDocName=pdf_conf_p48_s1_02_shim_v&allowInterrupt=1&noSaveAs=1&RevisionSelectionMethod=LatestReleased).

3.2. Cloud vertical structure

Cloud cover and cloud base height are only partial information of the complex geometry of cloudiness fields. For this reason the present study also focuses on the cloud vertical structure (CVS), since this allows a much more complete characterization which, in fact, includes the CBH of each cloud layer. When referring to CVS, we mean description of cloud boundaries (cloud

base height, CBH, and cloud top height, CTH) and cloud thicknesses of the (often more than one) cloud layers.

3.2.1. Remote sensing by active ground-based systems and value added products (ARSCL)

As already mentioned, clouds may occur in distinct layers or in layers that merge together, and layers can conceal and obscure each other. Therefore, human observations provide qualitative visual estimates of heights of clouds and number of layers, but these observations have many problems such as the approximate estimation of heights, cloud obscuration, subjective vision of the observer, etc. So, the primary alternative for observing important cloud properties are radar measurements (which provide cloud height, thickness, number of cloud layers), lidar measurements (for detection of cloud bases), and satellite radiance measurements (for cloud tops estimation). This subsection describes in a simplified manner radar, micro-pulse lidar, and Raman lidar technologies. In addition integrated systems (ARM Climate Research Facility, Cloudnet) and a value added product (ARSCL) provided by ARM are also described.

Cloud radars are active remote sensors that transmit at milli-meter wavelengths (MMCR) and are particularly suited for determining the properties of nonprecipitating clouds such as stratus, altostratus, and cirrus. They typically operate near 35 GHz (wavelength of 8.6 mm, Ka-band) or near 94 GHz (wavelength of 3.3 mm, W-band), which are frequency “window” regions where absorption by atmospheric gases shows at a minimum. Despite this, attenuation from atmospheric liquid water and vapor is more of an issue for these short-wavelength radars than for longer-wavelength (centimeter scale) weather radars. The short-wavelength of cloud radars combined with short power pulses, allows for high-resolution observations (on the order of tens of meters) capable of resolving the fine-scale clouds structure (Uttal, 2003). However, cloud radars often have range limitations of 20 km or less and are not suitable for observing clouds under conditions of moderate to heavy rainfall (Nowak et al., 2008). Other disadvantage of cloud radars is the elevated purchase and maintenance costs. Contrarily, the primary advantage of shorter-wavelength radars lies in their sensitivity to small ice particles and cloud droplets that can be two orders of magnitude smaller than typical raindrops. Some milli-meter wavelength cloud radar systems are ‘multiparameter’; in other words, they transmit and receive electromagnetic waves at more than one wavelength or polarization. Another advantage of cloud radars is that they provide comprehensive and detailed information on the geometrical morphology of clouds within the constraints of attenuation at one end of the detection scale and

non-detection of extremely small cloud hydrometeors at the other. But, in contrast, when interpreting cloud boundaries, it must be considered that there is often no significant difference in radar reflectivities between cloudy regions and adjacent regions of precipitation; so, despite radar is a more powerful instrument than a ceilometer, these regions must be distinguished by the change in structure of the Doppler velocities, the Doppler spectra, or with additional measurements as might be provided by another instrument such cloud base ceilometer or lidar (Uttal, 2003).

Milli-meter wavelength cloud radars were primarily research instruments, typically unique prototypes designed and operated by universities, governments, or private research organizations. In fact, the rapid development of MMCR in the 1990s was largely driven by the need to observe characteristics of non-precipitating clouds in order to determine cloud impacts on global atmospheric radiation and consequences for climate predictions by large global climate models. The 1990s were also the first decade when a few MMCR began operation on a continuous and long-term basis for climate research (Uttal, 2003).

Rotating beam ceilometers and typical ceilometers (e.g. Vaisala CL-31), provide good vertical resolution of CBH (they can locate the bottom of the cloud layers precisely) and higher temporal resolution than visual or satellite observations, as already explained (section 3.1.3). However, more sensitive lidar-based systems such as the Micropulse Lidar (MPL, www.micropulselidar.com) can also provide both column and vertically resolved aerosol and cloud structure and cloud phase. MPL is a zenith-pointing optical remote sensing system that emits laser pulses at 0.532 μm , and can be operated in a polarization mode. Polarization-sensitive detection of elastic backscattered light is useful for detection of cloud phase and depolarizing aerosols. The ARM program has deployed MPL at its instrumented sites, but without polarized detection. Adding an actively-controlled liquid crystal retarder provides the capability to identify depolarizing particles by alternately transmitting linearly and circularly polarized light. This represents a departure from established techniques, which transmit exclusively linear polarization or exclusively circular polarization. MPL presents other differences when compared to a conventional lidar: a high repetition-rate (2500 Hz) and a low-energy (~ 7 mJ) 'eye-safe' laser. The system is able to scan the atmosphere up to 30 km, well above the heights where tropospheric particles or cirrus clouds usually appear (izana.aemet.es), with a good enough signal-to-noise relation,

The NASA Micro Pulse Lidar Network (MPLNET) (Welton et al., 2001) is a federated network of Micro Pulse Lidar (MPL) systems designed to measure aerosol and cloud vertical structure

continuously, day and night, over long time periods required to contribute to climate change studies and provide ground validation for models and satellite sensors in the NASA Earth Observing System (EOS).

A Raman Lidar (RL, Figure 18) is an active, ground-based laser remote sensing instrument that operates by transmitting pulses of laser radiation at $0.355\ \mu\text{m}$ and recording radiation backscattered from the atmosphere as a function of time to provide range information similar to a radar system. The return signal contains a strong elastically scattered component due to scattering from clouds, aerosols, and molecular Rayleigh scattering, but the return also contains weaker inelastically scattered components that provide chemical-specific information. Selected species are detected by measuring the wavelength-shifted molecular return produced by Raman scattering. By taking the ratio of the signal at the water-vapor wavelength ($0.408\ \mu\text{m}$) to the signal at the nitrogen wavelength ($0.387\ \mu\text{m}$), most of the range-dependent terms drop out, and one is left with a quantity that is almost directly proportional to the water-vapor mixing ratio expressed as grams of water vapor per kilogram of dry air (a small correction for the wavelength dependence of the second attenuation term is easily taken into account). Similarly, by taking the ratio of the signal at the laser wavelength to the signal at the nitrogen wavelength, one is left with the aerosol backscatter ratio; this ratio is normalized such that it is unity in “clean air” (laser-wavelength scatter caused only by Rayleigh scattering), and is in excess of unity for scattering by parcels of air that contain aerosols (including cloud droplets/particles). Finally, analysis of the polarization dependence of the backscatter signal at the laser wavelength provides information on particle shape (phase); spherical particles (cloud droplets) do not depolarize the laser backscatter, whereas nonspherical particles (such as ice crystals in cirrus clouds) can significantly depolarize the laser backscatter. A particular mode of operation provides good daytime performance (discrimination of the weak Raman backscatter signal above the background daylight) without sacrificing nighttime performance (Newsom, 2009). In summary, RL can measure cloud base height, time resolved profiles of water vapor mixing ratio, relative humidity, and several aerosol-related quantities (such as aerosol scattering ratio, aerosol extinction, and aerosol depolarization ratio). The system used by ARM is a non-commercial custom-built instrument developed by Sandia National Laboratories (<http://www.sandia.gov/>) specifically for the ARM Program (Newsom, 2009).

Other organizations use RL such as Max-Planck Institute für Meteorologie and at NASA Goddard Space Flight Center. An important network which operates Raman Lidar in Europe is the Aerosols, Clouds, and Trace gases Research Infrastructure Network (ACTRIS) which have the

essential role to support building of new knowledge as well as policy issues on climate change, air quality, and long-range transport of pollutants. Actually, ACTRIS is building the next generation of the ground-based component of the EU observing system, and it integrates three existing research infrastructures: EUSAAR, CLOUDNET (see sections 1.2 and 3.2.1), and EARLINET. The European Aerosol Research Lidar Network to Establish an Aerosol Climatology (EARLINET) is a research lidar network with nowadays 27 stations distributed over Europe, centered in measuring aerosols and their main goal is to provide a comprehensive, quantitative, and statistically significant data base for the aerosol distribution on a continental scale. Note, however, that these networks are focused on aerosol observations, so no further mention to them will be made in this work.

It is usually accepted that most of the ground-based active instruments for cloud characterization must be combined with other instrumentation to avoid underestimation of cloud occurrence and in order to get comprehensive information about the sky condition. For example, Dupont et al. (2011) derived cloud properties from two lidars (RL and MPL) over the ARM SGP site. They concluded that MPL has a limited range compared to the RL and that this creates difficulties in the detection of high clouds, especially during daytime and summer periods: 2 km bias appeared for high clouds CBH. They warn MPL users that during daylight hours the increased noise from solar scattering at the lidar wavelength in essence poses a significant limit on the height of clouds that can be detected. Thus one must exercise caution in using MPL-generated cloud statistics as “truth” especially for high cloud occurrence, as it will be underestimated. Earlier, Moran et al. (1998) had affirmed that instruments that penetrate the cloud such as the milli-meter wavelength cloud radar (MMCR) may be combined with simultaneous measurements by radiometers and lidars to estimate several cloud properties. Similarly, Hogan et al. (2003) investigated the frequency of occurrence of clouds (derived from lidar, radar, and microwave radiometer observations) as a function of temperature obtained from a weather model. Forsythe et al. (2000) noted that the latter instruments do not usually have the spatial or temporal coverage necessary to make them useful for many applications; nowadays, however, these instruments can be operated with a high temporal resolution as in the Atmospheric Radiation measurement program (ARM) sites. Therefore, a combination of ground-based instruments such as MPL, cloud radar and ceilometers are usually applied at research facilities to observe and describe the CVS. They can provide cloud measurements with high accuracy and continuous temporal coverage. Note that radar and MPL are deployed at few locations around the world and their application is limited; ceilometers are commonly located at airports but they are used only for operationally purposes, not for research.



Figure 18. Raman Lidar (ARM webpage and Newsom, 2009).

More specifically, the integration of multiple ground based instruments to obtain a better cloud classification and characterization has been addressed by the ARM Climate Research Facilities (at its sites located in the Southern Great Plains (SGP), North Slope Alaska, and Tropical Western Pacific). At these ARM sites ground-based integrated observations of the sky consisting of several different instruments are provided. This includes in situ and remote sensing instrumentation: milli-meter wavelength cloud radar, micropulse lidars, microwave radiometers, ceilometers, several radar wind profilers, Raman lidar, balloon-borne atmospheric profiling, surface radiation measurements (pyrometers, multifilter rotating shadowband radiometer, rotating shadowband spectroradiometer) and total sky camera. Also, Cloudnet, which is an European research project of seven collaborating countries (UK, France, Germany, Finland, Ireland, Italy and the Netherlands) aiming to optimize the existing data sets from three weather stations and to develop cloud remote sensing algorithms, provides a similar suite of instrumentation at its sites (Illingworth et al., 2007).

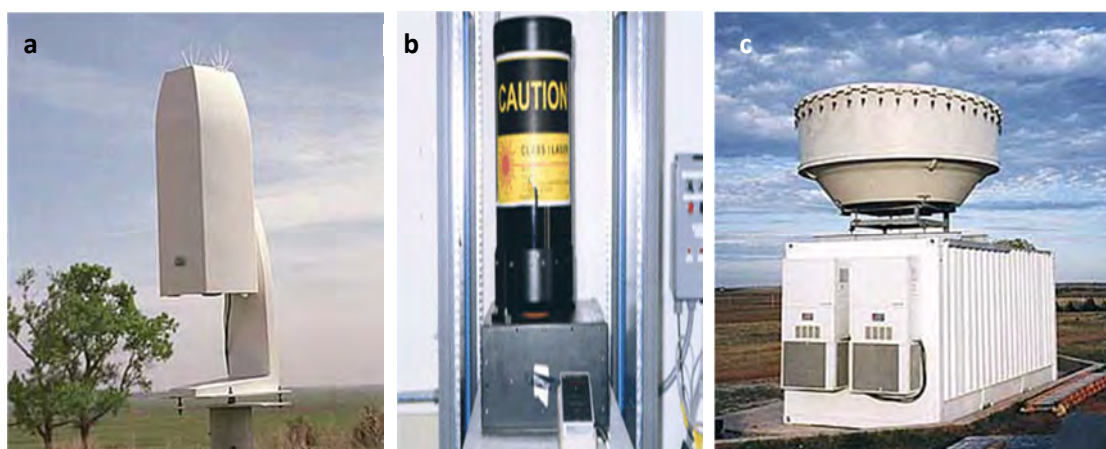


Figure 19. a) Ceilometer CT25K b) Micro Pulse Lidar (MPL), c) Milli-Meter wavelength Cloud Radar (MMCR) (ARM website).

The ARM value added product called ARSCL (Active Remote Sensing of Clouds) produces time series (with 10 s resolution) of vertical distributions of cloud hydrometeors in the main ARM sites: Southern Great Plains (SGP), Tropical Western Pacific (TWP), and North Slope of Alaska (NSA) (Clothiaux et al., 2000). ARSCL is considered the best approximation to the CVS that can be made from the ground, and integrates three ground-based instruments with different ranges of detection: a Vaisala CL25K ceilometer (VCEIL), a Micropulse Lidar (MPL), and a milli-meter wavelength cloud radar (MMCR) (Figure 19). Both MPL and VCEIL cannot penetrate thick low-level clouds to detect any more layers of clouds aloft. However, they can detect clouds that are visible from the ground within the observation ranges, though the MPL does sometimes label as layers with cloud optical thickness less than is typically used as a limit for human and sky imager observations. The greatest strength of the cloud radar is its ability to penetrate clouds and reveal multiple-layer structures but may miss some thin clouds composed of small hydrometeors. Yet the detection of cloud base heights from radar is often affected by the presence of large precipitation particles, as well as insects and bits of vegetation. If such particles are suspended in the atmospheric boundary layer, this may be mistakenly regarded as stratus clouds (Clothiaux et al., 2000).

The characteristics of the three instruments that compose ARSCL are specified in Table 4. Despite providing only a “pencil” beam, cloud radar–lidar systems can provide more accurate cloud vertical distributions and compensate for most of the shortcomings in cloud vertical distributions from surface observers and even from satellite imagery (Xi et al., 2010).

Table 4. Characteristics of instruments used as the basis of ARSCL value added product and, for comparison, the characteristics of the most used ceilometer (Vaisala CL-31, also used in Girona site) (extracted from the corresponding Handbooks from ARM Climate Research Facility).

	VCEIL (Vaisala CL25K ceilometer)	VCEIL (Vaisala Ceilometer CL-31)	MPL (Micropulse lidar)	MMCR (Milli-meter wavelength Cloud Radar)
Vertical range		7700 m	Up to 20 km	Up to 20 km
Maximum range for cloud base height	7500 m	7500 m	18 km	
Resolution	15.24 m (50ft) and 15s	10 m	15 m	
Wavelength	0.905 μm	0.910 μm (at 25°C)	0.532 μm	8.66 mm, Ka-band (Frequency 34.86 GHz)
Accuracy/uncertainty	$\pm 2\% \pm \frac{1}{2} \times$ [resolution]	$\pm 1\%$ or ± 5 m	$\pm 2\%$	
Minimum detection height	0 m	0 m	150 m	

Cloud boundaries (cloud base and top, CBH and CTH) are the most important variables for this study and the ARSCL product is taken here as a reference. The main product from ARSCL is the Cloud Base Best Estimate (CBBE) which is determined from MPL and VCEIL measurements only (no MMCR data are used). If the ceilometer first cloud base is between 0 and 3000 m, the ceilometer value is used; if the ceilometer cloud base is above 3000 m, but within 600 m of the MPL first cloud base, the ceilometer value is used. Otherwise, the MPL first cloud base is used. The difference between cloud height determination algorithms using VCEIL and MPL is that MPL uses a threshold variation to identify the cloud bottom, which ceilometers uses a calculated vertical visibility threshold of 100 m. This means that the ceilometer will not classify thin cloud regions that MPL would identify and usually gives a slightly higher cloud bottom height (Morris, 2012). Besides the CBBE, ARSCL provides bases and tops for up to 10 cloud layers, based on MMCR and MPL data. The best situation is when the cloud top is determined by MMCR; if

information from this instrument is not available, the cloud top is derived from MPL, and if the MPL beam is attenuated by the lower cloud then the cloud top is considered as not being retrieved.

3.2.2. Satellite observations (the A-train)

As already explained in section 3.1.5, satellites can observe the Earth in the visible, near-infrared and infrared wavelengths; and from a geostationary or polar –either sun-synchronous or non-sun-synchronous- orbit. Regarding CVS characterization, the altitude of the cloud top is inferred by relating the infrared emission temperature to the vertical profile of temperature obtained from radiosondes or other satellite sounders. Cloud optical thickness (opacity) is inferred from reflectance in the visible channel. If a second solar channel (in the near infrared) is available, then the vertically integrated liquid water content, and the effective radius of the droplets, can also be inferred (Warren and Hahn, 2003). More detailed information about clouds can be obtained from satellite instruments with finer spatial resolution (e.g., Landsat), and from satellites with more spectral channels (e.g., the Moderate Resolution Imaging Spectrometer (MODIS) on the Earth Observation Satellite (EOS)). An example of the use of radiosondes combined with satellites instruments (MODIS) was provided by Jin et al. (2007), which explored the detection of cloud vertical structures over the Arctic. Jin et al. (2007) also recalled the importance of obtaining the cloud vertical structure by using ground-based active instruments because, in the past, satellite-based cloud datasets retrieved from passive remote sensing techniques were unable to provide the CVS.

Table 5. The most interesting instruments, related to cloud characteristics, in the A-Train constellation and their primary purpose (adapted from L'Ecuyer and Jiang, 2010).

Satellite	Instrument	Primary data
Aqua	Atmospheric Infrared sounder (AIRS)	Temperature and humidity profiles and clouds
	Advanced Microwave Scanning Radiometer for EOS (AMSR-E)	Cloud liquid water path
	Advanced Microwave Sounding Unit-A (AMSU-A)	Temperature and humidity profiles
	Clouds and the Earth's Radiant Energy System (CERES)	Top-of-the-atmosphere radiation balance
	Moderate Resolution Imaging Spectroradiometer (MODIS)	Spatial distributions of aerosols and clouds
CloudSat	Cloud Profiling Radar (CPR)	Vertical structure of cloud properties
CALIPSO	Cloud-Aerosol Lidar with Orthogonal Polarization (CALIOP)	Vertical structure of thin clouds and aerosols
	Imaging Infrared Radiometer (IIR)	Cirrus cloud emissivity and particle size
	Wide Field Camera (WFC)	Imaging
AURA	Ozone Monitoring Instrument (OMI)	Total column ozone and other trace gases, including HCHO, NO ₂ , ClO, OCIO, and BrO
PARASOL (inoperative since 2009)	Polarization and Directionality of the Earth's Reflectances (POLDER)	Aerosol composition, cloud particle size and phase

Three-dimensional information about clouds can be obtained from satellites that look at the same scene from different angles (e.g., the Multi-angle Imaging Spectroradiometer, MISR onboard Terra Satellite). These instruments are useful for studying cloud properties but do not yet offer sufficiently long periods of record to produce a climatology (Warren and Hahn, 2003).

Nowadays, new instruments onboard of a new generation of satellites are providing details about the cloud vertical structure. This is particularly true for the so-called A-Train, a series of satellites that orbit all together (see some instruments onboard A-Train constellation and their primary purpose in Table 5). More specifically, we must highlight here two active sensors onboard of two satellites. First, the Cloud–Aerosol Lidar with Orthogonal Polarization (CALIOP, a two-wavelength polarization-sensitive lidar that provides high-resolution vertical profiles of aerosols and clouds (Kim et al., 2011; Rossow and Zhang, 2010) onboard a sun synchronous satellite which was launched in 2006 to study the impact of clouds and aerosols on the earth’s radiation budget and climate named CALIPSO (Cloud-Aerosol Lidar and Infrared Pathfinder Satellite Observation). Second, the Cloud Profiling Radar (CPR) onboard CloudSat, a satellite that provides observations about cloud amount, distribution, structure, and radiative properties. CloudSat was the first satellite that integrated the very sensitive milli-meter wavelength CPR that allows the detection of small particles of liquid water and ice, within large cloud masses (Kim et al., 2011; Rossow and Zhang, 2010). The combination of the measurements from these two satellites, CALIPSO and CloudSat, provides a 3-D perspective of how clouds and aerosols form, evolve, and affect weather and climate, and they are achieving notable results regarding the addition of a vertical dimension to traditional satellite images. However, because the repeat time for any particular location is very large, the time resolution of such observations is low (L’Ecuyer and Jiang, 2010; de Leeuw et al., 2012). In this sense, Kotarba (2009) discussed the matching between satellite and surface-based observations of clouds, and proved that surface data collected within 30 min before or after a pass by any satellite sensor can be used as a good approximation of exactly matched observations.

CloudSat was manufactured concurrently with CALIPSO to join three satellites already in orbit (Aqua, PARASOL, and Aura) building a constellation of five sun-synchronous satellites known as the A-Train (L’Ecuyer and Jiang, 2010). Furthermore, Aqua has onboard the MODIS imager and the Atmospheric Infrared Sounder (AIRS), designed to provide atmospheric temperature, water vapor profiles and cloud properties. Parasol (inoperative since 2009) had onboard the Polarization and Directionality of the Earth’s Reflectances (POLDER) instrument that retrieved the microphysical properties of clouds. POLDER had 9 spectral bands that cover a spectral range

from 0.443 μm to 0.910 μm (L'Ecuyer and Jiang, 2010) (CNES, website). The primary cloud monitoring instrument on Aura is the Ozone Monitoring Instrument (OMI). OMI is an UV/ VIS nadir solar backscatter spectrometer, covering a total spectral range from 0.27 μm to 0.5 μm , that measures cloud pressure and coverage and distinguishes different aerosols in the atmosphere in order to derive the ozone in the troposphere (L'Ecuyer and Jiang, 2010; Tapakis and Charalambides, 2012).

3.2.3. Aircraft in situ measurements

There are two kind of aircrafts that may take in situ measurements of atmospheric variables: those airplanes dedicated exclusively to collect cloud/aerosol characteristics (drop size, cloud base heights and tops, cloud water path, etc.) for research purposes (Chernykh and Aldukhov, 2004; Dimitrieva-Arrago and Shatunova, 1999); and the commercial airplanes which are not intended for sampling the atmosphere but which nevertheless may give some useful data (e.g.: temperature, humidity) (Ballish and Kumar, 2008).

Some examples of data taken from research aircraft to obtain the CBH in-situ can be seen in Chernykh and Aldukhov (2004) where the National Center for Atmospheric Research (NCAR) C-130Q research aircraft measurement are used. Dimitrieva-Arrago and Shatunova (1999) also used data from aircraft measurements (mostly for stratiform clouds) conducted by specialists of the Russian Hydrometeorological Scientific Research Center to obtain characteristic values of dew point depression in clouds and develop their method to obtain the CVS from radiosoundings. Previously, Dimitrieva-Arrago and Koloskova (1969) had carried out a comparison of CVS (location of cloud boundaries and cloud thickness) calculated using characteristic values of dewpoint depression (ΔT_d) with real cloud distributions derived from aircraft data. Moreover, in-situ measurements done by airborne instrumentation are quite common in cloud and/or aerosol microphysical studies, such as Leitch et al. (2010) who study the effect of carbonaceous aerosol particles on the reflectivity of sunlight by water clouds, or a more recent study by Delanoë et al. (2013) which illustrates the high potential of a French airborne radar–lidar instrument for studying cloud processes and evaluating satellite products when satellite overpasses are available.

Nowadays, there are specific databases (e.g. Aircraft Communications, Addressing, and Reporting Systems, ACARS) devoted to collect the temperature, humidity and wind profiles (among other variables) from commercial airplanes. In 2008 there were about 150,000

automated aircraft reports per day (Ballish and Kumar, 2008) and these profiles are growing in number. This kind of meteorological information is of good quality and can be a valuable source of wind and temperature data for operational weather forecasting (de Haan et al., 2013) and also for CVS determination. However, airplanes tend to avoid clouds because they can be directly affected by inclement weather. So, when major storms occur, airplanes often do not fly (Moninger et al., 2003). Thus, the use of aircraft in cloud related studies may potentially introduce a bias due to biased sampling. Other matters such as the warmer temperatures usually recorded by airplanes (Ballish and Kumar, 2008) and the trajectory of aircraft profiles (Schwartz and Benjamin, 1995) should be taken into account, if applying the methods to obtain the CVS to aircraft temperatures and humidity profiles.

3.2.4. Radiosoundings

Radiosounding is an in situ measurement technique performed by a radiosonde, which is an expendable, balloon-borne device that measures the vertical profile of meteorological variables and transmits the data to a ground-based receiving and processing station (Dabberdt et al., 2003). Historically, the first balloons were used as vehicles or were manned to make the first atmospheric observations: specifically, the first observations of scientific interest were those of Robertson in 1803 and of Gay-Lussac and Biot in 1804. They demonstrated the decrease of temperature, pressure, and moisture with height and the constant composition of air up to an altitude of 7000 m (Pommereau, 2003). The greatest progress in atmospheric science and meteorology came from the use of unmanned balloons. The first series of unmanned ascents for studying the upper atmosphere were launched by Hermite and Besançon in 1892 in France; they used an onboard recording thermometer, barometer, and hygrometer, which were recovered after the flight. The next important technical step forward was that of Assmann in Germany, who in 1901 suggested the use of small rubber dilatable balloons and a parachute for safe recovery of the instruments. With such a system, a record altitude of 37,700 m was reached at Pavia in Italy in 1912 (Pommereau, 2003). Another breakthrough in atmospheric science was the invention of the radiosonde by Idrac and Bureau in 1929, who added a radio transmitter which allow sending the air characteristics data acquired during the elevation of the balloon, thus eliminating the need to wait for an unpredictable and sometimes very time-wasting recovery of the sonde (Pommereau, 2003). Then, a computer rapidly reconverts the various radio signals into values of temperature, pressure and moisture (when winds are added, the observation is called a rawinsonde) (Dabberdt et al., 2003), and therefore a thermodynamic diagram can be

drawn (Figure 20). More recently, many improvements have been added: neoprene balloon material, much more sensitive sensors, miniaturized electronics, Omega navigation system, and the Global Positioning System for the location of the sonde.

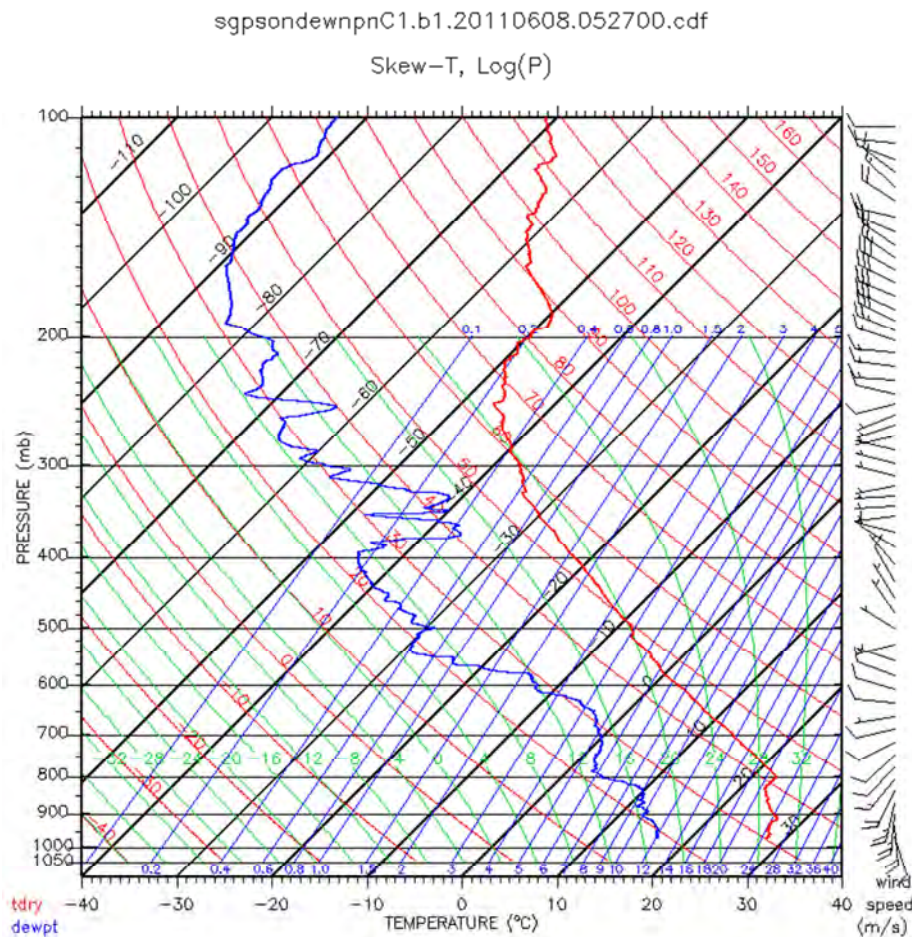


Figure 20. A thermodynamic diagram build from data collected by a radiosonde in Southern Great Plains on 8 June 2011 at 05:27h (Skew-T, Log(P) Diagram).

Currently available balloons allow a variety of in situ and remote sensors, making measurements from the ground up to about 40 km at relatively low cost, thus allowing the repetition of the measurements over a long period. The thermodynamic profiles are typically obtained twice each day (00.00 UTC and 12.00 UTC) and continue to be the backbone of an eclectic suite of measurement technologies used to provide data for input to numerical weather forecast models (Dabberdt et al., 2003). Other uses of radiosonde data include climate studies, air pollution investigations, aviation operations, and defense applications. There are also other special

radiosonde-based instruments, such as (extensive information to be found in Dabberdt et al., 2003):

- Automated Shipboard Aerological Program (ASAP): is a multinational effort to obtain upper-air soundings over the oceans. RS are launched from commercial ships using a special designed launch system.
- Dropsonde (or upsonde): these are ejected from research aircraft and float towards the surface on a special balloon-like parachute; they measure temperature, humidity, pressure and winds (*i.e.* dropwindsonde: specialized in forecasting hurricane movement).
- Driftsonde system: could fill the gaps in data coverage over oceanic and remote arctic and continental regions. The driftsonde concept seeks to obtain a large number of high-vertical-resolution GPS dropsonde profiles through the lower stratosphere and the entire troposphere by autonomous launching of dropsondes from specially designed balloon platforms.
- Rocketsonde: is similar to a dropsonde except that a rocket is used to carry the sonde to the desired deployment altitude where the sonde is ejected and floats to Earth on a small parachute.
- Ozonesondes: carry an ozone sensor, to get description of the stratospheric ozone layer.
- Radioactivity sondes.
- Pibals (pilot balloons): for determining the winds aloft.

In few words, a radiosonde (some models are shown in Figure 21) is a small, lightweight box equipped with various electronic weather instruments (thermometers, barometer and humidity sensor), a radiotransmitter, and a Global Positioning System (GPS) in order to track the exact displacement, all attached to a gas-filled balloon (Ahrens, 2009). The balloon is filled with hydrogen or helium in order to rise at an altitude of more than 30 km at a theoretical speed of approximately 5 m/s.

Additionally, thermodynamic profiles obtained by radiosondes may be used to guess the base, thickness and top height of clouds, by applying an adequate methodology. A major advantage of radiosounding is that multilayer clouds can be detected since the sonde crosses every level of the atmosphere (Chernykh and Eskridge, 1996; Zhang et al., 2010). Furthermore, the horizontal displacement of the balloon is an indication of the wind speed and direction at any given layers of the atmosphere, which at the same time become a double-edged sword when trying to characterize the cloudiness above a specific site, as it will be discussed later.



Figure 21. Most used worldwide radiosonde models: a) Vaisala RS-80 (public domain, Wikimedia commons); b) Vaisala RS-9 (Vaisala website); c) Vaisala RS41 radiosonde (Vaisala website); d) GPS Mark II Microsonde (Sippican website); e) M2K2-DC (Meteo Modem website); f) M10 GPSonde (Meteo Modem website); g) RS-06G GPS radiosonde from MEISEI (Japan); h) DFM-09 radiosonde (Graw website); i) Inside view of SRS-C34 radiosonde (Meteolabor website).

Thus, vertical profiles from radiosondes have been used by several authors to develop climatologies of CVS (Poore et al., 1995; Wang and Rossow, 1995; Wang et al., 1999, 2000), despite other studies like Elliott and Gaffen (1991) that and alert about the use of radiosoundings for climate studies due to their inhomogeneity. This later study explains that upper-air data is taken largely for weather forecasting purposes, not to study the climate. They made a register of which changes suffer the US RS from the early 1940s and conclude that the upper-air data

record for the US is not homogeneous, especially before 1973, because of problems with the humidity data in cold, dry conditions.

Radiosondes can penetrate atmospheric (and cloud) layers to provide in situ data. The vertical distributions of temperature, relative humidity and pressure measured by radiosondes are fundamental to the study of atmospheric thermodynamic and dynamic processes (Zhang et al., 2010). Actually, radiosoundings were probably the best method to obtain the CVS from the ground before the ARSCL development; currently they are the only solution to get a ground-based, global knowledge of CVS thanks to the global network of radiosonde launching stations. Moreover, radiosoundings are used as a reference against other techniques, for example in Wang et al. (2000) the CVS and its variations were studied from a 20 years of global rawinsonde dataset against ISCCP results, and in Zhang et al. (2010) an analysis of cloud layer structure was analyzed by using RS92 radiosonde aided by a 95GHz cloud radar, an MPL and a ceilometer. A recent study, Zhang et al. (2013), presents a radiosonde-based cloud layer detection method, based on Zhang et al. (2010), validated against ground-based remote sensing at multiple ARM sites.

There are available in the literature several methods to determine the CVS from radiosonde data. In the present study, six of these methods are applied to a number of atmospheric profiles obtained at the ARM Southern Great Plains (SGP) site, and their results are compared among them and with ARSCL. All methods establish some conditions on the relative humidity (or equivalent magnitudes, such as dew point depression) or its vertical variation to consider if there is a cloud in every atmospheric level/height. Some of them add other conditions related to cloud layers depth, and they are different, for example, regarding the vertical resolution required on the profile derived from the radiosonde data. The methods examined here are those by Poore et al. (1995); Wang and Rossow (1995); Chernykh and Eskridge (1996); Dimitrieva-Arrago and Shatunova (1999); Minnis et al. (2005) and Zhang et al. (2010). All these methods are extensively explained in next section (3.3.2-b).

The major reasons of using RS to provide the CVS are that the atmosphere profile data provided by the RS conveys valuable and independent information on the presence of clouds that could help identify any deficiencies of the ground-based remote product, and vice versa (Zhang et al., 2013); and because RS data from around the world have been collected routinely for many decades, whereas only a handful of ARM-like stations have been established over the past decade, such as the Cloudnet in Europe (e.g. Illingworth et al., 2007).

The most broadly used radiosondes at present are detailed next (Nash et al., 2011)(Figure 21, Table 6):

- Radiosondes RS41 and RS92 (Vaisala): Vaisala Company (headquartered in Helsinki) manufactures about 70% of the global supply of radiosondes. Vaisala was founded in 1936 by Professor Vilho Vaisala, who in 1931 invented one of the world's first radiosondes (Dabberdt et al., 2003). RS41 is the newest RS which offers higher resolution of temperature, humidity and pressure measurements than others. RS41 uses a platinum resistor as a temperature sensor, RS92 uses a capacitive wire, and both use a thin-film capacitor in order to measure the humidity (www.vaisala.com).
- M2K2-DC and M10 GPSonde (Meteo Modem): the use of M2K2-DC is widespread in the operational SYNOP upper air network of major and smaller National Meteorological Services. M10 GPSonde is the latest generation of Modem's radiosondes new generation (<http://www.meteomodem.com/rproduit.php?nom=M10>).
- GPS MARK II Microsonde (Sippican): has a thin rod thermistor as a temperature sensor, a carbon-made humidity sensor and a continuously variable capacitance aneroid as a pressure sensor (<http://www.sippican.com/>).
- RS-06G GPS (Meisei): is a Japan model of radiosonde with a thermistor tungsten helix as a thermometer sensor, and it is equipped with a GPS (http://www.meisei.co.jp/english/products/meteo/rs06g_gps_radiosonde.html).
- DFM-09 (Graw): is a German radiosonde with a thermistor as a temperature sensor, and a thin film capacitor as a pressure sensor (<http://www.graw.de/>).
- SRS-C34 (Meteolabor): is a Swiss model radiosonde with a thermocouple as a temperature sensor, a hypsometer as a pressure sensor, and a hygistor as a humidity sensor and optionally equipped with an H2C sensor (polymer) or SnowWhite hygrometer. Additionally, some models are GPS equipped (<http://www.meteolabor.ch/en/>).

Table 6. Currently used radiosondes (radiosonde brand websites; Nash et al., 2011).

Brand (Country)	Model	Temperature sensor				Humidity sensor				Pressure sensor				Op.T.* (h)	GPS height
		Type	Range (°C)	Res.* (°C)	Acc.* (°C)	Type	Range (%)	Res.* (%)	Acc.* (%)	Type	Range (hPa)	Res.* (hPa)	Acc.* (hPa)		
Vaisala (Finland)	RS41	Platinum resistor	+60 to -90	0.01	0.1 - 0.4	Thin-film capacitor	0 to 100	0.1	2 - 4	Calculated from GPS	Surface to 3	0.01	1 to 0.04	> 4	Yes
	RS92	Capacitive wire	+60 to -90	0.1	0.15 - 0.5	Thin-film capacitor, heated twin sensor	0 to 100	1	2 - 5	Silicon	1080 to 3	0.1	0.3 - 1	2.25	Yes
Meteo Modem (France)	M2K2-DC	Thermistor	+60 to -90	0.1	±0.5	Capacitor (polymer)	0 to 100	1	±5	-	1100 to 3	0.1	0.1 - 1	> 3	-
	M10	Thermistor	+60 to -90	0.1	0 - 0.5	Capacitor	0 to 100	1	±5	-	1100 to 3	0.1	0.1 - 1	> 3	-
Sippican (USA)	GPS Mark II Micro-sonde	Thin rod thermistor	+60 to -90	0.1	±0.2	Carbon	5 to 100	1	2	Continuously variable capacitance aneroid	1080 to 3	0.1	±0.5	-	-
Meisei (Japan)	RS-06G GPS	Thermistor (tungsten helix)	+40 to -90	0.1	±0.5	-	1 to 100	0.1	±7	Yes	1050 to 3	0.1	±0.5 to ±1	-	Yes
Graw (Germany)	DFM-09	Thermistor	-	0.1	< 0.2	Thin-film capacitor	-	1	< 5	-	-	0.3	-	-	-
Meteo-labor (Switzerland)	SRS-C34	Thermocouple	-100 to +60	0.01	0.1	Hygroclip Rotronic (hygristor)	5 to 100	1	2	Hypsometer	5 to 1100	0.1	0.2	3 to 5	Depending on the model
						H2C SENSOR (polymer, optional)	1 to 100	0.1	1						
						SnowWhite® hygrometer (optional)	2 to 100	0.1	1						

* Res.: resolution; Acc.: accuracy; Op.T.: operating time.

3.3 Methodology

3.3.1 Cloud cover and cloud base height from ceilometer measurements (Girona)

In Girona (NE of the Iberian Peninsula) the Environmental Physics Group of the University of Girona maintains, since December 2006, a laser ceilometer model *CL-31* from *Vaisala* (Figure 22), which is installed on the roof of a building of the Escola Politècnica Superior (41°57'48"N, 2°49'52"E, 110 m asl). This ceilometer takes backscattering profiles up to 7620 m, from which the CBH for up to three cloud layers are accurately retrieved by the algorithm provided by *Vaisala*. The central wavelength of the emitted light is about 910 nm, the vertical resolution has been programmed to 10 m, the measurement interval is 2 s, backscatter profiles are stored every 12 s, and accuracy (against reflector) is $\pm 1\%$ or $\pm 5\text{m}$ (Morris, 2012; Vaisala Oyj., 2006; and Vaisala website). This is a widely used instrumentation around the world, both in meteorological stations and airports, especially for the accuracy in its measures (see section 3.1.3).

It is also important to remind that ceilometer's maintenance is normally limited to window cleaning. Warnings and alarms are checked regularly (daily), and if there was a malfunction it will be reported in the data and status messages and fixed immediately. In addition, proper function of the window blower, the only mechanically moving part, is automatically checked every hour (Vaisala Oyj., 2006). The only major malfunction during the study period was a laser diode exhaust in 2010; consequently, the laser transmitter was changed in June 2010.

Other radiation (pyranometers, pyrgeometer, UV radiometer, pyrhelimeter, a multifilter radiometer (MFR7), etc.) and meteorological (barometer, thermometer, hygrometer, pluviometer, anemometer and weather vane) sensors, as well as an upwards looking hemispherical camera (Whole Sky Camera, WSC) operating continuously (Long et al., 2006b) are installed at the same place. The WSC takes images routinely on daytime and is provided of a shadowing system (it is installed on a sun tracker). The images are taken in two different formats: every minute as low-resolution jpg files (which is enough to infer cloud macrophysical properties, such as fractional sky cover, and potentially, the cloud type, see Long et al. (2006a) and Calbó and Sabburg (2008); and every fifteen minutes as high resolution bmp files (which are showed in the UdG website). Although the station is not part of any national or international network, it is running under the recommendations of the BSRN (Viúdez-Mora, 2011). There are also available surface cloud observations performed at Girona's airport, approximately 10 km away (143 m asl altitude) from the University site (Llach and Calbó, 2004); some of these data were used for comparison with cloudiness estimations made with the ceilometer.

The climate in Girona is predominantly Mediterranean, which main characteristic is that in summer the hottest temperatures coincide with the driest season (Girona's summer mean precipitation in the 1961-1990 period was 140-160 mm). This produces a lack of water and a dry soil and environment (Girona's annual hydric deficit is 100-200 mm, according to an evapotranspiration estimate using Thornthwaite formulation (Institut Cartogràfic de Catalunya, 2008)). The mean annual temperature in Girona is around 14-15°C and the annual temperature range is between 16-17°C. Girona has mild and dry winters (Girona's winter mean precipitation in the 1961-1990 period was 160-180 mm); in summer the anticyclonic stability domains and it is hot (temperatures often soar to about 30–40°C in the high season of July and August, and the minima do not descend under 20°C at night). The precipitation in the Mediterranean climate regions is not fairly sorted into the four seasons: the seasonal rainfall regime in Girona is Autumn-Spring-Winter-Summer. Rain is not frequent neither abundant but often has torrential characteristics. The dominant western fluxes become less wet as it cross the Iberian Peninsula, and when reach Girona they almost are unrecognizable as a maritime air mass. On the other hand, in warmer months the subtropical high pressures domain and then the Mediterranean Sea plays a major role in the precipitation. Specifically, Girona climate could be subclassified as Mediterranean climate with Catalan oriental "façade" (Martín Vide, 2001), which main characteristic is the pronounced rainfall maximum in autumn (Girona's autumn mean precipitation (1961-1990) was 240-260 mm), and its torrential character (Institut Cartogràfic de Catalunya, 2008). Moreover, Girona is a small city with approximately 100,000 inhabitants; it is lowly polluted and the load of atmospheric anthropogenic aerosol is low. The annual mean daily global irradiation is 14-14.5 MJ/m² (Institut Cartogràfic de Catalunya, 2008).

Using the instrumentation available at Girona, and in particular, data from the ceilometer, the temporal behavior of two cloudiness characteristics has been analyzed: cloud cover and cloud base height. For example, whole sky camera images, data from a pluviometer, some data from radiometers, and synoptic maps were used to check and illustrate the behavior of clouds as detected by the ceilometer in some case studies. Regarding cloud cover, it must be recalled that, strictly speaking, cloud cover is defined as the fraction of sky covered by clouds in a plain view. The term 'cloud fraction' is used to define the cloud cover measured by an angular vision instrument or by an observer. Both magnitudes, sometimes used indistinctly, are quantitative descriptors of cloudiness. Moreover, 'cloud occurrence' corresponds to the accounting of presence of clouds as detected by some instrument, and is sometimes used as an estimator of cloud cover. In Girona these estimations were made with the ceilometer and compared among observations from Girona's airport and from published climatologies.

In fact, the ceilometer's manufacturer (Vaisala) provides a sky condition algorithm, which is optional software that produces sky condition information from a single CL-31 ceilometer; this algorithm is generally used in automatic surface weather stations and airport weather monitoring systems. The purpose of the algorithm is to indicate the sky condition up to three layers (from clear sky to overcast) and the total cloud amount based on the ceilometer measurements only from one single point. The sky condition algorithm uses a time series of ceilometer data to calculate the cloud amount of different cloud layers and the corresponding layer heights. The conventional algorithms evaluate a histogram of cloud hits during the last 30 minutes. Instead of forming a histogram of hit heights, the algorithm uses both height and timing information to find those hits that are close to each other and are combined into clusters. After clusters have been formed a height value will be calculated for each cluster. The algorithm reports layers by combining those clusters whose heights are close to each other and then selecting those clusters that cover the greatest amount of the sky. The sky condition message is calculated every five minutes based on data collected during the last 30 minutes. The last 10 minutes are double-weighted (Vaisala Oyj., 2010).

Instead of this treatment, in this thesis another methodology to estimate the cloud cover from the ceilometer data is applied. Specifically, cloud occurrence is used here as an estimator of the cloud cover and it is defined as the ratio between the number of registers with detected clouds (i.e. at least one CBH value) with respect the total available records in a given period of time (one month in the present study). This, the estimation of the average monthly cloud cover from the monthly cloud occurrence, is the first analysis performed here with ceilometer data. The denomination (cloud occurrence) has also been used by Poore et al. (1995), Wang and Rossow (1995), Wang et al. (1999) and Wang et al. (2000), where cloud layers derived mainly from radiosonde profiles are reported and analyzed. However, they used the term with a different meaning, in order to account the existence (or not) of a cloud in a given level of the atmosphere.

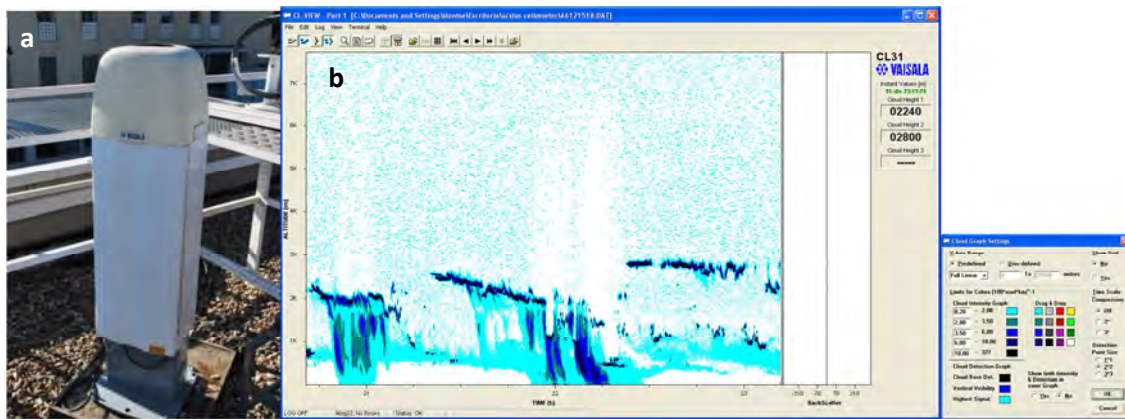


Figure 22. a) Vaisala CL-31 ceilometer and b) CL-View, the ceilometer's software (Girona, Spain).

A period of 4 years of ceilometer measurements, from January 2007 to December 2010, was analyzed, both for estimating cloud cover from cloud occurrence as explained, and also for statistically describing the behavior of the CBH. From the total possible measurements in this period, nearly the 92% is available. In fact, 17 months out of the 48 have 100% of data, and for most months there is more than 80% of the possible data to do the statistical analysis. Exceptions are May and June 2010, which present lower percentages of availability (54% and 45% respectively) because the ceilometer was in maintenance and calibration service, and July and August 2010 (60% and 68%) when power faults in the building caused by thunderstorm episodes resulted in some missing data. Since the amount of available data for these four months is still enough to make statistical statements, we have applied the same data treatment. Despite the relatively short period (4 years), the high frequency of measurements (12 s) results in a very large dataset with more than 9.5 million records.

3.3.2. Cloud vertical structure from radiosoundings and ARSCL (Southern Great Plains)

The Southern Great Plains Central facility (SGP, Lamont, OK) ($36^{\circ} 36' 18.0''$ N, $97^{\circ} 29' 6.0''$ W, 320m asl altitude) was the first field measurement site established by DOE's Atmospheric Radiation Measurement (ARM) Program. Scientists are using the information obtained from the SGP to improve cloud and radiative models and parameterizations and, thereby, the performance of atmospheric general circulation models used for climate research. The SGP was chosen as the first ARM field measurement site for several reasons including its relatively homogeneous geography and easy accessibility, wide variability of cloud type and surface flux properties, and large seasonal variation in temperature and specific humidity. Also, it already

had a large, existing network of weather and climate research and instrumentation. All this instrumentation contributes to the field of atmospheric research and furthering our understanding of atmospheric radiation and its interactions with clouds, aerosols, and gases. The SGP site consists of in situ and remote-sensing instrument clusters arrayed across approximately 55,000 square miles (143,000 square kilometers) in north-central Oklahoma, and is the largest and most extensive climate research field site in the world and can be viewed as a real "laboratory without walls". More than 30 instrument clusters have been placed around the SGP site, at the Central Facility and at Boundary, Extended, and Intermediate Facilities. The locations for the instruments were chosen so that the measurements reflect conditions over the typical distribution of land uses within the site (Ackerman and Stokes, 2003; Ackerman et al., 2004) (ARM website). This site was chosen from this study because it has such amount of instrumentation and measurements so it is very well suited for comparing measurements from RS with the ARSCL product.

The SGP represents the interior regions of many mid-latitude continents, where the clouds are driven by frontal systems or by heating and local convection. The convection is usually short lived over the SGP, and the site does not have the extensive cirrus clouds that are found in tropics (Mace and Benson, 2008). Shallow cumuli often form in spring and summer under stable synoptic conditions with a strong surface forcing and well-developed boundary layers (Qian et al., 2012).

3.3.2-a. Selecting suitable cases (horizontal displacement of the radiosonde and GOES images)

Data from 259 situations (corresponding to 65 days) from the SGP have been randomly selected and may be representative of all seasons of year 2009. The sonde model used at the SGP Central Facility in the year 2009 was the RS92-KL (Figure 21) manufactured by Vaisala and launched, in general, four times per day (Holdridge et al., 2011). The schedule for the routine launch operations is 2330, 0530, 1130, and 1730 UTC which corresponds to 6:30 pm, 12:30 am, 6:30 am, and 12:30 pm Central Daylight Time (CDT). The used profiles have a high vertical resolution (less than 10 m) as result of considering measurements every 2 s and an ascent rates in the range 2.5-5.5 m/s. Besides pressure, temperature and relative humidity, altitude and dew point temperature (among others) are provided in the radiosounding files.

Because of the movements of clouds (and also of the RS), comparisons of cloud boundaries cannot be limited to an instantaneous moment but must be made for a time range which is set to half an hour in this study (note that Zhang et al. (2013) used the same range in their study) . One radiosonde launch usually takes about 1.5 h to complete, but in the first half-hour, the balloon usually goes beyond the troposphere. Also balloon drift can cause a serious misalignment and thus degrade comparison results (Zhang et al., 2013). For this reason here some GOES images are used to assure the cloud situation of the radiosoundings studied.

The radiosonde horizontal displacement, due to the drift produced by the wind, must be taken into account because it could add some mismatch when comparing the clouds detected by the RS methods with the ARSCL “pencil view”. In order to address this issue, in Figure 23 the horizontal displacement depending on the vertical position has been represented as a box-plot diagram for the whole RS dataset. At maximum level of low clouds base (2 km), displacements are between 0.4 and 11 km. At 6 km height, the boundary between middle and high clouds, displacements are between 1.6 and 47 km. At 15 km height, the horizontal distance to the launch point ranges from 1.5 to 206.3 km. The median distance steadily grows with height, reaching 79 km at 15 km. As a conclusion, the horizontal drift of the RS can be an issue when comparing with fixed instrumentation, since half of the soundings go farther than 79 km. The horizontal positions of the RS when they reach 15 km height are represented in the inset of Figure 23. The RS drifts are always towards the East, due to the prevalence of the Westerlies in most of the troposphere at middle latitudes.

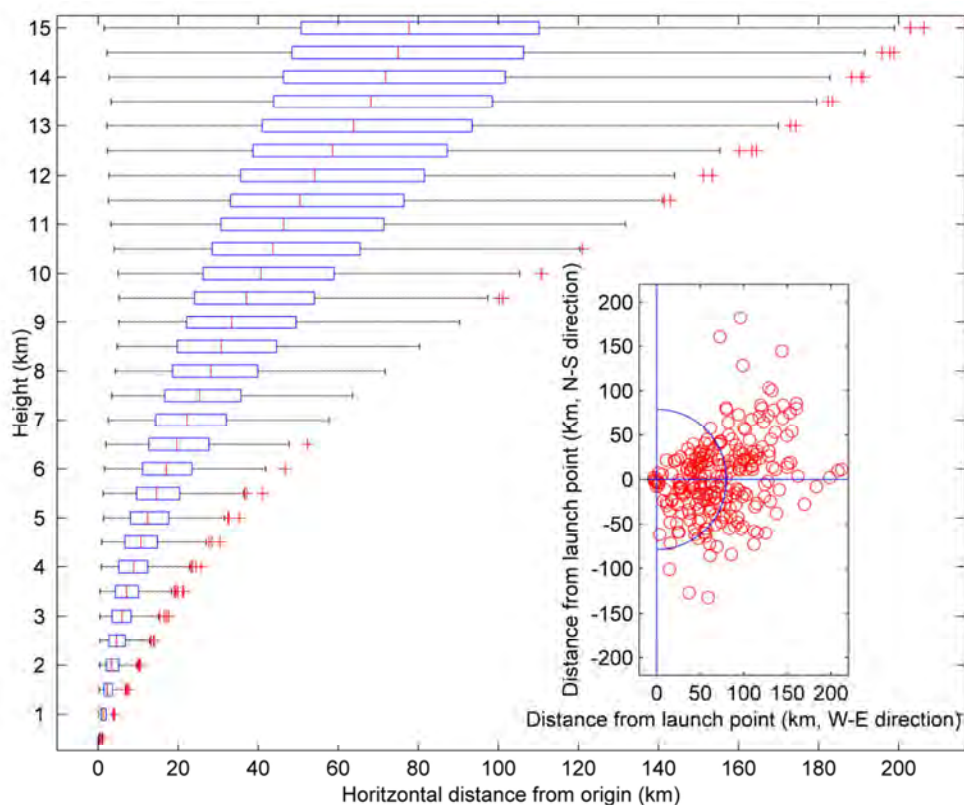


Figure 23. The boxplot shows the horizontal displacement, every 500 m height, of the 259 radiosondes launched from SGP (the boxplot shows the minimum, the first quartile, the median, the third quartile, the maximum and, if any, observations that might be considered outliers (plus symbols)). The inset shows the horizontal projection vision of the RS position with respect to the launch point when they reach 15 km. The semi-circle represents the median of all displacements (79 km).

Considering this large horizontal distances travelled by the RS, it may well happen that clouds crossed by RS differ from clouds over the ARSCL site. To help screen for those RS whose trajectory goes through a homogeneous cloud field, GOES images have been used to evaluate the cloudiness (or the lack thereof) in the area. Sequences of GOES images every 15 minutes have been analyzed corresponding to periods during the RS ascents. An area of 200 x 400 km² eastwards of the SGP site has been inspected. Both visible channel (band 1) images, when available and infrared atmospheric window channel (band 4) images have been used. Visible images make it possible to distinguish low clouds due to their high reflectance, while infrared images are more useful for detecting high clouds due to their low temperature. In addition, we check that the cloudiness derived from GOES images are compatible with what ARSCL produces over SGP. With these two conditions, some RS have been rejected from the original RS database,

so only 193 RS out of the initial 259 RS form the suitable dataset. These selected RS are still well distributed seasonally: winter 27%, spring 21%, summer 22%, and autumn 30%; and also well distributed through the day: 0530 UTC 25.4%, 1130 UTC 24.4%, 1730 UTC 26.9%, and 2330 UTC 23.3%. The entire procedure will be further explained by means of examples included in section 4.

Finally, a total sky imager (TSI-660 by Yankee Environmental Systems) provides time series of hemispheric sky images during daylight hours and retrievals of fractional sky cover for periods when the solar elevation is greater than 10 degrees. These animated images added some useful information when analyzing and interpreting results of ARSCL and radiosonde cloud vertical structure.

3.3.2-b. Radiosounding methods for cloud vertical structure estimation

There are several methods to obtain the CVS from radiosounding profiles, such as those in: Poore et al. (1995, PWR95), Wang et al. (1995, WR95), Chernykh and Eskridge (1996, CE96), Dimitrieva-Arrago and Shatunova (1999) and Dimitrieva (2012, personal communications) (DS99), Minnis et al. (2005, MNS05), and Zhang et al. (2010, ZHA10). Also, some authors have already performed comparison studies, but to our knowledge, none of these previous works has compared as many methods. For example, Naud et al. (2003) compared the methods by Wang and Rossow (1995) and Chernykh and Eskridge (1996), using data (November, 1996 – October, 2000) from surface-based active sensors placed at the ARM SGP site. In the same paper, the authors checked the effect of applying different thresholds on the relative humidity for the first method and modified the second method by making it dependent on the cloud cover and altitude for some occasions. They concluded that the Wang and Rossow (1995) method tends to classify moist cloudless layers as cloudy (especially at lower altitudes), furthermore, they suggested that the two methods tend to report high cloud top heights that are higher than the corresponding heights from radar observations. In a more recent comparison work, Zhang et al. (2012) conducted a campaign in China where a cryogenic frostpoint hygrometer, a Vaisala RS80 radiosonde, and a GTS1 radiosonde were deployed. They compared again the methods by Wang and Rossow (1995) and Chernykh and Eskridge (1996) and adapted them to the specific behavior of every radiosonde instruments that they used. Overall, results from these earlier comparison studies have clearly demonstrated the value of radiosonde data for determining cloud vertical structure. However, they have also shown that different methods produce slightly different

results, and that the cloud vertical structure derived from radiosondes data sometimes diverges from active sensor observations.

A more recent study from Zhang et al. (2013) presents a validation of a radiosonde-based cloud layer detection method against ground-based remote sensing at multiple ARM sites. Specifically, their study is based on Zhang et al. (2010) algorithm but expanding it to four regions and for 10 years of data, when available: Southern Great Plains (SGP), Tropical Western Pacific (TWP), North Slope of Alaska (NSA) and a shorter-term product for the ARM Mobile Facility (AMF) (Figure 24) deployed in Shouxian. They made some changes to the ZHA10 algorithm (in Zhang et al., 2010) to make it more reliable. They found that, overall, cloud layers derived from the ARSCL VAP and radiosonde data agree very well at the SGP and AMF-China sites; and at the TWP and NSA sites, the radiosonde tends to detect more cloud layers in the upper troposphere. They conclude that more studies are needed to improve the performance of radiosonde methods at different climate regions (in the Tropics and at high latitudes) and especially at upper parts of the atmosphere.



Figure 24. The ARM Mobile Facility (AMF, from ARM website).

In this thesis, to go a little further, six different methods to determine the CVS from radiosondes have been considered. However, as this work is based on techniques that have been developed and published earlier, we will not extensively describe their development; instead, Table 7 contains a summary of their main characteristics and a short description is given next.

Poore et al. (1995) developed a methodology (PWR95, see flowchart in Figure 25) with the aim to build a cloud climatology combining 14 years (1975-1988) of surface and upper-air observations (radiosoundings) at 63 sites in the Northern Hemisphere (0° to 80° N; 34

continental sites, 14 coastal sites, and 15 on islands). The main idea of PWR95 method is to estimate the cloud base and top heights from temperature-dependent dew point depression thresholds. In the PWR95 method, the radiosounding processing is limited to temperatures above -40°C or at a maximum of 10,668 m above ground level (agl). The radiosounding is linearly interpolated every 76 m and the dewpoint depression (ΔT_d) is calculated as the difference between the (dry) air temperature T and the dewpoint temperature T_{dew} :

$$\Delta T_d = T - T_{\text{dew}}$$

According with PWR95, a given atmospheric level has a cloud if

$$\Delta T_d < 1.7^{\circ}\text{C} \text{ at } T > 0^{\circ}\text{C}$$

$$\Delta T_d < 3.4^{\circ}\text{C} \text{ at } 0 > T > -20^{\circ}\text{C}$$

$$\Delta T_d < 5.2^{\circ}\text{C} \text{ at } T < -20^{\circ}\text{C}$$

which, in terms of RH, is approximately equivalent to

$$RH > 91.5\% \text{ at } T > 0^{\circ}\text{C}$$

$$RH > 83\% \text{ at } 0 > T > -20^{\circ}\text{C}$$

$$RH > 74\% \text{ at } T < -20^{\circ}\text{C}$$

Finally, some additional conditions are applied: specifically, a minimum cloud-layer thickness of 30.5 m (for low clouds, CBH < 1981 m) and 61 m (for middle and high clouds); cloud layers that extend to the top of the RS profile are discarded because they have indeterminate top heights.

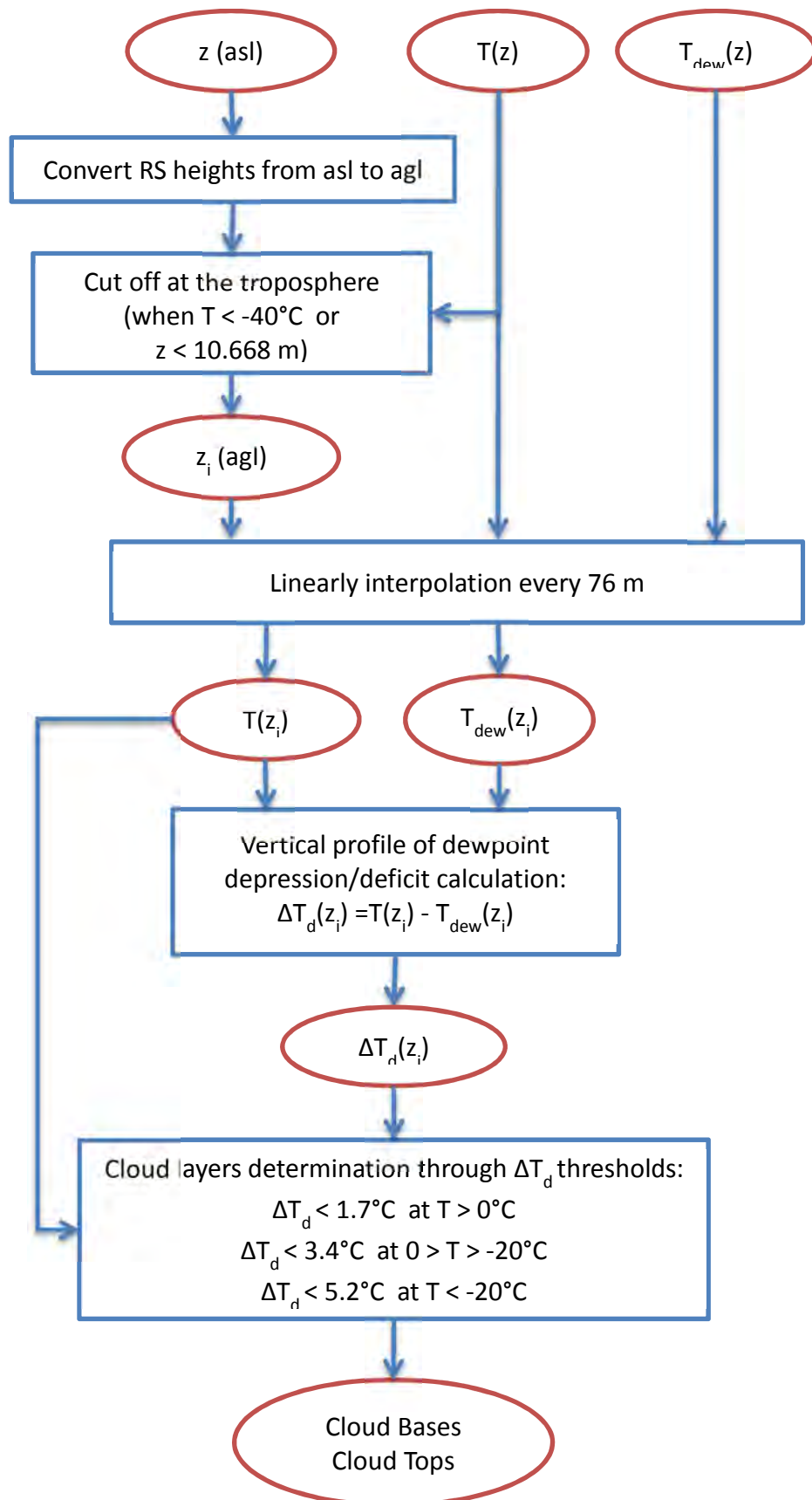


Figure 25. Simplified representation, or flowchart, of PWR95 method, as it has been applied. Red ovals are variables (measured from radiosonde or calculated by the methodology); blue rectangles are the method procedures. 'z' are heights, 'T' are temperatures, 'T_{dew}' are dewpoint temperatures, and ΔT_d are dewpoint depression or deficit.

Table 7. Summary of the applied RS methods.

Acronym	References	Cloud base and top height estimation methodology	Resolution (approx. number of levels)	Max. height	Data used	RH _{ice}	Min. thicknesses (m)	Min. CBH (m)
PRW95	<i>Poore, Wang and Rossow, 1995</i>	Temperature-dependent dew point depression thresholds	76 m (140)	Tropopause or 10668 m	z, T_{dry} and T_{dew}	No	30.5 (low) 61 (middle, high)	No
WR95	<i>Wang and Rossow, 1995</i>	Two RH thresholds (minRH = 84% and maxRH = 87%) and 3% jump.	Low* (180)	10 hPa	z, T_{dry}, P and RH	If $T < 0^{\circ}\text{C}$	No	500
CE96	<i>Chernykh and Eskridge, 1996; and Chernykh and Aldukhov, 2004</i>	Sign of the second-order derivatives with respect to height of the T and RH ($T''(z) \geq 0$ and $R''(z) \leq 0$)	Low* (180)	10 hPa	z, P, T_{dry}, T_{dew} and RH	If $T < 0^{\circ}\text{C}$	100	0
DS99	<i>Dimitrieva-Arrago and Shatunova, 1999; and Dimitrieva 2012 personal communications</i>	Pressure-dependent dew point depression thresholds	High** (3000)	300 hPa	z, P, T_{dry} and T_{dew}	No	No	0
MNS05	<i>Minnis et al., 2005</i>	Empirical parameterization calculating the probability of occurrence (Pcld) of a cloud layer using RH and T [Pcld (T, RH) > 67%]	25 hPa (36)	100 hPa	z, P, T_{dry} and RH	If $T < -20^{\circ}\text{C}$	No	0
ZHA10	<i>Zhang et al., 2010</i>	Improvement of the WR95 method (altitude dependent minRH and maxRH thresholds, without the 3% jump)	High** (3000)	Top of the profile	z, T_{dry} and RH	If $T < 0^{\circ}\text{C}$	30.5 (low) 61 (middle, high)	280

*A low resolution RS is built from the original RS (see text for details).

** High resolution means all available data in the RS (without any transformation).

Wang and Rossow (1995, WR95 method) slightly modified the PWR95 method. First, for levels with temperatures lower than 0°C, RH is computed with respect to ice instead of liquid water, which allows the use of a single threshold RH at all levels. This single threshold is set to 84% to identify a moist level; within a moist layer (i.e. several successive moist levels), the maximum RH must be greater than 87% to be considered as a cloud layer. In addition, if RH at the base (top) of the moist layer is lower than 87%, a RH jump exceeding 3% must exist from the underlying (above) level. All cloud layers, independent of their thickness, including single-level clouds, are retained in WR95. Another improvement is that cloud layers ending at the maximum observation altitude, which were discarded in PWR95, are kept in WR95. Finally, the minimum value of a cloud base height is set at 500 m above ground level.

The WR95 method was tested at 30 ocean sites by comparing with cloud properties derived from other independent data sources (visual observations and ISCCP data). The radiosonde data covered from 1946 to 1991; the sites were selected to supplement the poor ocean coverage of PWR95 dataset. The radiosounding dataset used by WR95 did not have as high resolution as the radiosounding data from the SGP that are used in the present study. For this reason, when applying WR95 method, we have first reduced the radiosonde resolution at approximately the same resolution of the original work (that is, mandatory pressure levels, significant points, and maximum distance between levels fixed at 200 m). The method for resolution reduction is based on Chernykh and Eskridge (1996), see immediately below.

The CE96 method (Chernykh and Eskridge, 1996), based on previous methods developed in the former Soviet Union, was evaluated using data from several United States radiosonde stations within different climates. Evaluation data was selected to include only situations where the observer could only see one cloud layer. Consequently, the evaluation is biased towards stratified cloud conditions. A few years later, Chernykh and Aldukhov (2004) further developed this method and applied it to one month of data from the Surface Heat Budget of the Arctic Ocean (SHEBA) experiment, along with satellite observations made during Phase II of the FIRE Arctic Cloud Experiment and sounding data from the National Center for Atmospheric Research (NCAR) C-130Q research aircraft.

The first step in the CE96 method is to build a new vertical profile with lower resolution. The new, coarse profile must include these levels (with the corresponding values obtained by interpolation between the original measured values):

- Mandatory pressure levels (where $P = 1000, 925, 850, 700, 500, 400, 300, 250, 200, 150, 100, 70, 50, 30, 20, 10$ hPa).
- Significant levels, to avoid differences greater than 0.5°C (air temperature) and 2.5% (relative humidity) between two consecutive levels
- Additional levels to obtain a maximum distance of 200 m between them.

In fact, Chernykh and Aldukhov (2004) used this technique to reduce the radiosonde data resolution and tested different values (from 100 m to 700 m) for the maximum distance between levels; based on their conclusions we have used a value of 200 m in the present work.

According to the CE96 method, the necessary condition for the existence of clouds in a given atmospheric level is that the second derivatives with respect to height (z) of temperature and relative humidity be positive and negative respectively:

$$T''(z) \geq 0 \text{ and } RH''(z) \leq 0$$

To calculate the second derivative, the temperature and relative humidity profiles are first approximated by cubic splines; in this way the second derivatives can be continuously estimated over the entire vertical profile as linear functions over each segment.

Then, when the previous conditions are met in a given level, the Arabey diagram (Chernykh and Eskridge, 1996) is applied to evaluate the cloud cover in it. If cloud cover is determined to be less than 20%, that level will not be considered as cloudy. In addition, for a succession of levels accomplishing both criteria to form a cloud layer, they must total a minimum thickness of 100 m.

Chernykh and Eskridge (1996) argued that this methodology makes physical sense because in a region of the atmosphere containing clouds, one expects higher relative humidity than in the layer above and below the cloud layer. Hence, a local maximum ($RH''(z) \leq 0$) must be reached. They also commented that clouds ordinarily have a more defined top than base and nearly always lie under a temperature inversion (so $T''(z) \geq 0$ at the cloud top). Condensation of water vapor and its accompanying release of latent heat make it reasonable for temperature to stop decreasing with height or to increase with height near the base of a cloud (hence, a local minimum, i.e. $T''(z) \geq 0$ is also expected at the cloud base).

The basis of the DS99 method (Dimitrieva-Arrago and Shatunova, 1999 and Dimitrieva, 2012, personal communications) is the vertical distribution of dew point depression (ΔT_d) in the atmosphere, as in the PWR95 method. Characteristic values of dew point depression in clouds are known from analysis of the great amount of aircraft data (mostly for stratiform clouds) conducted by specialists of the Hydrometeorological Scientific Research Center of Russia. Thus, Dimitrieva-Arrago and Koloskova (1969) carried out a comparison of cloud vertical structure (location of cloud boundaries and cloud thickness) calculated using characteristic values of ΔT_d with real cloud distributions derived from aircraft data. From this previous study, the method is quite simple. First, the dew point depression must be calculated at every radiosonde level. Then, three pressure-dependent dew point depression thresholds are applied to find the cloud layers:

$$\Delta T_d < 1.5^\circ C \text{ at } 1000 \text{ hPa} > P > 800 \text{ hPa}$$

$$\Delta T_d < 2.5^\circ C \text{ at } 800 \text{ hPa} > P > 550 \text{ hPa}$$

$$\Delta T_d < 5^\circ C \text{ at } 550 \text{ hPa} > P > 300 \text{ hPa}$$

Assuming the typical temperature found in the corresponding pressure range, ΔT_d thresholds can be expressed as RH (with respect to water) thresholds:

$$RH > 92.5\% \text{ at } 1000 \text{ hPa} > P > 800 \text{ hPa} \text{ (at } 15^\circ C \text{)}$$

$$RH > 87.5\% \text{ at } 800 \text{ hPa} > P > 550 \text{ hPa} \text{ (at } 0^\circ C \text{)}$$

$$RH > 75\% \text{ at } 550 \text{ hPa} > P > 300 \text{ hPa} \text{ (at } -20^\circ C \text{)}$$

Minnis et al. (2005, MNS05) provided a new cloud detection method derived from high temporal resolution ARSCL data, balloon-borne soundings, and satellite retrievals over the ARM SGP Central Facility between 1 March 2000 and 28 February 2001. MNS05 is an empirical parameterization that calculates the probability of occurrence of a cloud layer using RH and air temperature from radiosondes. First, RH values must be converted to RH with respect to ice when temperature is less than $-20^\circ C$; on the other hand, the profile has to be interpolated every 25 hPa up to the height of 100 hPa. Then an expression to estimate the cloud probability (P_{cld}) as a function of temperature and relative humidity is applied; in this formula, relative humidity is

given the maximum influence since it is the most important factor for cloud formation. Finally, a cloud layer is set wherever P_{cld} . Jin et al. (2007) slightly modified this method for its application to Arctic conditions (i.e. colder and less polluted). Minnis et al. (2005) developed their method to compare it with the Rapid Update Cycle (RUC) 40-km resolution model results (so a different goal than the other methods presented in this section, i.e. to create cloud climatologies). However, we have adapted and applied it in the present study given that the method produces what we would like to analyze: the CVS from vertical thermodynamic profiles.

Zhang et al. (2010, ZHA10) developed their methodology on the basis of data obtained during a campaign in Shouxian (China) from 14 May to 28 December 2008, where the ARM Mobile Facility (AMF) was deployed. Radiosonde data were used to analyze cloud vertical structure by taking advantage of the first direct measurements of cloud vertical layers from the 95 GHz radar. ZHA10 method is clearly an improvement of WR95 method. Instead of single WR95 threshold, ZHA10 is based on altitude dependent thresholds without the requirement of the 3% RH jump at the cloud base and top. Threshold values depending on height are shown in Table 8. According to their own results, Zhang et al. (2010) concluded that cloud layers retrieved using the ZHA10 method agree well with the surface active remote sensing observations (cloud radar, MPL, ceilometer) of cloud vertical distributions (the absolute differences in CBH from RS and MPL/ceilometer comparisons are less than 500 m for 77.1% / 68.4% of the cases analyzed).

Table 8. Summary of the values for min-RH, inter-RH and max-RH, from Zhang et al. (2010).

Altitude Range	ZHA10 min-RH	ZHA10 inter-RH	ZHA10 max-RH
0-2 km	92% - 90%	84% - 82%	95% - 93%
2-6 km	90% - 88%	82% - 78%	93% - 90%
6-12 km	88% - 75%	78% - 70%	90% - 80%
>12 km	75%	70%	80%

As a first step, the RH with respect to liquid water is converted to RH with respect to ice when the temperature is below 0°C . Then, moist layers are identified by applying four conditions: a) the base of the lowest moist layer is determined as the level where RH exceeds the minimum RH threshold (min-RH) corresponding to this level, b) above the base of the moist layer, contiguous levels with RH over the corresponding min-RH are treated as the same layer, c) the top of the moist layer is identified where RH decreases below the corresponding min-RH, and d) moist layers with bases lower than 120 m and thicknesses less than 400 m are discarded. Subsequently, cloud layers are defined through four additional steps: a) a moist layer is classified as a cloud layer if the maximum RH within this layer is greater than the corresponding maximum RH (max-RH) at the base of this moist layer, b) the base of cloud layers is set to 280 m agl, and cloud layers are discarded if their tops are lower than 280 m, c) two contiguous layers are considered as a single layer cloud if the distance between these two layers is less than 300 m or the minimum RH within this distance is greater than the maximum inter-RH value, and d) clouds are discarded if their thicknesses are less than 30.5 m for low clouds and 61 m for middle/high clouds.

3.3.2-c. Classification of the situations

The radiosonde trajectory (only the vertical position is considered) is graphically superposed to the temporal evolution of ARSCL CBBE and the first three CBH and CTH. From this representation, heights of cloud bases and tops are extracted by a visual inspection, obtaining what we call ARSCLv heights, which correspond to cloud bases and tops eventually crossed by the sonde during its ascent. These values will be the main reference considered in the present study for comparison. Additionally, the mean value of ARSCL cloud bases and tops is calculated, from the time when the RS is launched until half an hour later, will be denoted as ARSCLm. It has to be noted that the CBBE (from VCEIL/MPL) is considered the first cloud base layer unless the first CBH (from MMCR/MPL) is lower.

Then, the next step is comparing the behavior of the six methods above described with ARSCL observations. First, the sky situations were classified into four categories (according to ARSCLv): 'no clouds', '1 layer', '2 layers' or 'more than 2 layers'. Then, for every sky situation the methods were classified in several categories depending on the correspondence between the methods

and the observations. Further, every case was labeled as false negative, false positive, perfect agreement, approximate agreement, or not coincident, defined as follows.

'False negative' means that no clouds were detected by the method when ARSCLv gives one or more cloud layers. 'False positive' means that one or more cloud layers were detected by the method when ARSCLv does not give any cloud. 'Perfect agreement' occurs when the method detects the same cloud layer/s (number and heights) as ARSCLv. 'Approximate agreement' occurs when the method correctly detects at least one layer that ARSCLv gives, but disagrees on the whole cloud vertical structure. Finally, all other cases are labeled as 'not coincident'.

Regarding the matching between heights of cloud layers, the first step is to classify cloud layers (both from ARSCLv and the RS methods) as 'low' (CBH < 2000), 'middle' (2000 m < CBH < 6000 m) or 'high' (CBH > 6000 m) (according to WMO, 1975). For classifying the layers derived from the RS methods a tolerance interval of ± 300 m and ± 500 m is admitted when CBH is near a boundary (2000 m or 6000 m respectively). Secondly, a RS layer is considered as coincident to the ARSCLv layer if it belongs to the same class (low, middle or high) and (i) the ARSCLv cloud layer and the RS cloud layer are partly or totally superimposed each other, or (ii) the CBH from the RS method does not differ for more than 150 m (low clouds), 300 m (middle clouds) or 600 m (high clouds) from the ARSCLv CBH.

4. Results and discussion

As stated in the Introduction, there is a need for improvement of methods for automatic and continuous description of cloud characteristics and its description. Ceilometers constitute a priori a reliable instrumental method for sounding the atmosphere and describing cloudiness, specifically cloud cover and cloud base height (CBH). In this section, firstly the cloud occurrence as cloud cover estimator (subsection 4.1) and the behavior of CBH at different time scales (subsection 4.2) has been investigated at Girona (Spain), including a statistical analysis of the frequency distributions of CBH in monthly basis. These distributions are compared with previous results found in the literature concerning CBH behavior. The study covers four years (2007-2010) of high resolution (both in time and in the vertical direction) ceilometer measurements. Moreover, some specific atmospheric situations are described, adding some insight into the frequency distributions of CBH. These subsections are the core of the published paper Costa-Surós et al. (2013).

Secondly (subsection 4.3), methods based on atmospheric sounding profiles are compared with the CVS provided by ground-based active instruments (that is, the ARSCL cloud base and top heights) so strengths and weaknesses of the methods are revealed. All methods establish some conditions on the relative humidity, and differ on the use of other variables, the thresholds applied, or the vertical resolution of the profile. In this study these methods are applied to radiosonde profiles acquired at the ARM Southern Great Plains site (Oklahoma, US) during all seasons of year 2009 and endorsed by GOES images. These images were used to confirm that the cloudiness conditions were homogeneous enough across the radiosonde trajectory, so that the estimated CVS were comparable with the ARSCL observations (which determine the CVS exactly in the vertical direction). This last subsection contains the nucleus of two manuscripts recently submitted: Costa-Surós et al. (2014) and Viúdez-Mora et al. (2014).

4.1. Cloud occurrence as cloud cover estimator

The specific methodology and data for this study are explained in Section 3.3.1. Particularly, *cloud occurrence* for a determined time interval is defined as the ratio between the number of registers with detected clouds (i.e. at least one CBH value) with respect the total available

records. Cloud occurrence is used here as an estimator of the cloud cover, which is a quantitative descriptor of cloudiness.

Monthly estimations of cloud occurrence in percentage (Figure 26) have been obtained from the ceilometer data. Despite the year to year variability, some common features can be noted: most years follow a similar evolution, including a clear summer minimum (centered in July) (Figure 26a). However, some missing data in May-August 2010 might have affected the cloud occurrence values. In particular, it cannot be discarded that the absolute minimum in July 2010 be linked to the lost data precisely during cloudy situations (note that power faults due to thunderstorms produced the instrument failure).

Figure 26b shows the average of these four years of monthly cloud occurrence and the 1973-2003 cloud cover mean obtained from visual observations at Girona Airport (a few kilometers from the ceilometer site) processed by the same methodology as in Llach and Calbó (2004): monthly means in tenths are built from three daily observations (at 7h, 13h and 18h). Although it is unrealistic to expect complete similarity between the observer and any instrumental output (Boers et al., 2010) both evolutions agree well, showing a mean cloudiness around 40-50% along the year, except for the summer period, when the July minimum reaches around 30%. According with Boers et al. (2010) this agreement between monthly means may be hiding important differences in the distributions of cloud occurrence as compared to the human observations. Note, however, that the monthly cloud occurrence detected by the ceilometer is lower than the cloud cover from visual observations, all the year long, except in the winter season, that breaks this trend. We attribute this general underestimation to the limited vertical range of detection (7620 m). Of course, another reason for the mismatch between both series of data is that they correspond to different temporal periods. Nevertheless, the ceilometer cloud occurrence lies within the interannual variability described by the standard deviation of the monthly values.

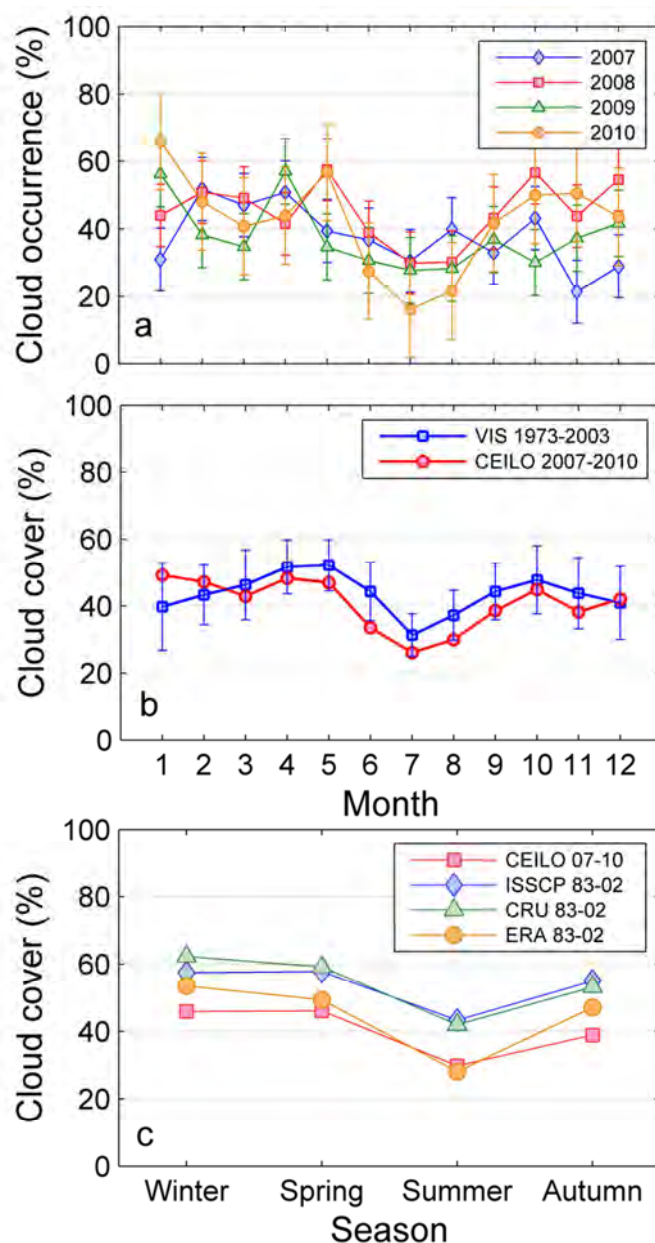


Figure 26. (a) Monthly cloud occurrence for the period 2007-2010, as derived from ceilometer data. Error bars indicate \pm one standard deviation of the original data. (b) Averaged monthly cloud occurrence as detected by the ceilometer for the period 2007-2010 and averaged cloud cover from visual observations at Girona Airport for the period 1973-2003. Error bars indicate \pm one standard deviation, as an estimation of the interannual variability. (c) Seasonal cloud cover in the Iberian Peninsula, series from the ISCCP, CRU and ERA datasets (several periods, see Calbó and Sanchez-Lorenzo, 2009) and seasonal averages of cloud occurrence from ceilometer data (December, January and February are considered as 'Winter'; March, April and May are 'Spring'; June, July and August are 'Summer'; and September, October and November are 'Autumn').

Moreover, Figure 26c shows that the cloud occurrence detected with the ceilometer at Girona is also consistent with the annual and seasonal total cloud cover (TCC) that can be derived from a climatic description of cloudiness in the Iberian Peninsula (Calbó and Sanchez-Lorenzo, 2009). This latter study was limited to the 1983-2002 period to allow comparing results from three different sources of data: the International Satellite Cloud Climatology Project (ISCCP) D2 data, the gridded data (TS 2.1) from the Climate Research Unit (CRU), and the European Centre for Medium-Range Weather Forecasts (ECMWF) Re-Analyses data (ERA-40). Results indicated that, in the Iberian Peninsula, the mean annual cloudiness ranges from 35–65% of fractional sky cover, depending on location and on data source. Seasonal evolution showed a very clear minimum of cloudiness that appears in summer and a maximum in winter. A similar behavior was also found by Rossow et al. (2005) regarding cloud amounts at these latitudes inferred from satellites (ISCCP) and radiosonde profiles. Some differences appeared among the three sources, probably due to the higher sensitivity of satellite observations to cirrus clouds, the underestimation of high clouds due to the obscuring effect in surface observations, and the satellite overestimation of low-level broken or scattered clouds (Calbó and Sanchez-Lorenzo, 2009). Thus, Figure 26c shows that seasonal cloud occurrence for Girona estimated from ceilometer measurements agree quite well with TCC values from the ERA dataset (ECMWF Re-Analyses data), and particularly in regards of the summer minimum.

Therefore, the estimated values of cloud cover from the ceilometer data (i.e., cloud occurrence) seem reasonable (although slightly lower) when compared either with visual observations taken at Girona airport or with the regional climatology based on surface and satellite observations. This is a notable fact, specially if one considers that device ceilometer has a very limited FOV and can hardly detect high clouds, and also recalling the shortness of the treated period (4 years) and the simplicity of the cloud cover estimation. Thus, when looking at long time series, the narrow FOV might be partially compensated: it can be assumed that clouds are advected over the ceilometer so a representative sample of the 2-D cloud field is obtained in most, but not all, cases.

4.2. Cloud base height from ceilometer measurements

4.2.1. Cloud layers and CBH distributions

Ceilometer measurements allow obtaining information on the vertical structure of the cloud field (although cloud top heights cannot be derived straightforwardly). For the 4-year period studied, the ceilometer detected a single cloud layer in 89.7% of the cases, whereas 9.4% were 2-layered systems, and 0.9% were 3-layered systems (relative to the number of cases where some cloud was detected; cases labeled as full or partial obscuration –usually due to heavy fog or precipitation–, when no cloud base is detected, have not been included). In principle, the frequency of multilayered cases is expected to be underestimated by the ceilometer since high clouds may often be occulted by the lower layers. Accordingly, from visual observations at Girona Airport (1973-2003), following SYNOP observation criteria, 46% of observations contain cloud types belonging to two different levels (low and middle, low and high, or middle and high).

In fact, the frequency of single layer occurrence in our database is very close to that found for the Cloud Layer Thickness Climatology (CLTC) presented in Poore et al. (1995, PWR95), where the frequency of occurrence of single-layer clouds at 63 sites (34 inland, 14 coastal and 15 island stations) in the Northern Hemisphere for 14 years (1975-1988) was analyzed. Cloud vertical structure (CVS) was determined from rawinsonde observations (RAOBS) of temperature and humidity and checked against (and sometimes combined with) surface weather observations (SWOBS). PWR95 found that over most sites the frequency of single-layer clouds was higher than 90%. However, they concluded that multilayered cases are underestimated in CLTC, when compared to another surface observation climatology (SOBS), from Hahn et al. (1982, 1984), which in turn seems to overestimate the multilayered occurrence.

Wang and Rossow (1995) performed also some statistical analysis on a database of cloud layers obtained from rawinsonde measurements taken at 30 oceanic or coastal stations. For the whole database, their method of cloud detection from the vertical profiles produced single layer cloud fields in only 60% of the cases, and about 26% corresponded to 2-layered conditions. Further, Wang et al. (1999) used various data sources from the Atlantic Stratocumulus Transition Experiment (ASTEX) including rawinsonde, radar, ceilometer, and satellite, to determine, among other features, the proportion between single and multi-layered conditions. They showed that the single layer frequency depends on the method of determination of the CVS. For the merged radar-ceilometer data (that is, using the ceilometer data to verify the radar-determined lowest

CBH), a single layer appeared 79% of cases, whereas the rawinsonde analysis gave only 52% of single layer cases. They also showed that single layers are more frequent for clouds below 3 km. In comparison, Wang et al. (2000, WRZ00) created a global CVS climatic dataset by analyzing a 20-year collection of twice-daily rawinsonde humidity profiles to estimate the height of cloud layers. They found that globally (for land and ocean profiles), 58% of clouds were single-layered and 42% multilayered, almost 67% of the latter being 2-layered clouds. Over land conditions they found 63% of single-layered structures, 27% of 2-layered systems, 7% of 3-layered, and 3% of systems with more than three layers.

Finally, global data from the study by Rossow and Zhang (2010) reveal that two satellite based systems, ISCCP in one hand and a combination of the CloudSat and CALIPSO (C&C) on the other hand, detected single cloud layers in 93.2% and 74.5% of the cases respectively, 2-layered systems in 6.3% and 18.0% of cases, and 3-layered systems 0.5% and 7.5% of the times. Note that C&C satellite combination is able to detect more multilayered situations because the powerfulness of their active (radar and lidar) instruments.

Therefore, our findings at Girona seem to confirm a tendency of ceilometers to overestimate the presence of single-layer cloud systems. The frequency of this kind of cloudiness according our measurements (89.7%) is almost the highest compared with the reviewed literature. There may be two reasons for such behavior: first, the effect of occultation by the first layer, which may hide other upper layers if it is thick enough, and second, the limited range reached by the ceilometer, so the highest clouds are not detected at all.

Figure 27 shows the frequency distributions of CBH retrieved with the ceilometer for the whole analyzed period. All histograms have been standardized (by dividing each absolute frequency by the total number of values for the analyzed period) in order to better comparing their shapes. The bins are 400 m wide, thus leading to 20 intervals in the total detection range of the ceilometer (0 to 7620 m, so the last bin corresponds to a width of only 20 m). In Figure 27a the distribution of CBH for all cases together (i.e. single-, two- and three- layered conditions) is presented, in comparison with the CBH distribution for cases with a single layer detected. As these single-layered cases represent near the 90% of the total, both distributions are very similar. Figure 27b and Figure 27c show the CBH distributions for 2-layered and 3-layered systems respectively.

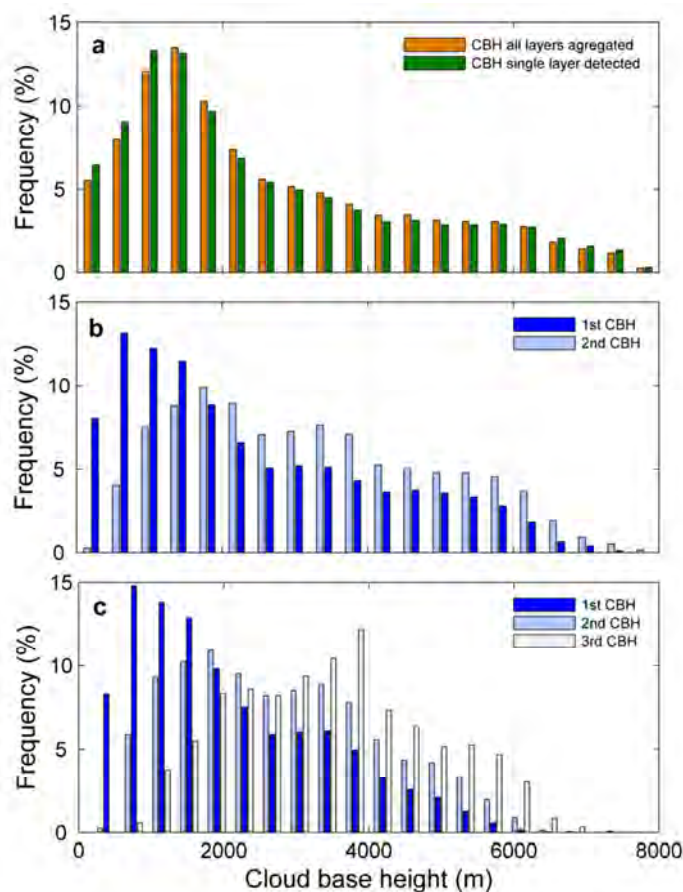


Figure 27. (a) Frequency distribution of CBH for all found layers aggregated, and when a single layer is detected. (b) Distribution of the CBH for the lower and higher layer when 2 layers are detected. (c) Distribution of the CBH for the lower, middle and higher layer when 3 layers are detected.

The histogram for all CBH together (Figure 27a) has the maximum for the bin centered at 1400 m (for the single-layered systems, the maximum is found for the bins centered at 1000 and 1400 m) and shows a progressive decreasing frequency up to the maximum level of detection of the ceilometer. Low clouds (below 2000 m) represent 49.6% of detected CBH (52% of single-layered systems), middle clouds (2000-6000 m) are the 42.9%, and high clouds (> 6000 m), the 7.5%. Combining the frequency of low clouds with the cloud occurrence specified in section 2.1 (40-50%), we can derive an approximate low cloud occurrence (25.7%) that agrees with the low cloud cover obtained from visual observations (i.e., from the already mentioned SYNOP observations at Girona Airport).

The mean and median of the distribution for all CBH together are 2560 m and 1970 m respectively, whereas for the single-layered systems these values are 2580 m and 1980 m. The mean of the distribution agrees well with WRZ00, who found that the CBH global average was at 2.4 km, being averaged CBH higher for land (2.8 km) than for ocean stations. Likewise, in PWR95, where the CLTC dataset was used, the latitudinal dependence of the averaged CBH is presented; according with their results (for land and latitudes near 42°), averaged CBH is around 2.4 km. For the Wang and Rossow (1995, WR95) dataset (which includes only stations that represent oceanic climatology), cloud bases are located 57% of the time below 2 km, with an even distribution above 2 km and a mean value of 2.6 km, so again very close to the mean value retrieved at Girona from our ceilometer measurements.

Despite this agreement with averaged values, the histogram (Figure 27a) shows some differences when compared with previous published results. For example, the histogram shown in WRZ00, both for land and ocean cases, is very biased to low CBH: about one-third of clouds have CBH below 0.5 km, with a sharp decrease of frequencies up to 1 km, followed by a smoother decrease above 2 km. Contrarily, the CBH distribution observed in Girona (with a clear maximum at 1400 m) is remarkably more similar to that in WR95, although this latter histogram has a much more peaked shape, with the maximum of the distribution centered at 1000 m. This could be explained by the fact that in WR95 all 30 stations were located at oceanic places, thus with a dominant contribution of low stratiform layers (marine *Stratocumulus*). Again, when comparing our results with Wang et al. (1999, WRUR99), several differences appear (dominant frequency for clouds below 2 km, and the peak of the distribution at around 700 m) owing to the fact that the focus of that study was put on marine boundary layer clouds.

Other authors have analyzed the vertical distribution of clouds observed at different locations by a suite of ground-based instruments (Ebell et al., 2011; Mace and Benson, 2008; Morcrette et al., 2012; Qian et al., 2012) or estimated by Global Circulation Models (Illingworth et al., 2007). All of them use the probability to find a cloud in a given level of the atmosphere, which is not directly and rigorously comparable with the frequency distribution of the CBH measured by the ceilometer. In any case, these works show an accumulation of cloudiness at approximately 1-2 km and a second maximum at higher altitudes (8-9 km), which again indicates a lower presence of high clouds when observed by the ceilometer when compared with other methods (e.g. MMCR, ARSCL, RS, models).

The distribution of CBH for 2-layered systems is shown in Figure 27b. For the lower layer, 70% of the retrieved CBH is below 3000 m. Strictly speaking, the maximum of the distribution is for the bin centered at 600 m, though high frequencies extend towards considerably higher CBH; the mean (median) of this distribution is 2400 m (1980 m). The upper layer detected with the ceilometer shows a bimodal distribution that has the main maximum for the bin centered at 1800 m, though appreciable frequencies extend also towards much higher values reaching the detection limit of the ceilometer (secondary maximum at 3400 m; mean and median are 3250 m and 3050 m respectively). These retrievals can be compared with the statistics for 2-layered systems in WR00, where the averaged CBH for the lower layer (for land stations) is 1.1 km, while average for the upper layer is 4.8 km.

Figure 27c shows the distributions of CBH for 3-layered systems as detected by the ceilometer. The distribution of the CBH for the lowest layer shows a maximum around 1000 m; for the middle layer, the distribution is bi-modal (with maxima at 1800 and 3400 m); the distribution for the highest layer has a peak around 3800 m and a secondary maximum at 2200 m. The mean (median) of the three distributions are 2050 m (1820 m), 2830 m (2690 m), and 3550 m (3480 m). Wang et al. (2000), regarding 3-layered cloud systems found the corresponding CBH averages at 0.8 km, 2.9 km and 5.5 km for land sites. The comparison of the latter results with ours seems to confirm that the derived CVS depends upon the detection system (radiosonde and ceilometer).

For multilayered cloud systems, distances between CBH of adjacent layers can be seen in Figure 28. The mean (median) of the distribution of CBH distances for 2-layered systems is 850 m (1070 m). When three layers are detected, the mean (median) distance between the lowest CBH and the middle CBH is 770 m (880 m), and between the middle and the highest CBH, 730 m (790 m). These values are quite different from separation between layers reported by WR95 (mean separation of 2.1 km, although most cases have separation between 0.5 and 1 km) and by WRZ00 (mean separation of 2.2 km and 2.3 km over ocean and land respectively). Therefore, important differences between methods used for finding the CBH arise again, considering that the latter values correspond to depth of clear air between adjacent cloud layers while our findings are distances between cloud bases.

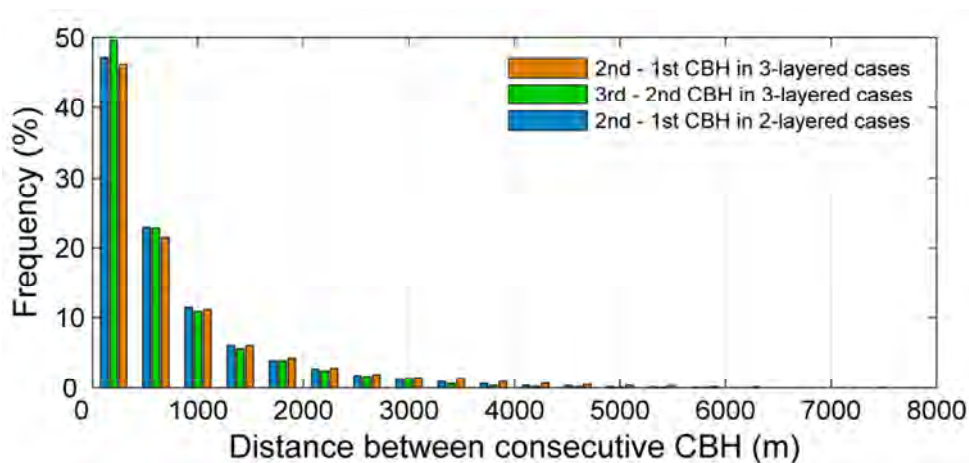


Figure 28. Frequency distribution of the distance between consecutive CBH detected by the ceilometer in multilayered cloud systems.

As it has been previously stressed, ceilometers have difficulties retrieving a second layer over a thick first layer, which add to the inability to determine the cloud top and the limited range of detection. On its side, CVS estimation from radiosonde profiles may have also its own limitations, starting from the horizontal trajectory of the RS while it is ascending, to the difficulty of establishing the humidity and temperature thresholds that correspond to a cloud layer. So, an extended analyses of methods based on RS are carried out in subsection 4.3.

4.2.2. Yearly evolution of the CBH distribution

Figure 29 shows the retrieved monthly distributions of CBH for single layer cases, for some representative months (January, April, July and October, i.e. the central month of every season), to figure out how CBH distribution evolves through the year. The remaining months have also been treated, but they are not included in the figure for sake of simplicity. In general, the monthly histograms show some common features: distributions are often multimodal, and frequencies decrease for high clouds. Despite these common characteristics, an evolution along the year appears clearly in Figure 29. January histograms are representative of the relatively homogeneous distributions for winter months, and have the maximum at the bin centered at 1000 m (January 2007 has a marked second maximum at 5800 m). In April, histograms have a

more compact shape, with the maximum ranging from 800 to 2400 m, except for the high contribution of very low clouds (with CBH < 400 m) in April 2007. In July (note that distributions for the four years are very similar) low clouds dominate again, with a much more peaked maximum always centered at 1400 m, possibly due to the predominantly anticyclonic and barometric swamps weather types, that favors the appearance of daily evolution clouds, and the eventual passing of weather fronts, both conditions favoring the accumulation of the CBH in low values. Finally, in October, the maxima of the distributions, which are less marked, extend from 400 m (for year 2010) to 1600 m (there is a second maximum centered at 3000 m in year 2007).



Figure 29. Standardized single layer CBH frequencies for some months, representative of each season, of the studied period.

Despite the diversity of observed CBH distributions, some standardized distributions were checked to fit them. The goal was to find an analytical distribution that could fit every real case by only changing its parameters (like it happens with other climatic characteristics as wind, which often matches the Weibull distribution, or precipitation, which usually fits an exponential distribution). No standardized distribution fitting all histograms was found, so this analysis was not continued. Only for illustrative purposes, the best distributions fitting two examples of real CBH histograms are shown in Figure 30a and b: Burr distribution (for July 2008) and uniform distribution (for November 2009), respectively.

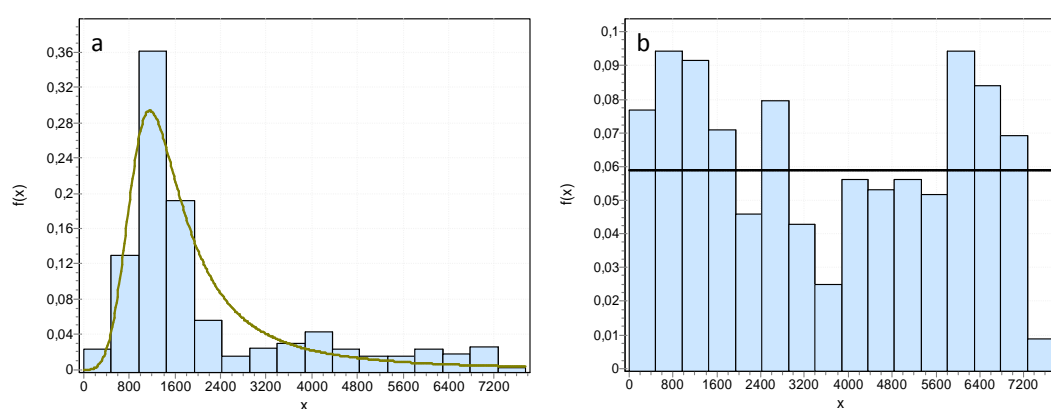


Figure 30. (a) July of 2008 histogram fits a Burr distribution; (b) November of 2009 histogram fits a uniform distribution.

Another way to make evident the seasonal evolution of the CBH distributions throughout the year is using cumulative CBH frequencies. Figure 31a presents all Januaries and Julies from 2007 to 2010 whereas Figure 31b presents Aprils and Octobers. It can be seen that Januaries and Julies are quite different since these months correspond to extreme seasons, whereas Aprils and Octobers are more similar, due to the fact that both correspond to transitional (equinoctial) seasons. Finally, Figure 31c shows the mean of the cumulative CBH frequencies for January, April, July and October, from 2007 to 2010, all together. All these figures show that, in July, there are (relative to the other months) few cases (25%) with CBH less than 1400 m, but 80% of clouds are below 3000 m. Contrarily, in January almost 40% of detected clouds have CBH less than 1000 m, so clouds up to 5000 m have to be accounted to reach 80% of cases. As already mentioned, the equinoctial seasons lay between these two extreme behaviors.

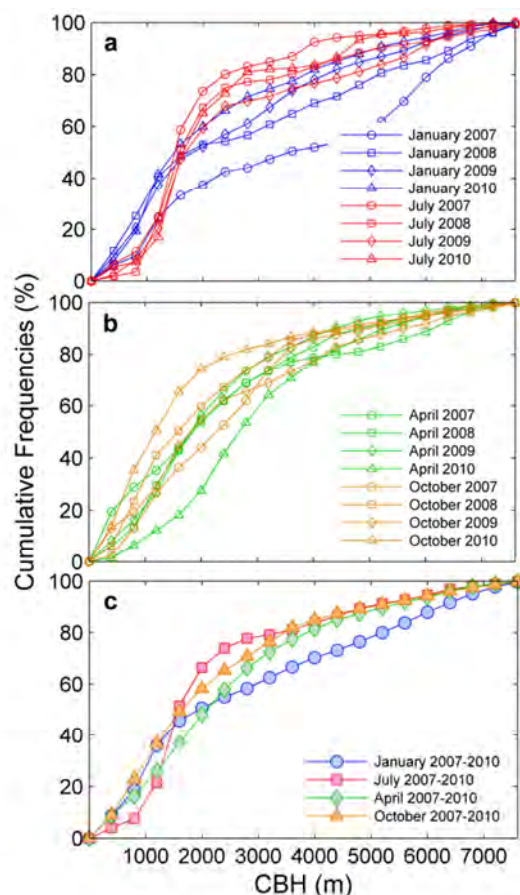


Figure 31. (a) January and July cumulative frequencies for the CBH of single layer cases; (b) April and October cumulative frequencies for the CBH of single layer cases; (c) Mean for the four years (2007-2010) cumulative frequencies for the CBH of single layer cases for January, April, July and October.

The asymmetry and ‘peakedness’ of the histograms (i.e. their shape) can be described through the skewness and kurtosis parameters respectively, which correspond to the third and fourth moments respect to the mean of the CBH frequency distributions. For the CBH distributions, skewness is always positive (which means that the right tail is more pronounced than the left tail) and presents a high negative correlation (Figure 32a, $r^2 = 0.83$, p -value < 0.0001) with the mean; it is also highly correlated (Figure 32b, $r^2 = 0.83$, p -value < 0.0001) with kurtosis. This means that distributions with a low mean CBH are very asymmetric having the tails biased to high values and show high peakedness (large kurtosis values). The best example is July, which presents large kurtosis and asymmetry values. These characteristics for July are probably due to

the contribution of convective clouds to high frequencies of low clouds, as already commented in previous sections. In other seasons, the origin of clouds is more diverse (including a large contribution of clouds associated to low pressure systems and their associated fronts) so cloud base heights are distributed along the histograms.

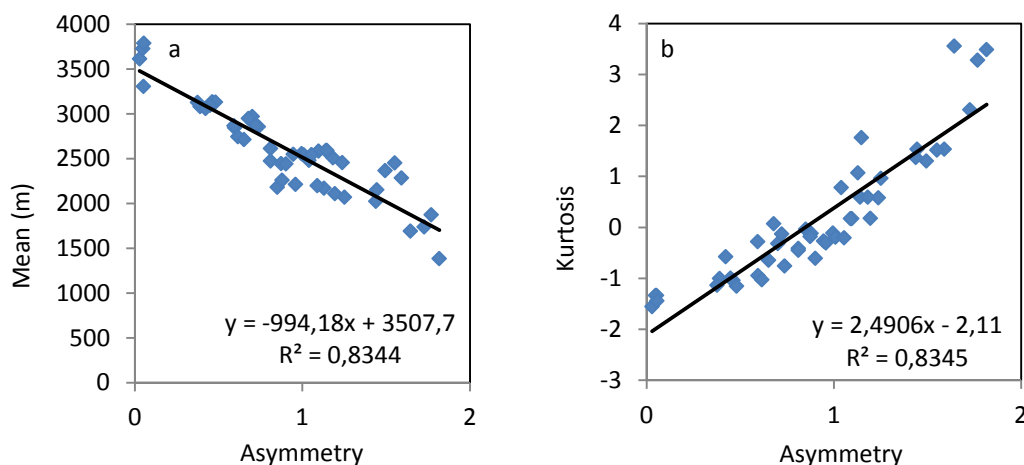


Figure 32. (a) Skewness (asymmetry) correlation with CBH mean; (b) skewness correlation with kurtosis.

4.2.3. CBH behavior during some atmospheric situations

Three typical cloudiness situations as seen by the ceilometer are explained, and their contribution to the frequency distributions of CBH are discussed next. One case for winter and two cases for summer are shown, as examples of expected conditions in these seasons. Most winter cloudiness is directly related with synoptic situations, and more specifically, with fronts that cross the area (see 4.2.3-a); in addition, there are fogs and some very low clouds (*Stratocumulus*, *Stratus*) related with local stability conditions below the subsidence thermal inversion associated to high pressure systems. On the other hand, in summer (subsection 4.2.3-b) there is cloudiness associated to synoptic situations (fronts crossing over the region) like in winter, but there is also another source of cloudiness: the surface heating and the subsequent convection that produces low clouds (*Cumulus humilis*) almost daily under low pressure gradients (persistent anticyclonic and swamp synoptic conditions).

4.2.3-a. Winter low pressure systems

The jet stream in winter usually adopts a zonal configuration, which allows a continuous western flux at the site latitude. This was the synoptic situation from 21 to 31 December 2009, when there was an episode of continued low pressure systems crossing the Iberian Peninsula from southwest to northeast. The weather fronts had lost power when arrived in the north-east of the peninsula, but they still left some precipitation over Girona (17.8 mm along these 11 days, according the rain gauge at the meteorological station placed side-by-side with the ceilometer). Figure 33a shows the CBH ceilometer data for the whole month. Between days 21 and 31 clouds formed along weather fronts and appeared day by day in an almost periodic way. During these days, there are first high and middle level clouds, from the maximum vertical range of the ceilometer going down towards the level of low clouds, but more often in the 4000-6000 m range. Then, when clouds reach low level (less than 2000 m) they remain at this level for several hours (6-12 h), and produce rainfall in most cases when the front overpasses the site (probably associated to the presence of *Nimbostratus*). Few hours after such an evolution of clouds, the sequence is repeated again. As the ceilometer detects CBH below 7620 m, the first, highest clouds that are expected with the arrival of a front (*Cirrus*, *Cirrocumulus*, *Cirrostratus*) cannot always be observed by this instrument. In addition, the highest clouds may appear when the low clouds are still present, and the latter may occult (both to an observer and to the ceilometer) the presence of the former. This can be seen for example in the transition between two consecutive systems the night of December 25 (Figure 33b, between 18-24 h): a layer of high-middle clouds (starting at CBH > 6000 m and descending to CBH < 4000 m) is apparent and occasionally detected by the ceilometer through the lower layer (CBH at 1000-2000 m).

Figure 33b corresponds to a detail for days 25 and 26 December 2009 and shows a particular example of a two consecutive low pressure systems. In fact, the synoptic maps of these two days (see synoptic maps of sea level pressure, temperature and geopotential height at 500hPa and 850hPa, along with Meteosat images, in annex 1) show the successive cold fronts and an occluded warm front. According to the weather type classification by Martin-Vide (2005), conditions change from a Northwest advection on day 25 to a South-Southeast advection on day 26, due to the changing position of the low pressure system center. The typical evolution of clouds and the descending CBH, as described above, is clearly detected by the ceilometer. Rain can also be observed in ceilometer plots, starting on day 26 at 5:25. On day 25, the hemispheric camera images (only for daylight hours, that is from 7:30 to 16:00 UTC approximately) show sometimes a clear sky (Figure 33i) but most time dominated by broken *Stratocumulus* clouds

(Figure 33ii). On day 26, clouds (mainly *Stratus*) totally cover the sky; these clouds sometimes show some vertical structure, so the ceilometer reports the cloud base at variable altitudes or even detects more than one layer (see Figure 33b, at around noontime, and Figure 33iii).

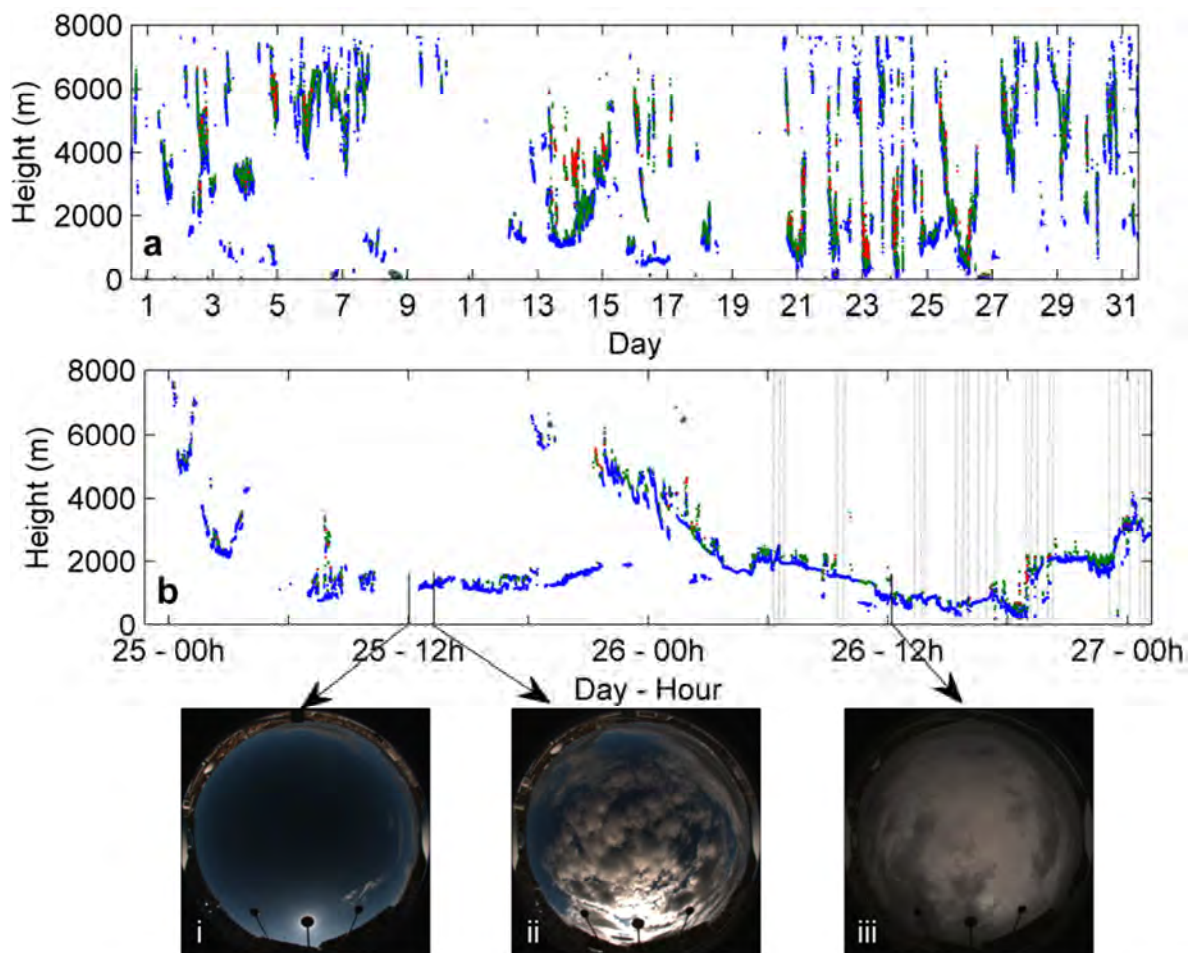


Figure 33. (a) Evolution of the ceilometer detected CBH in December 2009 (first CBH in blue, second CBH in green, third CBH in red). (b) A detail for 25-26 December 2009, including (dashed lines) the periods of rain, detected by the ceilometer itself and by the rain gauge and the sky camera. (i) Clear sky seen from the whole sky image from December, 25 at 12.00h. (ii) *Stratocumulus* clouds on December 25 at 12.45h. (iii) Sky image from December 26 at 12.06h where *Stratus* clouds cover all the sky and leave some precipitation.

Figure 34 shows the CBH frequency distribution for the period 21-31 December 2009, i.e., the period above described as an example of continuous front crossing. Thus, it is obvious that when fronts are passing, CBH is concentrated either at low altitudes or at middle levels. In fact, the distribution has two maxima, at 1000 m and 5000 m. Figure 34 also shows the CBH distribution for the short period (25-26 December 2009). The two histograms are bimodal, but the CBH distribution for the longer period is more uniform than the distribution for days 25-26, which has a much higher peak for low clouds (maximum at 1400 m). The reason is that not all the fronts of the longer period produced low level clouds as the passing fronts on the 25-26 did. For instance, on the 28-29 only few clouds reach the lower heights. On the other hand, the period previous to the start of the passing fronts shows a great variability of CBH, including some days with no clouds. All these facts contribute to make the histogram for the whole month (not shown) relatively uniform, as we have seen for winter months (subsection 4.2.2, Figure 29).

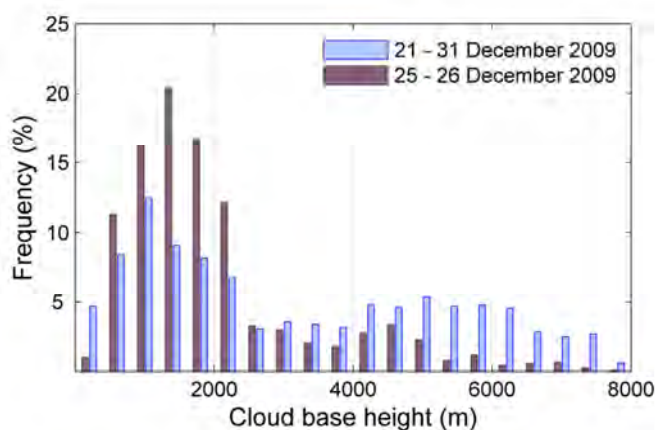


Figure 34. Frequency distributions of CBH for two different periods of December 2009.

4.2.3-b. Summer conditions

Figure 35a shows the CBH detected by the ceilometer in July 2009. From July 4-7, 2009, and according to the weather reports from the Meteorological Service of Catalonia and to weather maps (see synoptic maps of sea level pressure, temperature and geopotential height at 500hPa and 850hPa, along with Meteosat images, in annex 1), a low pressure system arrived in the area and made the temperature to cool down and the atmosphere to progressively unstabilize.

Specifically, on July 6 the weather front crossed over the site and left a very weak precipitation persisting until the next day; this can be seen in Figure 35b, where the detail of the ceilometer CBH detected for the period 6-7 July 2009 is shown. The typical evolution of clouds associated to a low pressure system (i.e., as above commented for a winter case) is clear, in particular from the later hours on day 6. Nevertheless, this summer cold front episode behaves slightly different, since low clouds stay longer than its winter counterparts shown in subsection 4.2.3-a. The sky camera images for day 7 confirm the evolution from high clouds to low thick clouds that remain over the site after noon (Figure 35i and Figure 35ii).

Other summer days show a very different behavior regarding cloudiness. For example, Figure 35a indicates that some days have mainly low level clouds, and only during a part of the day (days 12, 13, 18, 19, 30, 31). As an example of this characteristic evolution, Figure 35c shows the CBH for days 18-19 July 2009. This behavior, with low clouds appearing around noon, is typical of convective clouds of daily evolution: the surface heating and subsequent free convection forms low clouds, more specifically *Cumulus humilis* (fair weather clouds), which indicate warm weather, frequent in Girona summertime. The analyses of the synoptic maps for those days (see synoptic maps of sea level pressure, temperature and geopotential height at 500hPa and 850hPa, along with Meteosat images, in annex 1) confirm that conditions were favorable to convection: a slight Northwest advection on day 18 and a barometric swamp on day 19, with a trough in the south of Iberian Peninsula (classification from Martín-Vide, 2005). Moreover, the vertical profile obtained by radiosonde in Barcelona (90 km south of Girona) corroborates free convection conditions: the bulk Richardson number between 0 and 500 m agl at noontime is -2.7 and -10.7 respectively for days 18 and 19, due to super-adiabatic conditions and weak winds. In addition, *Cumulus* clouds are continuously forming and disappearing (Figure 35iii and Figure 35iv) within the field of view of the hemispheric sky camera. Some thin, high clouds (not seen by the ceilometer) seem to be present on day 19 (Figure 35iv), enhancing circumsolar radiation which is seen as a white circle in the image.

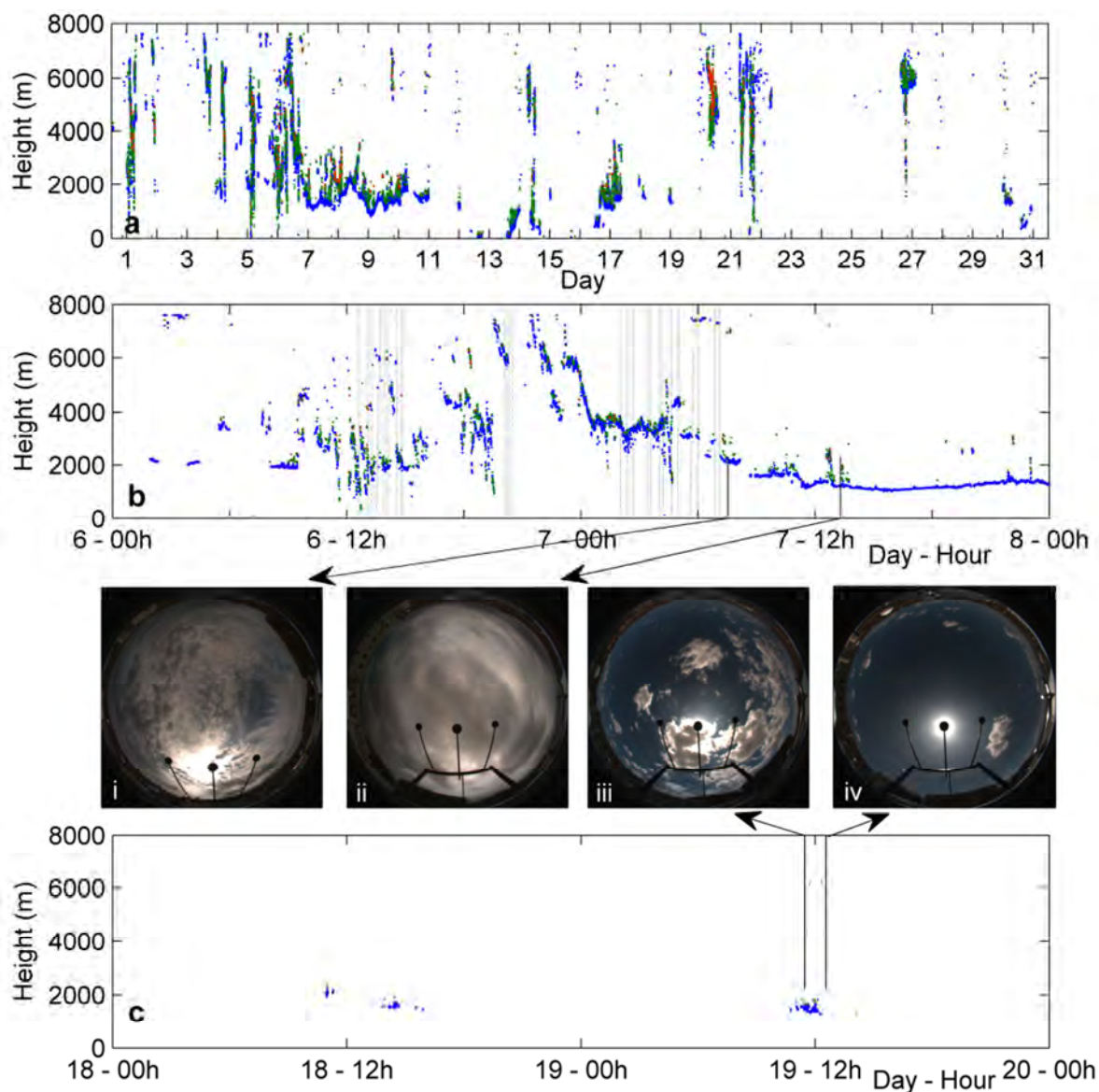


Figure 35. (a) Idem Figure 33 but for July 2009. (b) A detail for 6-7 July 2009, including (dashed lines) the periods of rain. (i) Whole sky image from July 7 at 7.30h where several cloud types in different layers can be seen and (ii) at 13.15h with *Stratus* that cover the sky (c) A detail for 18-19 July 2009. (iii) Whole sky image from July 19 at 11.30h, with *Cumulus humilis* clouds produced by convection; (iv) the image taken at 12.30h where clouds are disappearing.

The frequency distributions of CBH for these two different summer conditions (6-7 July and 18-19 July) are shown in Figure 36. Both histograms have marked peaks for low clouds. For the low pressure system, the maximum is at 1400 m, with a secondary maximum at 3400 m, although there are clouds at almost all altitudes during the whole episode. For the convective situation,

clouds for both days concentrate their bases within the bin centered at 1400 m, despite of some slightly higher clouds (bin centered at 2200 m) before noon of day 18. A more detailed analysis of this situation indicates that the mean CBH for the lowest layer was 1770 m (1500 m) for July 18 (July 19). This is in agreement with the lifting condensation levels, that according to surface conditions at the site (at noontime) was somewhat higher (1700 m) for day 18 than for day 19 (1200 m). In summary, both situations accumulate higher frequencies of CBH at low levels, in particular at 1400 m, where the two distributions have the maximum, contributing to the peakedness of CBH distributions for July (see Figure 29).

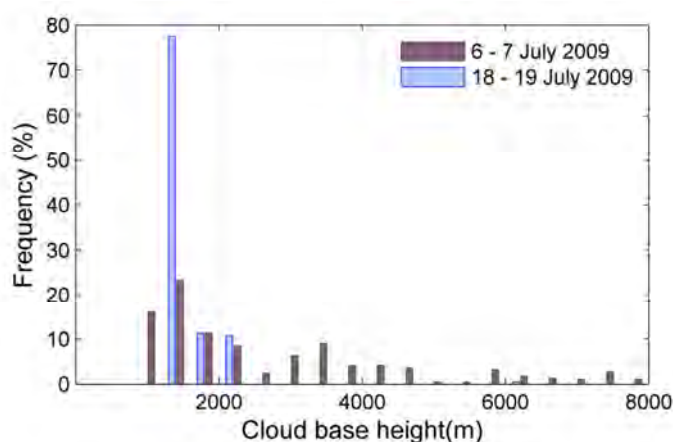


Figure 36. Frequency distributions of CBH for two different periods of July 2009.

To sum up with the results (of subsection 4.2), ceilometer measurements at Girona reveal a seasonal cycle, with important differences between “extreme” seasons (winter and summer) and the “transition” seasons (spring and autumn). Summer months in general and July in particular behave quite differently than other periods in the year, both regarding presence of clouds (with a minimum cloud occurrence of about 20-30%) and the distribution of CBH (with more than 25% of clouds having CBH around 1400 m and 80% of clouds with CBH lower than 3000 m). These CBH distributions of CBH are explained on the basis of some atmospheric situations that generate clouds, in particular conditions that produce the large number of low level clouds found. All these results are obtained despite the shortcomings of ceilometer observations, related to its limited vertical range, its reduced field of view, and its inability to detect clouds above a relatively thick layer of lower clouds.

4.3. Cloud vertical structure from atmospheric profiles and surface measurements

In this section, several methods to estimate the cloud vertical structure (CVS) based on atmospheric sounding profiles are compared, considering number and position of cloud layers, with a ground based system which is taken as a reference: the Active Remote Sensing of Clouds (ARSCl). All methods establish some conditions on the relative humidity, and differ on the use of other variables, the thresholds applied, or the vertical resolution of the profile. In this study these methods are applied to 193 radiosonde profiles acquired at the ARM Southern Great Plains site during all seasons of year 2009 and endorsed by GOES images, to confirm that the cloudiness conditions are homogeneous enough across their trajectory.

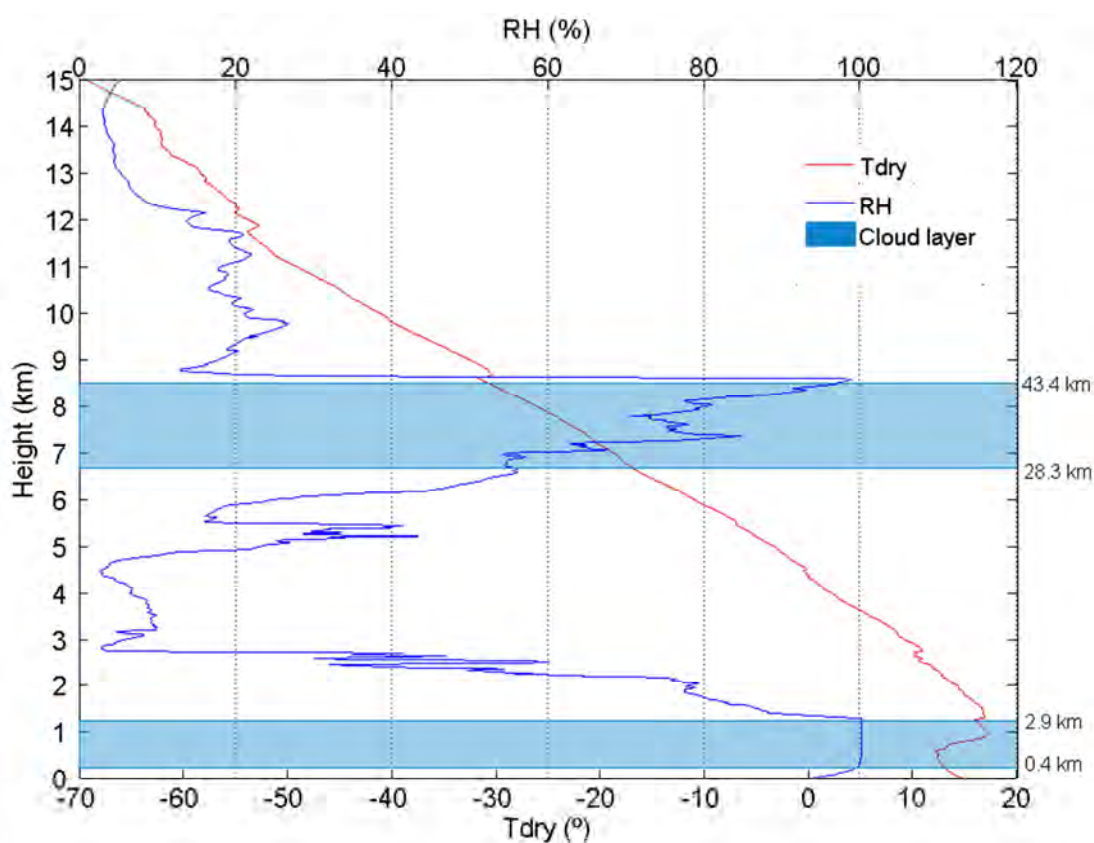


Figure 37. Temperature (T_{dry} ($^{\circ}\text{C}$), in red) and relative humidity with respect to water (RH (%), in blue) profiles above ground level from the radiosonde on October 5 of 2009 at 23.23h at SGP. Blue shading represents the cloud layers as detected by ARSCl. The values (on the right) related to every cloud layer boundary indicate the sonde horizontal distance from ARSCl site in kilometers when it reached those altitudes.

To illustrate the two sources of data that are combined in this study, an example of temperature and relative humidity profiles, as measured by the radiosonde and of two cloud layers as detected by ARSCL, is shown in Figure 37. See also in Figure 37 the sonde horizontal distance from the launching site when it reaches the altitudes where clouds are detected by ARSCL. The whole methodology is deeply explained in section 3.3.2.

4.3.1. CVS behavior during some atmospheric conditions

We present here four analyzed cases that correspond to different sky situations (no clouds, low, middle, and high clouds respectively). Figures 37 to 40 are composed of (a) the ARSCL and RS plots, (b) the cloud layers resulting from every applied method, and (c) GOES infrared images corresponding to approximately 25-45 minutes after the launch time (the SGP location and the position of the RS every 3 km in height are indicated in these images). Additionally, TSI images and animations, which are only available for daytime situations, can be found in the ARM archive (www.archive.arm.gov). All these figures and procedure allow guessing if the sonde may have crossed a cloud layer. In particular, taking into account the horizontal projection of the ascending RS, GOES images help to guess whether the trajectory of the RS went through clouds.

Specifically, panels (a) of each figure 37-41 show the ARSCL products around the RS launch time, that is the Cloud Base Height Best Estimate (CBBE) and up to three bottom heights and top heights of hydrometeor layers from composite MMCR/MPL. The vertical position of the radiosounding depending on the time is shown on the same panel. These figures allow visualizing if cloud layers were constant or not directly above the SGP site during and around the RS ascent. Panels (b) show, first of all, the cloud layers as detected by ARSCL (ARSCLm and ARSCLv), and second, the cloud layers found by the explained methods (PWR95, WR95, Chernykh and Eskridge (1996, CE96), Dimitrieva-Arrago and Shatunova (1999, DS99), Minnis et al. (2005, MNS05) and Zhang et al. (2010, ZHA10)).

Figure 38a, corresponding to 15 April 2009, shows that during the RS ascent there were no clouds above the site (except for a tiny high cloud at around 11:40 h). Moreover, GOES images confirm that the RS moved through a region free of clouds (see Figure 38c). Despite this, Figure 37b shows that some methods (CE96 and ZHA10) detect high clouds (producing a false positive); therefore these two methods find a moist layer, which could probably be related with

clouds present earlier, or moisture at that level downstream of the ARSCL location that the RS passed through, and interpreted it as a cloud. The other methods do not detect any cloud layers, as should be according to ARSCL and satellite images (perfect agreement).

In Figure 39a (15 October 2009) ARSCL data show that during the RS ascent there are two low, thin cloud layers below 1000 m, although the higher layer disappeared at 5:30 h. Probably, the RS crossed these two layers, since the horizontal displacement during the few minutes that are needed by the RS to reach 1000 m is very small (see Figure 39c). Despite a relatively large maximum horizontal displacement, GOES images confirm that the RS moved through a region of homogeneous low clouds (Figure 39c) so this profile is maintained in the dataset. Note that these low clouds, which have a temperature similar to the surface, are hardly distinguishable in a static infrared image but become perceptible when the image sequence is inspected. Only CE96 method (Figure 39b) detects these two layers, but it also finds other layers at middle and high levels of the troposphere that did not exist (therefore it is an approximate agreement). All other methods are also in approximate agreement with ARSCL because they detect the two layers as one layer.

For the case in Figure 40a (10 July 2009), ARSCL observed a cloud layer at about 5 km over SGP during the RS ascent, but PWR95 is the only method that detected it (Figure 40b), showing a perfect agreement. The other methods give false negatives. The TSI images/animation (available in ARM archive) show that on the launch time (11:30h UTC) and also on the time when the RS reached 5 km (11:48h) there are scattered clouds at SGP. GOES images show that the RS moved through a region with inhomogeneous mid-level cloudiness (Figure 40c) so this profile is not included in the database. In fact, this case could be an example of what Naud et al. (2003) already found: the disagreements between radar- (in our study ARSCL) and radiosonde-derived cloud boundaries may be caused by broken cloud situations when it is difficult to verify that fixed active sensors and radiosondes are observing the same clouds due to the horizontal drift of the latter.

For the case in Figure 41 (20 January 2009) ARSCL detected a high cloud during the ascent of the RS. WR95, CE96 and ZHA10 methods detected the high cloud that ARSCL observed as well. However, PWR95, WR95 and CE96 also detected a low cloud layer between 760 to 810 m, which in fact was observed by ARSCL quite later (at 15 h, not shown). Again, CE96 method estimated some middle and high layers that did not exist at the ARSCL location. Therefore, in this situation, there is an approximate agreement for WR95 and CE96, a perfect agreement for ZHA10, false

negative for DS99 and MNS05, and a not coincident qualification for PWR95. The TSI images/animation (available in ARM archive), at 13:44 h (two hours after the RS launch) does not seem to show any cloud layer that the ARSCL data show at that time. Despite the agreement of some methods, this case is not included in the database because the GOES image (Figure 41c) cannot confirm that high clouds were present neither over SGP nor over the region where the RS moved through.

The case in Figure 42 (5 October 2009) show a multilayer case with 2 layers of clouds as detected by ARSCL: a low cloud layer (from 250 to 1200 m) and a high layer (from 6700 to 8500 m). Results of PWR95, WR95 and ZHA10 methods are classified as “perfect agreement” because they detected the two cloud layers that ARSCL observed as well. CE96, DS99 and MNS05 are classified as “approximate agreement”, because CE96 detected two low layers, DS99 detect an additional high layer, and the MNS05 only detect the lower layer. The TSI image/animation (available in ARM archive) from the RS launch time (23:28 h UTC) to 00 h UTC shows that there are clouds over the location and some raindrops. Based on the scrutiny of the GOES infrared image (at 00:15 UTC of the next day, 6 October 2009), this multilayer case is included in the final dataset because it verify that at that time the satellite shows that there is indeed some clouds over SGP and over the region where the RS moved through.

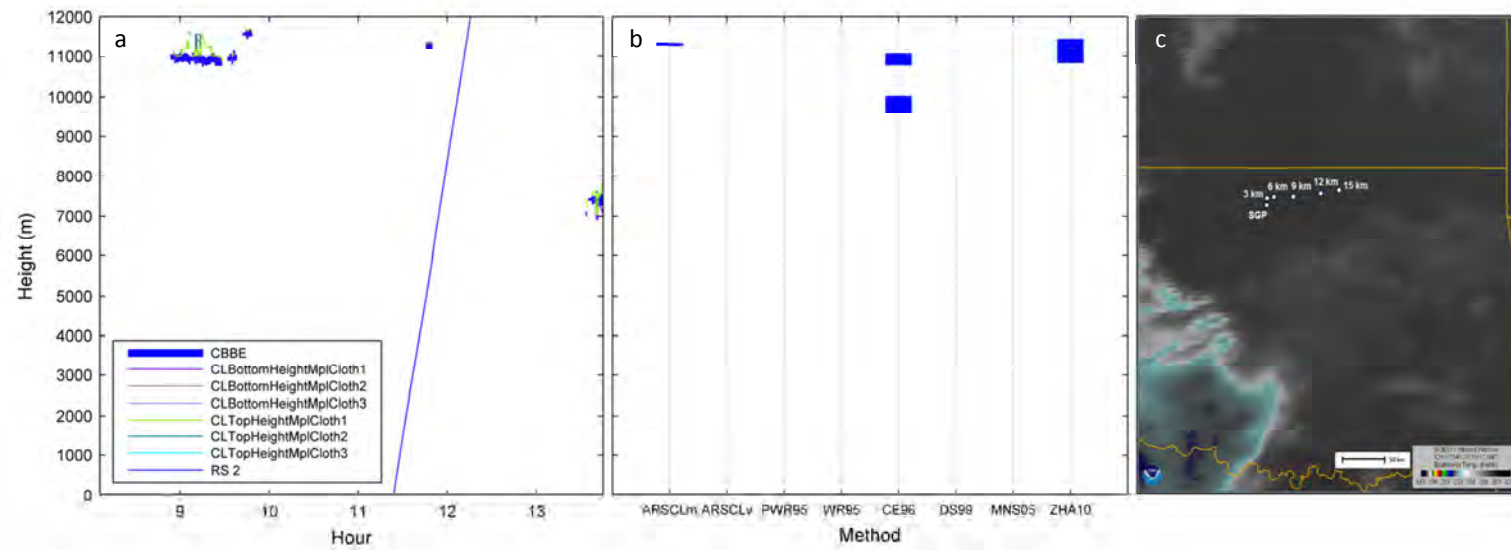


Figure 38. Case 1: 15 April 2009, No clouds. (a) Vertical position of the radiosounding depending on the time and the ARSCL products around the RS launch time (11:21 h UTC). (b) Cloud layers as detected by ARSCL (ARSCLm and ARSCLv), and as found by the explained methods (PWR95, WR95, CE96, DS99, MNS05 and ZHA10). (c) GOES image in the infrared channel at 12:00 UTC (approximately 25-45 min from the launch time). Dots indicate the horizontal position of the RS every 3 km height.

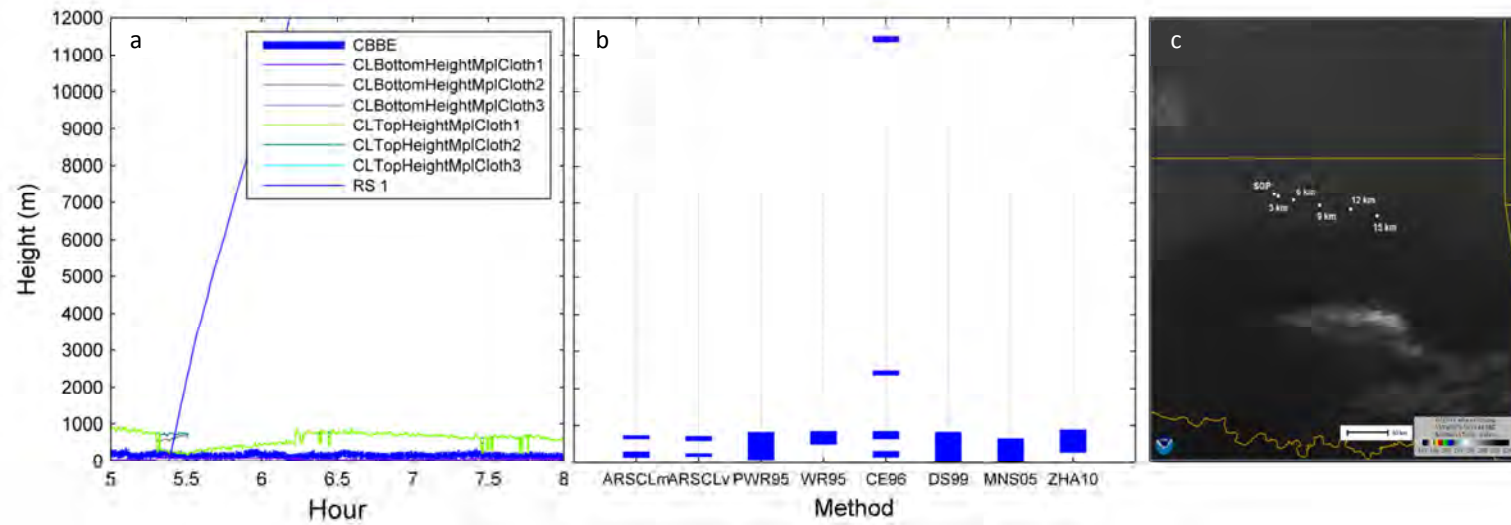


Figure 39. Idem as Figure 38, but for Case 2: 15 October 2009, Low clouds. RS launch time: 5:23 h UTC. GOES infrared image at 06:00 UTC.

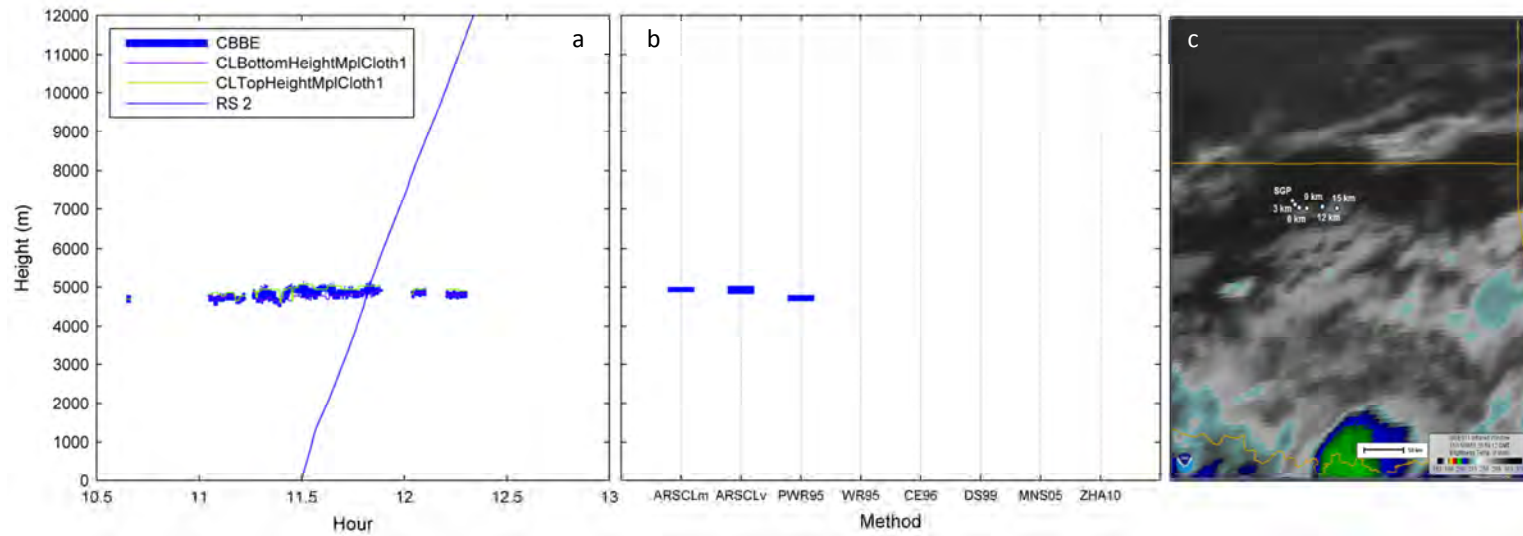


Figure 40. Idem as Figure 38, but for Case 3: 10 July 2009, Middle clouds. RS launch time: 11:30 h UTC). GOES infrared image at 12:00 UTC.

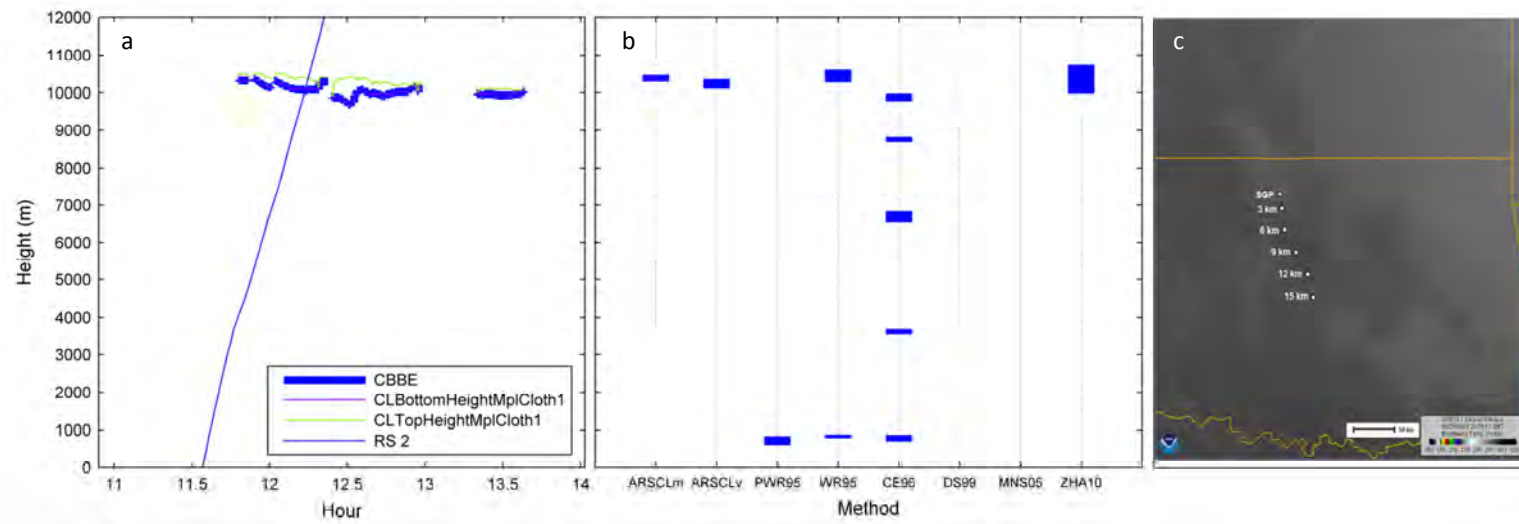


Figure 41. Idem as Figure 38, but for Case 4: 20 January 2009, High clouds. RS launch time: 11:34 h UTC. GOES infrared image at 12:00 UTC.

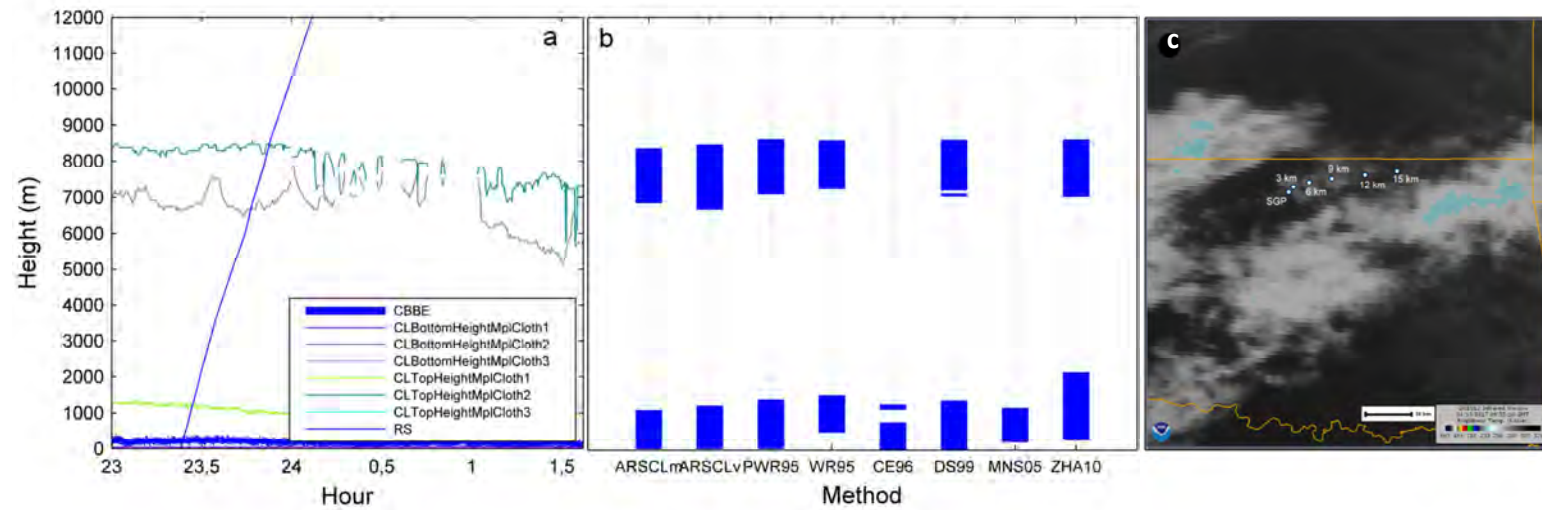


Figure 42. Idem as Figure 38, but for Case 5: 5 October 2009, 2 layers of clouds: low and high clouds. RS launch time: 23:28 h UTC. GOES infrared image at 00:15 UTC (6 October 2009).

4.3.2. General comparison of methods

Table 9 summarizes the behavior of the six methods for cloud detection from radiosoundings when compared to ARSCL observations, for all the 193 profiles considered. As commented in section 3.2.2, the sky situations are classified into four categories using ARSCL data: ‘no clouds’ (94 cases), ‘1 layer’ (58), ‘2 layers’ (32) or ‘more than 2 layers’ (9). Then, for every sky situation the methods are classified in several categories depending on the coincidence with the number and position of observed layers. Further, every comparison is accounted as false negative, false positive, perfect agreement, approximate agreement, or not coincident as previously defined.

In order to help to distinguish among the methods’ performance and support the general conclusions the 95% confidence intervals are also given for perfect agreement as an estimation of the statistical uncertainty. The confidence interval (CI_m), to a 95% confidence, has been calculated for each method with the formula:

$$CI_m = \frac{1.96 \cdot d_m}{\sqrt{n}}$$

where d_m is the dispersion:

$$d_m = \sqrt{\frac{PA_m \cdot \left[1 - \frac{PA_m}{n}\right]^2 + (n - PA_m) \cdot \left[0 - \frac{PA_m}{n}\right]^2}{n}}$$

PA_m is the number of cases of ‘Perfect Agreement’ for each method, and n is the total number of cases.

According to the results in Table 9, three methods (PWR95, MNS05 and ZHA10, see table 7 in section 3) have perfect agreements greater than 50%. Two of these methods, PWR95 and ZHA10, stand out for their high perfect agreement of 50.3% and 53.9%, and high approximate agreement of 35.8% and 29.5%, respectively, meaning that less than 17% of cases may be considered incorrect (false positive, false negative, not coincident) for both methods. MNS05 presents a very high ratio of perfect agreement (64.2%) but it gives false negative detections very often (that is, the method does not detect clouds in 18.1% of cases), so its approximate agreement is also very low (15.0%). The poorest results are obtained by CE96 (perfect agreement, 25.9%), which detects many layers that do not exist (for example, 24.4% of false positive, and 20.7% of not coincident with any ARSCL layer). If the analysis is done only with the

cloudy situations (so without considering the ‘no clouds’ cases) the perfect agreement worsens in all methods, as expected considering that the cloudless cases are the simplest. ZHA10 only reduces its perfect agreement to 32%, while in the other extreme, CE96 decreases its perfect agreement to 1%. However, the proportion of approximate agreement increases remarkably for all methods. In particular, PWR95, WR95 and DS99 improve their approximate agreement up to values from 70-80% (not shown in Table 9).

It is remarkable that the DS99 method is quite efficient despite its simplicity and the fact that it was developed mainly from stratiform situations. This method produces the highest value of approximate agreements (40.9%), due to a number of cases in which more layers than actually in existence (according to ARSCL) are detected. For example, from the 58 one-layer cases, DS99 detects this layer correctly in 56 cases, and at least one more layer, in 45 of these. Similarly, from the 32 two-layer cases, DS99 detects both layers in 19 cases, but at least one more layer in 14 of them.

The major problem with MNS05 is that it tends to underestimate the presence of clouds in many situations (e.g., 20 out of 58 one-layer cases, 25 out of 32 two-layer cases), for this reason its false negative percentage is high (18.1%) in comparison to the other methods. Accordingly, there are very few false positive from MNS05 (0.5%), while all other methods have significantly higher values (from 10.9% to 24.4%). For these reasons MNS05 worsens noticeably when only cloudy situations are considered.

The method CE96 stands out for its false positive detections: the method produces more cloud layers than observed in 47 out of 94 no cloud cases, 42 out of 58 one-layer cases, 25 out of 32 two-layer cases; it seems that this method is too sensitive. Zhang et al. (2012) found the same behavior for CE96, and remarked that this method identifies too many very thin cloud layers (our results indicate that CE96 detects high clouds 23% of the no clouds cases). In fact, Seidel and Durre (2003) had already criticized the use that Chernykh et al. (2001) made of CE96 method to analyze the trends in low and high cloud boundaries using radiosonde data obtained from 795 stations around the world. Specifically, Seidel and Durre (2003) claimed that (1) the CE96 method is very sensitive to vertical resolution, and (2) the vertical resolution of soundings has increased over recent decades, and concluded that these limitations “undermined the credibility of the reported trends”. Subsequently, Chernykh et al. (2003) replied to these criticisms arguing that the calculations in Chernykh et al. (2001) were accurate enough so the obtained trends represent atmospheric changes possibly due to climate change.

Table 9. Behavior of the six RS methods for cloud detection compared to ARSCL observations. Data in bold account for 'Perfect agreement' cases; data in italic account for 'Approximate agreement' cases.

ARSCL (Visu)			METHOD							
Situation	Num. Cases	%	Situation	PWR95	WR95	CE96	DS99	MNS05	ZHA10	
			No clouds	73	67	49	69	93	72	
No clouds	94	48.7	Clouds (1st CBH)							
			Low	12	10	18	10	1	6	
			Middle	9	12	7	13	0	6	
			High	0	5	22	2	0	10	
			No clouds	1	1	5	1	20	4	
1 layer	58	30.1	1 layer	Coincident	21	16	1	11	27	29
			Not coincident	2	0	8	1	1	2	
			<i>>1 layer</i>	<i>Some is coincident</i>	<i>33</i>	<i>40</i>	<i>17</i>	<i>45</i>	<i>9</i>	<i>23</i>
			Any coincidence	1	1	25	0	1	0	
			No clouds	1	1	2	0	11	1	
2 layers	32	16.6	1 layer	<i>One is coincident</i>	5	8	1	4	12	10
			No coincidence	0	0	1	0	2	0	
			2 layers	Coincident	3	5	0	5	4	3
			<i>One is coincident</i>	6	1	2	1	2	5	
			Any coincidence	0	0	1	1	0	1	
			<i>One is coincident</i>	7	4	14	7	1	7	
> 2 layers	9	4.7	<i>>2 layers</i>	<i>2 coincident</i>	<i>10</i>	<i>13</i>	<i>7</i>	<i>14</i>	<i>0</i>	<i>5</i>
			Any coincidence	0	0	4	0	0	0	
			No clouds	1	0	2	0	4	2	
			Perfect agreement	0	0	0	0	0	0	
			<i>Approximate agreement</i>	8	9	6	8	5	7	
			Any coincidence	0	0	1	1	0	0	
			False negative	1,6%	1,0%	4,7%	0,5%	18,1%	3,6%	
			False positive	10,9%	14,0%	24,4%	13,0%	0,5%	11,4%	
			Not coincident	1,6%	0,5%	20,7%	1,6%	2,1%	1,6%	
			<i>Approximate agreement</i>	<i>35,8%</i>	<i>38,9%</i>	<i>24,4%</i>	<i>40,9%</i>	<i>15,0%</i>	<i>29,5%</i>	
			Perfect agreement ± CI*	50,3 ± 7,1%	45,6 ± 7,0%	25,9 ± 6,2%	44,0 ± 7,0%	64,2 ± 6,8%	53,9 ± 7,0%	

*CI: confidence interval of Perfect agreement at 95% of confidence.

When the database is analyzed seasonally some interesting facts appear; the perfect agreement for each method and season is presented in Table 10. As can be seen in this table, the inter-seasonal variation of perfect agreement is greater than 30% for MNS05 and DS99, indicating that these methods have a distinct seasonal behavior. All methods show the maximum perfect agreement in winter, except for CE96 method. This is due to the high number of ‘no clouds’ situations in winter (71%), which in general are correctly identified. The good performance of WR95, PWR95, DS99 and ZHA10 methods when the clear sky cases are not considered is quite stable across the year (not shown).

Table 10. Seasonal values of perfect agreement (in parentheses the total number of cases) and its maximum difference for each method (W: winter, Sp: Spring, Su: Summer and A: autumn).

Method	Perfect agreement (%)				Max. Variation (%)
	W (52)	Sp (41)	Su (42)	A (58)	
PWR95	59.6	41.5	59.5	41.4	18.2
WR95	53.8	41.5	52.4	36.2	17.6
CE96	28.8	19.5	35.7	20.7	16.2
DS99	65.4	31.7	42.9	34.5	33.7
MNS05	84.6	48.8	64.3	56.9	35.8
ZHA10	69.2	41.5	54.8	48.3	27.7

4.3.3. ZHA10 tests and improvements

ZHA10 is an improvement of WR95, which in its turn is a modification of PWR95. The original reference of ZHA10 method (Zhang et al., 2010) presents a detailed comparison with cloud radar measurements that give the reference CVS, while the two earlier methods were compared against surface visual observations (and ISCCP data) which can hardly give an accurate description of the cloudiness structure. Our analyses produce similar results regarding these three methods, where the perfect agreement for ZHA10 is better than PWR95 and WR95 (Table 9) and also when only cloudy situations are considered. In addition, a slight change in the ZHA10 method produces a noticeable improvement in its performance (see below). Therefore, we have tested this method suitability for low resolution vertical profiles and checked the algorithm conditions for a moist layer to become a cloud layer and the conversion of relative humidity with respect to ice, besides the effect of coarsening RS vertical resolution.

The original ZHA10 method gives a relatively high number of false positive detections, in particular for thin clouds. Therefore, in order to reduce this percentage we extended to the whole atmospheric profile the condition of the minimum thickness (400 m) of a moist layer to be considered as a cloud layer. Recall that ZHA10 applies this condition only to moist layers with bases lower than 120 m. As expected, this new method, which will be denoted as ZHA10i, reduces false positive detections from 11.4% to 8.8% and improves the perfect agreement from 53.9% to 60.1%, (see Table 11). This improvement is mainly linked to a better detection ('coincident') of one-layer cases (35 out of 58) and is spread along all seasons and when only cloudy situations are considered.

In Figure 43 a comparison of the first CBH as derived from ZHA10 and ZHA10i estimation methods against the CBH from ARSCL measurements is shown. Among the 193 study cases, 95 have at least one CBH according to both ARSCL instruments and ZHA10 method; and 92 of the 193 for ZHA10i. The correlation between the first layer found with instruments and ZHA10 method is good ($r^2= 0.52$), and between ARSCL and ZHA10i is very good ($r^2= 0.84$). It is interesting to see that the points and the regression line for ZHA10i method is very close to the perfect agreement line (slope=1) It means that the ZHA10i method does not tend to underestimate nor overestimate the first CBH.

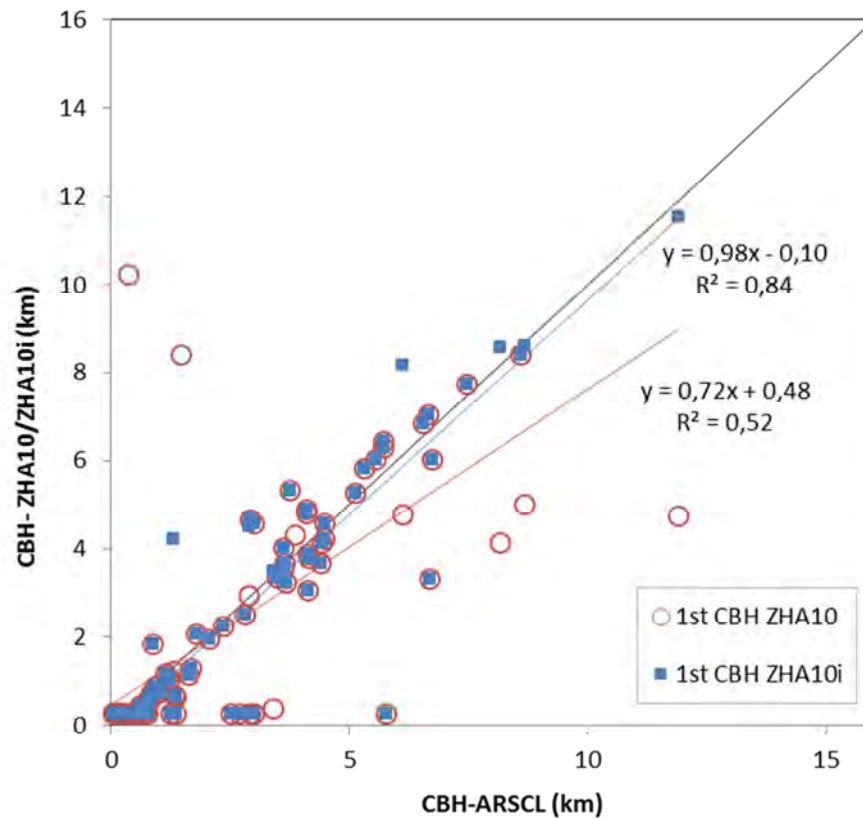


Figure 43. Comparison of cloud base height as derived from ZHA10 and ZHA10i methods estimation from RS vertical profile measurements against the cloud base height from ARSCL measurements (CBH-ARSCL) in SGP. The black diagonal is the line of the perfect agreement.

Several studies (including methods ZHA10, WR95, MNS05, but also Yi et al., 2004, for example) remark on the calculation of the relative humidity with respect to water or to ice when temperature is low enough. Therefore, we perform two tests: 1) removing the conversion of RH with respect to ice (ZHA10i-a); or 2) lowering the threshold temperature from 0°C to – 20°C (ZHA10i-b). As can be seen in Table 11, the overall behaviour of these two tests is worse than ZHA10i. In fact, ZHA10i-a is less effective in general than ZHA10i: it loses more layers (especially high cloud layers) which increases the false negative detections (from 3.6% to 12.4%) resulting in a perfect agreement improvement from 60.1% to 63.7% but an approximate agreement reduction from 26.4% to 19.2%. With ZHA10i-b, for the whole year neither the perfect agreement nor the approximate agreement changes much with respect to ZHA10i. However, results of ZHA10i-b are seasonally dependent: agreements for winter and spring are better than for ZHA10i, and for autumn and summer they are worse. Therefore, further analyses and tests

will be performed on ZHA10i, without any change regarding the treatment of relative humidity with respect to ice.

Despite the high vertical resolution of the current RS measurements, most sonde launching sites around the world release low vertical resolution profiles (GTS messages), so it is good to know if ZHA10i method works for lower resolution as well. It could be useful to check if this method could be used in reanalysis products. Reanalysis gives results on a coarse vertical resolution (see for example Table 2 in Crewell et al., 2004; or Table 1 in Illingworth et al., 2007). Specifically, the typical number of levels in the models and reanalyses is in the range of 30-60 (that is, resolution of around several hundred meters or several tenths of hectopascals), while the typical number of levels in radiosoundings is of the order of several thousands (that is, as previously mentioned, resolution of few meters or about one hectopascal). Therefore, we downgraded the resolution of the radiosoundings using the procedure from Minnis et al. (2005) to decrease the vertical resolution to 25 hPa (that is from around 3000 to 36 levels), and then applied the ZHA10i method.

Results of this test (ZHA10iLR hereinafter) show that the perfect agreement is significantly higher than ZHA10i (increasing from 60.1% to 66.3%). Combining perfect and approximate agreements, ZHA10iLR shows low variability along the year, with the minimum in summer (perfect 66.7%, approximate 16.7%) and the maximum in winter (perfect 86.5%, approximate 5.8%). We also find that false negative situations increase (from 3.6% to 7.8%), while false positive detections decrease (from 8.8% to 1%). Therefore, the use of lower resolution (ZHA10iLR) does not imply poorer results; contrarily, in many situations the detection of cloud layers improves.

ZHA10iLR results were inspected in detail and we found that the method tends to produce less cloud layers (which can explain the transfer from false positive towards false negative detections), while the layers found tend to be thinner (which make them more similar to the ARSCL reference). There are three reasons for this behavior: first, some moist layers were not found because the interpolated (averaged) RH values of the low resolution profile do not reach the min-RH threshold; second, some moist layers were not defined as cloud layers because the max-RH threshold that the method fixes within the layer is not reached. This is caused, in both cases, by the averaging of RH values involved when coarsening the resolution, which implies a smoothing of the RH vertical profile. The third reason is that some moist layers were not considered as cloud layers because the thickness threshold (>400 m) is harder to accomplish in the low resolution profile.

Table 11. Behavior of the tests performed on ZHA10 method compared to ARSCL observations. Data in bold account for 'Perfect agreement' cases; data in italic account for 'Approximate agreement' cases.

ARSCL (Visu)			METHOD							
Situation	Num. Cases	%	Situation	ZHA10	ZHA10i	ZHA10i-a	ZHA10i-b	ZHA10iLR	ZHA10 LRnew	
No clouds	94	48.7	No clouds	72	77	90	79	92	90	
			Clouds (1st CBH)	Low	6	4	2	4	1	2
				Middle	6	6	2	3	0	0
				High	10	7	0	8	1	2
1 layer	58	30.1	No clouds	4	5	16	6	12	7	
			1 layer	Coincident	29	35	31	33	34	36
				Not coincident	2	0	1	1	3	0
			<i>>1 layer</i>	<i>Some is coincident</i>	<i>23</i>	<i>18</i>	<i>10</i>	<i>17</i>	9	15
				Any coincidence	0	0	0	1	0	0
2 layers	32	16.6	No clouds	1	1	5	1	2	2	
			<i>1 layer</i>	<i>One is coincident</i>	<i>10</i>	<i>12</i>	<i>14</i>	<i>13</i>	<i>18</i>	<i>17</i>
				No coincidence	0	0	4	0	0	0
			2 layers	<i>Coincident</i>	3	4	2	3	2	3
				<i>One is coincident</i>	5	5	1	5	5	4
				Any coincidence	1	2	0	2	0	1
			<i>>2 layers</i>	<i>One is coincident</i>	<i>7</i>	<i>3</i>	<i>3</i>	<i>3</i>	<i>3</i>	<i>3</i>
				<i>2 coincident</i>	<i>5</i>	<i>5</i>	<i>3</i>	<i>5</i>	<i>2</i>	<i>2</i>
Any coincidence	0	0		0	0	0	0			
> 2 layers	9	4.7	No clouds	2	1	3	1	1	1	
			Perfect agreement	0	0	0	0	0	0	
			<i>Approximate agreement</i>	<i>7</i>	<i>8</i>	<i>6</i>	<i>8</i>	<i>8</i>	<i>8</i>	
			Any coincidence	0	0	0	0	0	0	
				False negative	3,6%	3,6%	12,4%	4,1%	7,8%	5,2%
				False positive	11,4%	8,8%	2,1%	7,8%	1,0%	2,1%
				Not coincident	1,6%	1,0%	2,6%	2,1%	1,6%	0,5%
				<i>Approximate agreement</i>	<i>29,5%</i>	<i>26,4%</i>	<i>19,2%</i>	<i>26,4%</i>	<i>23,3%</i>	<i>25,4%</i>
				Perfect agreement ± CI*	53,9 ± 7,0%	60,1 ± 6,9%	63,7 ± 6,8%	59,6 ± 6,9%	66,3 ± 6,7%	66,8 ± 6,6%

*CI: confidence interval of Perfect agreement at 95% of confidence

To overcome these issues, we tried to improve the ZHA10iLR method. First we removed the condition on minimum cloud thickness (>400 m) that we applied in ZHA10i. This means that no restriction for cloud layer thickness is imposed; note, however, that the low resolution profile implies that even a single layer cloud has at least a thickness of 25 hPa (i.e., 200 m at lower levels of the atmosphere or 1000 m at the higher levels). Second, the max-RH thresholds applied in ZHA10 original method were slightly reduced, to make the condition for a moist layer to become a cloud layer less restrictive. The new values are given in Table 12. In fact, the effect of RH thresholds in the retrieval of CVS (in relation with different climates or different radiosonde instruments) has been discussed in previous studies (Naud et al., 2003; Wang et al., 1999; Zhang et al., 2012; among others). Moreover, Zhang et al. (2013) presented a study about the suitable thresholds to be used depending on the particular RS used and on the specific site. The test with these two changes is labeled as ZHA10LRnew in Table 11. The perfect agreement rises up to 66.8%, and the false negative detections decreases down to 5.2%. So it appears that, with these modifications, the method suggested by Zhang et al. (2010) has potential to be successfully applied to low resolution profiles. Note that these results are in fact slightly better than those obtained by ZHA10i on the high resolution profile. So we also tested the change of the max-RH threshold on this case, but the results (not shown) turned out to be somewhat worse. In summary, the original values of max-RH seem adequate for high resolution profiles, while the new thresholds suggested here appear more suitable for low resolution profiles.

Table 12. Summary of the values for max-RH, from Zhang et al. (2010) and the new max-RH thresholds suggested for the low resolution test.

Altitude Range	ZHA10 max-RH	New max-RH
0-2 km	95% - 93%	93.5% - 91.5%
2-6 km	93% - 90%	91.5% - 89%
6-12 km	90% - 80%	89% - 77.5%
>12 km	80%	77.5%

4.3.4. ZHA10i application example

The proposed method has been applied, as an example of the usefulness of the CVS retrievals from radiosoundings, to study the role of CBH when modeling atmospheric longwave radiation at the surface during overcast skies (Viúdez-Mora et al., 2014). It is well known that the CBH is directly related to the cloud emission temperature, which is a main factor driving the longwave radiation at the surface. In this study, 82 cases of overcast situations observed at Girona were analyzed by using a one-dimensional radiative transfer model (RTM, SBDART, Ricchiazzi (1998)).

Figure 44 shows the longwave irradiance, $LW\downarrow$, as measured by a pyrgeometer (model CG1 from Kipp&Zonen, The Netherlands) against the CBH as determined by the ceilometer. Data points are representative of 10-minute periods, and distinction has been made between cases from the warm half of the year (climatic mean screen level temperature higher than 15°C, May to October, 38 cases) and those from the cold half of the year (temperature lower than 15°C, November to April, 44 cases). The CBH of all selected cases is between 0 and 5 km, most cases (61) having $CBH < 2$ km. The mean \pm standard deviation of CBH is 1.4 ± 1.0 km for the whole set of data, 1.5 ± 1.0 km for the warm period, and 1.3 ± 1.0 km for the cold period. In Figure 44, the whole set of points shows a large dispersion in $LW\downarrow$ values, and the dependence on CBH is not totally evident. However, taking separately each subset of data, a clear negative correlation (decreasing $LW\downarrow$ with increasing CBH) is noted. This is easily explained because the clouds closer to the surface are usually warmer than higher clouds, so enhancing its IR emission. As a first approximation, this dependence can be estimated to be about -12 Wm^{-2} per km, both for “warm” and “cold” points. There is some dispersion remaining in each subset coming from the fact that the represented cases correspond to different specific meteorological situations (temperature and humidity vertical profiles, cloud characteristics, etc).

For the Radiative Transfer Model (RTM) simulations of the longwave irradiance, the CBH were determined from ceilometer measurements and also estimated by applying the ZHA10i method to temperature and humidity profiles derived from the European Center for Medium range Weather Forecast (ECMWF), because radio soundings were not available in Girona. The high resolution ZHA10i method was applied here because the profiles were also high resolution: a mesoscale model was used to interpolate at finer (both horizontal and vertical) resolution the original coarse ECMWF analysis data. So, CBH ZHA10i estimations were proposed as an alternative to the direct measurements provided by the ceilometer (Viúdez-Mora et al., 2014).

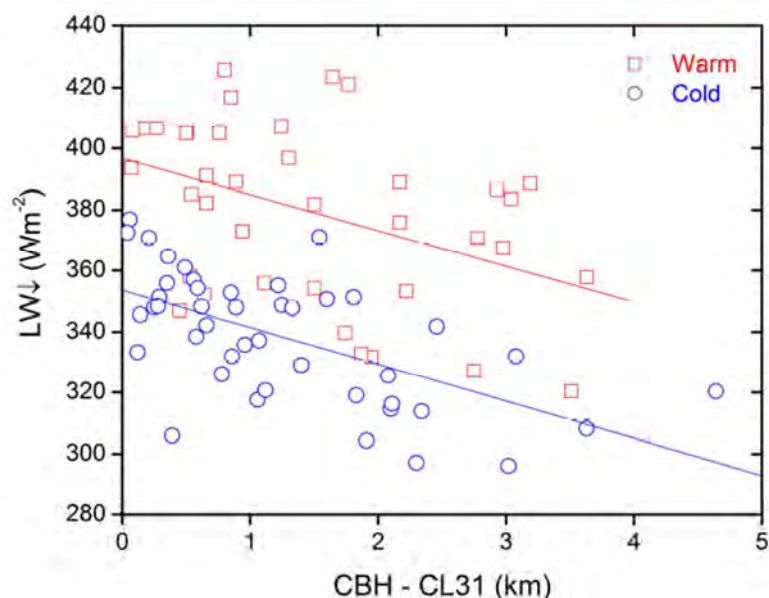


Figure 44. Downwelling longwave irradiance from pyrgeometer measurements against cloud base height measured with the ceilometer. Both values are ten minute averages. Lines correspond to the linear regression for each subset of points (Viúdez-Mora et al., 2014).

Figure 45 shows the CBH estimated from the vertical profile against the CBH from ceilometer measurements. The agreement between them is fair, although it is obvious that the estimation has some deficiencies. First, there are a number of cases when CBH-ZHA10i takes the minimum value (0.28 km) while the measurements indicate that clouds are quite higher. For these cases, the relative humidity in the first level of the synthetic atmospheric profile is higher than the required thresholds for a layer to be considered as a cloud. Second, there are two cases where the opposite occurs: CBH-ZHA sets a cloud much higher (around 9 km, so these cases do not appear in Figure 45) than the observed CBH. Finally, among the 82 cases, there are 4 cases for which the ZHA10i method does not detect any cloud since the relative humidity in the ECMWF-derived profile does not reach the specified thresholds at any level. It is remarkable that even when applied to synthetic profiles, CBH-ZHA10i captures in general the behavior of the cloud base height, since most values are arranged around the line of perfect agreement.

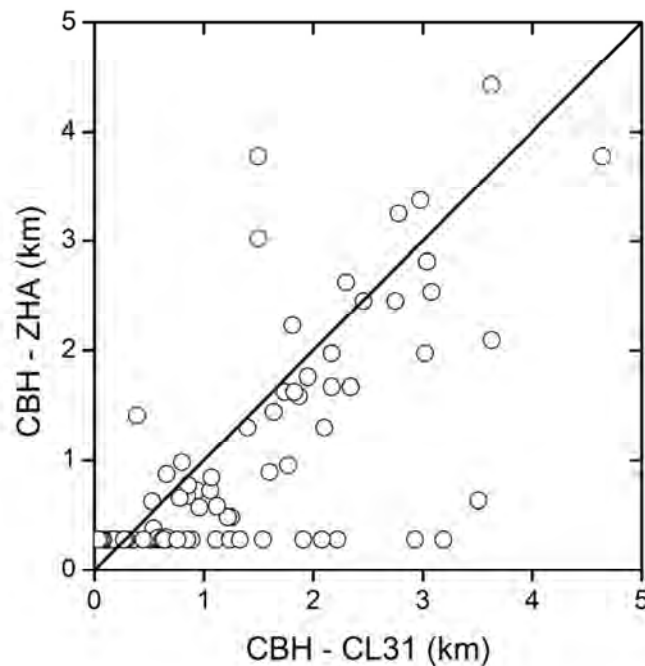


Figure 45. Comparison of cloud base height as derived from vertical profile (CBH-ZHA) against the cloud base height from ceilometer measurements (CBH-CL31). The diagonal is the line of the perfect agreement. Two outliers (CBH-ZHA \sim 9 km) are not shown (Viúdez-Mora et al., 2014).

Regarding the behavior of the longwave radiation as depending on CBH, Viúdez-Mora et al. (2014) results (Figure 46) show the general agreement between RTM estimations of $LW\downarrow$ and the corresponding observations. In total, three tests were performed and the best agreement indexes correspond to the 'CL31 test' (Figure 46 left), i.e. when the ceilometer observed CBH is used. In this test, dispersion of residuals is very low (6.2 Wm^{-2}) and bias is quite low too (1.6 Wm^{-2}). Results obtained with 'ZHA10 test' (right) are not much worse: bias is quite larger (4.3 Wm^{-2}), and dispersion is also increased (7.0 Wm^{-2}). These numbers may be compared with a more realistic estimation of the measurement uncertainty for $LW\downarrow$ which is calculated to be lower than 3 Wm^{-2} . Possible deficiencies in the synthetic profile (in particular, too high humidity at the lower levels) may explain the poorer results of ZHA10i method for CBH estimation and the general tendency towards overestimation that show the ZHA10i results. All these analyses confirm that the CBH plays a double role on $LW\downarrow$: first, CBH defines the temperature of the lowest cloud boundary (the cloud base); second, CBH somewhat discriminates between those

atmospheric layers that will add their effect on $LW\downarrow$ (i.e., layers between the cloud base and the ground) from those that will not have any effect (i.e., layers above the cloud).

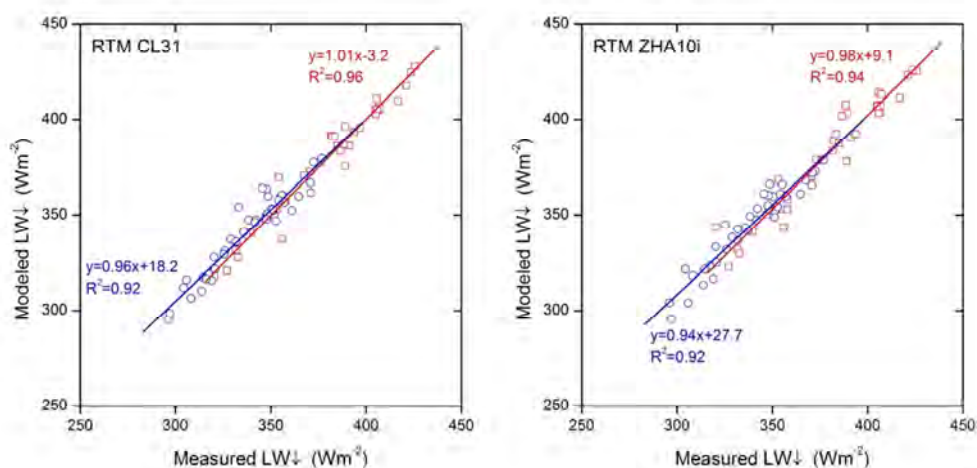


Figure 46. Comparison between calculated and measured $LW\downarrow$ at Girona, during overcast conditions and for the RTM results when using CBH measured by ceilometer (left) and for the ZHA10i results. See text for definition of tests. Warm season data (red) and cold season data (blue) are distinguished in the plots. Equally, the linear regression lines are given for both subsets of data (Viúdez-Mora et al., 2014).

To sum up with the results (of the subsection 4.3): The perfect agreement (i.e. when the whole CVS is correctly estimated) for the RS methods ranges between 26-64%; the methods show additional approximate agreement (i.e. when at least one cloud layer is correctly assessed) from 15-41%. When some changes are applied on one of these methods, the perfect agreement improves; moreover, this method is successfully adapted to make it suitable for low resolution vertical profiles. The perfect agreement, even when using low resolution profiles, reaches up to 67% (plus 25% of approximate agreement) if the thresholds for a moist layer to become a cloud layer are modified to minimize false negatives with the current data set, thus improving overall agreement. The ZHA10i method is subsequently applied in a study of the longwave irradiance reaching the ground under overcast conditions, when the CBH is a fundamental parameter driving this radiation.

5. Conclusions

This doctoral thesis has focused on a better description of both the horizontal and vertical distributions of the cloud field, by analyzing the cloud cover (CC), the cloud base height (CBH) and the entire cloud vertical structure (CVS) in many situations and from different sources. It may also constitute as a contribution to a broader exploitation of the large amount of experimental information that can be derived from instruments widely deployed (already in existence and being continuously extended), which can be used to characterize the cloudiness from a geometrical point of view. Two main sources of data have been considered: ceilometers and radiosoundings. Each of them has its own possibilities, which have been widely discussed in this work. Ceilometers can give high-precision measurements of the CBH (until a limited height range) and some estimation of the CC (cloud cover, assimilated to the vertical cloud occurrence) and radiosoundings can give an estimation of the CVS above the launch site. Specifically, several years of data acquired with a ceilometer located in Girona have been used to determine the ability of this instrumentation in obtaining the CC and the CBH vertical and temporal distributions. On the other hand, methods for deriving the CVS, based on RS profiles, have been compared with reliable retrievals from active surface instrumentation deployed at the Southern Great Plains site of the Atmospheric Radiation Measurement Program, and some improvements in the methodologies have been proposed.

This work has confirmed that ceilometers constitute a reliable instrumental method for sounding the atmosphere and describing cloudiness, specifically cloud base height, cloud cover, and even cloud vertical structure. The main conclusions (which will be detailed in following paragraphs) derived from the study in Girona are that ceilometer measurements reveal a seasonal cycle, with significant differences between the "extreme" seasons (winter and summer) and the "transition" seasons (spring and autumn). Summer months, in general, and July in particular, behave quite differently to other periods in the year, in terms of cloud occurrence). The study carried out at the Southern Great Plains reveals the strengths and weaknesses of the methods to retrieve the CVS based on radiosoundings. The six methods analyzed present significant differences in regards to their performance, although the best methods can reach agreements (perfect plus approximate) with observations higher than 80%. It appears that one method, provided that is conveniently modified, may successfully be applied to lower resolution profiles such as the WMO's Global Telecommunication System (GTS) vertical profiles or to the reanalysis temperature and humidity products.

From the ceilometer deployed in Girona, four years (2007-2010) of high resolution ceilometer measurements (both in time, 12 s; and in the vertical direction, 10 m) have been analyzed. The monthly cloud occurrence retrieved follows a similar evolution throughout the four years. Cloud occurrence has an average value of about 40-50%, with a summer minimum (down to 30%) centered in July. This behavior is also found in local climatology based on visual observations of CC, despite the different field of view associated to each methodology, and also despite the shortness (from the climatic point of view) of the ceilometer dataset. Moreover, the results are very consistent with regional climatology of CC based on surface and satellite observations.

The vertical distribution of the CBH has also been analyzed from the same dataset. The proportion of single layer cases, about 90%, is clearly an overestimation and linked to the missing very high layers (above 7620 m, the height range limit of the ceilometer) and to undetected layers above the lowest layer present. Comparison with other studies from the literature has confirmed this preferential assignation to single layer cases when a ceilometer is used for cloud detection.

Monthly CBH distributions have shown a yearly cycle, being more uniform or bimodal in winter (therefore with lower skewness) and more peaked (that is with higher kurtosis) in summer. The seasonal evolution has been confirmed by the cumulative frequencies for the CBH: in July, only 25% of cases have CBH less than 1400 m, but 80% of clouds are below 3000 m. To the contrary, in January almost 40% of detected clouds have CBH less than 1000 m, so clouds up to 5000 m have to be accounted as making up 80% of cases. The particular behavior of cloud occurrence in the summer has again been represented by the CBH distributions in July, which clearly peaked at the bin centered at 1400 m. Low clouds, originated from some typical synoptic conditions in summer on the one hand and from local convective activity on the other, can contribute to this relative accumulation. On the contrary, in winter months, (represented by January) CBH distributions appear more uniform because local convective activity is much less active in winter.

Despite the limited temporal extension of the ceilometer database used and that only measurements from one location have been used, some features that may be common to all ceilometer systems have been found. First, our ceilometer has confirmed its ability to operate throughout the year taking continuous measurements of the lowest CBH. In addition, it has been found that the estimations of average cloud cover for long periods (months, years) are reasonably good, and that the retrieved CBH distributions are, at least for single-layered cloud field structures, similar to those found using other methodologies. As expected, the ceilometer cannot provide a complete description of the CVS (that is, cloud tops and the number of cloud

layers actually present) in multilayered conditions, given their inherent limitations (limited range, obscured upper layers). In fact, the results indicate –as other authors have already pointed out- that ceilometers might be quite imperfect when describing these systems (i.e. with the presence of either both low and middle clouds, or both low and high clouds, for example). The use of ceilometers with a larger detection range (as the Vaisala CL51, or the Jenoptik CHM15k, Martucci et al. (2010)) would improve the CBH distributions retrieved, but only synergistic observations with other active instruments (e.g. cloud radar) would produce more reliable statistics of cloud vertical structure. The results obtained with our study, however, are sufficiently encouraging to assume that ceilometers may become a complement or even a replacement of human observations, at least for the average cloud occurrence for relatively long periods (months) and of course for the estimation of the CBH of the lowest cloud.

Furthermore, all methods to obtain the CVS based on radiosonde profiles that are available in the literature have been tested. In particular, six methods (PWR95, WR95, CE96, DS99, MNS05 and ZHA10) to detect cloud layers from thermodynamic vertical atmospheric profiles have been applied to 193 radiosoundings from the SGP ARM site. Their performance has been assessed by a comparison with the best estimated ARSCL boundaries taken as a reference, and a detailed comparison of the CVS revealing the strengths and weaknesses of the methods has been done.

Since large horizontal displacements can be achieved by the RS during their ascent, and in order to assure the homogeneity of the cloud field in the region, a suitable comparison has been made with GOES images used to screen the RS database. Ideal conditions for comparing RS retrievals with ARSCL estimations (e.g., RS totally vertical, RH and T measurements without any error, completely stationary meteorological situation) do not exist. It is obvious that none of these conditions can ever be accomplished as during the ascent, RS always suffer some horizontal displacement; all measurements bring some uncertainty; and the atmosphere is continuously changing. So, despite the effort towards the selection of homogeneous cloudiness cases, some disagreements could be attributed to the physical horizontal displacement of the sondes from the atmosphere directly above the ARSCL site. Using the satellite data has eliminated cases when there simply were not clouds at the ARSCL detected height where the sonde ended up at that height. However, there might still be some error the other way, as there may be cloud where the sonde is but no guarantee it is at the same height as the ARSCL cloud.

Three of the methods (PWR95, WR95, and ZHA10) perform reasonably well, giving perfect agreements at around 50% and approximate agreements of around 30% of the cases. The other methods give poorer results (lower perfect and/or approximate agreement, and higher false

positive, false negative or not coincident detections). When only cloud situations are considered, the latter methods produce even poorer results.

Despite the good agreements found for PWR95, WR95, and ZHA10, there are still some 15% of cases where these methods fail to estimate the CVS. In particular, there are a number of 'false negative' and 'false positive' cases. Disagreements correspond to cases when (1) the instruments (ARSCL) classify cloud layers that some radiosounding methods fail to detect, and (2) some of these radiosounding methods are capable of detecting moist layers in the atmosphere that the instruments (ARSCL) do not classify as a cloud layer but that may be potential cloud air masses because of their high relative humidity (so they might be forming or dissipating clouds). This is not surprising in the case of subvisual clouds and given the lack of a refined physical definition, i.e. threshold of what constitutes a cloud.

The ZHA10 method is the most recent version of the treatment initially proposed in PWR95 and WR95 and provides sufficiently good results (perfect agreement of 53.9% and approximate agreement of 29.5%) to be selected for further tests and improvements. Thus, several tests have been performed on this method by changing (1) the minimum thickness for a moist layer to be considered a cloud layer, (2) the threshold temperature to calculate RH with respect to water or with respect to ice, (3) the resolution of the atmospheric profile, and (4) the altitude dependent thresholds used to distinguish between moist and cloud layers. It has been found that by extending the condition of a minimum thickness for a cloud results in an overall improvement of the method (ZHA10i; perfect agreement, 60.1%; approximate agreement, 26.4%), but modifying the RH calculations does not produce any improvement. Hence, the method denominated as ZHA10i has been applied, as an alternative to ceilometer measurements, to estimate the CBH from profiles obtained from interpolated and adjusted ECMWF profiles. Its performance has been evaluated as fair, despite the use of synthetic profiles, and its potential use in modelling issues (specifically, in this latter study, in radiative transfer modeling of the downward longwave radiation) has been demonstrated.

A remarkable result of the present study comes from the tests performed with low resolution profiles. By slightly modifying the RH thresholds and one again removing the condition of minimum cloud thickness (the ZHA10LRnew method) better overall results (perfect agreement 66.8%; approximate agreement, 25.4%) are achieved than those obtained through the original method, even when it was applied to high resolution profiles. It appears that the method suggested by Zhang et al. (2010) (provided that it is conveniently modified) may be successfully applied to lower resolution profiles such as the WMO's Global Telecommunication System (GTS)

vertical profiles, or to the reanalysis temperature and humidity products, to see if clouds are produced as well to comparing them with the reanalysis data. For example, an estimate of the CVS from RS or computed atmospheric profiles may be needed for applications such as radiative transfer, agrometeorological or weather forecast studies.

Although this doctoral thesis has reached its proposed goals, some work is still needed; more studies especially have to be done in other climate zones. It would be recommendable to update an in depth comparison between ceilometer measurements and radiosonde estimation methods for detecting clouds (and their CBH and CVS). Such a comparison could be more comprehensive if a top-down view (i.e. satellite information) were added to describe the highest clouds. The specific algorithm that obtains CBH from the backscatter signal could be improved for detection of upper layers, although we realize that the signal extinction in the lowest layer may be difficult to overcome. The statistical analysis applied in the present work could be used to further describe cloud characteristics of extended (temporally or spatially, i.e. with similar databases from other sites) or improved (i.e. higher detection range, better multilayer detection) datasets containing ceilometer measurements.

Finally, the present study extends previous comparison studies on RS methods used to obtain CVS, such as those by Naud et al. (2003) and Zhang et al. (2012), as it considers more methods and accurately compares retrievals (layer by layer) against a reliable reference (ARSCL) and for an accurately selected set of cases. For example, Naud et al. (2003) found that WR95 and CE96 were generally consistent, but their analysis was limited to the lowest cloud bases and highest cloud tops. As previously mentioned, it would be of interest to extend our analyses to other sites (other climate regimes, such as in tropical and arctic regions), other datasets (e.g. aircraft profiles from the Aircraft Communications, Addressing, and Reporting System, ACARS), or other references (such as those provided by satellite platforms, i.e. CloudSat and CALIPSO; or by other projects like Cloudnet). When using other references with the aim of testing or comparing the retrieved CVS, the horizontal mismatch between the profile and the reference instruments (both ground and satellite based) should be taken into account. Further improvements of the methods for deriving cloud vertical structure from radiosoundings (for example by including other variables such as vertical velocity) should also be addressed as a priority. If these methods are to be applied massively to build climatologies of CVS, the issue of different brands and models of sondes must be addressed; similar caution should be taken into account when using aircraft profiles. In addition, the present study has shown that any of the methods is good enough to be used in climatological-oriented studies if a high accuracy of the CVS is sought. However, results

of the present paper are useful because they quantitatively assess the ability of the methods based on radiosoundings, which have been applied in the past in several studies. In addition, this research clearly shows which are the best methods and even suggests an improvement of one of them. In conclusion, although this study has met all its objectives, it has also opened up other challenges and questions that must be answered in the future.

BIBLIOGRAPHY

Ackerman, T. P., Genio, A. D. Del, Ellingson, R. G., Ferrare, R. A., Klein, S. A., McFarquhar, G. M., Lamb, P. J., Long, C. N., Verlinde, J. and Del Genio, A. D.: Atmospheric Radiation Measurement Program Science Plan, Office of Science, U.S. Department of Energy., 2004.

Ackerman, T. P. and Stokes, G. M.: The Atmospheric Radiation Measurement program, *Phys. Today*, 56(2), 38–44, 2003.

Acot, P.: Historia del clima, desde el big bang a las catástrofes climáticas, El Ateneo, Buenos Aires., 2005.

Ahrens, D. C.: *Meteorology Today, an introduction to Weather, Climate, and the Environment*, 9th ed., edited by Brooks/Cole, Belmont, CA (USA). [online] Available from: academic.cengage.com, 2009.

Angevine, W. M., Senff, C. J. and Westwater, E. R.: Observational Techniques-Remote, in *Encyclopedia of Atmospheric Sciences*, vol. 1, edited by J. R. Holton, J. A. Curry, and J. A. Pyle, pp. 271–279, Academic Press, cop. (an imprint of Elsevier Science), London (UK), San Diego (CA, US), 2003.

Argall, P. S. and Sica, R. J.: LIDAR: Atmospheric Sounding Introduction and evolution, in *Encyclopedia of Atmospheric Sciences*, vol. 2, edited by J. R. Holton, J. A. Curry, and J. A. Pyle, pp. 574–582, Academic Press, cop. (an imprint of Elsevier Science), London (UK), San Diego (CA, US), 2003.

Ator, J.: A Proposal for a new BUFR/CREX Table B descriptor for “Height above surface of the base of the lowest cloud seen,” in Meeting of expert team on data representation and codes, edited by WMO, p. 3, Prague (Czech Republic), 2002.

Ballish, B. a. and Kumar, V. K.: Systematic differences in aircraft and radiosonde temperatures. Implications for NWP and Climate Studies, *Bull. Am. Meteorol. Soc.*, 89(11), 1689–1708, doi:10.1175/2008BAMS2332.1, 2008.

Boers, R., de Haij, M., Wauben, W., Baltink, H., van Ulft, L., Savenije, M. and Long, C. N.: Optimized fractional cloudiness determination from five ground-based remote sensing techniques, *J. Geophys. Res.*, 115, 1–16, 2010.

Boucher, O., Randall, D., Artaxo, P., Bretherton, C., Feingold, G., Forster, P., Kerminen, V.-M., Kondo, Y., Liao, H., Lohmann, U., Rasch, P., Satheesh, S. K., Sherwood, S., Stevens, B. and Zhang, X. Y.: Clouds and Aerosols, in *Climate Change 2013: The Physical Science Basis. Contribution of Working Group I to the Fifth Assessment Report of the Intergovernmental Panel on Climate Change*, edited by J. B. Stocker, T.F., D. Qin, G.-K. Plattner, M. Tignor, S.K. Allen and V. B. and P. M. M. A. Nauels, Y. Xia, p. 1535, Cambridge University Press, Campridge and New York. [online] Available from: http://www.climatechange2013.org/images/report/WG1AR5_Chapter07_FINAL.pdf, 2013.

Brázdil, R., Pfister, C., Wanner, H., Storch, H. Von and Luterbacher, J.: Historical climatology in Europe - The state of the art, *Clim. Change*, 70(3), 363–430, doi:10.1007/s10584-005-5924-1, 2005.

Calbó, J., González, J. and Pages, D.: A method for sky-condition classification from ground-based solar radiation measurements, *J. Appl. Meteorol.*, 40(12), 2193–2199, 2001.

Calbó, J. and Sabburg, J.: Feature extraction from whole-sky ground-based images for cloud-type recognition, *J. Atmos. Ocean. Technol.*, 25(1), 3–14, doi:10.1175/2007JTECHA959.1, 2008.

Calbó, J. and Sanchez-Lorenzo, A.: Cloudiness climatology in the Iberian Peninsula from three global gridded datasets (ISCCP, CRU TS 2.1, ERA-40), *Theor. Appl. Climatol.*, 96(1-2), 105–115, doi:10.1007/s00704-008-0039-z, 2009.

Cazorla, A., Olmo, F. J. and Alados-Arboledas, L.: Development of a sky imager for cloud cover assessment, *J. Opt. Soc. Am. Opt. Image Sci.*, 25(1), 29–39, 2008.

Cazorla, A., Shields, J., Karr, M., Olmo, F., Burden, A. and Alados-Arboledas, L.: Technical Note: Determination of aerosol optical properties by a calibrated sky imager, *Atmos. Chem. Phys.*, 9(17), 6417–6427, 2009.

Cazorla Cabrera, A.: Development of a Sky Imager for Cloud Classification and Aerosol Characterization, 205 pp., Grupo de Física de la Atmósfera, Departamento de Física Aplicada, Universidad de Granada, Granada., 2010.

Chernykh, I., Alduchov, O. and Eskridge, R.: Trends in low and high cloud boundaries and errors in height determination of cloud boundaries, *Bull. Am. Meteorol. Soc.*, 82(9), 1941–1947, 2001.

Chernykh, I. and Aldukhov, O.: Vertical distribution of cloud layers from atmospheric radiosounding data, *Izv. Ocean. Phys.*, 40(1), 41–53, 2004.

Chernykh, I. and Eskridge, R.: Determination of cloud amount and level from radiosonde soundings, *J. Appl. Meteorol.*, 35(8), 1362–1369, 1996.

Chernykh, I. V., Alduchov, O. a. and Eskridge, R. E.: Comments on “Trends in low and high cloud boundaries and errors in height determination of cloud boundaries” - Reply, *Bull. Am. Meteorol. Soc.*, 84(2), 241–247, doi:10.1175/BAMS-84-2-241, 2003.

Clothiaux, E., Ackerman, T., Mace, G., Moran, K., Marchand, R. and Miller, M.: Objective determination of cloud heights and radar reflectivities using a combination of active remote sensors at the ARM CART sites, *J. Appl. Meteorol.*, 39(5), 645–665, 2000.

Clothiaux, E., Moran, K., Martner, B., Ackerman, T., Mace, G. and Uttal, T.: The atmospheric radiation measurement program cloud radars: Operational modes, *J. Atmos. Ocean. Technol.*, 16(7), 819–827, 1999.

Collett, J. L. and Herckes, P.: Cloud Chemistry, in *Encyclopedia of Atmospheric Sciences*, vol. 2, edited by J. R. Holton, J. A. Curry, and J. A. Pyle, pp. 451–458, Academic Press, cop. (an imprint of Elsevier Science), London (UK), San Diego (CA, US), 2003.

Costa-Surós, M., Calbó, J., González, J. A. and Long, C. N.: Comparing the cloud vertical structure derived from several methods based on radiosonde profiles and ground-based remote sensing measurements, *Atmos. Meas. Tech.*, (under rev, doi:doi:10.5194/amtd-7-3681-2014, 2014.

Costa-Surós, M., Calbó, J., González, J. A. and Martín-Vide, J.: Behavior of cloud base height from ceilometer measurements, *Atmos. Res.*, 127, 64–76, doi:10.1016/j.atmosres.2013.02.005, 2013.

Crewell, S., Bloemink, H., Feijt, a., Garcia, S., Jolivet, D., Krasnov, O. a., García, S. G., Van Lammeren, a., Löhnert, U., Van Meijgaard, E., Meywerk, J., Quante, M., Pfeilsticker, K., Schmidt, S., Scholl, T., Simmer, C., Schröder, M., Trautmann, T., Venema, V., Wendisch, M. and Willén, U.: The BALTEX Bridge Campaign - An integrated approach for a better understanding of clouds, *Bull. Am. Meteorol. Soc.*, 85(10), 1565–1584, doi:10.1175/BAMS-85-10-1565, 2004.

Cuadrat, J. M. and Pita, M. F.: *Climatología, Cátedra (Geografía)*, Grupo Anaya S.A., Madrid., 2009.

Dabberdt, W. F., Shellhorn, R., Cole, H., Paukkunen, A., Hörhammer, J. and Antikainen, V.: Radiosondes, in *Encyclopedia of Atmospheric Sciences*, vol. 5, edited by J. R. Holton, J. A. Curry, and J. A. Pyle, pp. 1900–1913, Academic Press, cop. (an imprint of Elsevier Science), London (UK), San Diego (CA, US), 2003.

Dai, A., Karl, T., Sun, B. and Trenberth, K.: Recent trends in cloudiness over the United States - A tale of monitoring inadequacies, *Bull. Am. Meteorol. Soc.*, 87(5), 597–606, doi:10.1175/BAMS-87-5-597, 2006.

Delanoë, J., Protat, A., Jourdan, O., Pelon, J., Papazzoni, M., Dupuy, R., Gayet, J.-F. and Jouan, C.: Comparison of Airborne In Situ, Airborne Radar-Lidar, and Spaceborne Radar-Lidar Retrievals of Polar Ice Cloud Properties Sampled during the POLARCAT Campaign, *J. Atmos. Ocean. Technol.*, 30(1), 57–73, doi:10.1175/JTECH-D-11-00200.1, 2013.

Dessler, a. E.: Observations of Climate Feedbacks over 2000-10 and Comparisons to Climate Models, *J. Clim.*, 26(1), 333–342, doi:10.1175/JCLI-D-11-00640.1, 2013.

Dimitrieva-Arrago, L. R. and Koloskova, L. F.: On approximate cloud boundary distribution method, *Meteorol. Hydrol.*, N6, 47–52, 1969.

Dimitrieva-Arrago, L. R. and Shatunova, M. V.: The Approximate Method of the Cloud Boundaries Definition and its Vertical Distribution Restoration, *Res. Act. Atmos. Ocean Model.*, 28, 4.5–4.6, 1999.

Dupont, J.-C., Haeffelin, M., Morille, Y., Comstock, J. M., Flynn, C., Long, C. N., Sivaraman, C. and Newson, R. K.: Cloud properties derived from two lidars over the ARM SGP site, *Geophys. Res. Lett.*, 38, L08814–L08814, doi:10.1029/2010GL046274, 2011.

Durr, B. and Philipona, R.: Automatic cloud amount detection by surface longwave downward radiation measurements, *J. Geophys. Res.*, 109(D5), 2004.

Eastman, R. and Warren, S. G.: A 39-Yr Survey of Cloud Changes from Land Stations Worldwide 1971–2009: Long-Term Trends, Relation to Aerosols, and Expansion of the Tropical Belt, *J. Clim.*, 26, 1286–1303, doi:10.1175/JCLI-D-12-00280.1, 2013.

Ebell, K., Crewell, S., Loehnert, U., Turner, D. D. and O'Connor, E. J.: Cloud statistics and cloud radiative effect for a low-mountain site, *Q. J. R. Meteorol. Soc.*, 137, 306–324, doi:10.1002/qj.748, 2011.

Eberhard, W. L.: Cloud Signals from Lidar and Rotating Beam Ceilometer Compared with Pilot Ceiling, *J. Atmos. Ocean. Technol.*, 3, 499–512, 1986.

Elliott, W. P. and Gaffen, D. J.: On the Utility of Radiosonde Humidity Archives for Climate Studies, *Bull. Am. Meteorol. Soc.*, 72(10), 1507–1520, doi:10.1175/1520-0477(1991)072<1507:OTUORH>2.0.CO 2, 1991.

Emeis, S., Munkel, C., Vogt, S., Muller, W. and Schafer, K.: Atmospheric boundary-layer structure from simultaneous SODAR, RASS, and ceilometer measurements, *Atmos. Environ.*, 38(2), 273–286, 2004.

Emeis, S., Schafer, K. and Munkel, C.: Long-term observations of the urban mixing-layer height with ceilometers, *14TH Int. Symp. Adv. Bound. LAYER Remote Sens.*, 1, U229–U237, 2008a.

Emeis, S., Schäfer, K. and Munkel, C.: Surface-based remote sensing of the mixing-layer height - a review, *Meteorol. Zeitschrift*, 17(5), 621–630, doi:10.1127/0941-2948/2008/0312, 2008b.

Enriquez, A., Calbó, J. and González, J. A.: Assessment of cloud cover in climate models and reanalysis databases with ISCCP over the Mediterranean region (poster), in *EGU General Assembly 2013, Vienna (AU)*, 2013.

Feister, U., Moeller, H., Sattler, T., Shields, J. and Goersdorf, U.: Comparison of macroscopic cloud data from ground-based measurements using VIS/NIR and IR instruments at Lindenberg, Germany, *Atmos. Res.*, 96(2-3), 395–407, doi:10.1016/j.atmosres.2010.01.012, 2010.

Feister, U. and Shields, J.: Cloud and radiance measurements with the VIS/NIR Daylight Whole Sky Imager at Lindenberg (Germany), *Meteorol. Zeitschrift*, 14(5), 627–639, 2005.

Forsythe, J., Haar, T. V and Reinke, D.: Cloud-base height estimates using a combination of meteorological satellite imagery and surface reports, *J. Appl. Meteorol.*, 39(12), 2336–2347, 2000.

Di Franco, F.: *Previsión del tiempo mirando al cielo*, Editorial Juventud, Barcelona., 1984.

Fu, Q.: Radiation (solar): Effects of clouds on solar radiation, in *Encyclopedia of Atmospheric Sciences*, vol. 5, edited by J. R. Holton, J. A. Curry, and J. A. Pyle, pp. 1859–1863, Academic Press, cop. (an imprint of Elsevier Science), London (UK), San Diego (CA, US), 2003.

Garrett, T. J. and Zhao, C.: Ground-based remote sensing of thin clouds in the Arctic, *Atmos. Meas. Tech.*, 6(5), 1227–1243, doi:10.5194/amt-6-1227-2013, 2013.

Gonzalez, Y., López, C. and Cuevas, E.: Automatic Observation of Cloudiness: Analysis of all-sky images, in *TECO-2012. WMO Technical Conference on Meteorological and Environmental Instruments and Methods of observation*, pp. 1–6, Brussels (Belgium), 2012.

De Haan, S., Bailey, L. J. and Können, J. E.: Quality assessment of Automatic Dependent Surveillance Contract (ADS-C) wind and temperature observation from commercial aircraft, *Atmos. Meas. Tech.*, 6(2), 199–206, doi:10.5194/amt-6-199-2013, 2013.

Hahn, C. J., Warren, S. J., London, J., Chervin, R. M. and Jenne, R.: Atlas of Simultaneous Occurrence of Different Cloud Types over the Ocean., Boulder, Colorado. [online] Available from: <http://nldr.library.ucar.edu/collections/technotes/asset-000-000-000-355.pdf>, 1982.

Hahn, C. J., Warren, S. J., London, J., Chervin, R. M. and Jenne, R.: Atlas of Simultaneous Occurrence of Different Cloud Types over Land, Boulder, Colorado. [online] Available from: <http://nldr.library.ucar.edu/collections/technotes/asset-000-000-000-355.pdf>, 1984.

Haij, M. De, Wauben, W. and Baltink, H. K.: Determination of mixing layer height from ceilometer backscatter profiles, *Remote Sens. Clouds Atmos.* XI, 6362, U176–U187, 2006.

Heinle, A., Macke, A. and Srivastav, A.: Automatic cloud classification of whole sky images, *Atmos. Meas. Tech.*, 3, 557–567, 2010.

Heintzenberg, J. and Charlson, R. J.: Clouds in the perturbed climate system: their relationship to energy balance, atmospheric dynamics, and precipitation, The MIT Press, Cambridge, Massachusetts; London., 2009.

Henderson-Sellers, A.: Continental cloudiness changes this century, *Geophys. J.*, 27, 255–262, 1992.

Hogan, R. J., Francis, P. N., Flentje, H., Illingworth, A. J., Quante, M. and Pelon, J.: Characteristics of mixed-phase clouds. I: Lidar, radar and aircraft observations from CLARE'98, *Q. J. R. Meteorol. Soc.*, 129(592), 2089–2116, doi:10.1256/qj.01.208, 2003.

Hogan, R., O'Connor, E. and Illingworth, A.: Verification of cloud-fraction forecasts, *Q. J. R. Meteorol. Soc.*, 135(643), 1494–1511, doi:10.1002/qj.481, 2009.

Holdridge, D., Prell, J., Ritsche, M. and Coulter, R.: Balloon-Borne Sounding System Handbook, U.S. Department of Energy, Office of Science., 2011.

Holejko, K. and Nowak, R.: Continuous wave laser ceilometer with code modulation for measurements of cloud base height, *Opto-electronics Rev.*, 8(2), 195–199, 2000.

Houghton, J.: Modelling the Climate, in *Global Warming. The complete Briefing.*, vol. 2nd, pp. 63–83, Cambridge University Press, Cambridge, United Kingdom and New York., 1997.

Hwang, P., Stowe, L., Yeh, H. and Kyle, H.: The Nimbus-7 Global Cloud Climatology, *Bull. Am. Meteorol. Soc.*, 69(7), 743–752, doi:10.1175/1520-0477(1988)069<0743:TGCC>2.0.CO;2, 1988.

Illingworth, a. J., Hogan, R. J., O'Connor, E. J., Bouniol, D., Brooks, M. E., Delanoë, J., Delanoë, J., Pelon, J., Protat, a., Gaussiat, N., Wilson, D. R., Donovan, D. P., Baltink, H. K., van Zadelhoff, G.-J., Eastment, J. D., Goddard, J. W. F., Wrench, C. L., Haeffelin, M., Krasnov, O. a., Russchenberg, H. W. J., Piriou, J.-M., Vinit, F., Seifert, a., Tompkins, a. M. and Willén, U.: Cloudnet - Continuous evaluation of cloud profiles in seven operational models using ground-based observations, *Bull. Am. Meteorol. Soc.*, 88(6), 883–898, doi:10.1175/BAMS-88-6-883, 2007.

Institut Cartogràfic de Catalunya: Atles Climàtic de Catalunya, Generalitat de Catalunya, Servei Meteorològic de Catalunya, Barcelona., 2008.

Jakob, C. and Miller, M.: Parameterization of physical processes: Clouds, in *Encyclopedia of Atmospheric Sciences*, vol. 4, edited by J. R. Holton, J. A. Curry, and J. A. Pyle, pp. 1692–1698, Academic Press, cop. (an imprint of Elsevier Science), London (UK), San Diego (CA, US)., 2003.

Janeiro, F., Ramos, P., Wagner, F. and Silva, A.: Developments of low-cost procedure to estimate cloud base height based on a digital camera, *Measurement*, 43(5), 684–689, 2010.

Jin, X., Hanesiak, J. and Barber, D.: Detecting cloud vertical structures from radiosondes and MODIS over Arctic first-year sea ice, *Atmos. Res.*, 83(1), 64–76, 2007.

Jones, D. W., Ouldrige, M. and Painting, D. J.: WMO International Ceilometer intercomparison, WMO, 1988.

Jones, P.: Historical climatology - a state of the art review, *Weather*, 63(7), 181–186, doi:10.1002/wea.245, 2008.

Kaiser, D. P.: Decreasing cloudiness over China: An updated analysis examining additional variables, *Geophys. Res. Lett.*, 27(15), 2193–2196, doi:10.1029/2000GL011358, 2000.

Kalb, C., Dean, A., Peppler, R. and Sonntag, K.: Intercomparison of Cloud Base Height at the ARM Southern Great Plains Site, in *Fifteenth ARM Science Team Meeting Proceedings*, pp. 1–23, Daytona Beach (Florida)., 2005.

Kassianov, E., Long, C. and Christy, J.: Cloud-base-height estimation from paired ground-based hemispherical observations, *J. Appl. Meteorol.*, 44(8), 1221–1233, 2005a.

Kassianov, E., Long, C. and Ovtchinnikov, M.: Cloud sky cover versus cloud fraction: Whole-sky simulations and observations, *J. Appl. Meteorol.*, 44, 86–98, 2005b.

Kim, S.-W., Chung, E.-S., Yoon, S.-C., Sohn, B.-J. and Sugimoto, N.: Intercomparisons of cloud-top and cloud-base heights from ground-based Lidar, CloudSat and CALIPSO measurements, *Int. J. Remote Sens.*, 32(4), 1179–1197, doi:10.1080/01431160903527439, 2011.

Klebe, D. I., Blatherwick, R. D. and Morris, V. R.: Ground-based all-sky mid-infrared and visible imagery for purposes of characterizing cloud properties, *Atmos. Meas. Tech.*, 7, 637–645, doi:10.5194/amt-7-637-2014, 2014.

Kotarba, A.: A comparison of MODIS-derived cloud amount with visual surface observations, *Atmos. Res.*, 92(4), 522–530, doi:10.1016/j.atmosres.2009.02.001, 2009.

Kreidenweis, S. M.: Aerosols: role in clouds physics, in *Encyclopedia of Atmospheric Sciences*, vol. 1, edited by J. R. Holton, J. A. Curry, and J. A. Pyle, pp. 40–47, Academic Press, cop. (an imprint of Elsevier Science), London (UK), San Diego (CA, US)., 2003.

Kreuter, A., Zangerl, M., Schwarzmann, M. and Blurnthaler, M.: All-sky imaging: a simple, versatile system for atmospheric research, *Appl. Opt.*, 48(6), 1091–1097, 2009.

L'Ecuyer, T. and Jiang, J. H.: Touring the atmosphere aboard the A-Train, *Phys. Today*, 63(7), 36–41, 2010.

Leaitch, W. R., Lohmann, U., Russell, L. M., Garrett, T. and Shantz, N. C.: Cloud albedo increase from carbonaceous aerosol, *Atmos. Chem. Phys.*, 10(16), 7669–7684, doi:10.5194/acp-10-7669-2010, 2010.

De Leeuw, G., Kokhanovsky, A. and Cermak, J.: Remote sensing of aerosols and clouds: Techniques and applications (editorial to special issue in Atmospheric Research), *Atmos. Res.*, 113, 40–42, doi:10.1016/j.atmosres.2012.04.017, 2012.

Van Lipzig, N. P. M., Schroeder, M., Crewell, S., Ament, F. and Chaboureau, J.-P.: Model predicted low-level cloud parameters - Part I: Comparison with observations from the BALTEX Bridge Campaigns, *Atmos. Res.*, 82(1-2), 55–82, doi:10.1016/j.atmosres.2006.01.010, 2006.

Liu, L., Sun, X., Chen, F., Zhao, S. and Gao, T.: Cloud classification based on structure features of infrared images, *J. Atmos. Ocean. Technol.*, 28(3), 410–417, doi:http://dx.doi.org/10.1175/2010JTECHA1385.1, 2011.

Liu, L., Sun, X., Gao, T. and Zhao, S.: Comparison of Cloud Properties from Ground-Based Infrared Cloud Measurement and Visual Observations, *J. Atmos. Ocean. Technol.*, 30(6), 1171–1179, doi:http://dx.doi.org/10.1175/JTECH-D-12-00157.1, 2013.

Llach, M. and Calbó, J.: Aproximación a la Climatología de la nubosidad en Cataluña, in *El clima, entre el mar y la montaña*, pp. 325–334, Asociación Española de Climatología, Santander., 2004.

Long, C. N. and Ackerman, T. P.: Identification of clear skies from broadband pyranometer measurements and calculation of downwelling shortwave cloud effects, *J. Geophys. Res. Atmos.*, 105(D12), 15609–15626, doi:10.1029/2000JD900077, 2000.

Long, C. N., Ackerman, T. P., Gaustad, K. L. and Cole, J. N. S.: Estimation of fractional sky cover from broadband shortwave radiometer measurements, *J. Geophys. Res. Atmos.*, 111(D11), doi:10.1029/2005JD006475, 2006a.

Long, C. N., Sabburg, J. M., Calbó, J. and Pagès, D.: Retrieving cloud characteristics from ground-based daytime color all-sky images, *J. Atmos. Ocean. Technol.*, 23(5), 633–652, doi:10.1175/JTECH1875.1, 2006b.

Long, C. N., Slater, D. W. and Tooman, T.: Total Sky Imager Model 880 Status and Testing Results, in *ARM Pr. Tech. Rep. ARM TR-006*, p. 36. [online] Available from: http://www.arm.gov/publications/tech_reports/arm-tr-006.pdf, 2001.

Lynch, P.: The origins of computer weather prediction and climate modeling, *J. Comput. Phys.*, 227(7), 3431–3444, doi:10.1016/j.jcp.2007.02.034, 2008.

Mace, G. G. and Benson, S.: The vertical structure of cloud occurrence and radiative forcing at the SGP ARM site as revealed by 8 years of continuous data, *J. Clim.*, 21(11), 2591–2610, doi:10.1175/2007JCLI1987.1, 2008.

Mancuso, R. L., Serebreny, S. M. and Blackmer, R. H. J.: A Cloud Simulation Model for Evaluating Automatic Ceilometer Systems, *J. Appl. Meteorol.*, 10, 1324–1330, 1971.

Martín Vide, J.: Clasificación de los climas, in *Climas y tiempos de España*, pp. 103–123, Alianza Editorial, Madrid., 2001.

Martín-Vide, J.: Catálogo de situaciones sinópticas, in *Los mapas del tiempo*, pp. 63–67, Ed. Davinci., 2005.

Martucci, G., Milroy, C. and O’Dowd, C. D.: Detection of Cloud-Base Height Using Jenoptik CHM15K and Vaisala CL31 Ceilometers, *J. Atmos. Ocean. Technol.*, 27(2), 305–318, doi:10.1175/2009JTECHA1326.1, 2010.

Mazón, J., Costa, M., Pino, D. and Lorente, J.: Clouds caused by human activities, *Weather*, 67(11), 302–306, doi:10.1002/wea.1949, 2012.

Min, Q. L. and Harrison, L. C.: Cloud properties derived from surface MFRSR measurements and comparison with GOES results at the ARM SGP site, *Geophys. Res. Lett.*, 23(13), 1641–1664, doi:10.1029/96GL01488, 1996.

Min, Q. L., Joseph, E. and Duan, M. Z.: Retrievals of thin cloud optical depth from a multifilter rotating shadowband radiometer, *J. Geophys. Res. Atmos.*, 109(D2), doi:10.1023/2003JD003964, 2004.

Minnis, P., Yi, Y. H., Huang, J. P. and Ayers, K.: Relationships between radiosonde and RUC-2 meteorological conditions and cloud occurrence determined from ARM data, *J. Geophys. Res.*, 110(D23), 1–19, 2005.

Moninger, W. R., Mamrosch, R. D. and Pauley, P. M.: Automated meteorological reports from commercial aircraft, *Bull. Am. Meteorol. Soc.*, 84(2), 203–216, doi:10.1175/BAMS-84-2-203, 2003.

Moran, J. M. and Morgan, M. D.: *Essentials of weather*, edited by R. McConnin, Prentice-Hall, Inc., New Jersey., 1995.

Moran, K. P., Martner, B. E., Post, M. J., Kropfli, R. A. and Welsh, D. C.: An unattended cloud-profiling radar for use in climate research, *Bull. Am. Meteorol. Soc.*, 79(3), 443–455, doi:10.1175/1520-0477(1998)079<0443:AUCPRF>2.0.CO 2, 1998.

Morcrette, C. J., O’Connor, E. J. and Petch, J. C.: Evaluation of two cloud parametrization schemes using ARM and Cloud-Net observations, *Q. J. R. Meteorol. Soc.*, 138(665), 964–979, doi:10.1002/qj.969, 2012.

Morris, V.: Vaisala Ceilometer (VCEIL) Handbook, ARM Clim. Res. Facil., 23 [online] Available from: http://www.arm.gov/publications/tech_reports/handbooks/vceil_handbook.pdf?id=25, 2012.

Morris, V. and Klebe, D.: A demonstration of the Solmirus all sky infrared visible analyzer, Poster Present. ASR Sci. Team Meet., 2010.

Morris, V., Klebe, D. and Costa-Surós, M.: Evaluation of Infrared Sky Imagers at the ARM Southern Great Plains Site, Poster Present. ASR II Sci. Team Meet., 2011.

Muenkel, C.: Mixing height determination with lidar ceilometers - results from Helsinki Testbed, *Meteorol. Zeitschrift*, 16(4), 451–459, 2007.

Muenkel, C., Emeis, S., Mueller, W. J. and Schaefer, K. P.: Aerosol concentration measurements with a lidar ceilometer: results of a one year measuring campaign, edited by K. Schaefer, A. Comeron, M. R. Carleer, and R. H. Picard, *Proc. SPIE--the Int. Soc. Opt. Eng.*, 5235, 486–496, doi:10.1117/12.511104, 2004.

Nash, J., Oakley, T., Vömel, H. and Wei, L.: WMO Intercomparison of high quality radiosonde systems. Report No. 107, Yangjiang (China). [online] Available from: <https://www.wmo.int/pages/prog/www/IMOP/intercomparisons.html>, 2011.

Naud, C. M., Muller, J. P. and Clothiaux, E. E.: Comparison between active sensor and radiosonde cloud boundaries over the ARM Southern Great Plains site, *J. Geophys. Res.*, 108(D4), 1–12, 2003.

Newsom, R. K.: *Raman Lidar Handbook*, ARM Program, Richland, WA., 2009.

Nowak, D., Ruffieux, D., Agnew, J. L. and Vuilleumier, L.: Detection of fog and low cloud boundaries with ground-based remote sensing systems, *J. Atmos. Ocean. Technol.*, 25(8), 1357–1368, doi:10.1175/2007JTECHA950.1, 2008.

Ogilvie, A. E. J.: Historical climatology, Climatic Change, and implications for climate science in the twenty-first century, *Clim. Change*, 100(1), 33–47, doi:10.1007/s10584-010-9854-1, 2010.

Peel, M. C., Finlayson, B. L. and McMahon, T. A.: Updated world map of the Köppen-Geiger climate classification, *Hydrol. earth Syst. Sci.*, 11(5), 1633–1644, 2007.

Pfister, G., McKenzie, R. L., Liley, J. B., Thomas, A., Forgan, B. W. and Long, C. N.: Cloud coverage based on all-sky imaging and its impact on surface solar irradiance, *J. Appl. Meteorol.*, 42(10), 1421–1434, doi:10.1175/1520-0450(2003)042<1421:CCBOAI>2.0.CO 2, 2003.

Pommereau, J.-P.: Observation Platforms: balloons, in *Encyclopedia of Atmospheric Sciences*, vol. 4, edited by J. R. Holton, J. A. Curry, and J. A. Pyle, pp. 1429–1438, Academic Press, cop. (an imprint of Elsevier Science), London (UK), San Diego (CA, US), 2003.

Poore, K., Wang, J. and Rossow, W.: Cloud Layer Thicknesses from a Combination of Surface and Upper-Air Observations, *J. Clim.*, 8(3), 550–568, 1995.

Probst, P., Rizzi, R., Tosi, E., Lucarini, V. and Maestri, T.: Total cloud cover from satellite observations and climate models, *Atmos. Res.*, 107, 161–170, doi:10.1016/j.atmosres.2012.01.005, 2012.

Qian, Y., Long, C. N., Wang, H., Comstock, J. M., McFarlane, S. A. and Xie, S.: Evaluation of cloud fraction and its radiative effect simulated by IPCC AR4 global models against ARM surface observations, *Atmos. Chem. Phys.*, 12(4), 1785–1810, doi:10.5194/acp-12-1785-2012, 2012.

Ramanathan, V., Cess, R. D., Harrison, E. F., Minnis, P., Barkstrom, B. R., Ahmad, E. and Hartmann, D.: Cloud-Radiative Forcing and Climate: Results from the Earth Radiation Budget Experiment, *Science* (80-.), 243(4887), 57–63, doi:10.1126/science.243.4887.57, 1989.

Rangno, A. L.: Clouds: classification, in *Encyclopedia of Atmospheric Sciences*, vol. 2, edited by J. R. Holton, J. A. Curry, and J. A. Pyle, pp. 467–497, Academic Press, cop. (an imprint of Elsevier Science), London (UK), San Diego (CA, US), 2003.

Ricchiazzi, P., Yang, S., Gautier, C. and Sowle, D.: SBDART: A research and teaching software tool for plane-parallel radiative transfer in the Earth's atmosphere, *Bull. Am. Meteorol. Soc.*, (9), 2101–2114, 1998.

Rossow, W. B. and Zhang, Y.: Evaluation of a Statistical Model of Cloud Vertical Structure Using Combined CloudSat and CALIPSO Cloud Layer Profiles, *J. Clim.*, 23(24), 6641–6653, doi:10.1175/2010JCLI3734.1, 2010.

Rossow, W. and Schiffer, R.: ISCCP Cloud Data Products, *Bull. Am. Meteorol. Soc.*, 72(1), 2–20, doi:10.1175/1520-0477(1991)072<0002:ICDP>2.0.CO;2, 1991.

Rossow, W., Zhang, Y. and Wang, J.: A Statistical Model of Cloud Vertical Structure Based on Reconciling Cloud Layer Amounts Inferred from Satellites and Radiosonde Humidity Profiles, *J. Clim.*, 18, 3587–3605, 2005.

Roulstone, I. and Norbury, J.: From lore to laws, in *Invisible in the storm. The role of mathematics in understanding weather.*, pp. 47–87, Princeton University Press, Princeton and Oxford., 2013.

Salazar, J. and Poveda, G.: Role of a simplified hydrological cycle and clouds in regulating the climate-biota system of Daisyworld, *Tellus.Series B, Chem. Phys. Meteorol.*, 61(2), 483–497, 2009.

Schade, N., Macke, A., Sandmann, H. and Stick, C.: Total and partial cloud amount detection during summer 2005 at Westerland (Sylt, Germany), *Atmos. Chem. Phys.*, 9(4), 1143–1150, 2009.

Schroeder, M., Ament, F., Chaboureau, J.-P. and Crewell, S.: Model predicted low-level cloud parameters Part II: Comparison with satellite remote sensing observations during the BALTEX Bridge Campaigns, *Atmos. Res.*, 82(1-2), 83–101, doi:10.1016/j.atmosres.2005.12.005, 2006.

Schwartz, B. and Benjamin, S. G.: A comparison of temperature and wind measurements from ACARS-Equipped Aircraft and Rawinsondes., *Weather Forecast.*, 10(3), 528–544, doi:10.1175/1520-0434(1995)010<0528:ACOTAW>2.0.CO;2, 1995.

Seidel, D. J., Durre, I., Chernykh, I. V., Alduchov, O. a. and Eskridge, R. E.: Comments on “Trends in low and high cloud boundaries and errors in height determination of cloud boundaries” - Reply, *Bull. Am. Meteorol. Soc.*, 84(2), 241–247, doi:10.1175/BAMS-84-2-237, 2003.

Seiz, G., Shields, J., Feister, U., Baltsavias, E. P. and Gruen, a.: Cloud mapping with ground-based photogrammetric cameras, *Int. J. Remote Sens.*, 28(9), 2001–2032, doi:10.1080/01431160600641822, 2007.

Shields, J. E., Johnson, R. W. and Koehler, T. L.: Imaging Systems for Automated 24-Hour Whole Sky Cloud Assessment and Visibility Determination, in *Proceedings of the Cloud Impacts on DOD Operations and Systems – 1991 Conference.*, pp. 137–142, San Diego, Calif., 1991.

Shields, J. E., Johnson, R. W. and Koehler, T. L.: Automated whole sky imaging systems for cloud field assessment, in Fourth Symposium on Global Change Studies, pp. 228–231, American Meteorological Society, San Diego, Calif. [online] Available from: [http://www-mpl.ucsd.edu/people/jshields/publications/pdfs/13 Shields AMS 93.pdf](http://www-mpl.ucsd.edu/people/jshields/publications/pdfs/13%20Shields%20AMS%2093.pdf), 1993.

Shields, J. E., Karr, M. E., Johnson, R. W. and Burden, A. R.: Day/night whole sky imagers for 24-h cloud and sky assessment: history and overview, *Appl. Opt.*, 52(8), 1605–1616 [online] Available from: http://www.opticsinfobase.org/view_article.cfm?gotourl=http://www.opticsinfobase.org/DirectPDFAccess/E4312735-CFFC-60D5-81E3ABF816D86AB5_249702/ao-52-8-1605.pdf?da=1&id=249702&seq=0&mobile=no&org=, 2013.

Shupe, M. D., Walden, V. P., Eloranta, E., Uttal, T., Campbell, J. R., Starkweather, S. M. and Shiobara, M.: Clouds at Arctic Atmospheric Observatories. Part I: Occurrence and Macrophysical Properties, *J. Appl. Meteorol. Climatol.*, 50(3), 626–644, doi:10.1175/2010JAMC2467.1, 2011.

Shuttleworth, W. J.: *Terrestrial Hydrometeorology*, edited by Wiley-Blackwell, West Sussex (UK). [online] Available from: http://books.google.es/books?id=1veoRTEJe2UC&printsec=frontcover&source=gbs_ge_summar_y_r&cad=0#v=onepage&q&f=false, 2012.

Smith, S. and Toumi, R.: Measuring cloud cover and brightness temperature with a ground-based thermal infrared camera, *J. Appl. Meteorol. Climatol.*, 47(2), 683–693, doi:10.1175/2007JAMC1615.1, 2008.

Solomon, S., Qin, D., Manning, M., Alley, R. B., Berntsen, T., Bindoff, N. L., Chen, Z., Chidthaisong, A., Gregory, J. M., Hegerl, G. C., Heimann, M., Hewitson, B., Hoskins, B. J., Joos, F., Jouzel, J., Kattsov, V., Lohmann, U., Matsuno, T., Molina, M., Nicholls, N., Overpeck, J., Raga, G., Ramaswamy, V., Ren, J., Rusticucci, M., Somerville, R., Stocker, T. F., Whetton, P., Wood, R. A. and Wratt, D.: Technical summary. *Climate change 2007: the physical science basis. Contribution of Working Group I to the Fourth Assessment Report of the Intergovernmental Panel on Climate Change*, edited by S. Solomon, D. Qin, M. Manning, S. Chen, M. Marquis, K. B. Averyt, M. Tignor, and H. L. Miller, Cambridge University Press, Cambridge, United Kingdom and New York., 2007.

Souza-Echer, M., Bins, L. and Andrade, M.: A simple method for the assessment of the cloud cover state in high-latitude regions by a ground-based digital camera, *J. Atmos. Ocean. Technol.*, 23(3), 437–447, 2006.

Stephens, G. L., Li, J., Wild, M., Clayson, C. A., Loeb, N., Kato, S., L'Ecuyer, T., Stackhouse, P. W., Lebsock, M. and Andrews, T.: An update on Earth's energy balance in light of the latest global observations, *Nat. Geosci.*, 5(10), 691–696, doi:10.1038/NGEO1580, 2012.

Stevens, B. and Bony, S.: Water in the atmosphere, *Phys. Today*, 66, 29–34, doi:10.1063/PT.3.2009, 2013.

Stowe, L. L., Yeh, H. Y. M., Eck, T. F., Wellemeyer, C. G., Kyle, H. and The Nimbus-7 Cloud data processing team: Nimbus-7 Global Cloud Climatology. Part II: First Year Results, *J. Clim.*, 2, 671–709 [online] Available from: [http://journals.ametsoc.org/doi/pdf/10.1175/1520-0442\(1989\)002<0671:NGCCPI>2.0.CO;2](http://journals.ametsoc.org/doi/pdf/10.1175/1520-0442(1989)002<0671:NGCCPI>2.0.CO;2), 1989.

Stull, R. B.: *Meteorology Today For Scientist and Engineers: A Technical Companion Book*, West Publishing Company, Minneapolis / St. Paul., 1995.

Sun, B. M. and Groisman, P. Y.: Cloudiness variations over the former Soviet Union, *Int. J. Climatol.*, 20(10), 1097–1111, doi:10.1002/1097-0088(200008)20:10<1097::AID-JOC541>3.3.CO 2-X, 2000.

Tapakis, R. and Charalambides, A. G.: Equipment and methodologies for cloud detection and classification: A review, *Sol. Energy*, (0), doi:10.1016/j.solener.2012.11.015, 2012.

Van Tricht, K., Gorodetskaya, I. V., Lhermitte, S., Turner, D. D., Schween, J. H. and Van Lipzig, N. P. M.: An improved algorithm for polar cloud-base detection by ceilometer over the ice sheets, *Atmos. Meas. Tech.*, 7(5), 1153–1167, doi:10.5194/amt-7-1153-2014, 2014.

Uttal, T.: Radar: Cloud Radar, in *Encyclopedia of Atmospheric Sciences*, vol. 4, edited by J. R. Holton, J. A. Curry, and J. A. Pyle, pp. 1795–1824, Academic Press, cop. (an imprint of Elsevier Science), London (UK), San Diego (CA, US), 2003.

Vaisala Oyj.: *Vaisala CL-31 user's guide*, Helsinki., 2006.

Vaisala Oyj.: *Sky Condition Algorithm for Vaisala Ceilometer's*. [online] Available from: [http://www.vaisala.com/Vaisala Documents/Brochures and Datasheets/Sky-Condition-CL31-Datasheet-B210507EN-B-LoRes.pdf](http://www.vaisala.com/Vaisala_Documents/Brochures_and_Datasheets/Sky-Condition-CL31-Datasheet-B210507EN-B-LoRes.pdf), 2010.

Viúdez-Mora, A.: Atmospheric downwelling longwave radiation at the surface during cloudless and overcast conditions. Measurements and modeling, Universitat de Girona. Departament de Física. [online] Available from: <http://hdl.handle.net/10803/31841>, 2011.

Viúdez-Mora, A., Costa-Surós, M., Calbó, J. and González, J. A.: Modeling Atmospheric Longwave Radiation at the Surface during Overcast Skies: The Role of Cloud Base Height, *J. Geophys. Res. - Atmos.*, (under revision), 2014.

Volken, E. and Brönnimann, S.: The thermal zones of the Earth according to the duration of hot, moderate and cold periods and to the impact of heat on the organic world, *Meteorol. Zeitschrift*, 20(3), 361–365, doi:10.1127/0941-2948/2011/0258, 2011.

Wallace, J. M. and Hobbs, P. V.: *Atmospheric Science, an introductory survey*, Academic Press, San Diego, Calif., 1977.

Wang, J. and Rossow, W.: Determination of Cloud Vertical Structure from Upper-Air Observations, *J. Appl. Meteorol.*, 34(10), 2243–2258, 1995.

Wang, J. and Rossow, W.: Effects of cloud vertical structure on atmospheric circulation in the GISS GCM, *J. Clim.*, 11(11), 3010–3029, 1998.

Wang, J., Rossow, W., Uttal, T. and Rozendaal, M.: Variability of cloud vertical structure during ASTEX observed from a combination of rawinsonde, radar, ceilometer, and satellite, *Mon. Weather Rev.*, 127(10), 2484–2502, 1999.

Wang, J., Rossow, W. and Zhang, Y.: Cloud vertical structure and its variations from a 20-yr global rawinsonde dataset, *J. Clim.*, 13(17), 3041–3056, 2000.

Warner, T. T.: Numerical Weather and Climate Prediction, Cambridge University Press, Cambridge, United Kingdom., 2011.

Warren, S. G., Eastman, R. M. and Hahn, C. J.: A survey of changes in cloud cover and cloud types over land from surface observations, 1971–96, *J. Clim.*, 20(4), 717–738, doi:10.1175/JCLI4031.1, 2007.

Warren, S. G. and Hahn, C. J.: Clouds: climatology, in *Encyclopedia of Atmospheric Sciences*, vol. 2, edited by J. R. Holton, J. A. Curry, and J. A. Pyle, pp. 476–483, Academic Press, cop. (an imprint of Elsevier Science), London (UK), San Diego (CA, US)., 2003.

Welton, E. J., Campbell, J. R., Spinhirne, J. D. and Scott, V. S.: Global monitoring of clouds and aerosols using a network of micro-pulse lidar systems, in *Lidar Remote Sensing for Industry and Environment Monitoring (SPIE)*, edited by U. N. Singh, T. Itabe, and N. Sugimoto, pp. 151–158, Sendai (Japan)., 2001.

Weng, F., Zou, X. and Turk, F. J.: Introduction to the Special Issue on the Chinese FengYun-3 Satellite Instrument Calibration and Applications, *IEEE Trans. Geosci. Remote Sens.*, 50(12), 4843–4844 [online] Available from: <http://ieeexplore.ieee.org/stamp/stamp.jsp?arnumber=06355808>, 2012.

Werner, T.: Transitioning to Operations: Lidars and Ceilometers, in *TECO-2012. WMO Technical Conference on Meteorological and Environmental Instruments and Methods of Observation*, p. 14, World Meteorological Organization, Brussels (Belgium). [online] Available from: http://www.wmo.int/pages/prog/www/IMOP/publications/IOM-109_TECO-2012/Programme_TECO-2012.html, 2012.

Wielicki, B., Cess, R., King, M., Randall, D. and Harrison, E.: Mission to Planet Earth: Role of Clouds and Radiation in Climate, *Bull. Am. Meteorol. Soc.*, 76(11), 2125–2153, 1995.

Wild, M.: Global dimming and brightening: A review, *J. Geophys. Res.*, 114, 1–31, doi:10.1029/2008JD011470, 2009.

Wild, M.: Enlightening Global Dimming and Brightening, *Bull. Am. Meteorol. Soc.*, 93(1), 27–37, doi:10.1175/BAMS-D-11-00074.1, 2012.

Willén, U., Crewell, S., Baltink, H. K. and Sievers, O.: Assessing model predicted vertical cloud structure and cloud overlap with radar and lidar ceilometer observations for the Baltex Bridge Campaign of CLIWA-NET, *Atmos. Res.*, 75(3), 227–255, doi:10.1016/j.atmosres.2004.12.008, 2005.

WMO: International Cloud Atlas. Manual on the observation of clouds and other meteors, WMO, I, 1975.

WMO: International Cloud Atlas. Manual on the observation of clouds and other meteors, Geneva (Switzerland)., 1987.

WMO: WMO Catalogue of Radiosondes and Upper-air wind Systems. [online] Available from: <http://www.wmo.int/pages/prog/www/ois/volume-a/vola-home.htm>, 2007.

WMO: Guide of Meteorological Instruments and Methods of Observation, in WMO, vol. I & II, pp. I.15–1 to I.15–11–II.2–10 to II.2–11., 2008.

Xi, B., Dong, X., Minnis, P. and Khaiyer, M.: A 10 year climatology of cloud fraction and vertical distribution derived from both surface and GOES observations over the DOE ARM SPG site, *J. Geophys. Res.*, 115, 1–12, doi:10.1029/2009JD012800, 2010.

Yi, Y. H., Minnis, P., Ayers, J. K., Huang, J. P., Doelling, D. R., Khaiyer, M. M. and Nordeen, M. L.: Relationships Between Meteorological Conditions and Cloud Properties Determined from ARM Data, 14th ARM Sci. Team Meet. Proceedings, Albuquerque, New Mex. March 22-26, 1–18, 2004.

Zelinka, M. and Hartmann, D.: Why is longwave cloud feedback positive?, *J. Geophys. Res.*, 115, 1–16, doi:10.1029/2010JD013817, 2010.

Zhang, J., Chen, H., Bian, J., Xuan, Y., Duan, Y. and Cribb, M.: Development of Cloud Detection Methods Using CFH, GTS1, and RS80 Radiosondes, *Adv. Atmos. Sci.*, 29(2), 236–248, doi:10.1007/s00376-011-0215-4, 2012.

Zhang, J., Chen, H., Li, Z., Fan, X. and Peng, L.: Analysis of cloud layer structure in Shouxian, China using RS92 radiosonde aided by 95 GHz cloud radar, *J. Geophys. Res.*, 115, 1–13, 2010.

Zhang, J., Li, Z., Chen, H. and Cribb, M.: Validation of a radiosonde-based cloud layer detection method against a ground-based remote sensing method at multiple ARM sites, *J. Geophys. Res. Atmos.*, 118(2), 846–858, doi:10.1029/2012JD018515, 2013.

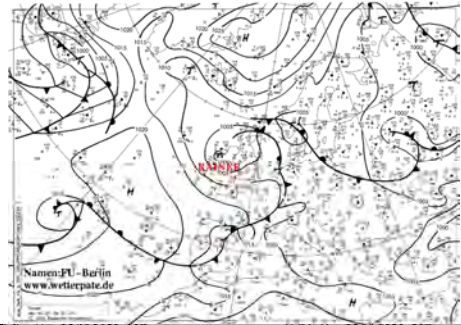
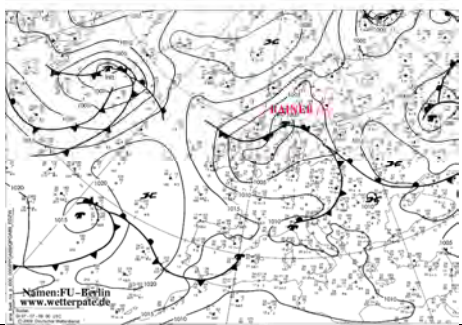
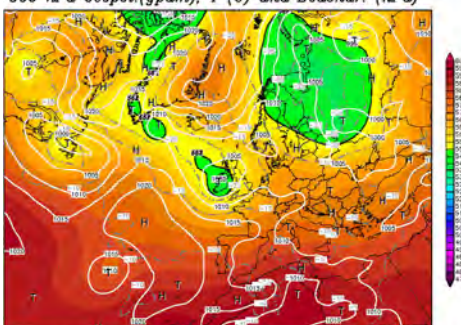
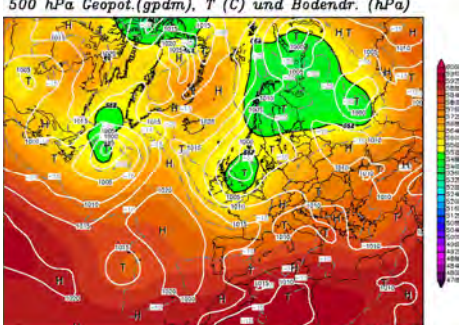
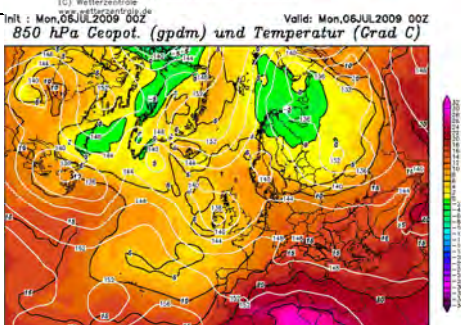
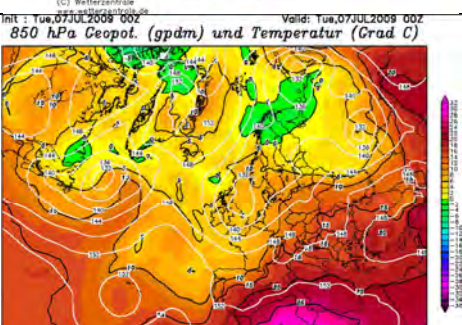
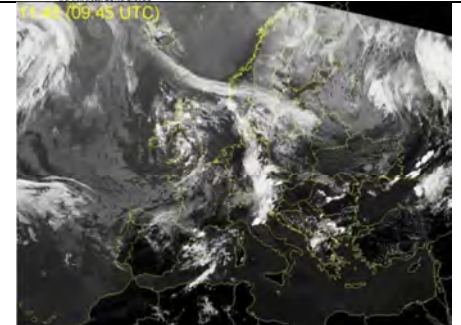
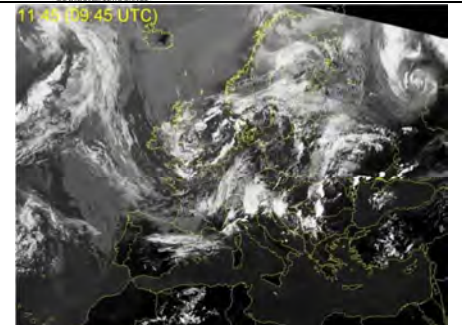
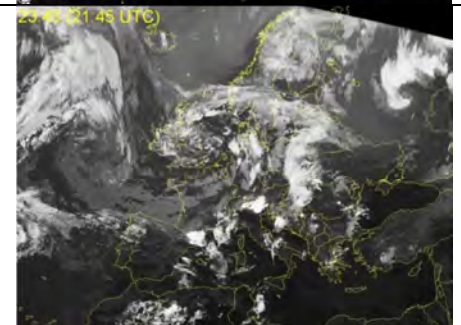
ANNEX 1: Synoptic maps of sea level pressure, temperature, and geopotential height at 500hPa and 850hPa; and Meteosat images; for some atmospheric situations (see section 4.2.3).

(1) source: Institut für Meteorologie: <http://www.met.fu-berlin.de/de/wetter/maps>

(2) source: Wetter Zentrale: <http://www.wetterzentrale.de/>

(3) source: EUMESAT: <http://www.eumetsat.int/>

	25/12/2009	26/12/2009
Sea level pressure map (00 UTC) (1)		
Temperature and Geopotential height at 500hPa (2)	<p>Int: Fri,25DEC2009 00Z Valid: Fri,25DEC2009 00Z 500 hPa Geopot.(gpm), T (C) und Bodendr. (hPa)</p>	<p>Int: Sat,26DEC2009 00Z Valid: Sat,26DEC2009 00Z 500 hPa Geopot.(gpm), T (C) und Bodendr. (hPa)</p>
Temperature and Geopotential height at 850hPa (2)	<p>Int: Fri,25DEC2009 00Z Valid: Fri,25DEC2009 00Z 850 hPa Geopot. (gpm) und Temperatur (Grad C)</p>	<p>Int: Sat,26DEC2009 00Z Valid: Sat,26DEC2009 00Z 850 hPa Geopot. (gpm) und Temperatur (Grad C)</p>
Meteosat Image (10.45 UTC) (3)	<p>11:45 (10:45 UTC)</p>	<p>11:45 (10:45 UTC)</p>
Meteosat Image (22.45 UTC) (3)	<p>11:45 (22:45 UTC)</p>	

	06/07/2009	07/07/2009
Sea level pressure map (00 UTC) (1)		
Temperature and Geopotential height at 500hPa (2)	<p>Init : Mon,06JUL2009 00Z Valid: Mon,06JUL2009 00Z 500 hPa Ceopot.(gpm), T (C) und Bodendr. (hPa)</p>  <p>Daten: GFS-Modell des amerikanischen Wetterdienstes (C) Wetterzentrale www.wetterzentrale.de</p>	<p>Init : Tue,07JUL2009 00Z Valid: Tue,07JUL2009 00Z 500 hPa Ceopot.(gpm), T (C) und Bodendr. (hPa)</p>  <p>Daten: GFS-Modell des amerikanischen Wetterdienstes (C) Wetterzentrale www.wetterzentrale.de</p>
Temperature and Geopotential height at 850hPa (2)	<p>Init : Mon,06JUL2009 00Z Valid: Mon,06JUL2009 00Z 850 hPa Ceopot. (gpm) und Temperatur (Grad C)</p>  <p>Daten: GFS-Modell des amerikanischen Wetterdienstes (C) Wetterzentrale www.wetterzentrale.de</p>	<p>Init : Tue,07JUL2009 00Z Valid: Tue,07JUL2009 00Z 850 hPa Ceopot. (gpm) und Temperatur (Grad C)</p>  <p>Daten: GFS-Modell des amerikanischen Wetterdienstes (C) Wetterzentrale www.wetterzentrale.de</p>
Meteosat Image (10.45 UTC) (3)		
Meteosat Image (22.45 UTC) (3)		

	18/07/2009	19/07/2009
Sea level pressure map (00 UTC) (1)		
Temperature and Geopotential height at 500hPa (2)	<p>Init : Sat,18JUL2009 00Z Valid: Sat,18JUL2009 00Z 500 hPa Geopot. (gpm), T (C) und Bodendr. (hPa)</p> <p>Daten: GFS-Modell des amerikanischen Wetterdienstes (C) Wetterzentrale www.wetterzentrale.de</p>	<p>Init : Sun,19JUL2009 00Z Valid: Sun,19JUL2009 00Z 500 hPa Geopot. (gpm), T (C) und Bodendr. (hPa)</p> <p>Daten: GFS-Modell des amerikanischen Wetterdienstes (C) Wetterzentrale www.wetterzentrale.de</p>
Temperature and Geopotential height at 850hPa (2)	<p>Init : Sat,18JUL2009 00Z Valid: Sat,18JUL2009 00Z 850 hPa Geopot. (gpm) und Temperatur (Grad C)</p> <p>Daten: GFS-Modell des amerikanischen Wetterdienstes (C) Wetterzentrale www.wetterzentrale.de</p>	<p>Init : Sun,19JUL2009 00Z Valid: Sun,19JUL2009 00Z 850 hPa Geopot. (gpm) und Temperatur (Grad C)</p> <p>Daten: GFS-Modell des amerikanischen Wetterdienstes (C) Wetterzentrale www.wetterzentrale.de</p>
Meteosat Image (10.45 UTC) (3)	<p>11.45 (09.45 UTC)</p> <p>© 2004 com (Source: EUMETSAT)</p>	<p>11.45 (09.45 UTC)</p> <p>© 2004 com (Source: EUMETSAT)</p>
Meteosat Image (22.45 UTC) (3)	<p>23.45 (21.45 UTC)</p> <p>© 2004 com (Source: EUMETSAT)</p>	

ANNEX 2: Website summary

European institutions and programs:

- British atmosphere datacenter, home: cedadocs.badc.rl.ac.uk (last access on 25 November 2013)
- Centre National d'Études Spatiales (CNES, France), home: www.cnes.fr (last access on 9 December 2013)
- Cloud-net Program: <http://www.cloud-net.org/> (last access on 21 February 2014)
- European Organization for the Exploitation of Meteorological Satellites, home: <http://www.eumetsat.int> (last access on 9 December 2013)
- European Space Agency, Envisat: <https://earth.esa.int/web/guest/missions/esa-operational-eo-missions/envisat> (last access on 9 December 2013)
- European Space Agency, ERS: <https://earth.esa.int/web/guest/missions/esa-operational-eo-missions/ers> (last access on 9 December 2013)
- European Space Agency, home: www.esa.int/ESA (last access on 9 December 2013)
- European Space Agency, meteorological missions (metop): http://www.esa.int/Our_Activities/Observing_the_Earth/The_Living_Planet_Programme/Meteorological_missions/MetOp (last access on 9 December 2013)
- Institut für Meteorologie (Berlin): <http://www.met.fu-berlin.de/de/wetter/maps> (last access on 21 February 2014)
- Izaña Atmospheric Research Center: <http://izana.aemet.es> (last access on 18 February 2014)
- Met Office: www.metoffice.gov.uk (last access on 21 February 2014)
- Servei Meteorològic de Catalunya: www.meteo.cat (last access on 21 February 2014)

- UdG meteorological and radiation station:
<http://www.udg.edu/Fisicaambiental/Estaciometeorologica/tabid/14749/Default.aspx>
(last access on 20 February 2014)
- Wetter Zentrale: <http://www.wetterzentrale.de/> (last access on 21 February 2014)

US institutions and programs:

- Atmospheric Radiation Measurement Climate Research Facility, home: www.arm.gov
(last access on 9 December 2013); archive: <http://www.archive.arm.gov/> (last access on 15 December 2013); Tech. Rep. "Total Sky Imager Model 880 Status and Testing Results" (Authors: Long, C.N., et al.): http://www.arm.gov/publications/tech_reports/arm-tr-006.pdf (last access on 9 April 2014); "Vaisala Ceilometer (VCEIL) Handbook" (Author: Morris, V.):
http://www.arm.gov/publications/tech_reports/handbooks/vceil_handbook.pdf?id=25
(last access on 9 April 2014).
- CERES ISCCP-D2like Product Information:
<http://ceres.larc.nasa.gov/products.php?product=ISCCP-D2> (last access on 4 April 2014)
- Colorado State University (CIRA): <http://amsu.cira.colostate.edu/> (last access 23 January 2014)
- Goddard Space Flight Center, home: trmm.gsfc.nasa.gov (last access on 9 December 2013)
- International Satellite Cloud Climatology Project, home: isccp.giss.nasa.gov (last access on 9 December 2013)
- Landsat Missions on US Geological Survey:
http://landsat.usgs.gov/band_designations_landsat_satellites.php (last access on 10 January 2014)
- Landsat program, home: landsat.gsfc.nasa.gov (last access on 9 December 2013)
- National Aeronautics and Space Administration (CERES), home:
<http://ceres.larc.nasa.gov/> (last access on 9 December 2013)

- National Oceanic and Atmospheric Administration, Advanced Very High Resolution Radiometer (AVHRR): noaasis.noaa.gov/NOAASIS/ml/avhrr.html (last access on 9 December 2013)
- National Oceanic and Atmospheric Administration, home: www.noaa.gov (last access on 9 December 2013)
- National Snow and Ice datacenter, home: nsidc.org (last access on 9 December 2013)
- National Space Science Data Center (NASA): nssdc.gsfc.nasa.gov (last access on 17 February 2014)
- NOAA's Surface Radiation Network (SURFRAD):
<http://www.esrl.noaa.gov/gmd/grad/surfrad/> (last access on 23 January 2014)
- Office of satellite operations, home: www.oso.noaa.gov (last access on 9 December 2013)

Private companies:

- Atmos Company, home: www.atmos-meteo.com (last access on 9 December 2013)
- Belfort Instrument: <http://belfortinstrument.com/products/80171-cloud-ceilometer/> (last access on 23 January 2014)
- Eliasson Engineering (Sweden): <http://www.eliasson.com/products/cbme80.shtml> (last access on 14 February 2014)
- Graw, home (Germany): <http://www.graw.de/> (last access on 12 February 2014)
- Jenoptik, home: www.jenoptik.com (last access on 9 December 2013)
- Meisei (Japan):
http://www.meisei.co.jp/english/products/meteo/rs06g_gps_radiosonde.html (last access on 12 February 2014)
- Meteo Modem, home (France): <http://www.meteomodem.com/> (last access on 12 February 2014)

- Meteolabor, home (Switzerland): <http://www.meteolabor.ch/en/> (last access on 12 February 2014)
- MTECH systems (Australia): <http://www.mtechsystems.com/meteorological/8200-CHS-Ceilometer.html> (last access on 14 February 2014)
- Nubiscope, home: www.nubiscope.eu (last access on 9 December 2013)
- Sandia National Laboratories, home: <http://www.sandia.gov/> (last access on 28 January 2014)
- Sieltec Canarias S.L (Spain):. <http://sonaspecs.zohosites.com> (last access on 21 January 2014)
- Sigma Space Micro Pulse Lidar division: <http://www.micropulselidar.com> (last access on 18 February 2014)
- Sippican Inc. (USA): <http://www.sippican.com/contentmgr/showdetails.php/id/306> (last access on 12 February 2014)
- Solmirus, home (USA): www.solmirus.com (last access on 9 December 2013)
- Vaisala Oyj, home (Finland): www.vaisala.com (last access on 9 December 2013); “Sky Condition Algorithm for Vaisala Ceilometer’s”: <http://www.vaisala.com/Vaisala Documents/Brochures and Datasheets/Sky-Condition-CL31-Datasheet-B210507EN-B-LoRes.pdf> (last access on 12 March 2014).
- Yankee Environment Systems Inc. (TSI-800) (USA): <http://www.yesinc.com/products/data/tsi880/> (last access on 20 January 2014)

Other agencies, networks and resources:

- Atlas of Simultaneous Occurrence of Different Cloud Types over Land (Authors: Hahn, C. J., et al.): <http://nldr.library.ucar.edu/collections/technotes/asset-000-000-000-355.pdf> (last access on 10 April 2014).

- Atlas of Simultaneous Occurrence of Different Cloud Types over the Ocean (Authors: Hahn, C. J., et al.): <http://nldr.library.ucar.edu/collections/technotes/asset-000-000-000-355.pdf> (last access on 10 April 2014).
- Aviation magazine: <http://avstop.com/ac/5-7.html> (last access on 4 April 2014)
- Book: “Meteorology Today, an introduction to Weather, Climate, and the Environment” (author: Ahrens, D. C., 9th edition): academic.cengage.com (last access on 9 April 2014).
- Book: “Terrestrial Hydrometeorology” (Author: Shuttleworth, W. J.): http://books.google.es/books?id=1veoRTEJe2UC&printsec=frontcover&source=gbs_ge_summary_r&cad=0#v=onepage&q&f=false (last access on 15 March 2014).
- Contribution of Working Group I to the Fifth Assessment Report of the Intergovernmental Panel on Climate Change “Climate Change 2013: The Physical Science Basis” (authors: Boucher, O., et al, by Cambridge University Press: http://www.climatechange2013.org/images/report/WG1AR5_Chapter07_FINAL.pdf (last access on 14 April 2014).
- Doctoral thesis: “Atmospheric downwelling longwave radiation at the surface during cloudless and overcast conditions. Measurements and modeling” (Author: Viúdez-Mora, A.): <http://hdl.handle.net/10803/31841> (last access on 5 March 2014).
- Hong Kong Observatory, home: http://www.hko.gov.hk/wxinfo/intersat/fy2e/satpic_s_vis.shtml (last access on 9 December 2013)
- India Space Research Organization, home: www.webcitation.org/5kf22DF7y (last access on 9 December 2013)
- Japan Aerospace Exploration Agency (JAXA), home: http://www.jaxa.jp/index_e.html (last access on 9 December 2013)
- Japan Aerospace Exploration Agency (JAXA), Marine Observation satellite “Momo-1”: http://www.jaxa.jp/projects/sat/mos1/index_e.html (last access on 9 December 2013)
- Japan Meteorological Agency, home: <http://www.jma.go.jp/jma/indexe.html> (last access on 9 December 2013)

- Korea Meteorological Administration/Meteorological Satellite Division (ESA and EUMESAT websites): <https://earth.esa.int/web/guest/missions/3rd-party-missions/historical-missions/kompsat-1> (last access on 14 January 2014), and https://www.eumetsat.int/cs/idcplg?IdcService=GET_FILE&dDocName=pdf_conf_p48_s1_02_shim_v&allowInterrupt=1&noSaveAs=1&RevisionSelectionMethod=LatestRelease (last access on 14 January 2014).
- Natural Resources Canada: <http://www.nrcan.gc.ca/earth-sciences/geomatics/satellite-imagery-air-photos/satellite-imagery-products/educational-resources/9387> (last access on 10 January 2014)
- Paper: “Automated whole sky imaging systems for cloud field assessment” (Authors: Shields, J. E., et al.): http://www-mpl.ucsd.edu/people/jshields/publications/pdfs/13Shields_AMS_93.pdf (last access on 8 March 2014).
- Paper: “Day/night whole sky imagers for 24-h cloud and sky assessment: history and overview” (Authors: Shields, J. E., et al.): http://www.opticsinfobase.org/view_article.cfm?gotourl=http://www.opticsinfobase.org/DirectPDFAccess/E4312735-CFFC-60D5-81E3ABF816D86AB5_249702/ao-52-8-1605.pdf?da=1&id=249702&seq=0&mobile=no&org= (last access on 8 March 2014).
- Paper: “Introduction to the Special Issue on the Chinese FengYun-3 Satellite Instrument Calibration and Applications” (Authors: Weng, F., et al.): <http://ieeexplore.ieee.org/stamp/stamp.jsp?arnumber=06355808> (last access on 9 April 2014).
- Paper: “Nimbus-7 Global Cloud Climatology. Part II: First Year Results” (Authors: Stowe, L. L., et al.): [http://journals.ametsoc.org/doi/pdf/10.1175/1520-0442\(1989\)002<0671:NGCCPI>2.0.CO;2](http://journals.ametsoc.org/doi/pdf/10.1175/1520-0442(1989)002<0671:NGCCPI>2.0.CO;2) (last access on 4 April 2014).
- Russia's space agency (Roscosmos): <http://www.russianspaceweb.com/elektro.html> (last access on 14 January 2014). Baseline Surface Radiation Network (BSRN): <http://www.ndsc.ncep.noaa.gov/coop/bsrn/> (last access on 23 January 2014).
- Tech. Rep.: “Transitioning to Operations: Lidars and Ceilometers” (Author: Werner, T.): http://www.wmo.int/pages/prog/www/IMOP/publications/IOM-109_TECO-2012/Programme_TECO-2012.html (last access on 15 March 2014).

- WMO Catalogue of Radiosondes and Upper-air wind Systems: <http://www.wmo.int/pages/prog/www/ois/volume-a/vola-home.htm> (last access on 9 April 2014).
- WMO Intercomparison of high quality radiosonde systems. Report No. 107 (Authors: Nash, J., et al.): <https://www.wmo.int/pages/prog/www/IMOP/intercomparisons.html> (last access on 5 April 2014).
- World Radiation Data Center (WRDC): <http://wrdc-mgo.nrel.gov/> (last access on 23 January 2014).